

**GEOSTATISTICAL ANALYSIS FOR  
SOIL DYNAMICS**

**A CASE STUDY FOR  
THE 1999 KOCAELI EARTHQUAKE**

**M.Sc. Thesis by  
Serkan Ülker, B.S.c**

**Department : Civil Engineering**

**Programme: Soil Mechanics and  
Geotechnical Engineering**

**DECEMBER 2006**

**GEOSTATISTICAL ANALYSIS FOR  
SOIL DYNAMICS**

**A CASE STUDY FOR  
THE 1999 KOCAELI EARTHQUAKE**

**M.Sc. Thesis by  
Serkan Ülker, B.S.c**

**Date of Submission : 20.11.2006**

**Date of Defence Examination : 22.12.2006**

**Supervisor (Chairman) : Assoc. Prof. Derin URAL SERPENGÜZEL**

**Members of Examining Committee : Prof . Dr. Ahmet SAĞLAMER**

**: Assoc. Prof. Dr. Mine ÇAĞLAR (K.Ü.)**

**DECEMBER 2006**

## PREFACE

Engineering Education for Bachelor and Master Science degree at Istanbul Technical University is the most important and valuable part of my life. Today, as a member of ITU family I want to express my special thanks to all, assist and trust me during last 7 years.

It was honestly, fortune that Assoc. Professor Derin URAL was my adviser. She never doubted my ability trusted, supported and encouraged me during my researches. I would like to express my grateful thanks to Professor Ahmet SAĞLAMER for his valuable support for my education and advices for the future.

I give thanks to TUBITAK (The Scientific and Technological Research Council of Turkey) for providing funds during my master science education and also appreciate the assistance of members working at TUBITAK-BİDEB.

Finally I specially thanks to my family and friends without their encouragement and support I couldn't finish my thesis.

December, 2006

Serkan ÜLKER

## TABLE OF CONTENTS

<b>ABBREVIATIONS</b>	vii
<b>LIST OF TABLES</b>	viii
<b>LIST OF FIGURES</b>	x
<b>LIST OF SYMBOLS</b>	xv
<b>ÖZET</b>	xvi
<b>SUMMARY</b>	xviii
<b>1 Introduction.....</b>	<b>1</b>
<b>2 Statistical Analysis of Soils.....</b>	<b>4</b>
2.1 Random Variables.....	5
2.2 Graphical Analysis of Variability.....	5
2.3 Quantitative Analysis of Variability.....	8
2.4 Theoretical Random Variable Models.....	12
2.4.1 Discrete Random Variables.....	12
2.4.2 Continuous Random Variables.....	14
2.5 Goodness of Fit Test.....	21
<b>3 Geostatistical Analysis for Soils.....</b>	<b>24</b>
3.1 Geostatistics.....	24
3.2 Stationarity.....	25
3.3 Intrinsic Hypothesis.....	25
3.4 Variogram.....	26
3.4.1 Properties of Variogram Function.....	27
3.4.2 Variogram Cloud.....	27
3.4.3 Experimental Variogram.....	28

3.4.4 Model Variogram.....	29
3.5 Autocovariance and Correlogram.....	33
3.6 Spatial Anisotropy.....	36
3.7 Kriging.....	36
<b>4 Earthquake in Turkey / 1999 Kocaeli Earthquake.....</b>	<b>40</b>
4.1 North Anatolian Fault.....	40
4.2 1999 Kocaeli Earthquake.....	42
4.2.1 Characteristics of the Earthquake.....	42
4.2.2 Fault Surface Ruptures .....	43
4.2.3 Strong Motion Records.....	44
4.3 Earthquake Effects on Adapazari.....	47
4.3.1 City of Adapazari.....	47
4.3.2 Geology of Adapazari.....	48
4.3.3 Researches in Adapazari.....	49
<b>5 Site Response Analysis.....</b>	<b>55</b>
5.1 Dynamic Soil Properties.....	56
5.2 Constitutive Models .....	59
5.3 Numerical Tools.....	60
5.4 Turkish Seismic Code for Soils and Earthquake Design.....	61
5.4.1 Determination of Soil Conditions.....	62
5.4.2 Determination of Elastic Seismic Loads.....	64
<b>6 Case Study: Geostatistical Analysis of Soil Deposits in Adapazari after 1999 Kocaeli Earthquake</b>	<b>67</b>
6.1 In-situ Testing and Interpretation.....	67
6.1.1 In-situ Testing in Adapazari.....	68
6.1.2 Sites Investigated.....	69
6.1.3 Interpretation of In-situ Tests.....	79

6.2. Statistical Analysis of Shear Wave Velocity.....	86
6.2.1 Graphical Analysis of Shear Wave Velocity.....	86
6.2.2 Quantitative Analysis of Shear Wave Velocity.....	88
6.3 Geostatistical Analysis of Shear Wave Velocity.....	97
6.3.1 Line description for Geostatistical Analysis.....	98
6.3.2 Variogram Estimation for Shear Wave Velocity.....	102
6.3.3 Kriging for Shear Wave Velocity.....	106
6.4 Site Response of Adapazari Soil Deposits.....	108
6.4.1 Input Motion.....	109
6.4.2 Soil Profile.....	109
6.4.3 Result of Analyses.....	114
<b>7 Conclusions</b>	<b>122</b>
<b>References</b>	<b>125</b>
Appendix -A In-situ Test Results	131
Appendix -B Statistical Analysis Results	200
Appendix -C Geostatistical Analysis Results	208
Appendix -D Ground Response Analysis	217
<b>CURRICULLUM VITAE</b>	<b>226</b>

## **ABBREVIATIONS**

CDF: Cumulative Distribution Function  
c.o.v: Coefficient of variation  
CPT: Cone Penetration Test  
EDF: Empirical Cumulative Distribution Function  
EERI: Earthquake Engineering Research Institute  
ERD: Earthquake Research Department Directorate for Disaster Affairs  
of the Ministry of Public Works  
KOERI: Kandilli Observatory and Earthquake Research Institute  
NSF: National Science Foundation  
PDF: Probability Density Function  
PEER: Pacific Earthquake Engineering Research Center  
PMF: Probability Mass Function  
SKR: Sakarya Ground Motion Station  
SPT : Standard Penetration Test  
S1A: (soil profile) Layer A at site 1  
USGS: United States Geological Survey

## LIST OF TABLES

	<b>Page No</b>
<b>Table 2.1</b> cov for Soil Properties	10
<b>Table 2.2</b> List of discrete random variable models and parameters used	13
<b>Table 2.3</b> List of continuous random variable models and parameters used.	16
<b>Table 2.4</b> Standard normal distribution (z) table	18
<b>Table 2.5</b> Critical Values for the Kolmogorov-Smirnov Statistics based on significance level and sample size	23
<b>Table 3.1</b> Variogram model, sill and nugget for various CPT parameters	32
<b>Table 3.2</b> Tabulated values of range and autocovariance distance for SPT and CPT Parameters	35
<b>Table 4.1</b> Devastating Earthquakes on North Anatolian Fault after 1939 Kocaeli Earthquake	41
<b>Table 4.2</b> Ground motion records in the region	46
<b>Table 5.1</b> Common values for Poisson's ratio	57
<b>Table 5.2</b> Geotechnical computer programs used in practice for site response analysis	61
<b>Table 5.3</b> Area and Estimated Population for each Earthquake Zone	62
<b>Table 5.4</b> Soil Groups from Turkish Seismic Code	63
<b>Table 5.5</b> Local Site Classes from Turkish Seismic Code	64
<b>Table 5.6</b> Effective Ground Acceleration from Turkish Seismic Code	64
<b>Table 5.7</b> Spectrum Characteristic Periods (TA and TB )	65
<b>Table 6.1</b> Specifications of CPT Equipment and Procedure	68
<b>Table 6.2</b> Specifications of SPT Equipment and Procedure	69
<b>Table 6.3</b> Elevations for in-situ tests for site 1	71
<b>Table 6.4</b> Elevations for in-situ tests for site 2	73
<b>Table 6.5</b> Elevations for in-situ tests for site 3	75
<b>Table 6.6</b> Elevations for in-situ tests for site 4	78
<b>Table 6.7</b> Corrections for SPT	79
<b>Table 6.8</b> Correlation coefficient, K, for different soil types	81
<b>Table 6.9</b> Soil groups based on standard penetration test values	83
<b>Table 6.10</b> Shear wave velocity values (m/sec) for site 1	84
<b>Table 6.11a</b> Shear wave velocity values (m/sec) for site 2	84
<b>Table 6.11b</b> Shear wave velocity values (m/sec) for site 2	85
<b>Table 6.12</b> Shear wave velocity values (m/sec) for site 3	85
<b>Table 6.13</b> Shear wave velocity values (m/sec) for site 4	85
<b>Table 6.14</b> Descriptive Statistics for Shear Wave Velocity in 4 Sites	90
<b>Table 6.15</b> Proposed distributions for 12 layers in the area of interest	92

<b>Table 6.16</b>	Distribution Parameters for the layers investigated	93
<b>Table 6.17</b>	Results for K-S Test	94
<b>Table 6.18</b>	Shear wave velocity (m/sec) distribution and probability to observe for each layer	96
<b>Table 6.19</b>	Soil groups based on shear wave velocities (m/sec)	96
<b>Table 6.20</b>	Probability to observe shear wave velocity below the given limits	97
<b>Table 6.21</b>	Experimental variogram result for line 1	105
<b>Table 6.22</b>	Parameters for the model variogram for defined lines	106
<b>Table 6.23</b>	Vs values computed based on geostatistical analysis (line 1)	112
<b>Table 6.24</b>	Vs values computed based on statistical analysis (line 1)	113
<b>Table 6.25</b>	Modulus reduction curves and damping curves for analysis	113
<b>Table 6.26</b>	Site response analysis results for 4 lines	120
<b>Table B-1</b>	Descriptive Statistics for Layers already investigated	201

**ZEMİN DİNAMIĞINDE  
GEOİSTATİSTİKSEL DEĞERLENDİRME  
1999 KOCAELİ DEPREMİ ÖRNEĞİ**

**YÜKSEK LİSANS TEZİ  
İnşaat Müh. Serkan Ülker**

**Tezin Enstitüye Verildiği Tarih : 09.11.2006**

**Tezin Savunulduğu Tarih : 22.12.2006**

**Tez Danışmanı: Doç. Dr. Derin URAL SERPENGÜZEL  
Diğer Jüri Üyeleri : Prof. Dr. Ahmet SAĞLAMER  
: Doç. Dr. Mine ÇAĞLAR (K.Ü.)**

**ARALIK 2006**

## LIST OF FIGURES

		<b>Page No</b>
<b>Figure 2.1</b>	Types of uncertainty in geotechnical soil properties	4
<b>Figure 2.2</b>	A typical histogram for total unit weight data	6
<b>Figure 2.3</b>	A typical frequency plot for total unit weight	6
<b>Figure 2.4</b>	Cumulative frequency plot for total unit weight data	7
<b>Figure 2.5</b>	Frequency plot of hydraulic conductivity data	7
<b>Figure 2.6</b>	Frequency plot of log-hydraulic conductivity data	8
<b>Figure 2.7</b>	Mode, median and mean values for non-symmetrical distribution	9
<b>Figure 2.8</b>	Probability density function for unit weight variable	14
<b>Figure 2.9</b>	Cumulative distribution function for unit weight variable	15
<b>Figure 2.10</b>	Probability density function and frequency density plot for unit weight variable	15
<b>Figure 2.11</b>	Typical normal distribution curve, fitted on frequency density histogram	17
<b>Figure 2.12</b>	Standard normal distribution and corresponding properties for standard deviation limits	19
<b>Figure 2.13</b>	PDF for hydraulic conductivity observations	19
<b>Figure 2.14</b>	Typical shapes for gamma distribution for different shape and scale factors	21
<b>Figure 2.15</b>	Theoretical and empirical cumulative distribution and process for K-S tests	22
<b>Figure 3.1</b>	General view of spatial distribution	24
<b>Figure 3.2</b>	General view of a variogram cloud	27
<b>Figure 3.3</b>	Typical view of a experimental variogram	28
<b>Figure 3.4a</b>	Analysis of random variables with a lag distance, 1m	28
<b>Figure 3.4b</b>	Analysis of random variables with a lag distance, 2m	29
<b>Figure 3.5</b>	General view of model variogram and variogram parameters	29
<b>Figure 3.6</b>	Variogram models represented by graphically	31
<b>Figure 3.7</b>	The relationship between autocovariance and variogram	35
<b>Figure 3.8</b>	Variograms for different directions	36
<b>Figure 4.1</b>	North Anatolian Fault Zone including devastating earthquakes with lateral slip values	40
<b>Figure 4.2</b>	Location of the epicenter for 1999 Kocaeli Earthquake	43
<b>Figure 4.3</b>	Right Lateral Offsets, produced by 1999 Kocaeli Earthquake, vertical offset shown in parentheses	43
<b>Figure 4.4</b>	2.7 meters right lateral offset along surface rupture near Resitbey	44

<b>Figure 4.5</b>	Peak Accelerations for the Each Observation Station	45
<b>Figure 4.6</b>	Acceleration records obtained from SKR station	47
<b>Figure 4.7</b>	General subsurface conditions and shear wave profile for Adapazari	48
<b>Figure 4.8</b>	General Map of Adapazari showing the geology and main streets and also SKR ground motion station	50
<b>Figure 4.9</b>	General Map of Adapazari showing heavily damaged distribution	50
<b>Figure 4.10</b>	Loss of bearing capacity and bulging of pavements	51
<b>Figure 4.11</b>	Overturning of a five-storey building with aspect ratio about four	51
<b>Figure 4.12</b>	Lateral movement observed in earthquake vicinity	52
<b>Figure 4.13</b>	Liquefied buildings with no structural damage	53
<b>Figure 4.14</b>	Sand boil on sidewalk	53
<b>Figure 5.1</b>	Definition of motion types	55
<b>Figure 5.2</b>	Change on equivalent number of cycles due to earthquake magnitude	58
<b>Figure 5.3</b>	Modulus under cyclic loading conditions	59
<b>Figure 5.4</b>	Earthquake Zonation Map	62
<b>Figure 5.5</b>	Design Response Spectrum from Turkish Seismic Code	65
<b>Figure 5.6</b>	Normalized Spectral Acceleration for 5 stations and minimum requirements in seismic code in both directions	66
<b>Figure 6.1</b>	Location of the sites on Adapazari City Map	70
<b>Figure 6.2</b>	Plan view of Site 1 and location of the boring logs	71
<b>Figure 6.3</b>	Soil profile for site 1.	72
<b>Figure 6.4</b>	Plan view of Site 2 and location of the boring logs	73
<b>Figure 6.5</b>	Soil profile for site 2.	74
<b>Figure 6.6</b>	Plan view of Site 3 and location of the boring logs	75
<b>Figure 6.7</b>	Soil profile for site 3.	76
<b>Figure 6.8</b>	Plan view of Site 3 and location of the boring logs	77
<b>Figure 6.9</b>	Soil profile for site 4	78
<b>Figure 6.10</b>	Relationship between N'60 and Elevation for Site 1	81
<b>Figure 6.11</b>	Relationship between N'60 and Elevation for Site 2	82
<b>Figure 6.12</b>	Relationship between N'60 and Elevation for Site 3	82
<b>Figure 6.13</b>	Relationship between N'60 and Elevation for Site 4	83
<b>Figure 6.14</b>	Histogram plot for S3B	87
<b>Figure 6.15</b>	Frequency plot for Vs variable in S3B	87
<b>Figure 6.16</b>	Cumulative Histogram for Vs variable in S3B	88
<b>Figure 6.17</b>	Frequency plot for Vs variable in S3B with fitted normal curve	91
<b>Figure 6.18</b>	Histogram plot for lnVs variable in S3B	92
<b>Figure 6.19</b>	K-S Test application to S3B data set	94
<b>Figure 6.20</b>	Line 1 defined for geostatistical analysis in site 1	98
<b>Figure 6.21</b>	Line 2 defined for geostatistical analysis in site 2	98
<b>Figure 6.22</b>	Line 3 defined for geostatistical analysis in site 3	99

<b>Figure 6.23</b>	Line 4 defined for geostatistical analysis in site 4	99
<b>Figure 6.24</b>	Shear wave velocity values (m/sec) shown in elevation distance map for line 1	100
<b>Figure 6.25</b>	Shear wave velocity values (m/sec) shown in elevation distance map for line 2	100
<b>Figure 6.26</b>	Shear wave velocity values (m/sec) shown in elevation distance map for line 3	101
<b>Figure 6.27</b>	Shear wave velocity values (m/sec) shown in elevation distance map for line 4	101
<b>Figure 6.28</b>	Squared-differences variogram cloud for line 1	103
<b>Figure 6.29</b>	Experimental Variogram and Model fitting for line 1	104
<b>Figure 6.30</b>	2-D kriging map of shear wave velocity (m/sec) for line 1	107
<b>Figure 6.31</b>	3-D Surface Map for kriging of line 1	108
<b>Figure 6.32</b>	SKR Station, E-W record from 1999 Kocaeli Earthquake used as input motion	109
<b>Figure 6.33</b>	Finite element mesh for top 10 m for statistically modeled soil profile (line 1)	110
<b>Figure 6.34</b>	Finite element mesh for top 10 m for geostatistically modeled soil profile (line 1)	110
<b>Figure 6.35</b>	Finite element mesh used in analysis including the imported soil profile from Bray et al (2004) (line 1)	111
<b>Figure 6.36</b>	Modulus Reduction and Damping Curves for Clay	113
<b>Figure 6.37</b>	Modulus Reduction and Damping Curves for Sand	114
<b>Figure 6.38</b>	Statistically modeled soil profile (line 1)	114
<b>Figure 6.39</b>	Acceleration time history at ground surface for statistically modeled soil profile (line 1)	115
<b>Figure 6.40</b>	Peak acceleration vs distance, computed at ground surface for statistically modeled soil profile (line 1).	115
<b>Figure 6.41</b>	Peak Acceleration distribution for statistically modeled soil (line 1).	116
<b>Figure 6.42</b>	Response Spectrum for statistically modeled profile (line 1)	116
<b>Figure 6.43</b>	Geostatistically modeled soil profile (line 1)	117
<b>Figure 6.44</b>	Acceleration time history for Geostatistically modeled soil profile (line 1)	117
<b>Figure 6.45</b>	Peak Acceleration distribution for geostatistically modeled soil (line 1).	118
<b>Figure 6.46</b>	Relationship between acceleration versus distance for the ground surface (line 1)	118
<b>Figure 6.47</b>	Response Spectrum for geostatistically modeled profile (line 1)	119
<b>Figure 6.48</b>	Acceleration (g) and distance (m) at the ground surface (line 1)	119
<b>Figure 6.49</b>	Computed peak accelerations on sites in Adapazari	120
<b>Figure 6.50</b>	Normalized Spectral Acceleration for the lines and soil classes defined in Turkish Seismic Code	121
<b>Figure C-1</b>	Variogram clouds of shear wave velocity for line 1	209

<b>Figure C-2</b>	Variogram clouds of shear wave velocity for line 2	209
<b>Figure C-3</b>	Variogram clouds of shear wave velocity for line 3	210
<b>Figure C-4</b>	Variogram clouds of shear wave velocity for line 4	210
<b>Figure C-5</b>	Experimental Variogram and Model fitting for line 1	211
<b>Figure C-6</b>	Experimental Variogram and Model fitting for line 2	211
<b>Figure C-7</b>	Experimental Variogram and Model fitting for line 3	212
<b>Figure C-8</b>	Experimental Variogram and Model fitting for line 4	212
<b>Figure C-9</b>	2-D Kriging map of shear wave velocity (m/sec) for line 1	213
<b>Figure C-10</b>	2-D Kriging map of shear wave velocity (m/sec) for line 2	213
<b>Figure C-11</b>	2-D Kriging map of shear wave velocity (m/sec) for line 3	214
<b>Figure C-12</b>	2-D Kriging map of shear wave velocity (m/sec) for line 4	214
<b>Figure C-13</b>	3-D Kriging map of shear wave velocity (m/sec) for line 1	215
<b>Figure C-14</b>	3-D Kriging map of shear wave velocity (m/sec) for line 2	215
<b>Figure C-15</b>	3-D Kriging map of shear wave velocity (m/sec) for line 3	216
<b>Figure C-16</b>	3-D Kriging map of shear wave velocity (m/sec) for line 4	216
<b>Figure D-1</b>	Statistically Modeled soil profile for line 1	218
<b>Figure D-2</b>	Geostatistically Modeled soil profile for line 1	218
<b>Figure D-3</b>	Peak acceleration distribution for statistically Modeled soil profile for line 1	218
<b>Figure D-4</b>	Peak acceleration distribution for geostatistically Modeled soil profile for line 1	219
<b>Figure D-5</b>	Peak acceleration distribution along the line 1 recorded at ground surface for statistically and geostatistically modeled soil profiles	219
<b>Figure D-6</b>	Statistically Modeled soil profile for line 2	220
<b>Figure D-7</b>	Geostatistically Modeled soil profile for line 2	220
<b>Figure D-8</b>	Peak acceleration distribution for statistically Modeled soil profile for line 2	220
<b>Figure D-9</b>	Peak acceleration distribution for geostatistically Modeled soil profile for line 2	221
<b>Figure D-10</b>	Peak acceleration distribution along the line 2 recorded at ground surface for statistically and geostatistically modeled soil profiles	221
<b>Figure D-11</b>	Statistically Modeled soil profile for line 3	222
<b>Figure D-12</b>	Geostatistically Modeled soil profile for line 3	222
<b>Figure D-13</b>	Peak acceleration distribution for statistically Modeled soil profile for line 3	222
<b>Figure D-14</b>	Peak acceleration distribution for geostatistically Modeled soil profile for line 3	223
<b>Figure D-15</b>	Peak acceleration distribution along the line 3 recorded at ground surface for statistically and geostatistically modeled soil profiles	223
<b>Figure D-16</b>	Statistically Modeled soil profile for line 4	224
<b>Figure D-17</b>	Geostatistically Modeled soil profile for line 4	224
<b>Figure D-18</b>	Peak acceleration distribution for statistically Modeled soil profile for line 4	224

- Figure D-19** Peak acceleration distribution for geostatistically Modeled soil profile for line 4 225
- Figure D-20** Peak acceleration distribution along the line 4 recorded at ground surface for statistically and geostatistically modeled soil profiles 225

## LIST OF SYMBOLS

<b><i>a</i></b>	Range
$\alpha, \beta, \lambda$	gamma distribution parameters
<b><i>E<sub>s</sub></i></b>	Stress strain modulus
<b><i>G</i></b>	Shear modulus
<b><i>h</i></b>	lag distance
<b><i>N</i></b>	Number of observations
<b><i>N<sub>m</sub></i></b>	SPT blow number
<b><i>(N<sub>1</sub>)<sub>60</sub></i></b>	SPT blow number (corrected)
<b><i>PI</i></b>	Plasticity index
<b><i>V<sub>s</sub></i></b>	Shear wave velocity
<b><math>\mu</math></b>	Mean
<b><math>\mu</math></b>	Poisson' ratio
<b><math>\sigma</math></b>	Standard deviation
<b><math>\rho</math></b>	Correlation coefficient
<b><math>\delta</math></b>	coefficient of variation
<b><math>\lambda</math></b>	weight parameter
<b><math>\kappa</math></b>	kurtosis
<b><math>\Psi</math></b>	skewness
<b><math>\gamma</math></b>	semivariance
<b><math>\rho</math></b>	Density of soil
<b><math>\xi</math></b>	Damping

## ZEMİN DİNAMİĞİNDE GEO-İSTATİSTİKSEL DEĞERLENDİRME,

### 1999 KOCAELİ DEPREMİ ÖRNEĞİ

#### ÖZET

Yerel zemin koşullarının sismik etkiler altında incelenmesi üç bileşen altında toplanabilir. Deprem kaydı, zeminin modellenmesi ve analiz yöntemi olarak sayılabilecek bu bileşenler arasında zeminin modellenmesi belirsizliklerin en sık rastlandığı bileşen olarak karşımıza çıkmaktadır.

Bu çalışma kapsamında zemin dinamiği analizlerinde kullanılmak üzere belirsizliklerin en aza indirgeneceği, daha doğru ve güvenilir sonuçlara ulaşılacağı ön görüşüyle zemin modellemesinde, geoistatistiksel analiz yöntemi kullanılmıştır.

1999 Kocaeli depremi sonrası Adapazarı'nda yapılmış olan 31 CPT ve 22 SPT; arazi deneyleri sonuçları yorumlanarak analizler için kayma dalgası hız verileri hazırlanmıştır..

İstatistiksel ve geoistatistiksel analizler kullanılarak, 4 farklı sahada ilk on metrelik zemin tabakası için kayma dalgası hız değişkeni modellenmiştir.

İstatistiksel analizler sonucunda zemin tabakaları istatistiksel dağılımlar şeklinde modellenmiş bu sahalarda ölçülebilecek kayma dalgası hız değerleri olasılıklarıyla verilmiştir. İstatistiksel değerlendirmeler, sonucunda kayma dalgası hız değişkenine ait varyasyon katsayısı 0.13 olarak hesaplanmıştır.

Geoistatistiksel analizler ile birlikte zeminde belirsizliklere neden olan kayma dalgası hız değişkenleri için korelasyon mesafesi ve değişimin varyasyonu hesaplanarak zemin için kayma dalgası hız profili belirlenmiştir. Geoistatistiksel değerlendirme sonucunda korelasyon mesafesi 3.5m olarak bulunmuştur.

İstatistiksel ve geoistatistiksel olarak modellenen zemin profilleri 1999 Kocaeli depremi sonrası SKR istasyonundan elde edilen deprem kaydının kullanıldığı iki boyutlu eşdeğer lineer analiz yöntemiyle çözülmüştür. Geoistatistiksel analiz sonrası oluşturulan zemin profilinde ölçülen en yüksek ivme değeri istatistiksel analiz sonrası modellenen zemin profilinden elde edilen en yüksek ivme değerine göre ortalama 0.01 g daha az çıkmıştır.

Geoistatistiksel analiz, Geoteknik mühendisliği uygulamalarında rastsal değişkenlerin konuma bağlı olarak belirlenmesinde kullanılan yeni bir yöntemdir. Zemin dinamiği analizlerinde geoistatistiksel modelleme kullanılmasıyla belirsizlikler azaltılarak daha doğru ve güvenilir sonuçlar elde edilmektedir.

## **GEOSTATISTICAL ANALYSIS FOR SOIL DYNAMICS**

### **A CASE STUDY FOR 1999 KOCAELI EARTHQUAKE**

#### **SUMMARY**

Site response analysis can be considered as composed of three components namely, input motion, soil model and method of analysis. All components has uncertainty but Soil model is the component consisting highest uncertainty if it is compared to others.

In this study, geostatistical analysis is used for modeling the soil in order to minimize the uncertainty and obtain more accurate and reliable results.

Field investigations including 31 CPT and 22 SPT performed in Adapazari after 1999 Kocaeli earthquake are interpreted to obtain shear wave velocity values. By using statistical and geostatistical analysis, first ten meters in 4 sites in Adapazari, shear wave velocity profiles are modeled

Firstly, by using statistical analysis, soil layers are modeled on the basis of statistical distributions. Descriptive statistics for shear wave velocity variable are computed. Moreover, probabilities to observe shear wave velocity values at site are calculated. Coefficient of variation is generalized as 0.13 for shear wave velocity variable.

Secondly, correlation coefficient and variation for shear wave velocity are computed by using geostatistical analysis.  $V_s$  profiles are defined for soil models by using three main components of geostatistics, range nugget effect and sill. Range value is generalized as 3.5m for shear wave velocity variable.

Statistically and geostatistically modeled soil profiles are used as input soil models for site response analysis. As input motion, earthquake data recorded at SKR station

after 1999 Kocaeli earthquake is used. Method of analysis is selected as equivalent linear two dimensional models.

Peak accelerations recorded at ground surface on geostatistically modeled soil profiles are generally 0.01 g lower than the values computed on statistically modeled soil profiles.

Geostatistical analysis, is a new tool for geotechnical engineering discipline to model the soil profile with limited sample of data by using their own location. Minimizing the uncertainty, obtaining more accurate and reliable results are advantages of geostatistics during soil dynamic analysis

## **1.Introduction**

Assessment of uncertainty is an integral part of all engineering projects. Every engineering project requires the commitment of financial and human capital and it is the responsibility of the engineer to develop a design that performs satisfactorily while providing an appropriate level of safety and minimal the use of financial and human resources. Assessment of uncertainty is particularly important for those projects that involve significant interaction with earth materials. For geotechnical applications, the engineer uses data from a site investigation to interpret the structure and potential behavior of the subsurface. Often these data consist of samples that represent 1/100,000 or less of the total volume of soil. These samples and the associated field and lab testing provide the information used to estimate soil parameter values.

For a reliable design, the uncertainties must be identified, characterized, and taken into account. Tang, (1984), Christian et al. (1994), Fenton (1999), Duncan (2000), Whitman (2000), Zhang et al (2004) among others have described general principles for organizing and characterizing geotechnical uncertainties and have presented examples that illustrate the use of probability theory to include uncertainties in geotechnical design.

Uncertainty could be considered by using statistical methods. Theory of random variable, probability and descriptive statistics the ways to analyze the nature of soil. Distribution functions indicate the trend of the variability of the soil and a simple way in order to estimate the limits of the range.

Advanced statistics, geostatistics is another tool to determine soil variability. Geostatistics deals with spatial data; data for which each value is associated with a location in space. In such analysis it is assumed that there is some connection between location and data value. From known values at sampled points, geostatistical analysis can be used to predict spatial distributions of properties over large areas or volumes. To determine geotechnical and geological conditions, such as the

stratigraphy of soil or rock layers at a project site, boreholes are drilled at specified locations. Often, and as expected, one finds that measurements from boreholes close to each other tend to be more similar compared to those from distant boreholes.

In what way does geostatistics differ from conventional statistics? Conventional statistics is used to analyze and interpret the uncertainty caused by limited sampling. For example, a conventional statistical analysis of core samples from a site investigation program might show that measured cohesion values of a material can be described by a normal distribution. However, this distribution only describes the population of values gathered in the investigation; it does not convey information on which zones are likely to have high cohesion values and which areas low values. Geostatistical analysis, on the other hand, is utilized to interpret statistical distribution of data and to examine spatial relationships. For the example given, the method capable of exhibiting cohesion values variation over distance, and assists in predicting areas of high and low cohesion values. The method provides tools for capturing maximum information on a phenomenon from few, often biased, and often under-sampled data. It produces predictions of the probable distribution of properties in space.

Geostatistics, dealing with spatial data and location can be considered as well defined method for analysis in geotechnical engineering problems. One of the problems can be defined as earthquakes. Modeling the soil by geostatistical analysis to determine site response could bring a new method in dynamic analysis of soil.

An earthquake with a magnitude of 7.4(Mw) occurred on 17 August 1999, between Gölcük and Izmit in Kocaeli Province of Turkey. This earthquake is officially called Kocaeli Earthquake. The earthquake caused disastrous damage to a huge number of buildings resulting in significant casualties in the provinces of Istanbul, Kocaeli, Sakarya, Bolu, Bursa, Zonguldak, Eskisehir, Yalova. According to preliminary report, the earthquake caused the loss of more than 17.000 lives and injured more than 23.000 people, and collapsed 2000 buildings totally. This earthquake caused severe structural damages in Gölcük, Izmit, Düzce, Yalova, Adapazari and the suburbs of Istanbul. Direct economic lost was estimated due to only structural damages is about 6 billion US dollars.

It is now well known that improper design and construction practices played a big role in the performance of more than 20,000 structures during the Kocaeli Earthquake(Celebi, 2000) This being a given, the main goal must be to improve design and construction practices. Initial part of the design process is assessments on the soil, in other words geotechnical design.

Therefore, the objective of this study is to characterize the soil in the city of Adapazari by using statistical and geostatistical methods and the results of the analysis are to be used in site response analysis for the 1999 Kocaeli Earthquake

The data used in this research is obtained from the investigations executed by Bray in 2000 under the sponsorship of Pacific Earthquake Engineering Research Center.

The research performed in the following order the definition of the statistical and geostatistical methods in chapter 2 and chapter 3. For the application of the methods the 1999 Kocaeli Earthquake are discussed in chapter 4

The seismic behavior of the soil under earthquake loading and site response analysis is expressed in chapter 5. The Turkish Seismic Code is examined in this chapter

Chapter 6 covers the analysis of soil deposits in Adapazari, statistical and geostatistical methods applied to the shear wave velocity values computed with the correlations. Statistically and geostatistically modeled soil profiles are used as soil models for site response analysis.

## 2. Statistical Analysis of Soils

Certainty is when the outcome of an event or the value for a parameter is known. On the contrary, a situation can be accepted as “uncertain” if there are at least two possible values for the result. Uncertainty analysis requires estimation and simulation techniques for data. The approach for dealing with uncertainty in geotechnical engineering was presented by Arthur Casagrande in his 1964 Terzaghi Lecture.

Uncertainty in geotechnical soil properties can be grouped into aleatory and epistemic uncertainty (Lacasse et al., 1996). Aleatory uncertainty represents natural randomness of the soil whereas, epistemic uncertainty results because of lack of information and shortcomings in measurements. Sources of uncertainty in geotechnical design are listed in figure 2.1.

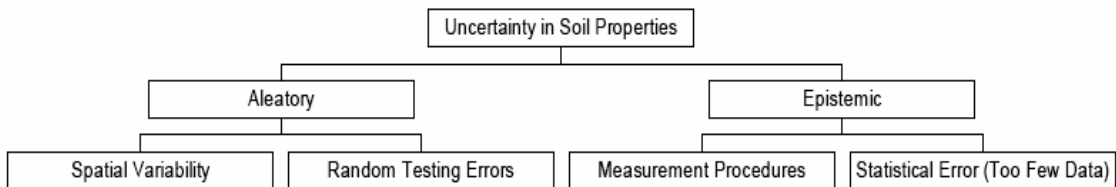


**Figure 2.1** Types of uncertainty in geotechnical soil properties (Lacasse et al., 1996)

As an example to uncertainty, Jones et al (2002) investigated the randomness of a SPT sampling in a deposit of loose sand. Source of aleatory uncertainty in the measured SPT resistance would include the natural variability of the soil and random testing errors. Sources of epistemic uncertainty contain non-standard equipment such as; sampler size and insufficient data such as one boring for entire site. It is important that, epistemic uncertainty can be reduced by additional data or repeating the process with the corrected equipment. However it is not possible to reduce the effect of aleatory uncertainty which includes the inherent stochasticity of the soil.

## 2.1 Random Variables

In order to explain uncertainty, fundamentals of probability need to be discussed. Probability concept is on the basis of random variable. A random variable represents a quantity that varies. Specifically, a random variable model describes the possible values that a quantity can take on, and the respective probabilities for each of these values.

If a random variable takes on a specific value, in other words measured, then it is no longer random and it will be shown with a lowercase letter. Therefore,  $x$  is an observation of  $X$ . The range of possible values that  $X$  can be observed is defined as the sample space of  $X$ . For example, water content of the soil could be any value greater than zero. The probability of the sample space will be equal to 1. The probability distribution for a random variable is a function describing the probability that it takes on different values.

## 2.2 Graphical Analysis of Variability

Soil has heterogeneous material properties. Evaluation process for variability should include graphical analysis of the data obtained from the site. In this study histograms and frequency plots are presented to depict variability.

A histogram is obtained by dividing the data into groups, and then counting the number of values corresponding to each data set. The histogram gives information about the variability in the data set. It shows the range of the data, the most frequently occurring values, the amount of scatter about the values in the set.

There are several issues to consider in determining the number of intervals for a histogram. First, the number of intervals should depend on the number of data. If the number of data increases, the number of interval should be increased. Second, number of the intervals affects the distribution of the variable. Too few interval or too many intervals couldn't symbolize the behavior of the population. There is no rule to compute the number of intervals. However there are empirical formulas used to compute number of intervals in literature. Gilbert(1997) suggests to use the following equation in order to have a view for the number of intervals.

$$k = 1 + 3.3 \log_{10}(n) \quad (2.1)$$

where  $k$  is the number of intervals and  $n$  is the number of data points. Typical histogram for unit weight data is shown in figure 2.2.

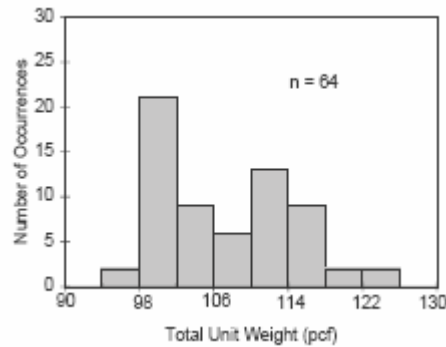


**Figure 2.2** A typical histogram for total unit weight (Gilbert,1997)

The frequency of occurrence in each histogram interval is obtained by dividing the number of occurrences to the total number of data points. A bar chart plot of the frequency occurrence in each interval is called a frequency plot. Figure 2.3 shows the frequency plot of the unit weight data which is graphed as a histogram in figure 2.2

Frequency plot and histogram have the same shape and information but in a frequency plot, the vertical axis is the frequency of occurrence.

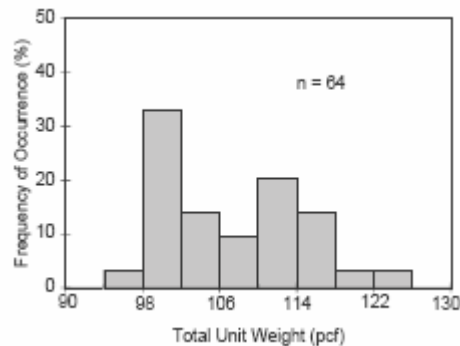


**Figure 2.3** A typical frequency plot for total unit weight (Gilbert,1997)

The cumulative frequency plot is a third graphical tool presented for variability analysis. Cumulative frequency is the frequency of data points that have values less than or equal to the upper bound of an interval in the frequency plot. The cumulative frequency is obtained by summing up the interval frequencies for all intervals below the upper bound. A plot of cumulative frequency versus the upper bound is called the cumulative frequency plot.

A percentile value for the data set corresponds to the cumulative frequency. For example, the 50th percentile value for the unit weight data set is 106 pcf (50 percent of the values are less than or equal to 106 pcf), while the 90th percentile value is equal to 117 pcf (Figure 2.4)

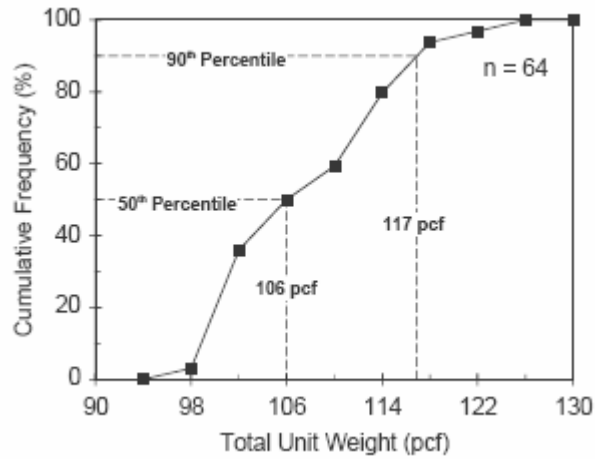


**Figure 2.4** Cumulative frequency plot for total unit weight data (Gilbert,1997)

In some cases, it is useful to transform the data before plotting it. One example is a data set of measured hydraulic conductivity values for a compacted clay liner. The frequency plot for these data is shown on figure 2.5. It does not convey much about the data set because the hydraulic conductivity values range over several orders of magnitude. A more useful representation of the data is to develop a frequency plot for the logarithm of hydraulic conductivity, as shown on figure 2.6.

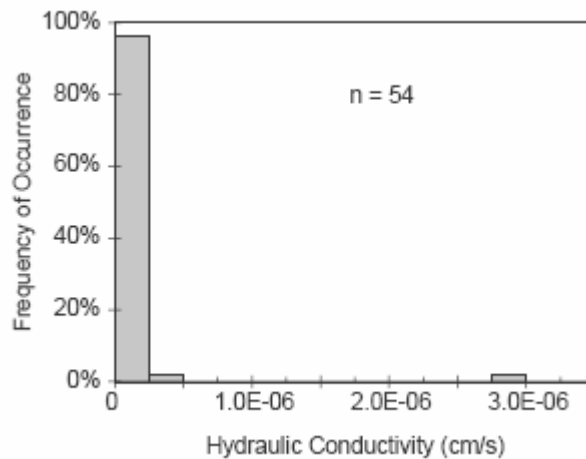


**Figure 2.5** Frequency plot of hydraulic conductivity data (Gilbert,1997)

Now it can be seen that the most likely interval is between  $10^{-8.4}$  and  $10^{-8.2}$  cm/s and that most of the data are less than or equal to  $10^{-7}$  cm/s.

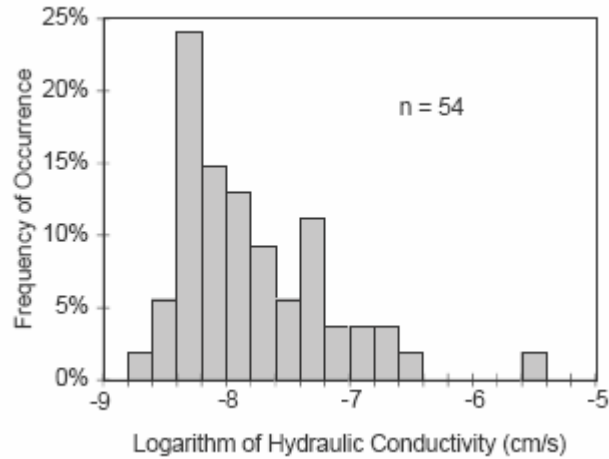


**Figure 2.6** Frequency plot of log-hydraulic conductivity data (Gilbert,1997)

### 2.3 Quantitative Analysis of Variability

In addition to the graphical analysis, the variability in a data set can also be analyzed quantitatively. The statistics of a data set provide quantitative measures of variability. Mathematical expectation, also known as mean, variance, coefficient of variation, skewness, kurtosis and correlation between data points are discussed in this section.

The most common measure for the center of a data set is the average value, which is also called the sample mean. The sample mean is obtained as follows

$$\mu = \frac{1}{n} \sum_{i=1}^n x_i \quad (2.2)$$

Where  $\mu$  is the sample mean  $x_i$  is each data value and  $n$  is the total number of the data points.

The sample median and mode are other measures of central tendency for a data set. As shown in Figure 2.7. Sample median is the 50<sup>th</sup> percentile value, while the sample is the most likely value. The mean, median and mode are not equal unless the data distribution (the frequency plot) is symmetrical and has a single mode (peak).

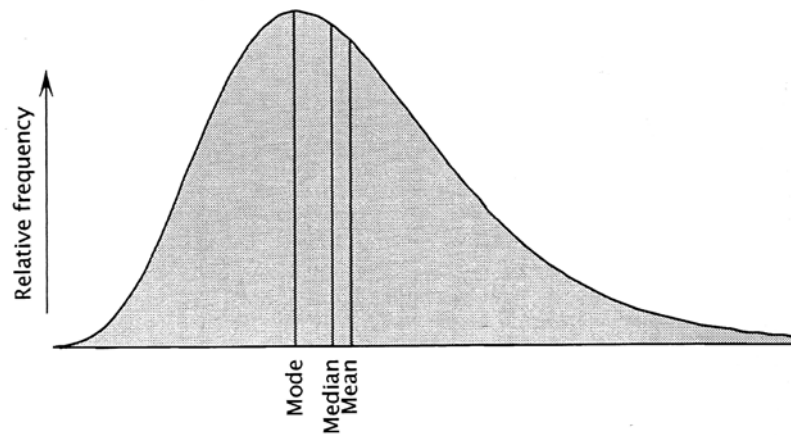


**Figure 2.7** Mode, median and mean values for non-symmetrical distribution. (Davis,2002)

The amount of scatter in a data set is most easily measured by the sample range. The sample range is the maximum value in the data set minus the minimum value. The sample variance is a measure of dispersion about the mean value of the data set. The sample variance is obtained as follows

$$\sigma_x^2 = \frac{1}{n} \sum_{i=1}^n (x_i - \mu_x)^2 \quad (2.3)$$

where  $\sigma^2$  is the sample variance. The sample variance is the average of the square of the distance between individual data points and the sample mean. Its value will always be greater than or equal to zero.

The sample standard deviation,  $\sigma$  is the square root of the sample variance, while the sample coefficient of variation (c.o.v.), is the standard deviation divided by the mean value.

$$\delta_x = \frac{\sigma_x}{\mu_x} \quad (2.4)$$

Because the standard deviation has the same units as the mean value, the c.o.v. is a dimensionless measure of dispersion.

Coefficient of variation commonly used to describe the variation of many geotechnical soil properties. c.o.v can be defined as normalization of standard deviation due to mean. Typical c.o.v. values for various soil properties are summarized in Table 2.1 by Kim(2005). A comprehensive listing can be found in Jones et al(2002)

**Table 2.1** c.o.v. for Soil Properties (Kim, 2005)

Parameter	Coefficient of variation [%]	Source
Porosity	10	Schultze (1972)
Specific gravity	2	Padilla and Vanmarcke (1974)
Water content (Silty clay)	20	Padilla and Vanmarcke (1974)
Water content (Clay)	13	Fredlund and Dahlman (1972)
Degree of saturation	10	Fredlund and Dahlman (1972)
Unit weight	3	Hammitt (1966)
Coefficient of permeability	240 at 80% saturation	Nielsen et al. (1973)
	90 at 100% saturation	Nielsen et al. (1973)
Compressibility factor	16	Padilla and Vanmarcke (1974)
Preconsolidation pressure	19	Padilla and Vanmarcke (1974)
Compression index (Sandy clay)	26	Lumb (1966)
Compression index (Clay)	30	Fredlund and Dahlman (1972)
Standard penetration test	26	Schultze (1972)
Standard cone test	37	Schultze (1972)
Friction angle (Gravel)	7	Schultze (1972)
Friction angle (Sand)	12	Schultze (1972)

Since the sample variance is the average of the square distance from the sample mean, data values the same distances above and below the sample mean contributes equally. Therefore, the sample variance provides no indication of how symmetrical the data are dispersed about the mean. The sample skewness, which is essentially the average of the cubed distance from the sample mean, provides a measure of symmetry for a data set.

The sample skewness coefficient, a dimensionless measure of skewness, is given by the following formula

$$\psi = \frac{1}{n} \frac{\sum_{i=1}^n (x_i - \mu_x)^3}{\sigma_x^3} \quad (2.5)$$

where  $\psi$  is the sample skewness coefficient. A skewness coefficient of zero means that the data values are distributed symmetrically about the mean value. A negative skewness coefficient indicates that the data are skewed about the mean to the right

(toward larger values), while a positive skewness coefficient indicates that the data are skewed to the left (toward smaller values).

Kurtosis is an expression called as fourth moment, a tendency for a distribution to form a sharp narrow peak or a broad plateau. It is a unitless parameter. A positive kurtosis indicates that the tails of distribution are longer and has a peak, whereas a negative kurtosis is the sign of short tail distribution. For normally distributed models kurtosis model is zero defined as mesokurtic. More peaked distributions are leptokurtic and less peaked distributions are called as platykurtic. Kurtosis parameter can be computed by the given formula,

$$k = \frac{1}{n} \frac{\sum_{i=1}^n (x_i - \mu_x)^4}{\sigma_x^4} - 3 \quad (2.6)$$

In some cases, there are two random variables in a probability space. The relationship between two variables must be analyzed. Therefore, joint moments can be used to describe the relationship in statistics. The first joint moment is a measure of the interdependence between the variables,  $X$  and  $Y$ . It is the covariance of  $X$  and  $Y$  and defined as;

$$\text{cov}(x, y) = \sum_{i=1}^n [x_i - \mu_x](y_i - \mu_y) \quad (2.7)$$

where  $x_i$  and  $y_i$  are paired observations of the two variables. if  $X$  and  $Y$  are independent than  $\text{cov}(x,y)$  will be equal to zero. Nevertheless, positive covariance means one variable increases, while the other increasing. In the same way if negative covariance exists, the variable is decreasing with the increase of the other. Therefore covariance can be described as relative measurement of variables,  $X$  and  $Y$ .

The relative measurement between the variables can be computed by correlation coefficient;

$$\rho_{xy} = \frac{\sum_{i=1}^n [(x_i - \mu_x)(y_i - \mu_y)]}{\sqrt{\sum_{i=1}^n (x_i - \mu_x)^2 \sum_{j=1}^n (y_j - \mu_y)^2}} \quad (2.8)$$

The sample correlation coefficient ranges between -1.0 and 1.0, The closer the absolute value of  $\rho$  is to 1.0 the stronger the linear relationship between the two variables.

In geotechnical practice, correlation coefficient should be used to estimate the dependency of the data. Jones et al(2002) applied the method to water content data obtained from a boring log. Relationship between water content data and depth investigated and correlation coefficient computed -0.937 which means as depth increases, water content of soil decreases.

## 2.4. Theoretical Random Variable Models

Why is a theoretical random variable model needed to describe a data set? First, a data set is limited in size. It is required to measure the variable at every point in the soil in order to obtain the "true" statistics. A random variable is a theoretical model of these "true" statistics.

There are two types of random variables already defined in literature, one is discrete and the other is continuous, corresponding to discrete probability space and continuous probability space, respectively. To realize the random variables, USCS soil type is an example for discrete random variable whereas, friction angle and permeability are called as continuous random variables.

### 2.4.1 Discrete Random Variables

Discrete random variables can only take on discrete values within the sample space. As an example, SPT blow numbers, applied in a field. The probability mass function (PMF) for a discrete random variable describes its probability distribution

$$P[X = x] = p_x(x) \quad (2.9)$$

The cumulative distribution function (CDF) describes the probability that the random variable takes on a value less than or equal to a given value. It is obtained as follows

$$F_X(x) = P[X \leq x] = \sum_{\text{all } x_i \leq x} p_X(x_i) \quad (2.10)$$

The mean value for a discrete random variable is obtained as follows,

$$\mu_X = \sum_{all x_i} x_i p_X(x_i) \quad (2.11)$$

where  $\mu_x$  is the mean value of  $X$ . Similarly, the variance is obtained as follows,

$$\sigma_X^2 = \sum_{all x_i} (x_i - \mu_x)^2 p_X(x_i) \quad (2.12)$$

where  $\sigma_x$  is the standard deviation of  $X$ .

An important tool when working with random variables is expectation. The expectation of a quantity is the weighted average of that quantity, where the possible values are weighted by their corresponding probabilities of occurrence. For example, the expected value of  $X$  is

$$E[X] = \sum_{all x_i} x_i p_X(x_i) \quad (2.13)$$

It is obvious that, the mean value of  $X$ ,  $\mu_x$  is equal to its mathematical expectation. In the same way, variance of  $X$  will be the mathematical expectation of  $(X - \mu_x)^2$

$$E[(X - \mu_x)^2] = \sum_{all x_i} (x_i - \mu_x)^2 p(x) \quad (2.14)$$

Table 2.2 explains the common used discrete random variable models (Gilbert,1997)

**Table 2.2** List of discrete random variable models and parameters used.

Distribution	PDF	Mean	Variance
Binomial	$p_X(x) = \frac{n!}{x!(n-x)!} p^x (1-p)^{n-x}$ $x = 0, 1, \dots, n$	$np$	$np(1-p)$
Geometric	$p_X(x) = p(1-p)^{x-1}$ $x = 1, 2, \dots$	$\frac{1}{p}$	$\frac{1-p}{p^2}$
Poisson	$p_X(x) = \frac{(vt)^x}{x!} e^{-vt}$ $x = 0, 1, \dots$	$vt$	$vt$

## 2.4.2 Continuous Random Variables

Continuous random variables can take on any value within the sample space. Total unit weight is an example of a continuous random variable; it can take on any value greater than zero.

The probability density function (PDF) for a continuous random variable describes its probability distribution. While the PDF is similar to the PMF in the information that it expresses, there is significant difference in these two functions. For a continuous random variable, there are large numbers of possible values within the sample space. Hence, unlike a discrete random variable, it is not possible to define the probability of the event that  $X$ . The PDF is denoted by  $f(x)$ . A typical probability density function plotted for unit weight variable is shown in figure 2.8

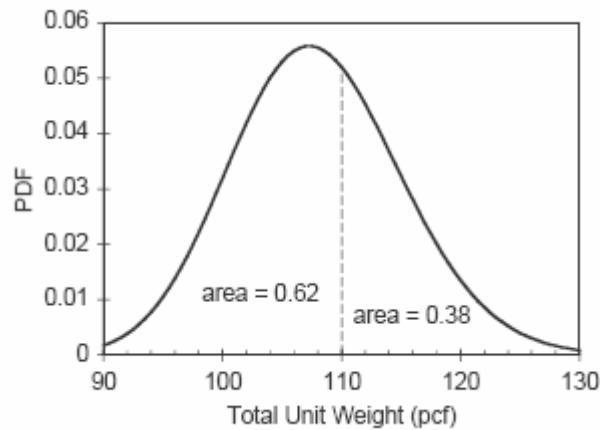


**Figure 2.8** Probability density function for unit weight variable (Gilbert,1997)

Similar to Cumulative Distribution Function (CDF) in discrete random variables, CDF for continuous random variables is can be computed by,

$$F_X(x) = P[X \leq x] = \int_{-\infty}^x f_X(\xi) d\xi \quad (2.15)$$

A typical cumulative distribution function plotted for unit weight variable is shown in figure 2.9. CDF can be analyzed as the area under the PDF. Since the probability of the sample space is equal to 1.0, the area under the PDF must equal 1.0. The area under the curve in figure 2.9 till the value 110 pcf is equal to 0.62. That means the probability of the observations, obtained up to 110 pcf is 62%.

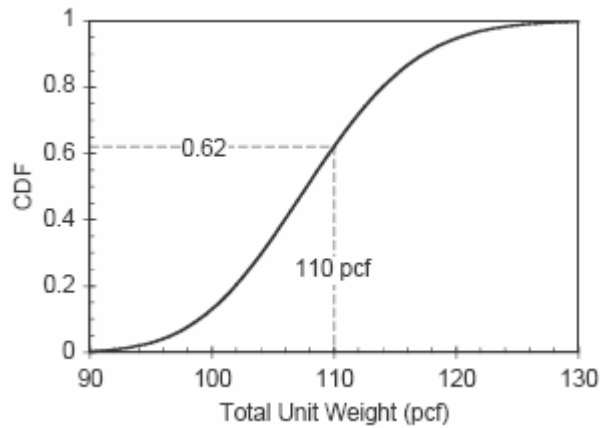


**Figure 2.9** Cumulative distribution function for unit weight variable (Gilbert,1997)

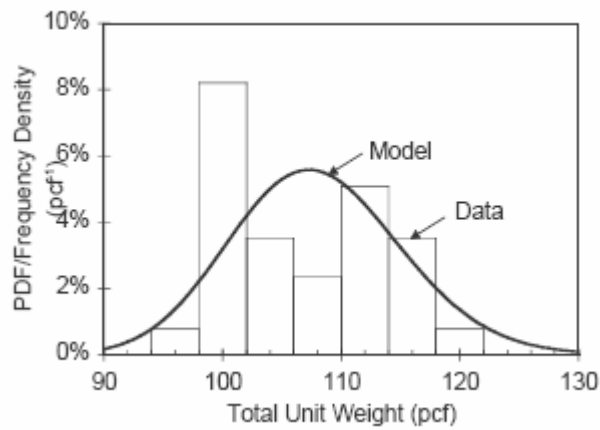


**Figure 2.10** Probability density function and frequency density plot for unit weight variable (Gilbert,1997)

The expectation for a continuous random variable is defined in the same way as for a discrete random variable. However, since there is large number of possible value in the sample space, the process of summing up values weighted by their possibility is an integration.

$$E[g(X)] = \int_{-\infty}^{\infty} g(x) f_X(x) dx \quad (2.16)$$

Similarly, the mean, variance, skewness and kurtosis for a continuous random variable are found as follows

$$\mu_X = E[X] = \int_{-\infty}^{\infty} x f_X(x) dx \quad (2.17)$$

$$\sigma_X^2 = E[(X - \mu_X)^2] = \int_{-\infty}^{\infty} (x - \mu_X)^2 f_X(x) dx \quad (2.18)$$

$$\psi_X = \frac{E[(X - \mu_X)^3]}{\sigma_X^3} = \frac{\int_{-\infty}^{\infty} (x - \mu_X)^3 f_X(x) dx}{\sigma_X^3} \quad (2.19)$$

$$K_X = \frac{E[(X - \mu_X)^4]}{\sigma_X^4} = \frac{\int_{-\infty}^{\infty} (x - \mu_X)^4 f_X(x) dx}{\sigma_X^4} \quad (2.20)$$

Common models for continuous random variables and parameters are listed in Table 2.3.

**Table 2.3** List of continuous random variable models and parameters used.

Distribution Name	pdf, $f_X(x)$	CDF, $F_X(x)$	E(X)	V(X)
Uniform	$\begin{cases} \frac{1}{b-a}, & \text{if } a < x < b \\ 0, & \text{otherwise} \end{cases}$	$\begin{cases} 0, & \text{if } x \leq 0 \\ \frac{x-a}{b-a}, & \text{if } 0 < x < 1 \\ 1, & \text{if } x \geq 1 \end{cases}$	$\frac{b+a}{2}$	$\frac{(b-a)^2}{12}$
Normal	$\frac{1}{\sigma\sqrt{2\pi}} e^{-(x-\mu)^2/2\sigma^2}$ <p>for all real x</p>	$\int_{-\infty}^x \phi(z) dz$ <p>where</p> $\phi(z) = \frac{1}{\sqrt{2\pi}} e^{-z^2/2}$ $Z = (X - \mu)/\sigma$	$\mu$	$\sigma^2$
Exponential	$\begin{cases} \lambda e^{-\lambda x}, & \text{if } x > 0 \\ 0, & \text{otherwise} \end{cases}$	$\begin{cases} 0, & \text{if } x \leq 0 \\ 1 - e^{-\lambda x}, & \text{if } x > 0 \end{cases}$	$\frac{1}{\lambda}$	$\frac{1}{\lambda^2}$
Gamma	$\begin{cases} \frac{\lambda^\alpha}{\Gamma(\alpha)} x^{\alpha-1} e^{-\lambda x}, & \text{if } x, \lambda, \alpha > 0 \\ 0, & \text{otherwise} \end{cases}$ $\Gamma(\alpha) = \int_0^{\infty} x^{\alpha-1} e^{-x} dx = \frac{n!}{\lambda^{n+1}}$ <p>for any <math>\lambda &gt; 0</math> and <math>n = 0, 1, 2, \dots</math></p>	There is no convenient formula unless $\alpha$ is positive	$\frac{\alpha}{\lambda}$	$\frac{\alpha}{\lambda^2}$

The normal distribution (also known as the Gaussian distribution) is the classic bell-shaped curve, faced frequently in data sets. For example, the undrained shear strength to depth ratio data from figure 2.11 is fit well by a normal distribution.

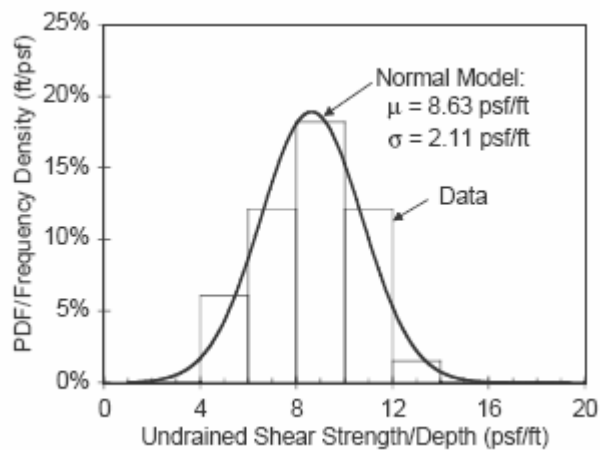


**Figure 2.11** Typical normal distribution curve, fitted on frequency density histogram (Gilbert,1997)

The CDF for a normal distribution cannot be derived analytically. That is why it is needed to normalize the variable with the given formula below,

$$Z = \frac{X - \mu_X}{\sigma_X} \quad (2.21)$$

The mean value is subtracted from each variable and then divided to the standard deviation of  $X$ .  $Z$  is the standard normalized form of  $X$  with the parameters mean is zero and standard deviation is one. Table 2.4 is the CDF values for standard normal distribution

**Table 2.4** Standard normal distribution (z) table

z	0.00	0.01	0.02	0.03	0.04	0.05	0.06	0.07	0.08	0.09
0.00	0.000	0.004	0.008	0.012	0.016	0.019	0.024	0.028	0.032	0.036
0.10	0.040	0.044	0.048	0.052	0.056	0.060	0.064	0.068	0.071	0.075
0.20	0.079	0.083	0.087	0.091	0.095	0.099	0.103	0.106	0.110	0.114
0.30	0.118	0.122	0.126	0.129	0.133	0.137	0.141	0.144	0.148	0.152
0.40	0.155	0.159	0.163	0.166	0.170	0.174	0.177	0.181	0.184	0.188
0.50	0.192	0.195	0.199	0.202	0.205	0.209	0.212	0.216	0.219	0.222
0.60	0.226	0.229	0.232	0.236	0.239	0.242	0.245	0.249	0.252	0.255
0.70	0.258	0.261	0.264	0.267	0.270	0.273	0.276	0.279	0.282	0.285
0.80	0.288	0.291	0.294	0.297	0.300	0.302	0.305	0.308	0.311	0.313
0.90	0.316	0.319	0.321	0.324	0.326	0.329	0.332	0.334	0.337	0.339
1.00	0.341	0.344	0.346	0.349	0.351	0.351	0.355	0.358	0.353	0.362
1.10	0.364	0.367	0.369	0.371	0.373	0.375	0.377	0.379	0.381	0.383
1.20	0.385	0.387	0.389	0.391	0.393	0.394	0.396	0.398	0.400	0.402
1.30	0.403	0.405	0.407	0.408	0.410	0.412	0.413	0.415	0.416	0.418
1.40	0.419	0.421	0.422	0.424	0.425	0.427	0.428	0.429	0.431	0.432
1.50	0.433	0.435	0.436	0.437	0.438	0.439	0.441	0.442	0.443	0.444
1.60	0.445	0.446	0.447	0.448	0.450	0.451	0.452	0.453	0.454	0.455
1.70	0.455	0.456	0.457	0.458	0.459	0.460	0.461	0.462	0.463	0.463
1.80	0.464	0.465	0.466	0.466	0.467	0.468	0.469	0.469	0.470	0.471
1.90	0.471	0.472	0.473	0.473	0.474	0.474	0.475	0.476	0.476	0.477
2.00	0.477	0.478	0.478	0.479	0.479	0.480	0.480	0.481	0.481	0.482
2.10	0.482	0.483	0.483	0.483	0.484	0.484	0.485	0.485	0.485	0.486
2.20	0.486	0.486	0.487	0.487	0.488	0.488	0.488	0.488	0.489	0.489
2.30	0.489	0.490	0.490	0.490	0.490	0.491	0.491	0.491	0.491	0.492
2.40	0.492	0.492	0.492	0.493	0.493	0.493	0.493	0.493	0.493	0.494
2.50	0.494	0.494	0.494	0.494	0.495	0.495	0.495	0.495	0.495	0.495
2.60	0.495	0.496	0.496	0.496	0.496	0.496	0.496	0.496	0.496	0.496
2.70	0.497	0.497	0.497	0.497	0.497	0.497	0.497	0.497	0.497	0.497
2.80	0.497	0.498	0.498	0.498	0.498	0.498	0.498	0.498	0.498	0.498
2.90	0.498	0.498	0.498	0.498	0.498	0.498	0.499	0.499	0.499	0.499
3.00	0.499	0.499	0.499	0.499	0.499	0.499	0.499	0.499	0.499	0.499
3.10	0.499	0.499	0.499	0.499	0.499	0.499	0.499	0.499	0.499	0.499
3.20	0.499	0.499	0.499	0.499	0.499	0.499	0.499	0.500	0.500	0.500
3.30	0.500	0.500	0.500	0.500	0.500	0.500	0.500	0.500	0.500	0.500
3.40	0.500	0.500	0.500	0.500	0.500	0.500	0.500	0.500	0.500	0.500

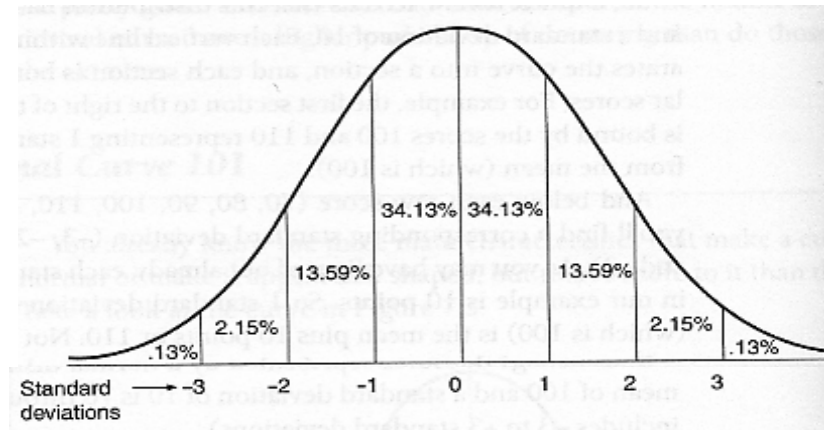


**Figure 2.12** Standard normal distribution and corresponding properties for standard deviation limits

From the table 2.4 and figure 2.12 , it can be determined that 68.3% of scores will fall within 1 standard deviation above and below the mean, 95.4% of scores will fall within 2 standard deviations above and below the mean and that 99.7% of scores will fall within 3 standard deviations below or above the mean

If the logarithm of a variable has a normal distribution, then the variable has a lognormal distribution. The lognormal distribution is commonly used for three reasons. First, it results if you multiply many individual random variables together. Second, the lognormal distribution model variables that cannot be less than zero. Since many engineering properties, such as strength, are non-negative, the lognormal distribution is a reasonable model. Finally, the lognormal distribution is convenient for modeling quantities that vary over several orders of magnitude, such as hydraulic conductivity. Distribution of hydraulic conductivity is plotted and decided to be analysed as log-normal distribution

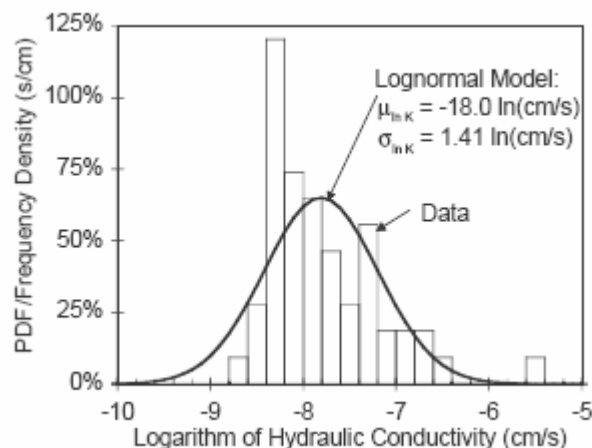


**Figure 2.13** PDF for hydraulic conductivity observations (Gilbert,1997)

Similarly for the values accepted as lognormally distributed, normalization can be applied with the formula,

$$Z = \frac{\ln X - \mu_{\ln x}}{\sigma_{\ln x}} \quad (2.22)$$

The lognormal distribution provides a convenient model for random variables with relatively large coefficients of variation (>30%) for which an assumption of normality would imply a significant probability of negative values (Jones et al, 2002). Random variables often assumed to be lognormally distributed include the coefficient of permeability, the undrained shear strength of clay, and factors of safety (Jones et al, 2002).

The Gamma distribution is widely used in engineering, science, and business, to model continuous variables that are always positive and have skewed distributions. The Gamma distribution has the following probability density function:

$$f(x) = \begin{cases} \frac{\left(\frac{x}{\beta}\right)^{\alpha-1} \exp\left(-\frac{x}{\beta}\right)}{\beta\Gamma(\alpha)} & x \geq 0 \\ 0 & \text{otherwise} \end{cases} \quad (2.23)$$

where  $\Gamma(\alpha)$  is the Gamma function, and the parameters  $\alpha$  and  $\beta$  are both positive,  $\alpha > 0$  and  $\beta > 0$ .  $\alpha$  is known as the shape parameter, while  $\beta$  is referred to as the scale parameter.  $\beta$  has the effect of stretching or compressing the range of the Gamma distribution. A Gamma distribution with  $\beta = 1$  is known as the standard Gamma distribution.

The Gamma distribution represents a family of shapes. As suggested by its name,  $\alpha$  controls the shape of the family of distributions. The fundamental shapes are characterized by the following values of  $\alpha$ :

Case I: ( $\alpha < 1$ )

The Gamma distribution is exponentially shaped and asymptotic to both the vertical and horizontal axes.

Case II: ( $\alpha = 1$ )

A Gamma distribution with shape parameter  $\alpha = 1$  and scale parameter  $\beta$  is the same as an exponential distribution of scale parameter (or mean)  $b$ .

Case III: ( $\alpha > 1$ )

When  $\alpha$  is greater than one, the Gamma distribution assumes a unimodal, but skewed shape. The skewness reduces as the value of  $\alpha$  increases.

The shape and scale parameters of a Gamma distribution can be calculated from its mean  $\mu$  and standard deviation  $\sigma$  according to the relationships:

$$\alpha = \left(\frac{\mu}{\sigma}\right)^2 ; \quad \beta = \frac{\sigma^2}{\mu} \quad \text{and} \quad \lambda = \frac{1}{\beta} \quad (2.24)$$

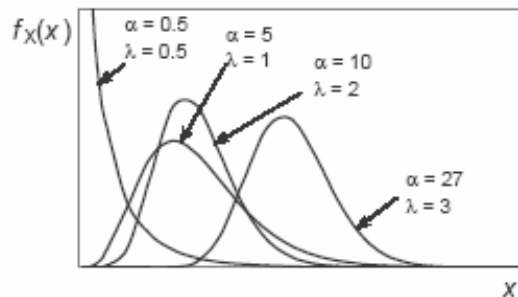


**Figure 2.14** Typical shapes for gamma distribution for different shape and scale factors.

The Gamma distribution is sometimes called the Erlang distribution, when its shape parameter  $\alpha$  is an integer.

## 2.5. Goodness of Fit Test

A commonly faced problem in elementary statistics is comparing a distribution of sample observations to some specified model distribution. It is expected to apply statistical tests that assume the data are drawn from a population having certain characteristics, such as a normal or lognormal distribution. The frequency distribution of the sample may be compared to the hypothetical distribution to see if this assumption is warranted.

There are two type of methods, one is parametric and other is non-parametric, to evaluate the random sampling. Parametric methods assume that the calculated test values have distributions whose shapes are of known form. These test distributions ( $t$ ,  $F$ , and  $X^2$ ) all describe the results of random sampling from normal populations, and are defined by equations that have only a few simple parameters. Sometimes it is needed to work with a small sample whose size can't be increased and whose population doesn't fit to normal distribution. In that situation it is recommended to turn the computation to non-parametric statistical tests. (Davis, 2002). There are some well-defined tests namely, Mann-Whitney test, Kruskal-Wallis test, Kolmogorov-Smirnov tests in literature. Kolmogorov-Smirnov tests are discussed in the study.

Kolmogorov-Smirnov tests compare cumulative distribution functions directly which is an advantage.

In general, a sample is selected from some unknown population and wished to test its goodness of fit to a hypothetical model of a specific population. Both the sample and the hypothetical model are plotted together in cumulative form, each scaled so their cumulative sums are 1.0. (Figure 2.15)

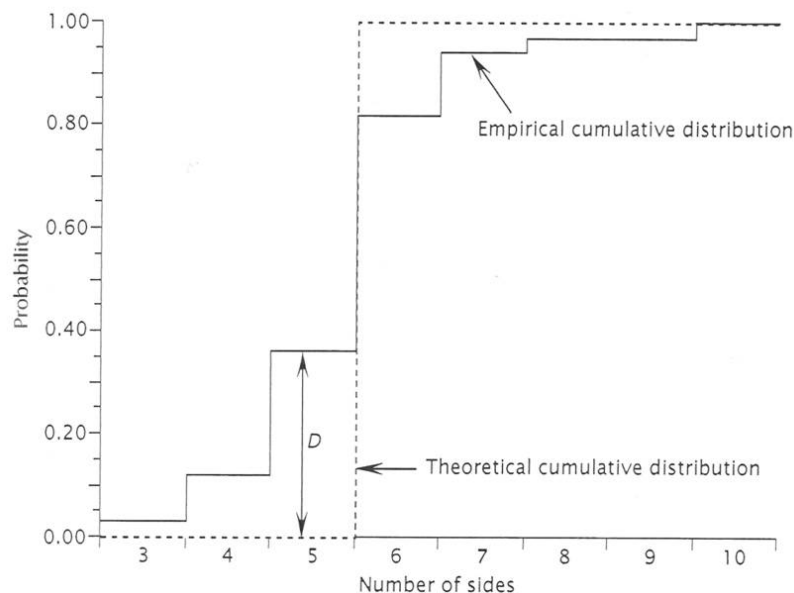


**Figure 2.15** Theoretical and empirical cumulative distribution and process for K-S tests (Davis,2002)

The greatest difference between the two plots are examined. This maximum difference is the Kolmogorov-Smirnov statistic, D

$$D = \max | \text{CDF} - \text{EDF} | \quad (2.25)$$

Critical values of D are listed in Table 2.5, for number of observations and significance level. Table 2.5 gives critical values for the Kolmogorov-Smirnov statistic, and can be used for either one-tailed or two-tailed hypotheses.

**Table 2.5** Critical Values for the Kolmogorov-Smirnov Statistics based on significance level and sample size (Bayazit,1996)

n	0.20	0.10	0.05	0.01
5	0.45	0.51	0.56	0.57
10	0.32	0.37	0.41	0.49
15	0.27	0.30	0.34	0.40
20	0.23	0.26	0.29	0.36
25	0.21	0.24	0.27	0.32
30	0.19	0.22	0.24	0.29
35	0.18	0.20	0.23	0.27
40	0.17	0.19	0.21	0.25
45	0.16	0.18	0.20	0.24
50	0.15	0.17	0.19	0.23
>50	$1.07/\sqrt{n}$	$1.22/\sqrt{n}$	$1.36/\sqrt{n}$	$1.63/\sqrt{n}$

The two-tailed null hypothesis states that classes of the distribution from which the sample is obtained are equal to those of the hypothetical model for all values of x.

The one-tailed null hypothesis states that all classes of the sample distribution are equal or less than those of the hypothetical model (maximum positive difference is used) or similarly, all classes of the sample distribution are equal or greater than those of the hypothetical model (maximum negative difference is used). In most cases, two tailed hypothesis is used.

### 3. Geostatistical Analysis for Soils

In chapter 2, basic statistical and probabilistic methods are discussed to characterize soil variability. Soils are expected to be spatially analyzed. Characterization of the spatial distribution of soil properties requires the use of regionalized variables, which has a particular structure consisting random variable and completely deterministic parameter. (Jones et al, 2002). It means that the properties of the regional variable at the points  $X$  and  $X+\Delta h$  are correlated. (Figure 3.1) Traditional methods of classification and statistical analysis do not consider this aspect directly (Trangmar et al, 1985)

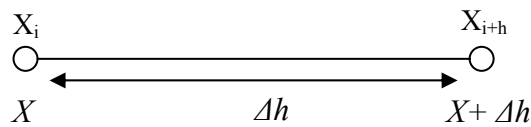


**Figure 3.1** General view of spatial distribution

Geostatistics, based on the regionalized variable theories have made it possible to analyze spatial relationships of the soil variability and interpolate values at unsampled locations. Spatial structure and random characteristics are considered in geostatistical analysis.

#### 3.1. Geostatistics

Geostatistics are based on the concepts of regionalized variables, random functions and stationarity assumptions (Trangmar et al, 1985). Geostatistical methods have two components, one is variography and the other is kriging. Variography is dealing with the structural dependence of the regionalized variable and modeling the spatial variability. Kriging provides optimal and unbiased estimates of the regionalized variable at unsampled locations, using the variogram model and the original values taken at sample locations.

### 3.2. Stationarity

In order to analyze the regionalized variable, there are some assumptions of stationarity (Cressie, 1993). Stationarity assumptions are related to the moment of the random function.

First assumption is stationarity of mean, which means the expected value of the random function is same at all locations in entire site of the study.

$$E[X] = \mu \quad (3.1)$$

where  $\mu$  is the mean and  $X$  is the random function. If there is a separation distance between two points in the site, since the mean value is same at all region,

$$E[X_i - X_{i+h}] = 0 \quad (3.2)$$

Mathematical expectation of the difference at any two locations is equal to zero.

Second assumption is stationarity of variance, which means sample variance is same in the entire space and regardless of position.

$$E\{[X_i - \mu][X_{i+h} - \mu]\} = \sigma^2 \quad (3.3)$$

It is clear that, position of the sample,  $x$ , has no effect on variance.

Second-order stationarity does not apply if a finite variance and covariance can't be defined, therefore a weaker form of stationarity called the intrinsic hypothesis is assumed (Journel and Huijbretgts, 1978)

### 3.3. Intrinsic Hypothesis

Secondary order stationarity assumption is not widely used and suitable for most of the dataset. Since the expected value of  $X$  is not constant, covariance and variance can not be computed directly and must be estimated. The intrinsic hypothesis is expressed in terms of differences of  $X_{i+h} - X_i$  of the regionalized variable. There are two common assumptions for the hypothesis (Omonode,2001)

1. Stationarity of the mean, which is same as in the second order stationarity

$$E[X_i - X_{i+h}] = 0 \quad (3.4)$$

For any  $x$  and  $h$ , the expected value of any  $X$  is constant

2. Stationarity of the squared differences.

$$\gamma(h) = \left(\frac{1}{2}\right)E\{[X_i - X_{i+h}]^2\} \quad (3.5)$$

The above statement is defined as variogram<sup>1</sup>,  $\gamma(h)$ . It only depends on the separating vector  $h$ . The equation is zero if the separation distance is zero in other words if there is no difference in positions the result of the formula will be definitely zero.

### 3.4. Variogram

It is expected to have a relationship between the points, random variables already located and normally, decrease on distance should increase the correlation. In other words, differences of regionalized variables in a population are a function of distance. Variogram function is the indicator of the distance variable relation. The function is defined as the variance of the difference of two regionalized variables, separated with a distance  $\Delta h$ ,

$$2\gamma(h) = Var[X_i - X_{i+h}] \quad (3.6)$$

by using the properties of the variance function,

$$2\gamma(h) = Var[X_i - X_{i+h}] = E[X_i - X_{i+h}]^2 - \{E[X_i - X_{i+h}]\}^2 \quad (3.7)$$

$$= E[X_i - X_{i+h}]^2 - \{E[X_i] - E[X_{i+h}]\}^2 \quad (3.8)$$

Assumption of stationarity process  $E[X_i] = E[X_{i+h}]$  is included to the formula above and variogram is defined as a function of mathematical expectation.

$$2\gamma(h) = E[X_i - X_{i+h}]^2 \quad (3.9)$$

---

<sup>1</sup> In literature there is a conflict on the name of the function. Some authors call the equation as semivariogram. In this study it is used as variogram.

Hence, a formula is used, in order to evaluate correlation, based on the method of moments, as shown in equation 3.10.

$$\gamma(h) = \frac{1}{2N(h)} \sum_{N(h)} [X_i - X_{i+h}]^2 \quad (3.10)$$

### 3.4.1 Properties of Variogram Function

- As an interpretation of the formula, at the point  $h=0$  the value of the variogram will be equal to zero;  $\gamma(0)=0$
- Variogram is defined as the variance of the regionalized variables, so there are no negative values for the variogram;  $\gamma(h) \geq 0$
- Variogram is a symmetrical function;  $\gamma(h) = \gamma(-h)$
- Increase of the variogram at infinity is less than the increase of  $h^2$ ;  
 $\lim_{h \rightarrow 0} \gamma(h) / h^2 = 0$

### 3.4.2 Variogram Cloud

The variogram cloud is the distribution of the variance between all pairs of points at all possible distances. It is computed by the formula;  $0.5(X_i - X_{i+h})^2$  and separation distance,  $h$ . A typical variogram cloud is illustrated in figure 3.2.

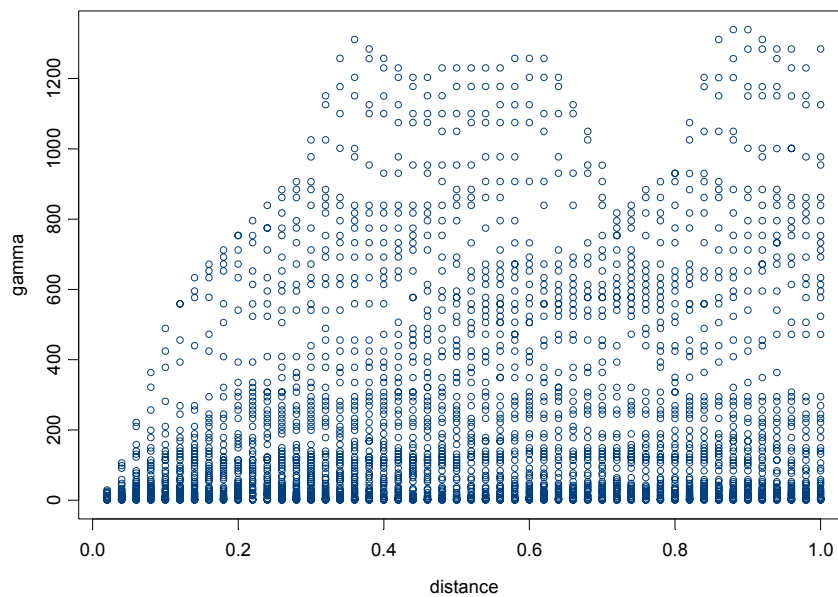


**Figure 3.2** General view of a variogram cloud

### 3.4.3 Experimental Variogram

An experimental variogram is computed by taking average of variogram cloud diagram for each lag distance. Thus, the experimental variogram for the distance is calculated by the formula,

$$\gamma(h) = \frac{1}{2N(h)} \sum_{i=1}^{N(h)} [X_i - X_{i+h}]^2 \quad (3.11)$$

where  $N(h)$  is the number of pairs for the distance  $h$ . Figure 3.3 is a general view of an experimental variogram.

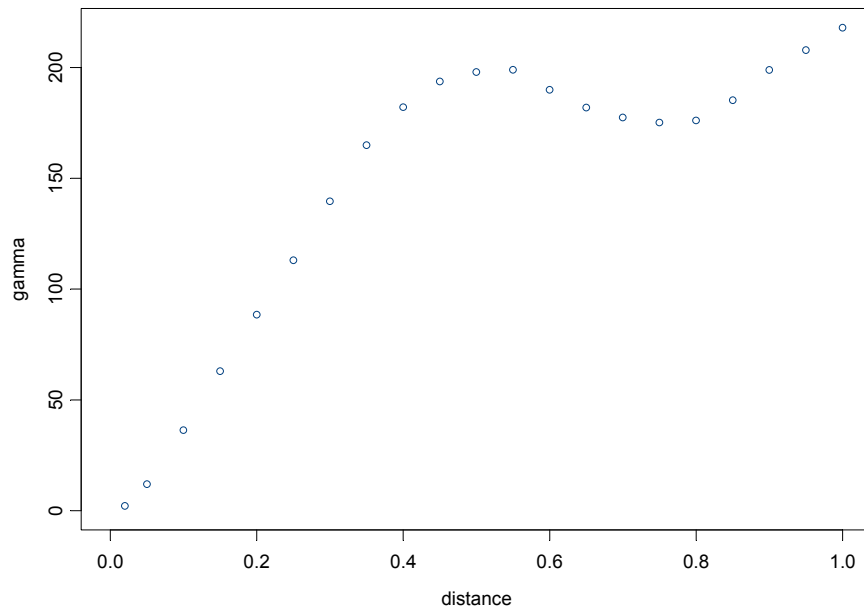


**Figure 3.3** Typical view of an experimental variogram

Experimental variogram is examined for the selected lag distance. As an example,  $k$  values are obtained at 20 different locations with a 1m interval. Experimental variograms are analyzed along a line with a lag distance 1m. in figure3.4a and figure 3.4b

Variogram values for 1m distance

$$\gamma(1) = \frac{1}{2} \frac{1}{19} [(k_1 - k_2)^2 + (k_2 - k_3)^2 + (k_3 - k_4)^2 + \dots + (k_{19} - k_{20})^2]$$

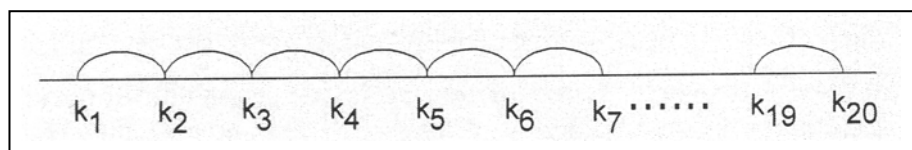


**Figure 3.4a** Analysis of random variables with a lag distance, 1m

Variogram values for 2m distance

$$\gamma(2) = \frac{1}{2} \frac{1}{18} \left[ (k_1 - k_3)^2 + (k_2 - k_4)^2 + (k_3 - k_5)^2 + \dots + (k_{18} - k_{20})^2 \right]$$

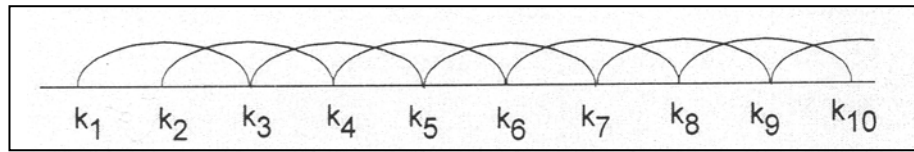


**Figure 3.4b** Analysis of random variables with a lag distance, 2m

In general, the values on experimental variogram could be computed with the given formula.

$$\gamma(h) = \frac{1}{2} \frac{1}{N-h} \sum_{i=1}^{N-h} (k_i - k_{i+h}) \quad (3.12)$$

The basic principle for geostatistical analysis is correct estimation and modeling of the variogram.. Variogram modeling is an estimation method. What is done along the process is modeling the experimental points using a mathematical function. Further steps depend on the accuracy of the variogram modeling.

### 3.4.4 Model Variogram

Variogram models are used for interpolation. The model depicts the change of  $\gamma$  when separation distance or lag distance increases. A general view and parameters of variogram is given in figure 3.5.

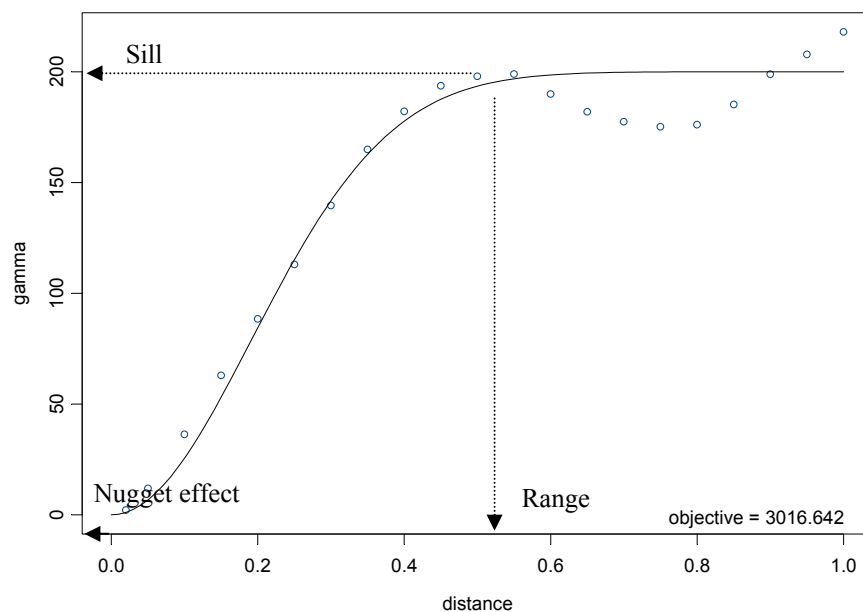


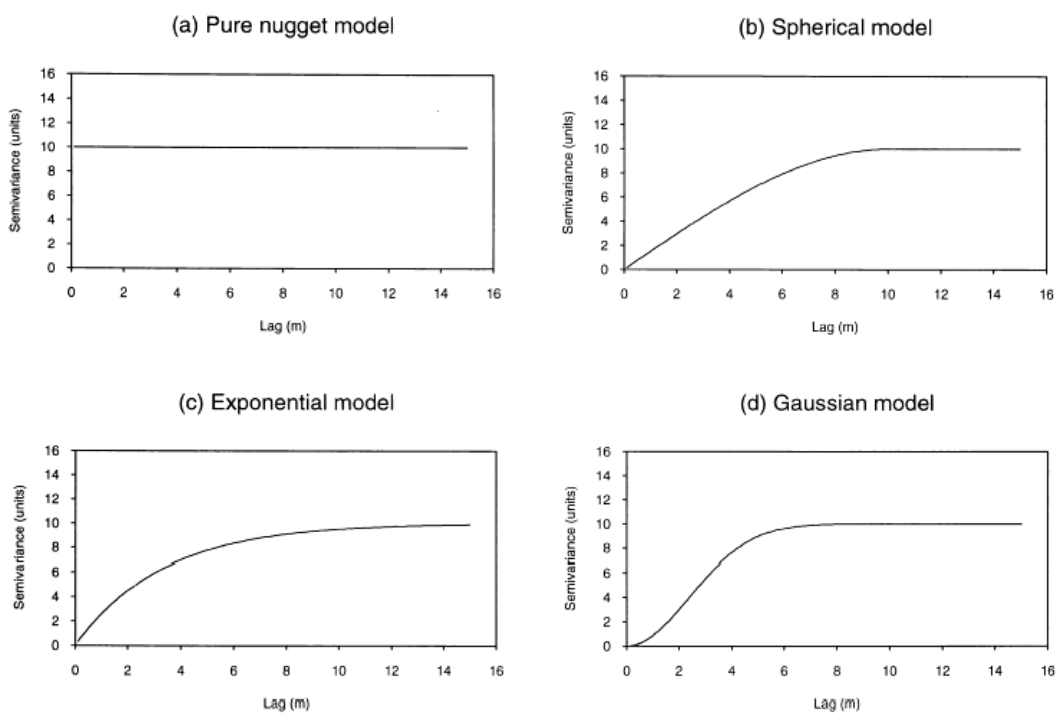
**Figure 3.5** General view of model variogram and variogram parameters

Semivariance value is the average of the squared differences between all observations, separated by the corresponding lag distance.

According to distribution of the sample data, the shape of variogram may take many forms. In general, since the data set provides secondary order stationarity, variogram value increases as lag distance increases and converges to a value, in other words aims to reach a plateau. An ideal variogram, shown in figure 3.5 is defined by three parameters, namely the sill, the range and the nugget (Trangmar,1985)

The sill in a variogram is the value about which the function becomes stable. The sill value can be assumed as equal to the semivariance of the stationarity data. The separation distance where the variogram function approaches the sill is called range. Samples having closer distances than the range are assumed spatial correlated.

The ideal variogram should start from the origin. However, many soil properties have nonzero semivariances as  $h$  tends to zero. This nonzero semivariance is the nugget variance or nugget effect. Nugget effect is a random variance often caused by measurement error or microvariability. (Omonode,2001).It varies from 0% to 100% of the sill value. 0% means there is no possible effect of measurement error or microvariability on the variance, in the same way 100% indicates a constant value for variance at different sill values, this situation is the pure nugget effect (Figure 3.6a).



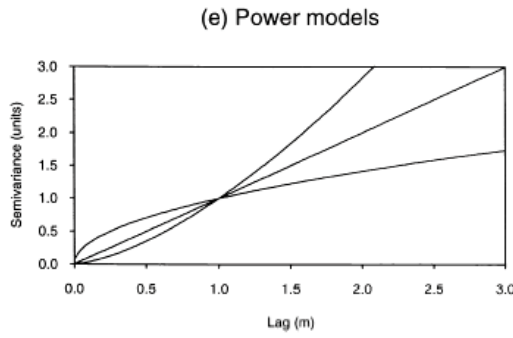


**Figure 3.6** Variogram models represented by graphically (Atkinson and Tate, 2000)

For bounded models, the semivariance reaches a maximum point as the sill. Typical bounded variogram models are, as shown in figure 3.6, spherical, exponential and gaussian models.

A spherical model increases linearly from the origin and includes a normal transition at a range of influence. Its variogram function is given by

$$\gamma(h) = \begin{cases} a^2 + (\sigma^2 - a^2) \left[ \frac{3}{2} \frac{h}{h_r} - \frac{1}{2} \frac{h^3}{h_r^3} \right], & \text{for } 0 \leq h \leq h_r \\ \sigma^2, & h \geq h_r \end{cases} \quad (3.13)$$

Where  $a^2$  is the nugget,  $h_r$  is the range and  $\sigma^2$  is the sill.

An exponential model approaches sill with the given formula

$$\gamma(h) = \begin{cases} a^2 + (\sigma^2 - a^2) \left[ 1 - e^{-\frac{h}{c}} \right], & \text{for } h \geq 0 \end{cases} \quad (3.14)$$

Where  $c$  is the constant for effective range which means it will never reach to sill.

A gaussian model is parabolic at the origin. Its variogram function can be computed by

$$\gamma(h) = \begin{cases} a^2 + (\sigma^2 - a^2) \left[ 1 - e^{-\frac{h^2}{c^2}} \right], & \text{for } h \geq 0 \end{cases} \quad (3.15)$$

The effective range is at  $h_r = c\sqrt{3}$

Attributes of each model are well documented in Journel and Huijbregts(1978). The gaussian model best describe the characteristics that are continuous and vary gradually. The spherical model becomes more appropriate when the distance between unexpected changes are not clearly defined. The exponential model describes the characteristics affected by unexpected changes at all distances and lastly the pure nugget model shows no spatial correlation between the sample characteristics (Omonode, 2001).

A number of researchers have investigated the spatial variability of soils interpolated the data in terms of standard variogram models. CPT data is the most convenient and economical data for variogram models Therefore many of the available data are based on CPT parameters (Jones et al, 2002). Tabulated values for variogram model, sill and nugget are listed in table 3.1.

**Table 3.1** Variogram model, sill and nugget for various CPT parameters (after Hegazy et al,1996; listed in Jones et al,2002)

Soil Property	Soil Type	Direction	Variogram Model	Nugget (atm <sup>2</sup> )	Sill (atm <sup>2</sup> )
CPT Tip Resistance	Sandy fill	Vertical	Spherical	0–7	2.8–127
	Sandy clay	Vertical	Spherical	0	14–2000
	Clayey sand to silty sand	Vertical	Exponential/ Spherical	0	1940–3312
	Clays	Vertical	Exponential/ Spherical	0–4	0.6–21.6
	Sandy fill	Non-directional	Exponential	0.00	70
	Sandy clay	Non-directional	Spherical	0.00	4200
	Clayey sand to silty sand	Non-directional	Spherical	0.00	1700
	Clays	Non-directional	Exponential	4.50	27
CPT Sleeve Friction	Sandy fill	Vertical	Exponential/ Spherical	0.00–0.03	0.03–0.13
	Sandy clay	Vertical	Exponential/ Spherical	0	0.03–0.80
	Clayey sand to silty sand	Vertical	Spherical	0.00–0.05	0.13–0.83
	Clays	Vertical	Exponential/ Spherical	0	0.00–0.26
	Sandy fill	Non-directional	Exponential	0.00	0.12
	Sandy clay	Non-directional	Spherical	0.00	0.85
	Clayey sand to silty sand	Non-directional	Exponential	0.00	0.47
	Clays	Non-directional	Exponential	0.00	0.25

**Table 3.1**(continued) Variogram model, sill and nugget for various CPT parameters (after Hegazy et al,1996; listed in Jones et al,2002)

Soil Property	Soil Type	Direction	Variogram Model	Nugget (atm <sup>2</sup> )	Sill (atm <sup>2</sup> )
CPT Pore Pressure	Sandy fill	Vertical	Exponential/ Spherical	0	0.00–0.12
	Sandy clay	Vertical	Spherical/ Gaussian	0	0.02–0.37
	Clayey sand to silty sand	Vertical	Exponential/ Spherical	0	0.03–7.17
	Sandy fill	Non-directional	Exponential	0.00	0.05
	Sandy clay	Non-directional	Spherical	0.00	1.16
	Clayey sand to silty sand	Non-directional	Exponential	0.00	0.10

### 3.5 Autocovariance and Correlogram

Variograms are useful tools to define the spatial structure of the observations and estimate unknown values at unobserved points by using interpolation techniques. However, to determine the spatial relationship between two variables and understand the spatial correlation requires crosscorrelation analysis and correlogram.

The spatial relation between two variables x and y is determined with the cross covariance function computed by using the formula,

$$C(h) = E\{[X_i - \mu_{X_i}][Y_i - \mu_{Y_i}]\} \quad (3.16)$$

Therefore, the autocovariance of X as a function of the separation distance, h, becomes:

$$C(h) = E\{[X_i - \mu_{X_i}][X_{i+h} - \mu_{X_{i+h}}]\} \quad (3.17)$$

The autocovariance is calculated between series and itself displayed by a lag distance. The autocovariance at lag 0 is the variance of the regionalized variable. The autocovariance can be symbolized by  $Cov_h$ ,  $C(h)$  or  $\sigma_h^2$ . The autocorrelation function or correlogram is obtained by normalizing the autocovariance by the variance.

$$r_h = \frac{Cov(X_i, X_{i+h})}{Var(X)} \quad (3.18)$$

At a separation distance,  $h=0$ , correlogram is equal to zero and with the increase on lag distance it should be expected to decrease. Variables with periodic characteristics will have autocorrelation functions that decrease and increase periodically with the lag distance (Jones et al, 2002)

Some basic properties for correlogram are,

1. It takes values from the range -1 to 1. At lag distance ( $h$ ) is equal to zero, due to the similarity of the variable pair; it is 1 or -1. For large distances it goes to zero which means there is no correlation or spatial dependence
2. For the variables not correlated in the space, only  $r_h(0)$  is equal to one, the others,  $r_h(h)$  are equal to zero.
3. The correlogram could show a cyclic effect such that as the distance increases, the correlation becomes alternatively positive and negative and at large distances eventually approaches zero.

There is also a strong relationship between the variogram and autocovariance. By using Equation 3.9 and Equation 3.17, semivariance can be computed as:

$$\gamma(h) = C(0) - C(h) \quad \text{where } C(0) = \sigma^2 \quad (3.19)$$

$C(0)$  means the autocovariance value at the lag distance,  $h=0$ . The relationship is shown in figure 3.7

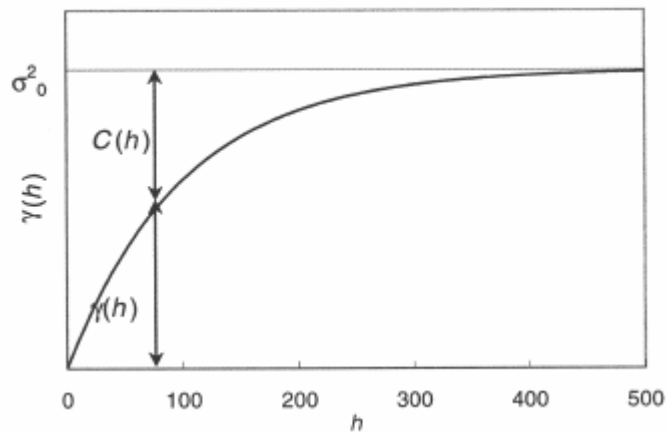


**Figure 3.7** The relationship between autocovariance and variogram (Jones et al,2002)

Data on the distances over which the soil properties correlated have been reported by De Groot, Lacasse and Nadim, and Hegazy et al. By fitting the data to standard

variogram models, the autocovariance distances in other words ranges can be determined. Table 3.2 shows some of the outcomes for discussions on data.

**Table 3.2** Tabulated values of range and autocovariance distance for SPT and CPT Parameters (listed in Jones et al,2002)

Soil Property	Soil Type	Direction	Range (a) or Autocovariance Distance ( $r_0$ ) (m)*	Note
SPT N Value	Dune sand	Horizontal	$r_0 = 20$	1
	Alluvial sand	Horizontal	$r_0 = 17$	
CPT Resistance	Offshore soils	Horizontal	$r_0 = 30$	2
	Offshore soils	Horizontal	$r_0 = 14-38$	
	Silty clay	Horizontal	$r_0 = 5-12$	
	Clean sand	Vertical	$r_0 = 3$	
	Mexico clay	Vertical	$r_0 = 1$	
	Clay	Vertical	$r_0 = 1$	
	Sensitive clay	Vertical	$r_0 = 2$	
	Silty clay	Vertical	$r_0 = 1$	
CPT Tip Resistance	North Sea clay	Horizontal	$r_0 = 30$	1
	Copper tailings	Vertical	$r_0 = 0.5$	
	Clean sand	Vertical	$r_0 = 1.6$	
	North Sea	Horizontal	$r_0 = 14-38$	
	Sensitive clay	Vertical	$a = 2$	
	Sandy fill	Vertical	$a = 0.27-0.94$	3
	Sandy clay	Vertical	$a = 0.30-1.22$	
	Clayey sand to silty sand	Vertical	$a = 1.83-2.90$	
	Clays	Vertical	$a = 0.70-2.65$	
	Sandy fill	Non-directional	$a_1 = 1.07, a_3 = 0.57$ <sup>(a)</sup>	
Sandy clay	Non-directional	$a_1 = 0.98, a_3 = 0.69$ <sup>(b)</sup>		
Clayey sand to silty sand	Non-directional	$a_1 = 3.05, a_3 = 2.32$ <sup>(c)</sup>		
Clays	Non-directional	$a_1 = 3.05, a_3 = 1.32$ <sup>(d)</sup>		
CPT Sleeve Friction	Sandy fill	Vertical	$a = 0.61-0.82$	3
	Sandy clay	Vertical	$a = 0.34-1.77$	
	Clayey sand to silty sand	Vertical	$a = 1.37-3.05$	
	Clays	Vertical	$a = 0.46-4.42$	
	Sandy fill	Non-directional	$a_1 = 1.83, a_3 = 0.74$ <sup>(a)</sup>	
	Sandy clay	Non-directional	$a_1 = 1.22, a_3 = 1.20$ <sup>(b)</sup>	
	Clayey sand to silty sand	Non-directional	$a_1 = 3.66, a_3 = 2.36$ <sup>(c)</sup>	
	Clays	Non-directional	$a_1 = 4.57, a_3 = 2.39$ <sup>(d)</sup>	
Sensitive clay	Vertical	$a = 2$		
CPT Pore Pressure	Sandy fill	Vertical	$a = 0.46-1.68$	3
	Sandy clay	Vertical	$a = 0.37-1.37$	
	Clayey sand to silty sand	Vertical	$a = 2.59-3.66$	
	Sandy fill	Non-directional	$a_1 = 1.52, a_3 = 1.04$	
	Sandy clay	Non-directional	$a_1 = 1.22, a_3 = 0.81$	
	Clayey sand to silty sand	Non-directional	$a_1 = 3.96, a_3 = 2.16$	
	Sensitive clay	Vertical	$a = 2$	
<p>* <math>a_1</math> = major range, <math>a_3</math> = minor range  (a) 312 points  (b) 126 points  (c) 450 points  (d) 636 points  Notes:  (1) DeGroot (1996)  (2) Lacasse and Nadim (1996)  (3) Hegazy, et al. (1996)</p>				

### 3.6 Spatial Anisotropy

A spatial data is said to be anisotropic if its variability is not the same in every direction. Type and direction of the anisotropy can be determined by computing the experimental variogram. Figure 3.8 shows the variograms for vertical and horizontal directions. It is adequate to examine the variogram for four main directions in order to estimate the anisotropy (Tercan and Sarac, 1998).

Two types of anisotropy; geometric and zonal are described in literature. First one, geometric anisotropy occurs if Sill values remain constant, whereas range values vary. The other anisotropy, zonal anisotropy is the result of having same sill values and different range values. Tercan and Sarac, (1998) discuss the types of anisotropies and how to consider anisotropy in practice

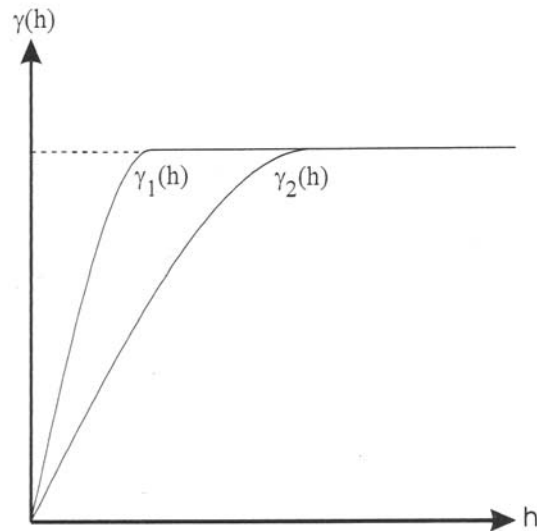


**Figure 3.8** Variograms for different directions (Tercan and Sarac, 1998)

### 3.7. Kriging

If measurements have been made at random locations and the correlation between the samples is known, it is possible to estimate values at unsampled locations. This is done by using the kriging interpolation technique. Kriging is a weighted, moving average interpolation procedure that minimizes the estimated variance of the interpolated value with the weighted average of its neighbors. The weighting factors and the variance are computed using the variogram model. Since the correlation is related to the distance, the locations of the samples are the source of weights. The

simplest one of the interpolation technique is ordinary kriging. It uses weighted linear combinations of the sample values to interpolate the unknown values at required locations. The mathematical formula for interpolation is given below,

$$X_0^* = \sum_{i=1}^n \lambda_i X_i \quad (3.20)$$

Where  $X_0^*$  is the unknown and estimated value at the location  $x_0$ ;  $X_i$  is the known value taken from the location  $x_i$  and used in interpolation technique.  $\lambda_i$  is the weight of each individual location.

In geostatistics, assigned weights are calculated by assuming the mean of interpolation errors is zero and the variance is the minimum possible (Tercan and Sarac, 1998). These conditions are discussed with corresponding formulas below

The first condition known as unbiased condition and defined with the formula;

$$E[X_0 - X_0^*] = 0 \quad (3.21)$$

It can be written as;

$$E[X_0 - X_0^*] = E\left[X_0 - \sum_{i=1}^n \lambda_i X_i\right] = 0 \quad (3.22)$$

$$E[X_0] = \sum_{i=1}^n \lambda_i E[X_i] \quad (3.23)$$

and

$$\mu = \sum_{i=1}^n \lambda_i \mu \iff \sum_{i=1}^n \lambda_i = 1 \quad (3.24)$$

As the second step, the minimum variance ( $E[X_0 - X_0^*]^2$ ) must be minimized.

Under the unbiased condition,

$$\left[X_0 - \sum_{i=1}^n \lambda_i X_i\right]^2 = -\sum_{i=1}^n \sum_{j=1}^n \lambda_i \lambda_j 0.5[X_i - X_j]^2 + 2\sum_{i=1}^n \lambda_i 0.5[X_0 - X_j]^2 \quad (3.25)$$

and taking the mathematical expectation,

$$E\left[X_0 - \sum_{i=1}^n \lambda_i X_i\right]^2 = -\sum_{i=1}^n \sum_{j=1}^n \lambda_i \lambda_j 0.5E[X_i - X_j]^2 + 2\sum_{i=1}^n \lambda_i 0.5E[X_0 - X_j]^2 \quad (3.26)$$

the semivariance value is computed as  $\gamma(h) = 0.5E[X_i - X_j]^2$  so, it is replaced with the equation above.

$$E\left[X_0 - \sum_{i=1}^n \lambda_i X_i\right]^2 = -\sum_{i=1}^n \sum_{j=1}^n \lambda_i \lambda_j \gamma(x_i - x_j) + 2\sum_{i=1}^n \lambda_i \gamma(x_i - x_j) \quad (3.27)$$

by using the methods of Lagrange multipliers and under unbiased condition, the solution can be obtained by the following formulas.

$$\sum \lambda_i \gamma(x_i - x_j) + m = \gamma(x_0 - x_j) \quad (3.28a)$$

$$\sum_i \lambda_i = 1, \quad j = 1, \dots, n \quad (3.28b)$$

It can be written as,

$$\begin{aligned} \lambda_1 \gamma_{11} + \lambda_2 \gamma_{12} + \dots + \lambda_n \gamma_{1n} + m &= \gamma_{01} \\ \lambda_1 \gamma_{21} + \lambda_2 \gamma_{22} + \dots + \lambda_n \gamma_{2n} + m &= \gamma_{02} \\ \dots & \\ \dots & \\ \lambda_1 \gamma_{n1} + \lambda_2 \gamma_{n2} + \dots + \lambda_n \gamma_{nn} + m &= \gamma_{0n} \\ \lambda_1 + \lambda_2 + \dots + \lambda_n &= 1 \end{aligned} \quad (3.29)$$

It can be shown in a matrix form as,

$$\begin{pmatrix} \gamma_{11} & \gamma_{12} & \cdot & \gamma_{1n} & 1 \\ \gamma_{12} & \gamma_{22} & \cdot & \gamma_{2n} & 1 \\ \cdot & \cdot & \cdot & \cdot & \cdot \\ \gamma_{n1} & \gamma_{n2} & \cdot & \gamma_{nn} & 1 \\ 1 & 1 & \cdot & 1 & 0 \end{pmatrix} \begin{pmatrix} \lambda_1 \\ \lambda_2 \\ \cdot \\ \lambda_n \\ m \end{pmatrix} = \begin{pmatrix} \gamma_{01} \\ \gamma_{02} \\ \cdot \\ \gamma_{0n} \\ 1 \end{pmatrix} \quad (3.30)$$

$\gamma_{ij}$  points the variogram of the pair,  $x_i$  and  $x_j$  and  $m$  is the Lagrange constant.

The kriging variance, an estimate of the estimation variance, can be obtained as:

$$\sigma_k^2 = 2 \sum_{i=1}^n \lambda_i \gamma(x_0 - x_i) - \sum_{i=1}^n \sum_{j=1}^n \lambda_i \lambda_j \gamma(x_i - x_j) \quad (3.31)$$

The information needed as input to kriging estimation includes the sample values and their spatial coordinate locations of blocks or points to be estimated and estimated variogram function. Computationally, the process consists of following steps: (Jones et al, 2002)

1. Entry in the data file of data points and selection of samples that influence the block of interest
2. Computation of covariance between the selected samples
3. Computation of covariance between the selected samples and estimation point
4. Assembly of the kriging equation
5. Solution of the kriging equations to obtain the weights
6. Computation of estimated values using computed weights and
7. Calculation of Kriging variance.

## 4. Earthquakes in Turkey / 1999 Kocaeli Earthquake

Earthquakes are natural disasters that causes tremendous damage around the world each year. As being in an active zone, Turkey has stays on the focus of earthquakes for many centuries. In this section, North Anatolian Fault and earthquake history of Turkey are briefly introduced 1999 Kocaeli Earthquake and effects of earthquake in Adapazari are discussed as a background for the study.

### 4.1 North Anatolian Fault

The North Anatolian Fault is one of the largest strike-slip fault systems of the world with 1500 km length . It could be defined by the ends, in the east, Karliova and in the west Gulf of Saros. There are lots of basins along the 1500 km-long fault system. Erzincan, Tasova, Havza, Tosya, Bolu, Duzce, Adapazari basins are the examples. These districts are the popular places for the human settlements, agricultural productivity and other social facilities. Besides most of the industrial facilities located on the fault controlled basins. In last decades, the industrial regions are the focus of population in Turkey due to economic demands. Recently more than 40% of Turkey's population lives on the North Anatolian Fault and its branches (Tuysuz and Genc,2000) North Anatolian Fault is shown in figure 4.1

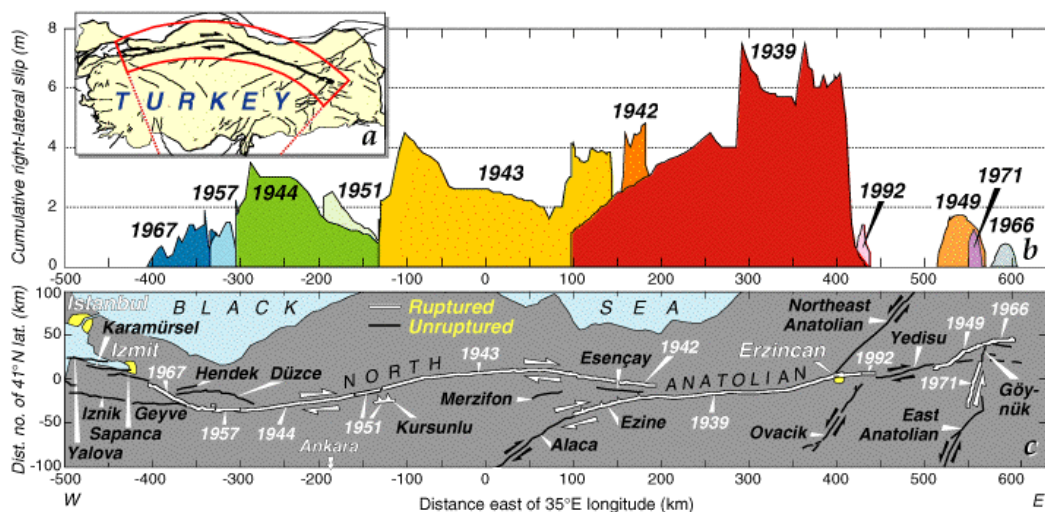


**Figure 4.1:** North Anatolian Fault Zone including devastating earthquakes with corresponding lateral slip values (Stein et al 1997)

As can easily be seen in figure 4.1, earthquakes migrated to the west on North Anatolian Fault. Stein et al (1997) pointed to the possibility of a large magnitude earthquake occurrence in the Izmit bay within thirty year probability and in 1999 expected earthquake occurred in Kocaeli and there is also a possibility to face a devastating earthquake near future.

Indeed, North Anatolian Fault is a well defined fault by Barka(1992). Barka performed various researches on North Anatolian Fault and its branches. He indicated that North Anatolian Fault Zone has been active for approximately 12 million years.

Numerous large earthquakes have occurred on the zone and caused loss of life to thousands and extensive damage to infrastructures and buildings. In the period of 1900-1999 in Turkey, There were 149 devastating earthquakes that led to 578,544 collapsed or heavily damaged buildings and 97,203 casualties (Özmen,2000).

It is obvious that, on average, there is an earthquake, striking entire site in approximately every 7 months. Meanwhile every year, approximately 5844 buildings are damaged and 982 people are killed due to the earthquakes in Turkey. Table 4.1 shows the earthquake records in Turkey that affected large areas and caused heavily damages

**Table 4.1** Devastating Earthquakes along North Anatolian Fault after the 1939 Kocaeli Earthquake

Year	Location	Moment Magnitude
1939	Erzincan	8.1
1942	Niksar-Erbaa	6.9
1943	Tosya	7.7
1944	Bolu-Gerede	7.5
1949	Karlıova	7.1
1951	Kurşunlu	6.8
1957	Abant	6.8
1966	Varto	6.6
1967	Mudurnu	7.0
1971	Bingöl	6.8
1992	Erzincan	6.5
1999	İzmit	7.4
1999	Düzce	7.2

In the 60 years period, earthquakes have migrated towards west on the North Anatolian .fault. 17 August 1999 Kocaeli earthquake is the largest natural disaster of the 20<sup>th</sup> century in Turkey after the 1939 Erzincan earthquake.

## **4.2. 1999 Kocaeli Earthquake**

On August 17, 1999 a devastating earthquake hit the northwestern side of Turkey. The earthquake was the deadliest one around the world in the year 1999 based on the United States Geological Survey (USGS) records.

The earthquake affected a widespread area. It covered about 65,000 km<sup>2</sup> in area and more than 15 million in population. It means that one fourth of the people, living in Turkey felt the strong motion. The data, provided by Ministry of Public Works indicates that more than 66,000 homes were heavily damaged or collapsed in the area. More than 250,000 people were forced to live in temporary shelter. \$25 billion was the estimated total loss as the economic impact by United Nations, However the most grievous one the loss of lives with the number 17479 and injured of 43.953 people

### **4.2.1. Characteristics of the Earthquake**

By the local time 3:02 a.m. on August 17, 1999, earthquake caught the residents in their sleep. The moment magnitude was reported as 7.4 by the Kandilli Observatory and Research Center whereas; USGS documented the magnitude as 7.6. The Epicenter of the earthquake was pointed at 40.70N and 29.86E, about 11km far from the city of Izmit (Capital city of Kocaeli province). Location of the epicenter for 1999 Kocaeli Earthquake is shown in figure 4.2.

The location indicates that the earthquake occurred in the northernwest stand of the North Anatolian fault system. The earthquake originated at a depth of 17 kilometers and caused right-lateral strike slip movement on the fault.

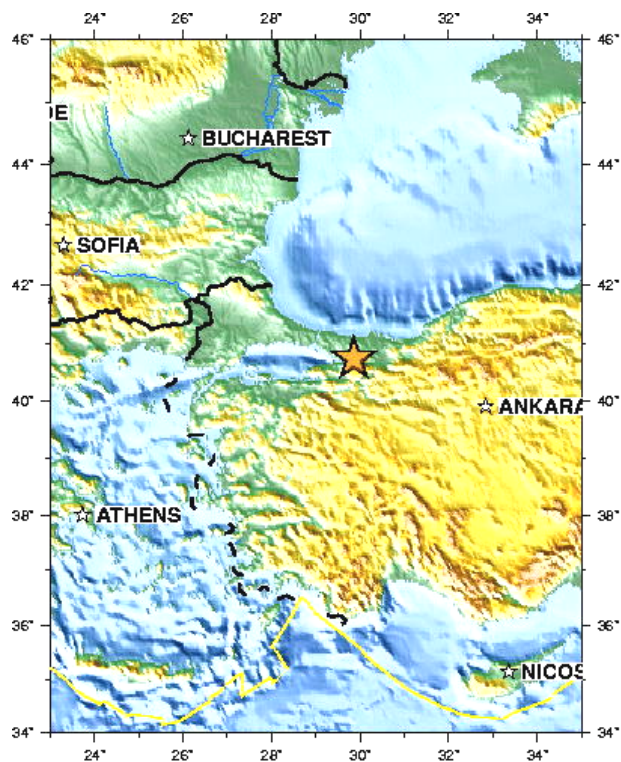


**Figure 4.2** Location of the epicenter for 1999 Kocaeli Earthquake (40.70N, 29.86E)  
Source: USGS

#### 4.2.2 Fault Surface Ruptures

The earthquake produced at least 100 km surface rupture and right lateral offsets around 4 meters.(USGS, 1999) Additionally the vertical offset is measured 2.3 meters in Golcuk. The offsets are depicted in the figure 4.3.

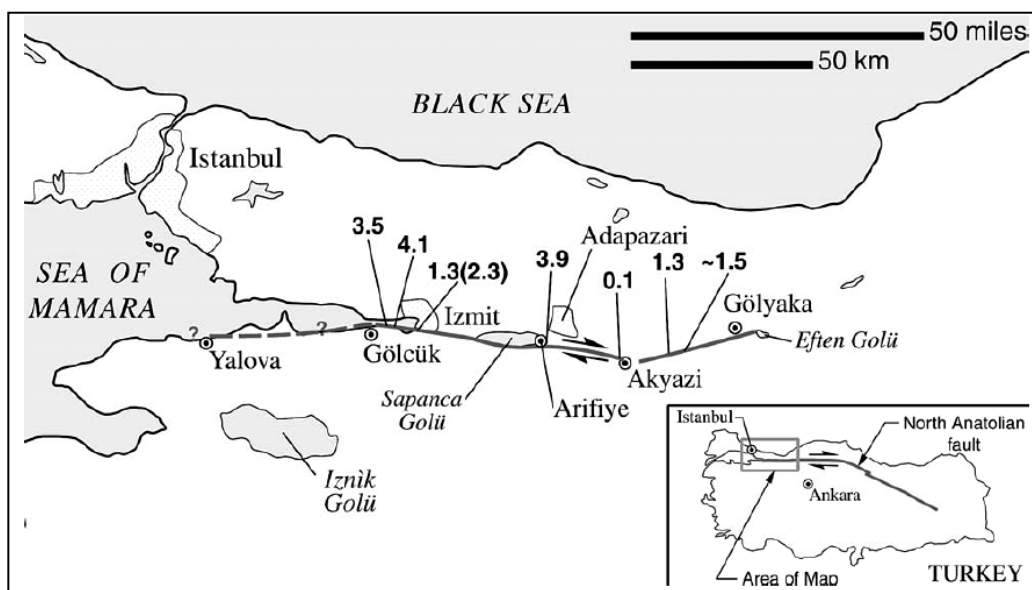


**Figure 4.3** Right Lateral Offsets, produced by 1999 Kocaeli Earthquake, vertical offset shown in parentheses (USGS,1999)

Lateral offsets can easily be observed from the existing positions of the fences or trees standing in an order. Figure 4.4, was taken by Heidi Stenner, a member of USGS research team who expressed the lateral movement distance as 2.7 meters.



**Figure 4.4** 2.7 meters right lateral offset along surface rupture near Resitbey (photo taken by Heidi Stenner)

The Kocaeli Earthquake is one of the first earthquakes in modern times where a major fault ruptured directly through a heavily urbanized and industrialized area (Bardet, 2000). In addition many apartment buildings, schools, hospitals, bridges were built close to the fault lines as the North Anatolian Fault runs parallel to the Marmara Sea and Izmit Bay.

Although the line for the fault is known, there are no restrictions for the construction process. Not only the trees, fences but also railways, bridges highways were damaged as they were close to fault line.

#### **4.2.3. Strong Motion Records**

To evaluate and understand the effect of the earthquake it is the best way to analyze the ground motion records taken by the network stations. There are 5 main earthquake stations in the vicinity and 38 ground motion records were listed.

The institutions, recorded the data and number is given in an order and listed below,

Earthquake Research Department, Directorate for Disaster Affairs of the Ministry of Public Works(ERD).....	24 Records
Kandilli Observatory and Earthquake Research Institute(KOERI).....	10 Records
Istanbul Technical University(ITU).....	4 Records

There were also three sets of structural records one from the Middle East Technical University (METU), and others from KOERI. In addition, National Institute of Dam Agency has stations on the dams in the region but there were no motion records already taken.

The distribution of the stations, as pointed in figure 4.5, is not uniform, centralizing near the Sea of Marmara, also in Istanbul. 17 of 38 ground motion stations are listed in the table 4.2 in the distance to epicenter order. The stations in Istanbul recorded the motion with the one fourth of the peak acceleration except Avcilar.

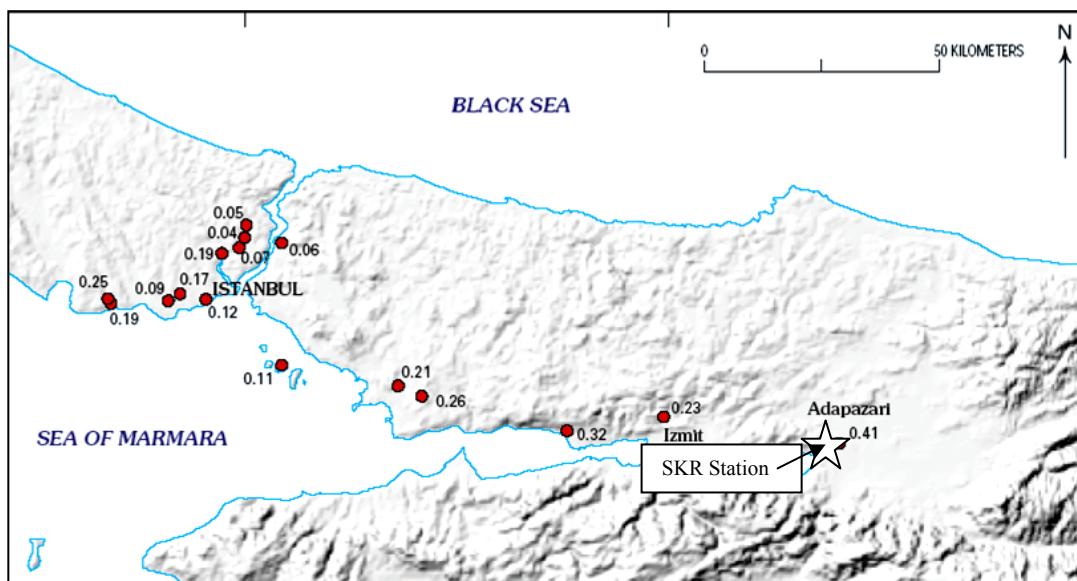


**Figure 4.5** Peak Accelerations for the Each Observation Station (USGS,1999)

**Table 4.2** Ground motion records in the region (Celebi et al,2000; USGS,1999)

Station	Owner	Site Class	Distance (km)	L (g)	T (g)	L (+)	T (+)	V (g)	Lat N.	Lat. E
SKR	Sakarya	ERD	3.3	*	0.407	S	E	0.259	40.737	30.384
YPT	Yarimca	KOERI	4.4	0.230	0.322	W	N	0.241	40.763	29.761
IZT	Izmit	ERD	7.7	0.171	0.225	S	E	0.146	40.790	29.960
DZC	Duzce	ERD	14.2	0.374	0.315	W	S	0.480**	40.850	31.170
GBZ	Gebze	ERD	17	0.264	0.142	N	W	0.199	40.820	29.440
ARC	Arcelik	KOERI	17	0.211	0.134	N	W	0.083	40.83	29.36
IZN	Izmit	ERD	29.7	0.092	0.123	S	E	0.082	40.440	29.750
IST	Istanbul	ERD	60.7	0.061	0.043	S	E	0.036	41.080	29.090
MCK	Mecidiyekoy	ITU	62.3	0.054	0.070	N	W	0.038	41.065	28.990
YKP	Yapi Kredi	KOERI	62.6	0.041	0.036	S	W	0.027	41.081	29.007
ZYT	Zeytinburnu	ITU	63.1	0.120	0.109	N	W	0.051	40.986	28.908
MSK	Maslak	ITU	63.9	0.054	0.038	N	W	0.031	41.104	29.010
FAT	Fatih	KOERI	64.5	0.189	0.162	S	E	0.131	41.054	28.950
BRS	Bursa Sivil Savunma	ERD	66.6	0.054	0.046	S	E	0.025	40.183	29.131
ATK	Atakoy	ITU	67.5	0.103	0.168	N	W	0.068	40.989	28.849
DHM	Hava Alani	KOERI	69.3	0.090	0.084	S	W	0.055	40.982	28.820
ATS	Ambarli Termik Santrali	KOERI	78.9	0.252	0.180	N	W	0.081	40.980	28.692

L, longitudinal, T, transverse, V, vertical; the components L and T are instrument components and do not correspond to north-south and east-west automatically. Refer to each network for the correct orientation of each horizontal component.

\* L, component did not function;

\*\* , based on a single spike (actual value may be smaller)

The closest and also the largest peak acceleration was taken from the station SKR located in Adapazari district. The acceleration was graphed in figure 4.6

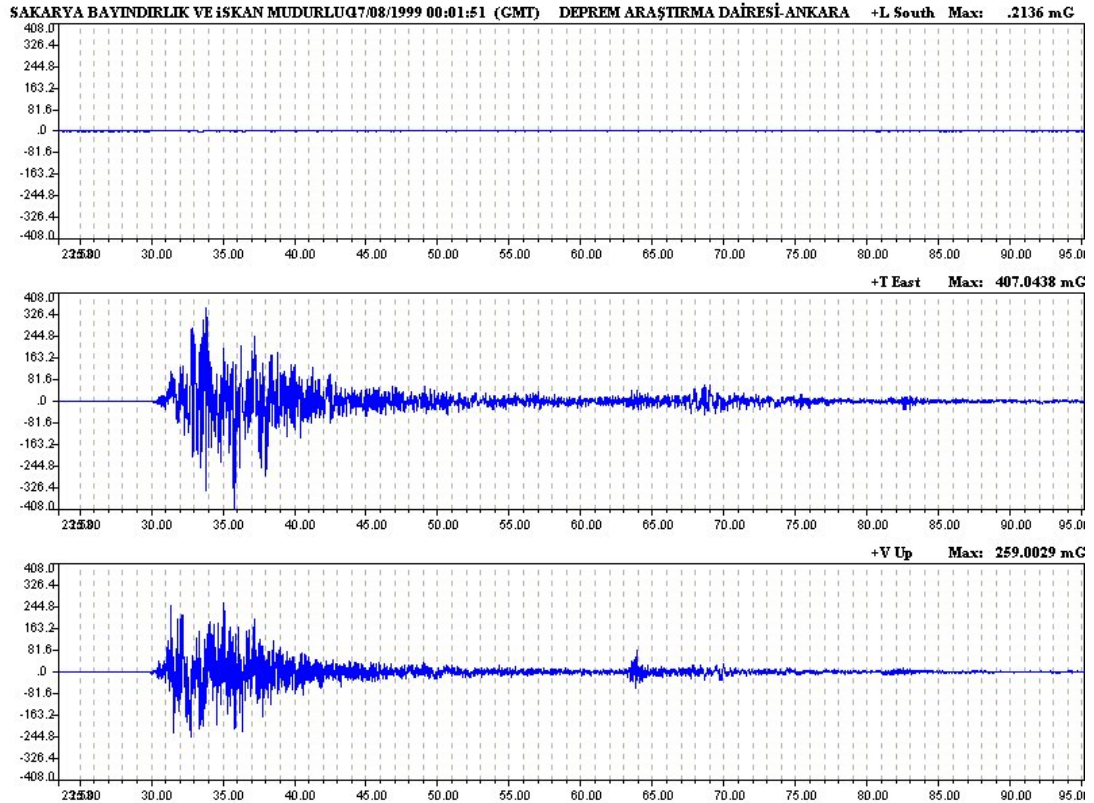


**Figure 4.6** Acceleration records obtained from SKR station

Although maximum offset records were obtained in the area, there is no motion record station near by the vicinity. The closest station as mentioned before was SKR but, actually, there was no acceleration record in the longitudinal direction. The only available record was transverse data with the 0.41g. The station is situated in a one floor building in undamaged part of the Adapazari.

### 4.3. Earthquake Effects on Adapazari

Adapazari (Capital City of Sakarya Province) suffered the highest level of gross building damage and life loss of any city faced by the 1999 Kocaeli Earthquake (Baturay et al, 2000).

#### 4.3.1 City of Adapazari

As the capital city of Sakarya, Adapazari is an important city in the northwest of Turkey. It is home for over 180,000 people. As stated in Turkish Government

earthquake research data, the official loss of life was 3690 and buildings, heavily damaged or collapsed, were about 5000. The city is densely developed and most of the dwellings are 3-5 storey reinforced concrete and 1-2 storey timber/brick buildings. Most of the reinforced concrete buildings constructed with stiff mat foundations; depths are about 1.5m due to groundwater conditions(Sancio,2003) Data from ground surveys indicates that, 20% of reinforced concrete and 56% of timber/brick buildings were severely damaged or collapsed.

#### 4.3.2 Geology of Adapazari

Adapazari is in an alluvium plain formed by River Sakarya on a sedimentary basin. The city is located 50 km far from the Black Sea. Most of the city lies on deep sediments. It is reported that, Federal Dam Agency reached bedrock at 200 m depth in Yenigun District. (Figure 4.7)

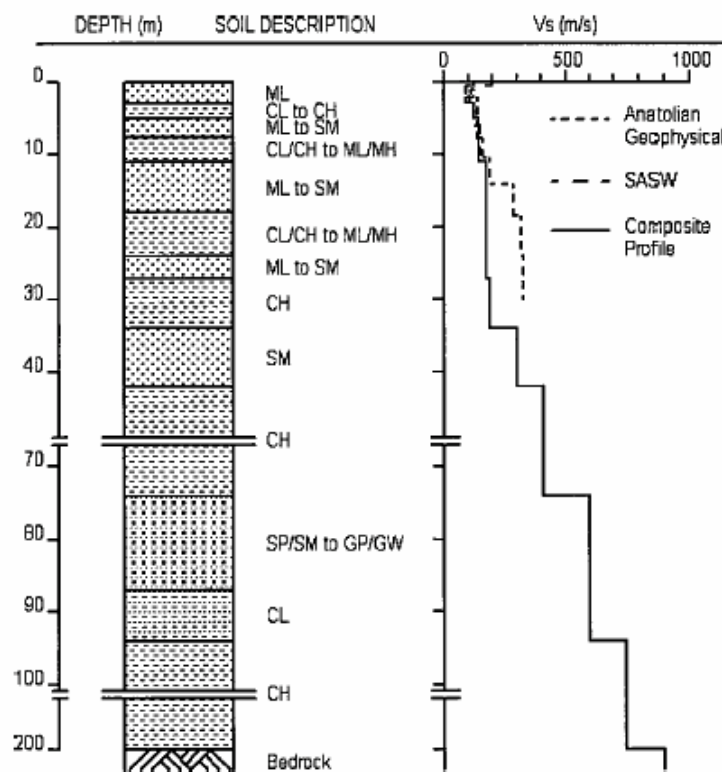


**Figure 4.7** General subsurface conditions and shear wave profile for Adapazari (Bray et al, 2004)

Indeed, the name Adapazari is derived from “Ada” meaning island and “Pazar” meaning market. Originally, the site was an island in a shallow lake, where a bazaar was held. Time by time the site was filled and people started to live on a fill.

Due to the active sedimentation, the subsurface conditions at Adapazari are changing quickly in both directions, vertical and horizontal. The soils reported in boring logs include clean fine sands, silty sands, silty clays and gravels. The ground water level varies seasonally in the range of 1-2 meters.

As demonstrated in figure 4.8 and figure 4.9, the dominant geology is holocene alluvium. There are some small regions consisting of bedrock in the southwest of the city. SKR ground motion station is the other place pointed in the map. As mentioned in section 4.2.3, It is located in stiff soil in undamaged area of the city. Damage was concentrated in Holocene Alluvium parts of the city.

### **4.3.3 Research in Adapazari**

Following the Kocaeli earthquake, a large number of engineers and researchers from USA, Turkey and also other countries, were dispatched to the epicentral area to define the damage and collect any information. As a result of preliminary researches, Kocaeli earthquake caused noticeable geotechnical hazards in different forms such as; liquefaction, bearing capacity loss, subsidence and lateral spread. Sucuoglu(2000) claims that site response amplification was mainly responsible for the remarkable increase of damage over young alluvial soil layers.

Because of the shallow groundwater level, few buildings in the basin had basements. Buildings with basements were located in light ground failure areas and also ground water level was relatively deep at the sites. Settlements of shallow foundations were observed up to 150 cm, which is the largest settlement in Adapazari (Baturay et al, 2000).

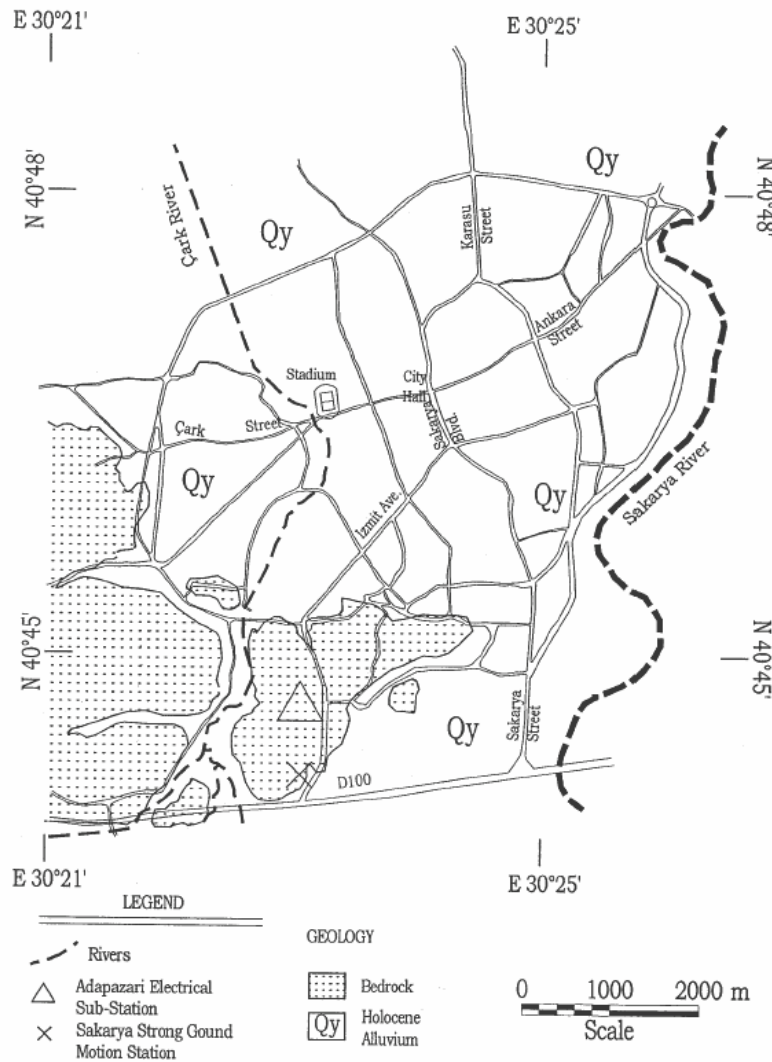


**Figure 4.8** General Map of Adapazari showing the geology and main streets and also SKR ground motion station (Bardet et al, 2000)

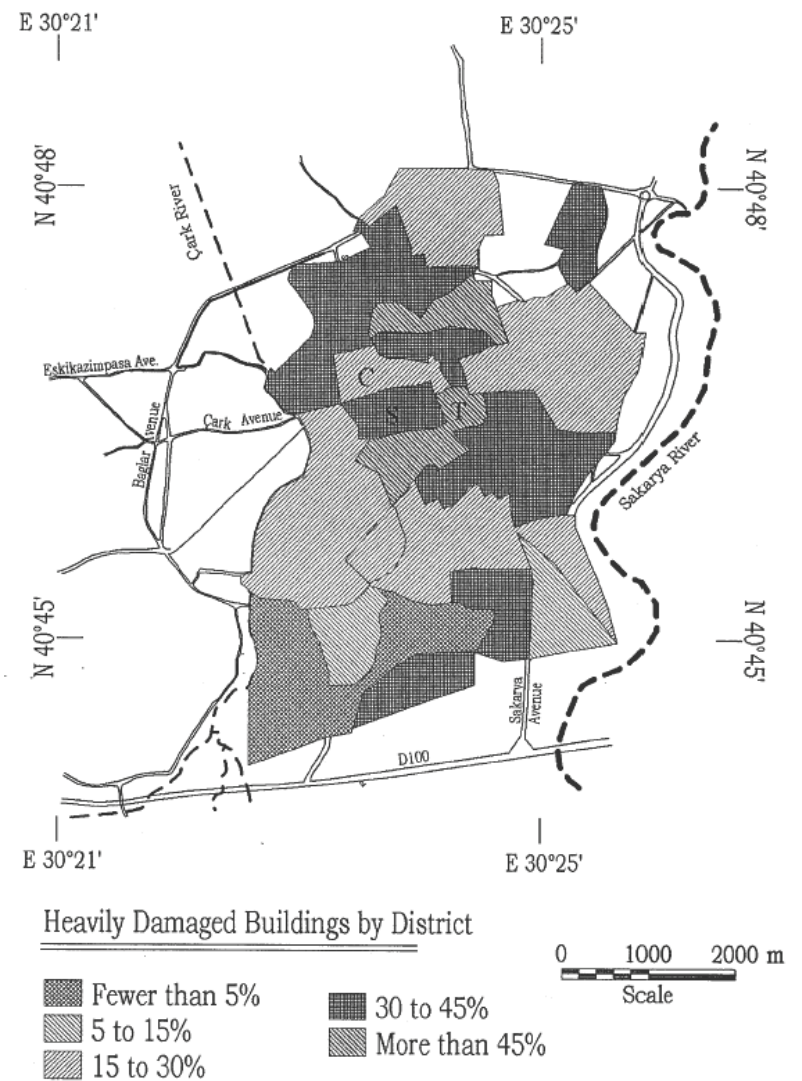


**Figure 4.9** General Map of Adapazari showing heavily damaged distribution ( Bardet et al,2000)

The bearing failure was typically observed by large settlements. As an evidence, paved areas around the settled buildings bulged as demonstrated in figure 4.10



**Figure 4.10** Loss of bearing capacity and bulging of pavements (PEER,1999).

The most common picture in the city was swelling of the sidewalks, in other words the near soil of the structures. In several cases, bearing failure led to rotation of the structures, and caused overturning problems. As a result of bearing failure analysis, Bray and Stewart noticed that buildings that overturned had aspect ratios (height to width) in excess of two. In figure 4.11, a building was chosen as an example of overturning. It has an aspect ratio about four. By the strong shaking and without an adjacent building on the left side, it laid to the roof of the three storey building. The building has a shallow foundation with the depth around one meter.



**Figure 4.11** Overturning of a five-storey building with aspect ratio about four (PEER,1999)

Lateral movements were faced in the ground failure areas. The behavior of the structure was as a rigid body; movement of stiff mat foundation as a whole. In addition, there was no significant damaged building by the lateral movements. Lateral movements were limited due to the surrounding conditions. The largest lateral movement, observed in the damaged area occurred at a five-storey building. As shown in figure 4.12, lateral movements were approximately 100 cm away from photographer and 55cm from sidewalk.(Baturay et al, 2000)



**Figure 4.12** Lateral movement observed in earthquake vicinity (PEER,1999)

There were only three pile supported buildings reported in the Adapazari region along the examined lines by personal conversations to residents and local engineers. The locations of pile supported buildings, had negligible ground failures although two of them had significant structural damages.(Baturay, 2000) The reason for non-ground failure could be the effect of piles on soil improvement.

Geotechnical investigations expressed that groundwater level fluctuates in a range of first 3-4 meters due to seasonable variation. Top 15 meters defined as loose and medium stiff sandy layers containing different amounts of low plasticity clay and silt, and gravel. Most of the soils contain significant fines (more than 35% passing the #200 sieve)(Bray et al 2004). The conditions are pointing the possibility of liquefaction. Thus, USGS research team noticed that, main reason for the over-estimated ground deformations was the liquefaction of unconsolidated river deposit on the northern part of the city.

During the earthquake neither the only two buildings on pile foundations nor any of the 1-2 storey buildings located on these soils was affected from liquefaction. However, 3-6 storey buildings having shallow mat foundations had significant settlements or overturned. The sunken buildings in the region were less damaged when compared to the adjacent buildings in non-liquefied area (Figure 4.14). The interpretation of the USGS researchers was that seismic waves were unable to propagate through the liquefied soils and shake the buildings as violent as adjacent buildings. The primary evidence of the liquefaction, sand boils were also observed near the sidewalks (Figure 4.14).



**Figure 4.13** Liquefied buildings with no structural damage (Photo: National Inst. of Standards and Technology)



**Figure 4.14** Sand boil on sidewalk (Photographed by Mehmet Celebi,USGS)

With so many affected buildings, Adapazari provided a natural laboratory for the study of the effects of liquefaction on building performance. Lots of scientists and researches; Bardet et al.(2000), Ural(2001), Cox(2001), Ural et al(2003),

Sancio(2003) and Bray et al (2004) examined the subsurface conditions and effects on liquefaction. A comprehensive research done by PEER research team, comprising researchers from U.C. Berkeley, Brigham Young Univ. and UCLA with ZETAS, Sakarya Univ. and Middle East Technical Univ., documented the liquefaction potential along the intended lines, lying out through the damaged area.

## 5. Site Response Analysis

Site response analyses are often used to modify earthquake motions in bedrock to account for the effects of a soil profile at a site. Steps involved in ground response analyses to develop site-specific response spectra at a soil site are briefly summarized below and are illustrated by the sites investigated during the study.

Site response analysis can be discussed with 4 main components as described by Ansal(2004b). The first component is the input ground motion. The second component is the site characterization based on geomorphologic and geotechnical conditions. The third component is the soil model and the fourth component is the method of site response analysis.

Input motion is the earthquake record obtained in strong ground motion stations. Due to the geological characteristics, the motion should be modified. Earthquake records are sometimes called outcrop records. An outcrop record is the record obtained at a rock outcrop. Such a record does not necessarily represent the motion in the same rock if the rock has a soil cover as illustrated in figure 5.1

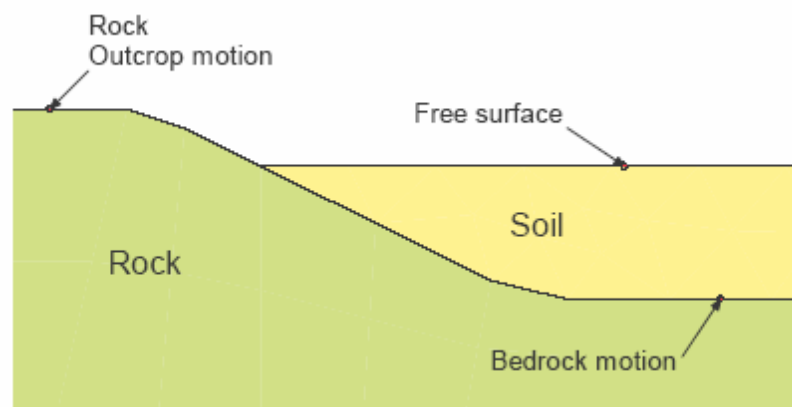


**Figure 5.1** Definition of motion types (Krahn, 2004)

Site characterization is defined by site investigations composed of in situ and laboratory testing programs. In situ tests are considered as 3 categories. The first category is penetration tests namely, SPT and CPT. Second category is expansion tests such as pressuremeter. Third category is seismic wave velocity measurement based on down-hole, cross hole, PS logging and SASW.

Laboratory test such as cyclic triaxial, cyclic shear, cyclic torsional triaxial, resonant column can be studied to analyze behavior of soil under dynamic loading.

Computer programs have generally analyzed the site response models in three categories; Linear elastic, Equivalent linear and non linear models.

Site response analysis are performed by using computer programs based on one-dimensional, two-dimensional and three-dimensional finite element models.

Dynamic properties of soils, soil models and computer programs used for site response analysis are briefly discussed in this chapter. At the end of the chapter the earthquake aspect of Turkey, and the Turkish seismic code is briefly introduced.

## 5.1 Dynamic Soil Properties

In an elastic homogenous soil mass dynamically stressed, three elastic waves travel at different steps. These are P waves, S waves and Rayleigh waves. The velocity of rayleigh wave is less than shear wave (Bowles, 1996). The relationship between P wave and S wave is defined as

$$0 \leq V_s \leq 0.707V_p \quad (5.1)$$

Shear wave velocity can be obtained from field tests or by using empirical correlations. Survey on site response analysis pointed out that most of the researchers used empirical correlations to obtain shear wave velocity (Kramer and Paulsen, 2004).

Shear modulus can be obtained by using mass density of soil and shear wave velocity computed by making field measurements.

$$G = \rho \times V_s^2 \quad (5.2)$$

The Relationship between shear modulus and stress strain modulus can be expressed by the formula below,

$$E_s = 2(1 + \mu) \times G \quad (5.3)$$

$\mu$  is poisson's ratio. It is defined as the ratio of axial compression to lateral expansion strains. Common values for poisson's ratio are given in table 5.1

**Table 5.1** Common values for Poisson's ratio (Bowles, 1996)

$\mu$	Soil Type
0.40-0.50	Most clay soils
0.45-0.50	Saturated clay soils
0.30-0.40	Cohesionless – medium and dense
0.20-0.35	Cohesionless – loose to medium

Dynamic laboratory testing of soils usually involves applying uniform cyclic stresses. The behavior of the soil is consequently known relative to a number of uniform cycles. Earthquake shaking however involves highly irregular cycles. It is necessary therefore to equate the two somehow. Seed et al. (1975a), determined that a uniform shear stress cycle equal to 65% of the maximum shear stress cycle from an irregular earthquake ground motion record would produce a similar pore-pressure response.

There also needs to be an equivalent number of uniform cycles. The issue is, how many uniform cycles will give a response similar to the many irregular cycles in an earthquake record? The equivalent number of uniform cycles is related to the magnitude of the earthquake. The value can be read from figure 5.2

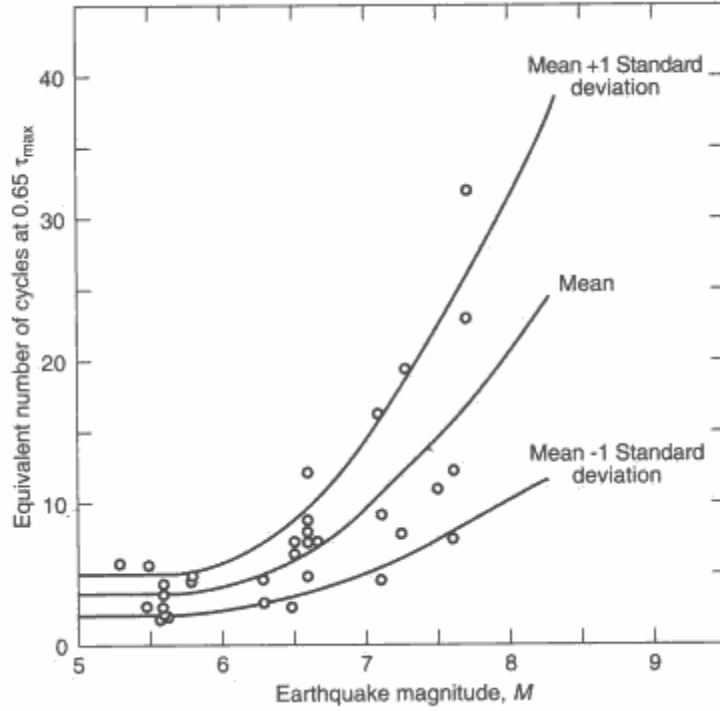


**Figure 5.2** Change on equivalent number of cycles due to earthquake magnitude (Kramer, 1996)

The damping ratio and shear modulus reduction changes during the analysis should be known. Kramer(1996) suggested formulas listed below to define damping and G reduction during the analysis.

$$\xi = 0.333 \frac{1 + \exp(-0.0145PI^{13})}{2} \left[ 0.586 \left( \frac{G}{G_{max}} \right)^2 - 1.547 \frac{G}{G_{max}} + 1 \right] \quad (5.4)$$

$$\frac{G}{G_{max}} = K(\gamma, PI) (\sigma'_m)^{m(\gamma, PI) - m_0} \quad (5.5)$$

$$K(\gamma, PI) = 0.5 \left\{ 1 + \tanh \left[ 1n \frac{0.000102 + n(PI)^{0.492}}{\gamma} \right] \right\} \quad (5.6)$$

$$m(\gamma, PI) - m_0 = 0.272 \left\{ 1 - \tanh \left[ 1n \left( \frac{0.000556}{\gamma} \right)^{0.40} \right] \right\} \exp(-0.0145PI^{13}) \quad (5.7)$$

There are also damping and G reduction curves already defined for the different type of soils. Vucetic-Dobry; Constant; Sun, Golesorkhi, and Seed; Rock; Ishibashi-Zhang; Seed-Idriss are available curves for damping function whereas Vucetic-Dobry; Gravel; Sun, Golesorkhi, and Seed; Ishibashi-Zhang; Rock; Seed-Idriss are available curves for G reduction function. (Proshake, 2001)

## 5.2 Constitutive Models

There are 3 constitutive models defined for site response analysis, linear elastic, equivalent linear and non linear.

Linear elastic model is the simplest model for which stress is directly proportional to the strain. The proportional constants are stress-strain modulus and poisson's ratio.

$$\sigma = E \times \varepsilon \quad (5.8)$$

The linear elastic model is not useful for actual field problems, since in reality the stress strain relationship is fairly nonlinear.

The equivalent linear elastic model is very similar to the linear elastic model. The difference is that the soil stiffness is modified in response to computed strains. Laboratory tests have shown that the soil stiffness changes with cyclic amplitude under dynamic cyclic loading condition. (Geo-slope, 2002) The secant shear modulus of soils decrease with increase of cyclic shear strain amplitude as shown in Figure 5.3.

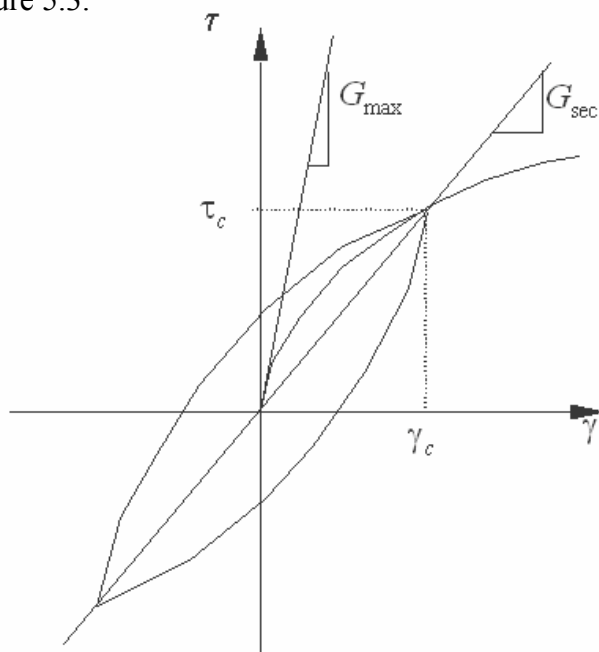


**Figure 5.3** Modulus under cyclic loading conditions. (Geo-slope, 2002)

The variation of  $G_{sec}$  is defined with the G reduction function.

Kramer and Paulsen (2004) expressed the equivalent linear model as,

*The method is computationally efficient and provides reasonable results for many cases, especially for those where small strains (< 1-2%) and modest accelerations (<0.3-0.4 g) develop. The linear approach allows computation of the bedrock motion from a given free surface motion, or deconvolution.*

There are some limitations for the model. Since it is linear there is no possibility to observe permanent displacement. Moreover the model is not capable of modeling the pore pressures because total stress approach is used in analysis (Kramer and Paulsen, 2004)

Nonlinear models can account for the nonlinear behavior of soil using various constitutive soil models. The constitutive models include different features, updated stress-strain relationships, pore-pressure generation. These features, unavailable in the equivalent linear model, allow more accurate calculations of soil behavior. Because they may be formulated in terms of effective stresses, unlike equivalent linear models, nonlinear models can account for the build up of pore water pressure that can cause the soil to soften. An important application of nonlinear soil models is in liquefaction hazard analysis (Makdisi and Wang, 2004). Nonlinear models can also predict permanent deformations since the strain does not return to zero following cyclic loading. Nonlinear models tend to be necessary for analyses where large strains or displacements are expected. ( Kramer and Paulsen, 2004).

### **5.3 Numerical Tools**

A significant number of computer programs are now available for site response analyses. The programs can be categorized into groups as the type of constitutive models, dimension and interface.

Constitutive models that are already explained in section 5.2 are the equivalent linear model and non linear model. Dimensions are described as one-dimensional, two-dimensional and three dimensional finite element models. Windows and DOS are the interface options in order to use computer programs. Widely used codes for site response analysis are listed in Table 5.2

**Table 5.2** Geotechnical computer programs used in practice for site response analysis (Kramer and Paulsen, 2004).

Dimensions	OS	Equivalent Linear	Nonlinear
1-D	DOS	Dyneq, Shake91	AMPLE, DESRA, DMOD, FLIP, SUMDES, TESS
	Windows	ShakeEdit, ProShake, Shake2000, EERA	CyberQuake, DeepSoil, NERA, FLAC, ShearBeam
2-D / 3-D	DOS	FLUSH, QUAD4/QUAD4M, TLUSH	DYNAFLOW, TARA-3, FLIP, VERSAT, DYSAC2, LIQCA
	Windows	QUAKE/W, SASSI2000	FLAC, PLAXIS

One dimensional codes are can be categorized as Shake and its derivatives. For two and three dimensional codes and with the increase of mesh complexity the computer run time may take hours. Some of the programs are general geotechnical codes which includes dynamic modules.

#### **5.4 Turkish Seismic Code for Soils and Earthquake Design**

The two codes that influence design and construction in Turkey are TS-500 Building Code Requirement for Reinforced Concrete (2000) and Specification for Structures to be built in Disaster Areas (2006), shortly the Turkish Seismic Code.

TS-500/2000 includes basic principles for reinforced construction and a revision of TS-500/1985.

The last and current seismic code is the 2006 Turkish Seismic Code. An earthquake zonation map was published for the country due to the risk assessment in 1997 by Ministry of Public Works as illustrated in figure 5.4. The map remains the same in the seismic code revised in 2006. It divides Turkey into 5 zones due to the expected ground acceleration values. Zone 1 is for the values greater and equal to 0.40g, zone 2 is between 0.30- 0.40g, zone 3 is for the range 0.20-0.30g , zone 4 is between 0.10-0.20g and lastly less than 0.10g the zone is the fifth.

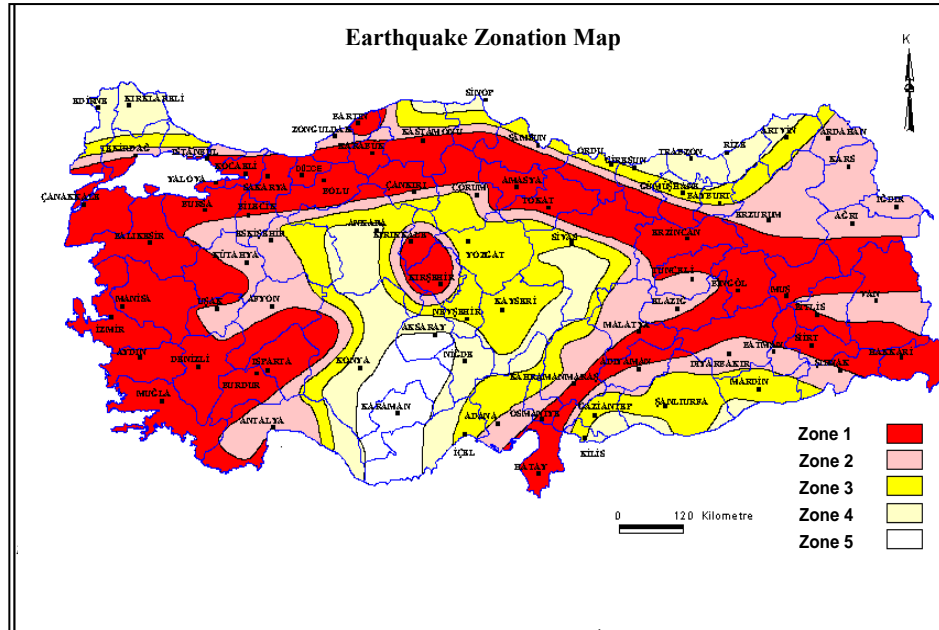


**Figure 5.4** Earthquake Zonation Map (1997)

The red region pointed the high risk of earthquake. There is only a small part around the city Karaman defined with the minimum risk. The area and corresponding population for each zone is listed below in table 5.3

Total area of zone 1 and zone 2 contains three fourths of the population in Turkey.

**Table 5.3** Area and Estimated Population for each Earthquake Zone (Özmen,2000)

Zone	Area (km <sup>2</sup> )	Estimated Population
Zone 1	328,995	28,498,740
Zone 2	186,411	16,674,656
Zone 3	139,594	9,334,138
Zone 4	97,894	8,129,711
Zone 5	32,051	1,107,757
Total	784,945	63,745,000

#### 5.4.1 Determination of Soil Conditions

Based on the studies and observations discussed the site categories in the 1997 Turkish Seismic Code are defined in terms of the shear wave velocity. If shear wave velocities are available for the site, they should be used to classify the site. However, in recognition of the fact that in many cases the shear wave velocities are not

available, alternative definitions of the site classes also are included in the 1997 Regulations. They use the standard penetration resistance for cohesionless, cohesive soils, and rock, and the undrained shear strength for cohesive soils only. These alternative definitions are rather conservative since the correlation between site amplification and these geotechnical parameters is more uncertain than the correlation with  $V_s$ . Table 5.4 describes the soil groups on the basis of  $N_{30}$ , relative density, unconfined compression strength and shear wave velocity.

**Table 5.4** Soil Groups from Turkish Seismic Code

<i>Soil Group</i>	<i>Description of Soil Group</i>	<i>Stand. Penetr. (N/30)</i>	<i>Relative Density (%)</i>	<i>Unconf. Compres. Strength (kPa)</i>	<i>Shear Wave Velocity (m/s)</i>
(A)	1. Massive volcanic rocks, unweathered sound metamorphic rocks, stiff cemented sedimentary rocks	---	---	> 1000	> 1000
	2. Very dense sand, gravel...	> 50	85-100	---	> 700
	3. Hard clay, silty lay.....	> 32	---	> 400	> 700
(B)	1. Soft volcanic rocks such as tuff and agglomerate, weathered cemented sedimentary rocks with planes of discontinuity.....	---	---	500-1000	700-1000
	2. Dense sand, gravel.....	30-50	65-85	---	400-700
	3. Very stiff clay, silty clay...	16-32	---	200-400	300-700
(C)	1. Highly weathered soft metamorphic rocks and cemented sedimentary rocks with planes of discontinuity	---	---	< 500	400-700
	2. Medium dense sand and gravel.....	10-30	35-65	---	200-400
	3. Stiff clay, silty clay.....	8-16	---	100-200	200-300
(D)	1. Soft, deep alluvial layers with high water table.....	---	---	---	< 200
	2. Loose sand.....	< 10	< 35	---	< 200
	3. Soft clay, silty clay.....	< 8	---	< 100	< 200

In order to take into account the groups; there is a need to classify the soil groups with the change on topmost layer thickness. Table 5.5 presents the description of the local site classification.

**Table 5.5** Local Site Classes from Turkish Seismic Code

<i>Local Site Class</i>	<i>Soil Group according to Table 5.4 and Topmost Layer Thickness (<math>h_1</math>)</i>
Z1	Group (A) soils Group (B) soils with $h_1 \leq 15$ m
Z2	Group (B) soils with $h_1 > 15$ m Group (C) soils with $h_1 \leq 15$ m
Z3	Group (C) soils with $15 \text{ m} < h_1 \leq 50$ m Group (D) soils with $h_1 \leq 10$ m
Z4	Group (C) soils with $h_1 > 50$ m Group (D) soils with $h_1 > 10$ m

#### 5.4.2 Determination of Elastic Seismic Loads

In order to determine seismic loads, spectral acceleration coefficient,  $A(T)$  corresponding to 5% damped elastic design acceleration spectrum normalized by the acceleration of gravity ( $g$ ) is used.

$$A(T) = A_0 IS(T) \quad (5.9)$$

where  $A_0$  is the effective ground acceleration coefficient,  $I$  is the building importance factor and  $S(T)$  is the spectrum coefficient.

Effective ground acceleration is specified in table 5.6. It changes due to the seismic zone already defined in the earthquake zonation map in figure 5.4.

**Table 5.6** Effective Ground Acceleration from Turkish Seismic Code

<i>Seismic Zone</i>	$A_0$
<b>1</b>	<b>0.40</b>
<b>2</b>	<b>0.30</b>
<b>3</b>	<b>0.20</b>
<b>4</b>	<b>0.10</b>

The building importance factor, I, is a coefficient used to increase the design loads. Residential and office buildings have a coefficient of 1.0, whereas, buildings required to be utilized immediately after the earthquake have a value of 1.5 which is a 50% increase on earthquake load in consideration.

Spectrum Coefficient, S(T) is the component of spectral acceleration coefficient which depends on the local soil conditions and building natural period, T.

$$\begin{aligned}
 S(T) &= 1 + 1.5T/T_A & 0 \leq T \leq T_A \\
 S(T) &= 2.5 & T_A < T \leq T_B \\
 S(T) &= 2.5(T_B/T)^{0.8} & T \geq T_B
 \end{aligned}
 \tag{5.10}$$

$T_A$  and  $T_B$  are the spectrum characteristic periods depending on the local site conditions defined in table 5.5. Values for  $T_A$  and  $T_B$  are listed for various soil conditions in table 5.7

**Table 5.7** Spectrum Characteristic Periods ( $T_A$  and  $T_B$ )

Local Site Class acc.to Table 5.5	$T_A$ (sec)	$T_B$ (sec)
Z1	0.10	0.30
Z2	0.15	0.40
Z3	0.15	0.60
Z4	0.20	0.90

Design response spectrum is plotted in figure 5.5

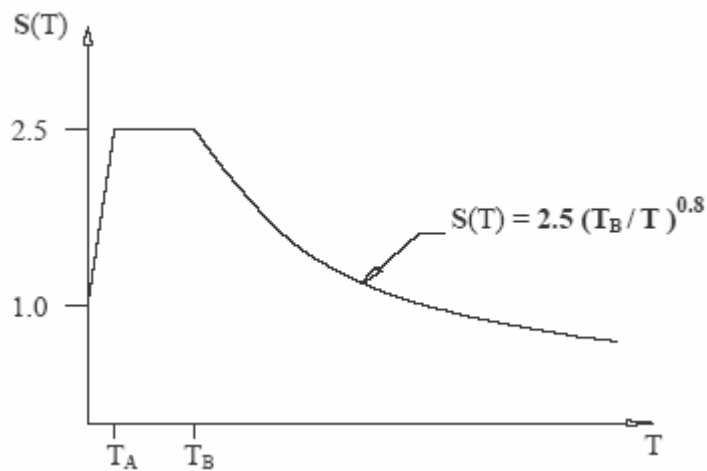


**Figure 5.5** Design Response Spectrum from Turkish Seismic Code (1997)

When required, elastic acceleration spectrum may be determined through special investigations by considering local seismic and site conditions. However spectral acceleration coefficients computed for the specific site couldn't be less than the values already calculated in the seismic code. Normalized spectral acceleration for the 1999 Kocaeli earthquake and the value proposed to used in regulations are given in figure 5.6.

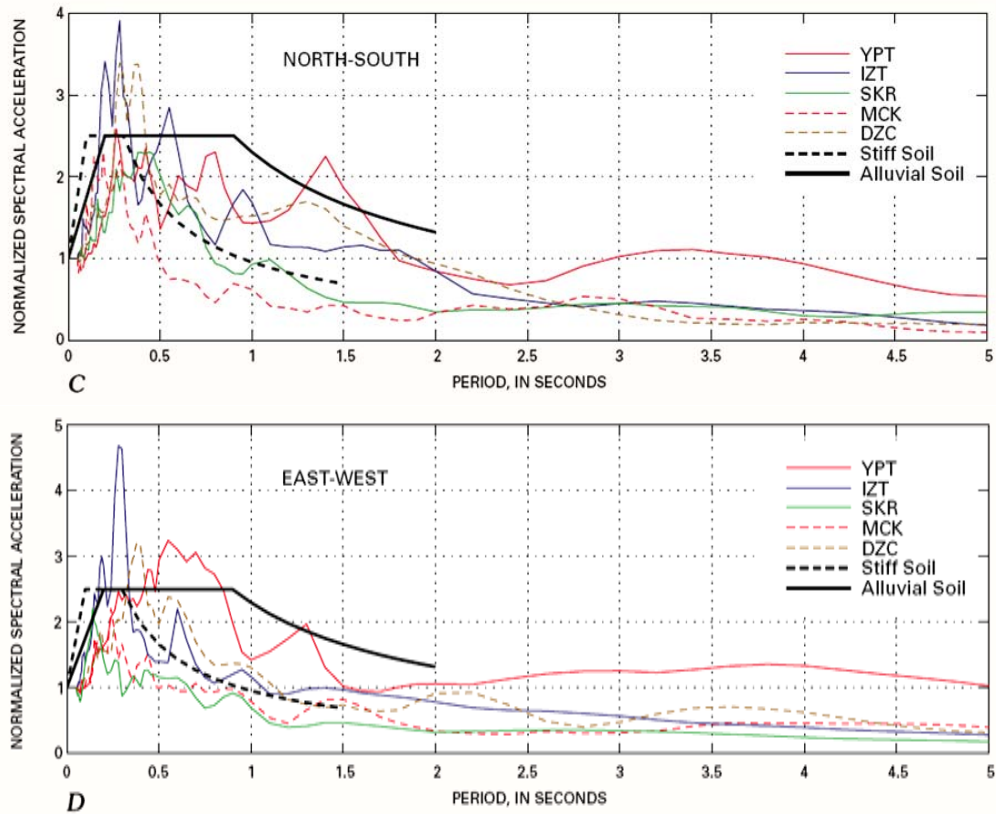


**Figure 5.6** Normalized Spectral Acceleration for 5 stations and minimum requirements in seismic code in both directions (USGS,1999)

## **6. Case Study: Geostatistical Analysis of Soil Deposits in Adapazari after 1999 Kocaeli Earthquake**

As a case study, in this chapter subsurface response against earthquake is investigated for the soil profiles defined by geostatistical analysis.

During the study, first the in-situ test results are discussed and 4 sites located in Adapazari city center are defined. In order to analyze with statistical and geostatistical methods, shear wave velocity values are determined by using empirical correlations. Ground motion record taken after the earthquake in SKR station is applied to modeled soil profiles. Consequently, the seismic behavior of the soil deposits in selected sites is described and compared to the current seismic code already used in Turkey.

### **6.1 In-situ Testing and Interpretation**

Following the Kocaeli earthquake on August 17,1999, a large number of engineers and researchers from the U.S.A. and Turkey, as well as from other countries, were dispatched to the epicentral area to assess the damage caused by the event and to collect information valuable for the documentation of the performance of earth structures and buildings. This study relies on such data collected by the US-Turkey reconnaissance effort funded by the National Science Foundation (NSF) and the Earthquake Engineering Research Institute (EERI). As documented by these parties, a large number of buildings in the city of Adapazari experienced poor performance of the foundation system and exhibited vertical displacement, tilt, and at times, horizontal translation. Patterns of ground failure and liquefaction were observed and documented by careful building-by-building surveys of damage and performance (Bardet et al, 2000)

### 6.1.1 In-situ Testing in Adapazari

A total of 135 Cone Penetration Test (CPT) profiles and 46 soil borings with multiple Standard Penetration Testing (SPT) were completed in the City of Adapazari, Turkey to document the subsurface conditions at sites of interest. Most of the site investigation was limited to a depth of 10 m, but 28 CPT profiles and 5 soil borings were extended deeper to characterize soils to depths of up to 30 m. (Bray et al., 2004). This study covers a small district of Adapazari. 31 CPT and 22 SPT were used to model 4 sites located in the city center of Adapazari during the study.

Procedures and equipment properties of cone penetration test and standard penetration test should be given as they are the starting points for the study.

Table 6.1 lists the specifications of the equipment employed, which consists of a 60° apex angle cone, with a cross-sectional area of approximately 10 cm<sup>2</sup>. The length of the rod increment was 50 cm and the depth interval at which the tip resistance, sleeve friction, and pore water pressure were measured was 2 cm. The rate of penetration was kept constant at 2 cm/s. (Sancio, 2003)

**Table 6.1** Specifications of CPT Equipment and Procedure

Tip Area	10 cm <sup>2</sup>
Internal Angle of Cone	60
Sleeve Area	150cm <sup>2</sup>
Cone Area Ratio	0.75
Penetration rate	2 cm/s
measurement interval	at every 2 cm
rod interval length	50 cm

Table 6.2 presents a list of the methods used to perform the SPT in the Adapazari soils. A rope and cathead system was used to perform the Standard Penetration Test. The diameter of the rope used was 2 cm and the diameter of the cathead was approximately 11.2 cm. The driving energy was delivered by the 76 cm-high drop of a safety hammer weighing approximately 63.5 kgf. The safety hammer was custom made in Ankara, Turkey. The sampler used had an outer diameter of 50.8 mm, a constant inner diameter of 35 mm and a total length of 600 mm. After performing the SPT and bringing the sampler back to the surface, soil samples were visually identified, removed from the sampler and placed in a plastic bag that was taken to the

geotechnical laboratory of Sakarya University for index testing and grain size analysis. (Sancio, 2003)

**Table 6.2** Specifications of SPT Equipment and Procedure

Drilling Technique	Rotary Wash
Borehole Support	Casing, ID=10 cm
Drill Bit	Tri-cone bit
Drill Rod	AWJ type
Length of Rod Section	152 cm
Sampler	OD=50.8 mm ID=35 mm Length=600 mm
Cathead Diameter	11.2 cm
Rope Diameter	2 cm
Rope & Cathead	2.25 turns on a clockwise rotating cathead
Hammer Type	Safety Hammer
Penetration Resistance	Blows recorded over three intervals, each of the 15 cm N=number of blows over the last 2 intervals

### 6.1.2 Sites Investigated

Sancio(2003) examined the liquefaction analysis of the city of Adapazari by using in-situ test results in 12 different sides as a part of PEER research project. In this study, shear wave velocity profiles of 4 redefined sites are evaluated. Each site has its own coordinate system and is analyzed independently. They are shown in the map of Adapazari City in figure 6.1.

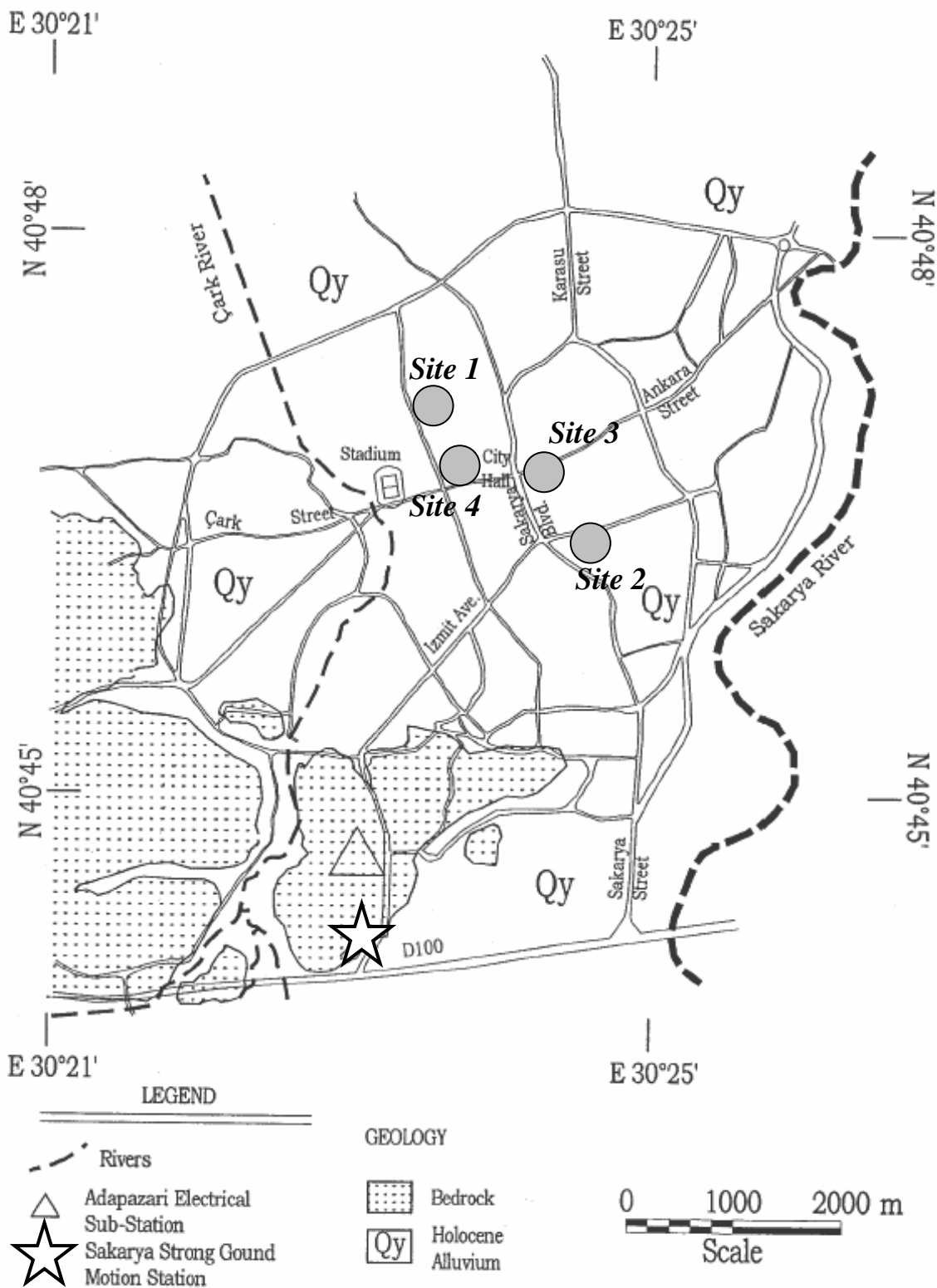
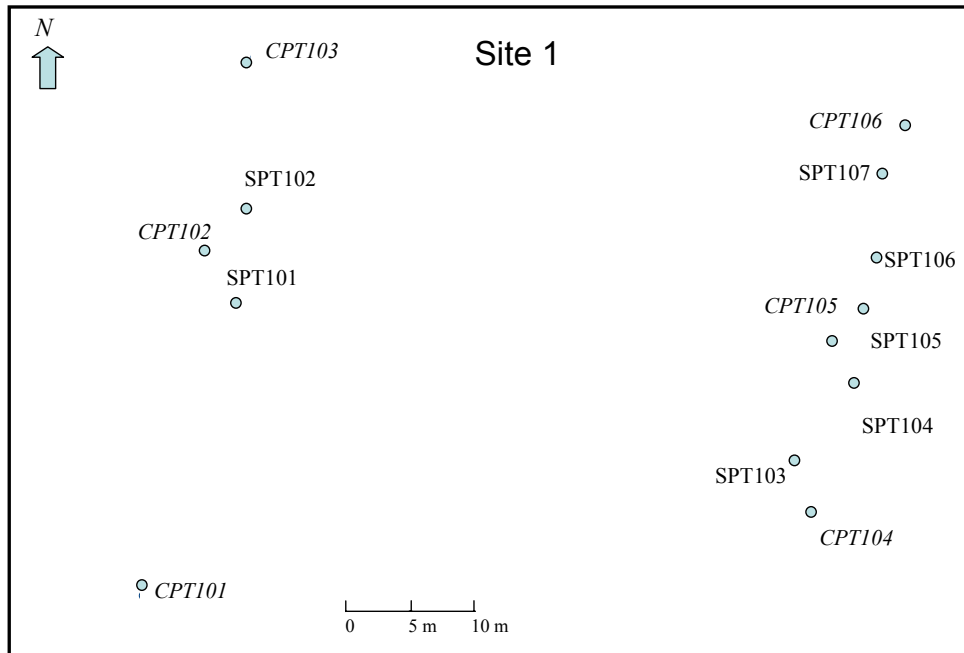


Figure 6.1 Location of the sites on Adapazari City Map

*Site 1*

As shown in figure 6.2, 6 Cone Penetration Tests (CPT) and 7 exploratory borings with implementation of Standard Penetration Tests (SPT) were performed in order to identify and characterize subsurface conditions for the first 10 meters.



**Figure 6.2** Plan view of Site 1 and location of the boring logs

Results of in-situ tests are presented in the appendix of this thesis. Each exploratory boring log has samples which is helpful to analyze the soil beneath the damaged part of the earthquake vicinity. Site 1 covers 3 to 5 storey apartment buildings which is a residential area. The elevation of the site is around 31.0 m. In order to determine the soil profile CPT and SPT locations are shown in figure 6.1 and elevation for each test is listed in table 6.3

**Table 6.3** Elevations for in-situ tests for site 1

Study ID	Elevation (m)	Study ID	Elevation (m)
CPT101	30.56	SPT101	30.76
CPT102	30.78	SPT102	30.76
CPT103	30.78	SPT103	30.60
CPT104	30.63	SPT104	30.61
CPT105	30.66	SPT105	30.62
CPT106	30.69	SPT106	30.62
		SPT107	30.67

Soil profile of site 1 is plotted in figure 6.3.

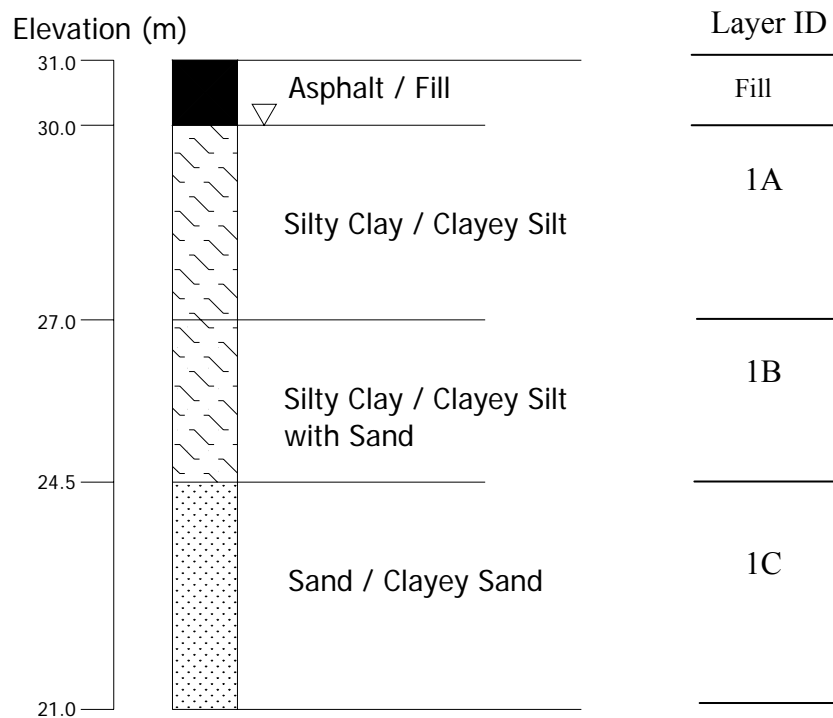


**Figure 6.3** Soil profile for site 1.

Since the ground surface is variable, the top elevation for the site is assumed as 31.0 m. Because of the residential area, first meter of the profile includes pavement and fill. The soil, from 30 m to 27 m is a mixture of fine graded soil and could be defined as silty clay / clayey silt. Most of the foundations are lying at a depth of approximately 1.5m which is in the silty clay / clayey silt strata. As the second layer although the soil has a general behavior of fine graded soils, the distribution covers some sand seams in different regions. It is the reason for sudden differences, faced in in-situ tests. So it is defined as silty clay / clayey silt with sand seams. At approximately 24.5 m clayey sand and clean sand was found. It continues till the exploratory depth (~10m)

The liquid limit of the soil samples recovered in this deposit is in the range of 14 to 45, whereas the natural water content is close to the liquid limit in the order of higher than 0.9 LL

## Site 2

As shown in figure 6.3, 11 Cone Penetration Tests (CPT) and 7 exploratory borings with implementation of Standard Penetration Tests (SPT) were performed in order to identify and characterize subsurface conditions for first 10 meters.

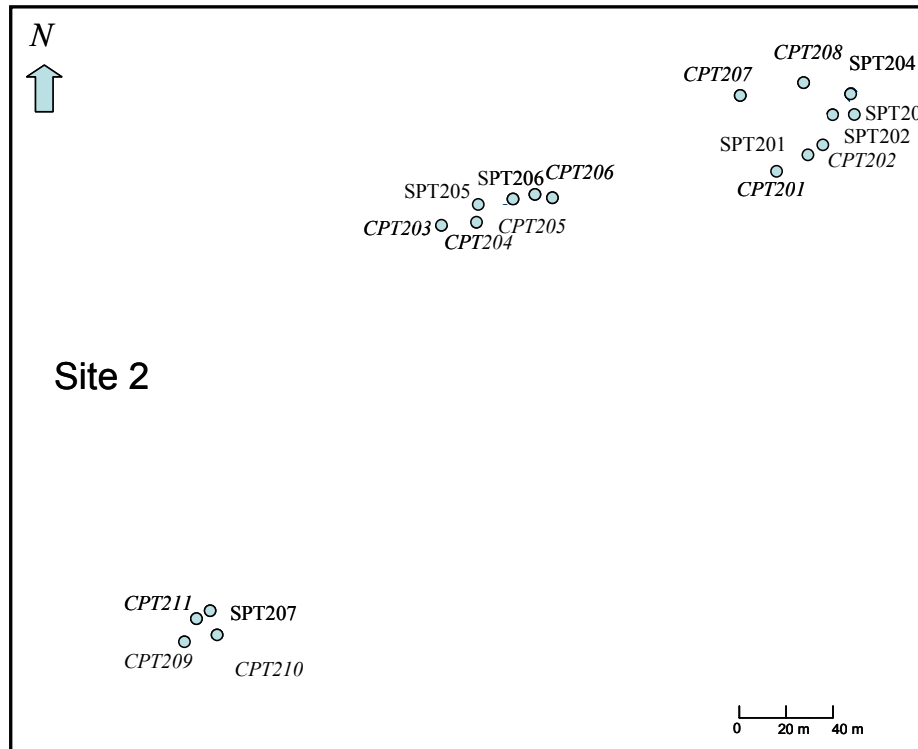


**Figure 6.4** Plan view of Site 2 and location of the boring logs

Results of in-situ tests are presented in appendix part of the study. Site 2 is also a residential area with the damaged and collapsed buildings. The foundations are typical mat foundations and in general lying at a depth of approximately 1.5m. In the southwest part of the site, evidence of liquefaction was observed (Sancio, 2003). The elevation of the site is around 31.1 m. In order to determine the soil profile CPT and SPT locations are pointed in figure 6.4 and elevation for each test is found out and listed in table 6.4

**Table 6.4** Elevations for in-situ tests for site 2

Study ID	Elevation (m)	Study ID	Elevation (m)
CPT201	31.11	CPT210	31.39
CPT202	31.09	CPT211	31.12
CPT203	30.98	SPT201	31.08
CPT204	31.09	SPT202	31.15
CPT205	31.07	SPT203	31.09
CPT206	31.07	SPT204	31.09
CPT207	31.19	SPT205	31.02
CPT208	31.09	SPT206	31.06
CPT209	30.97	SPT207	31.11

Soil profile of site 2 is plotted in figure 6.5.

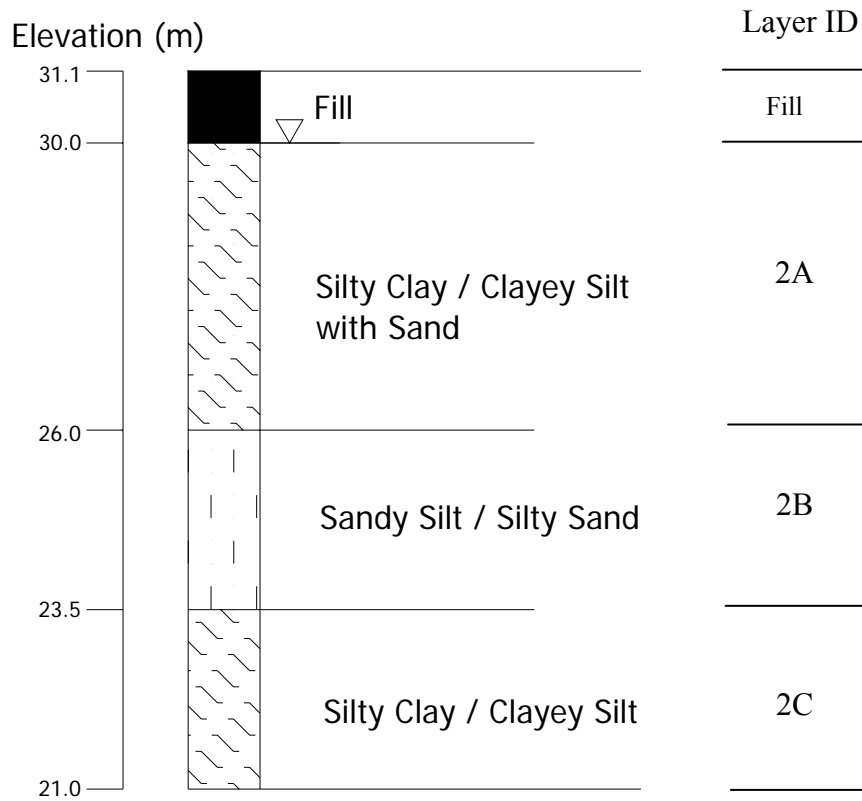


**Figure 6.5** Soil profile for site 2.

A fill layer and also pavement and concrete slabs were observed for the first meter beneath the ground surface. Since the ground surface is variable, the top elevation for the site is assumed as 31.1 m. The soil, from 30 m to 26 m is a mixture of fine graded soil and for limited area, sand particles was observed. Following the first strata,

between the elevations 26m and 23.5m sandy soil is dominant. The samples, recovered in the layer, indicated the existence of sand and silt as a mixture. Hence the soil is defined as silty sand / sandy silt. Beneath the second layer till the exploratory depth general characteristic of the soil is fine graded soil.

Natural water contents are found very close to the liquid limit. Moreover, for some regions, it exceeds the liquid limit values and changes to liquid state.

### Site 3

As shown in figure 6.5, 8 Cone Penetration Tests (CPT) and 4 exploratory borings with implementation of Standard Penetration Tests (SPT) were performed in order to identify and characterize subsurface conditions for first 9 meters.

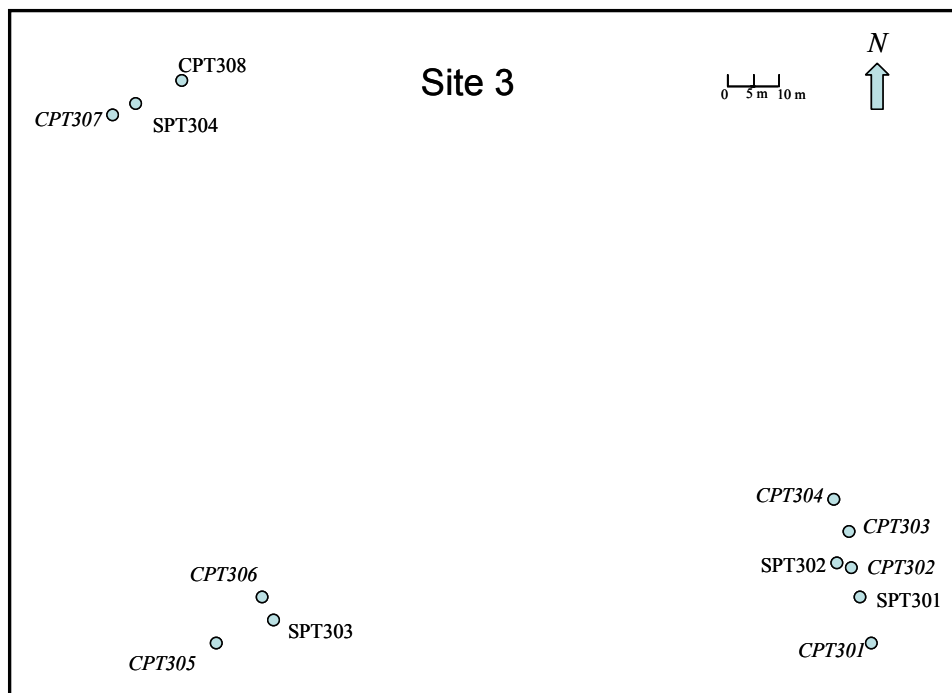


**Figure 6.6** Plan view of Site 3 and location of the boring logs

Results of in-situ tests are presented in the appendix of this thesis. Site 3 is located in the center of Adapazari. The district covers heavily damaged buildings with a ratio more than 45%. 3-5 storey apartment buildings are dominant in the vicinity. In order to determine the soil profile CPT and SPT locations are pointed in figure 6.5 and elevation for each test is found out and listed in table 6.5

**Table 6.5** Elevations for in-situ tests for site 3

Study ID	Elevation (m)	Study ID	Elevation (m)
CPT301	32.87	CPT307	32.61
CPT302	32.92	CPT308	32.58
CPT303	33.01	SPT301	32.92
CPT304	32.98	SPT302	32.92
CPT305	32.61	SPT303	32.63
CPT306	32.64	SPT304	32.60

It is obvious that the elevation of the site is almost 32.7 m.

Soil profile of site 3 is plotted in figure 6.7.

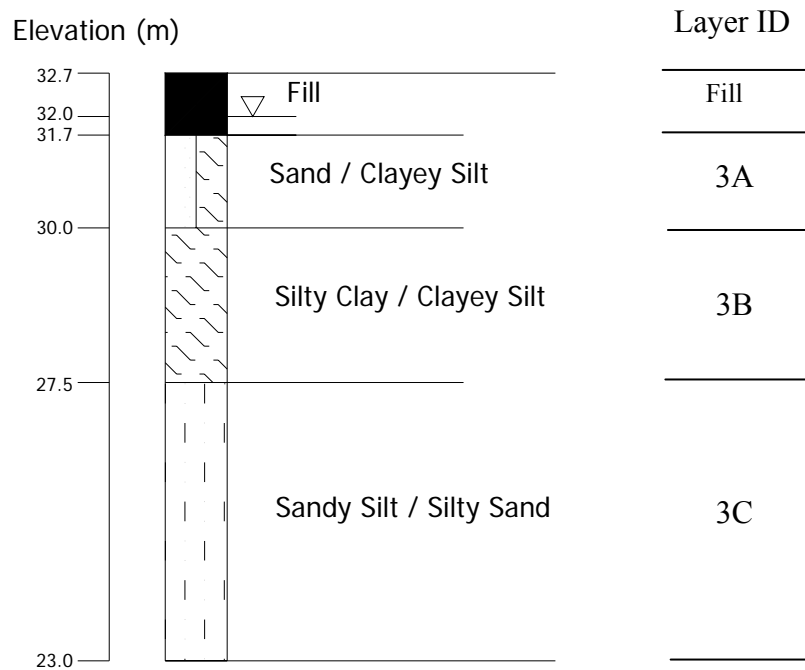


**Figure 6.7** Soil profile for site 3

The ground water level was measured at a depth of 0.7m. There is one meter layer contains fill and other materials, used to stabilize the ground surface. For the southeast part of the site between 31.7m and 30m elevations sand deposits are found whereas the other sides of the region can be defined as clayey silt. There are also some evidence of liquefaction (Sancio, 2003). The soil stratum beneath the first layer is a mixture of fine graded soil up to the elevation 27.5 m. Following the layer up to exploratory depth(~10m), sand and silt mixture namely, sandy silt and silty sand is observed.

#### Site 4

As depicted in figure 6.7, 6 Cone Penetration Tests (CPT) and 4 exploratory borings with implementation of Standard Penetration Tests (SPT) were performed in order to identify and characterize subsurface conditions for first 9 meters.

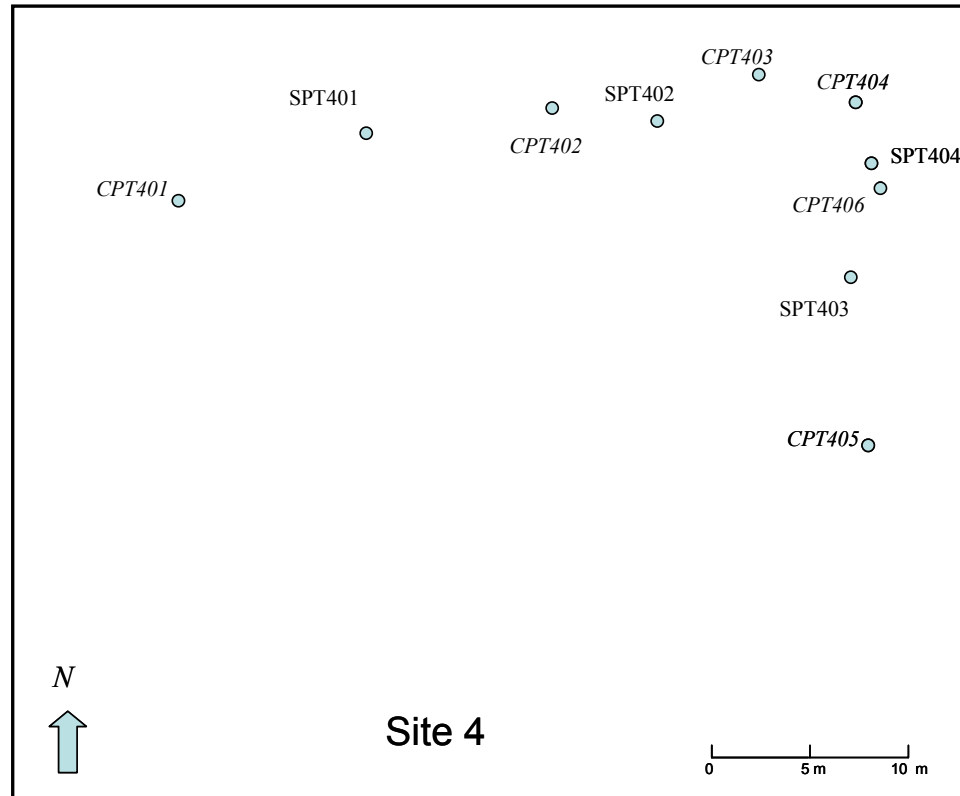


**Figure 6.8** Plan view of Site 3 and location of the boring logs

Results of in-situ tests are presented in appendix part of the study. Site 4 is located in the west of Adapazari. There are 5 storey apartment buildings in the research area. Excessive settlements and rotations are already observed however, building's structural frame was undamaged by earthquake (Sancio, 2003). In order to determine the soil profile CPT and SPT locations are pointed in figure 6.8 and elevation for each test is found out and listed in table 6.6.

**Table 6.6** Elevations for in-situ tests for site 4

Study ID	Elevation (m)	Study ID	Elevation (m)
CPT401	31.63	CPT406	31.03
CPT402	31.09	SPT401	30.95
CPT403	30.91	SPT402	31.09
CPT404	30.95	SPT403	31.04
CPT405	30.99	SPT404	30.95

It is obvious that the elevation of the site is almost 31.0m. CPT401 located in the northeast part of the site has a great difference whereas the other exploratory boring logs lie nearly at same elevation.

Soil profile of site 4 is plotted in figure 6.9.

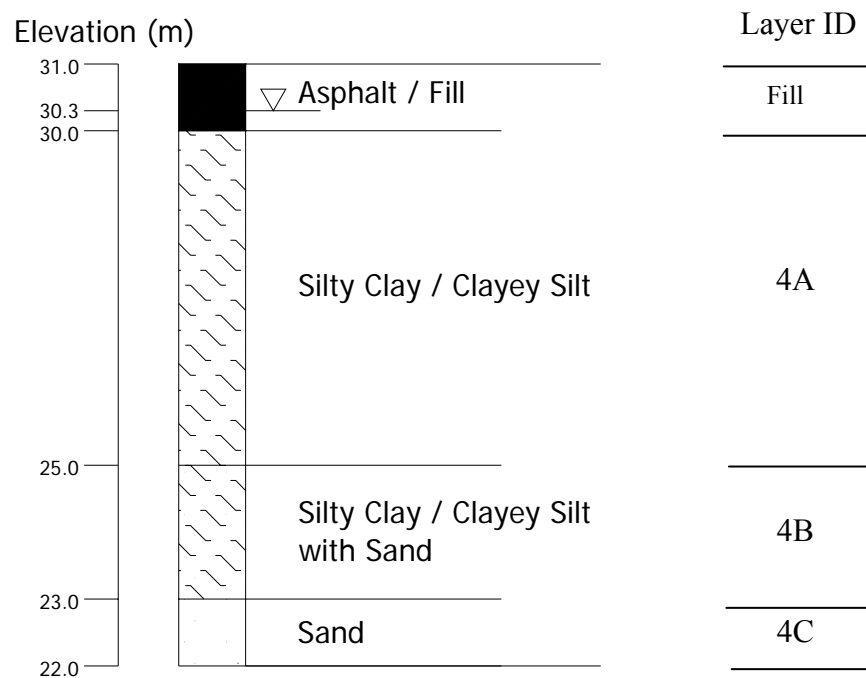


**Figure 6.9** Soil profile for site 4.

The ground water level varies in the range of 0.7m to 1.0m below the sidewalk level. Beneath the fill / asphalt layer, 5m thick silty clay / clayey silt strata is observed. The deposit of fine graded soil with sand seams is underlain by approximately 2m thick strata. At elevation of 23m up to 22m, clean sand is founded. The fine content of the upper strata fall in the range of 75% to 100% and most of the samples have fine content higher than 90%. As observed in the other sides the natural water contents are close to the liquid limit values which is generally higher than 35.

### 6.1.3. Interpretation of In-situ Tests

In this section, sites already discussed in section 6.1.2 are examined by using the Cone Penetration Tests (CPTs) and Standard Penetration Tests (SPTs). In order to use the results of the tests in correlations it is necessary to correct them. Hence, the first step during the interpretation process is correction of the SPT data and then by using CPT-SPT correlations, conversion of CPT values to SPT-N blow numbers and lastly computing the shear wave velocity for the required points by using empirical correlations.

Although the SPT has been standardized, it is not actually easy to apply the process in the field. The significant problem is for the energy ratio. In most cases, the amount of energy transmitted to the system is not equal to the theoretical energy. For the reason stated, Skempton (1986) and Robertson and Wride (1997) suggested corrections for the SPT-N blow numbers.

$$(N_1)_{60} = N_m C_n C_E C_B C_R C_S \quad (6.1)$$

Where  $N_m$  = measured standard penetration resistance;  $C_N$  = factor to normalize  $N_m$  to a common reference effective overburden stress;  $C_E$  = correction for hammer energy ratio ( $E_R$ );  $C_B$  = correction factor for borehole diameter;  $C_R$  = correction factor for rod length; and  $C_S$  = correction for samples with or without liners. Values are listed in table 6.7.

For the SPT, performed in 4 different sites, energy ratio and rod length terms are checked out and listed in boring logs as attached in appendixes part. Maximum value for overburden pressure coefficient is limited to the 1.7. Although there are some suggested values for energy ratio coefficient, Energy ratio already measured in field is preferred to use. Samples are retrieved by using standard sampler.

**Table 6.7** Corrections for SPT modified Skempton (1986) as listed by Robertson and Wride (1997)

Factor	Equipment variable	Term	Correction
Overburden pressure	---	$C_N$	$(P_a / \sigma'_{v0})^{0.5}$
Overburden pressure	---	$C_N$	$C_N < 1.7$
Energy ratio	Donut hammer	$C_E$	0.5-1.0
Energy ratio	Safety hammer	$C_E$	0.7-1.2
Energy ratio	Automatic-trip Donut-type hammer	$C_E$	0.8-1.3
Borehole diameter	65-115 mm	$C_B$	1.0
Borehole diameter	150 mm	$C_B$	1.05
Borehole diameter	200 mm	$C_B$	1.15
Rod length	< 3	$C_R$	0.75
Rod length	3-4 m	$C_R$	0.8
Rod length	4-6 m	$C_R$	0.85
Rod length	6-10 m	$C_R$	0.95
Rod length	10-30 m	$C_R$	1.0
Sampling method	Standard sampler	$C_S$	1.0
Sampling method	Sampler without liners	$C_S$	1.1-1.3

For computational purposes, the SPT N blow numbers are assumed same at the closest integer elevation. For example, a blow number obtained from the elevation 29.2m is assumed to be taken at 29.0m. That is why, for the following chapters, the data will be investigated as a horizontal layer.

In order to model the soil profile, it is recommended to use much more and reliable data. In the area of interest, there are only SPT and CPT tests, already performed. So, CPT tests are needed to convert SPT blow numbers to increase the data set by using empirical correlations. Ramaswamy et al (1982) suggested a formula for the intended correlation. (Bowles,1996)

$$N = K.q_c \quad (6.2)$$

where  $q_c$  is in the units of Mpa and coefficient K tends to range from 0.1 to 1.0 as in the following table which uses  $N'_{60}$  :

**Table 6.8** Correlation coefficient, K, for different soil types (Bowles,1996)

Soil Type	$q_c/N_{60}$
Silts, sandy silts and slightly cohesive silt-sand mixtures	0.1-0.2
Clean fine to medium sands and slightly silty sands	0.2-0.3
Coarse sands and sands with little gravel	0.5-0.7
Sandy gravels and gravel	0.8-1.0

Soil types already observed in the field are generally corresponds to the first two groups. There is no evidence of gravel in in-situ tests. Tip resistance values for 31 Cone Penetration Tests at the integer elevations are converted to the SPT blow numbers.

Relationship between corrected SPT blow number and elevation for 4 sites are plotted in the figures 6.10 to 6.13.

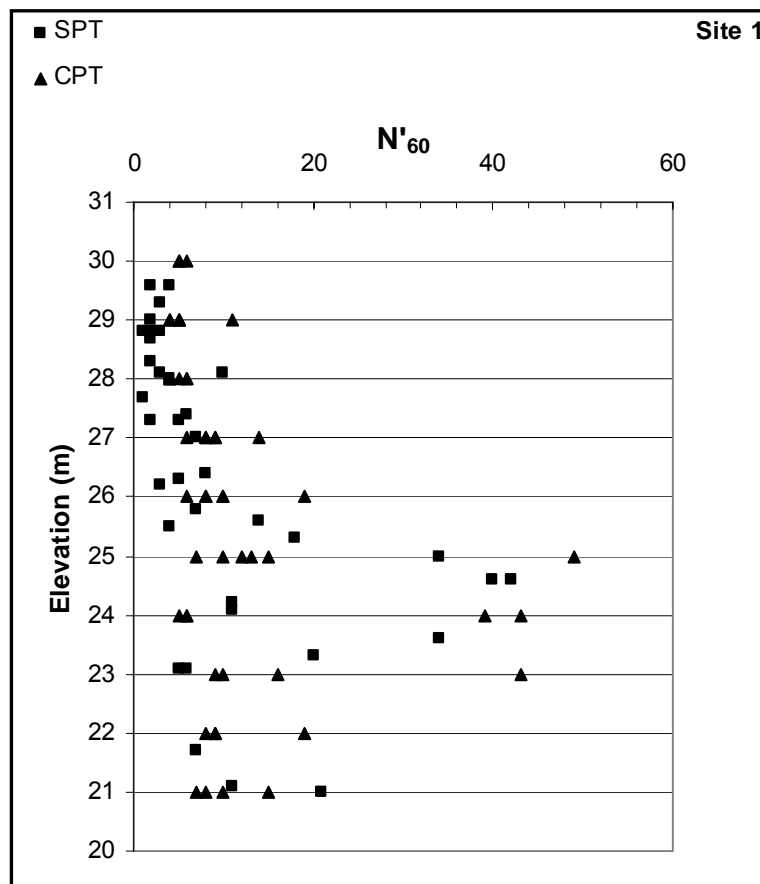


**Figure 6.10** Relationship between  $N'_{60}$  and Elevation for Site 1



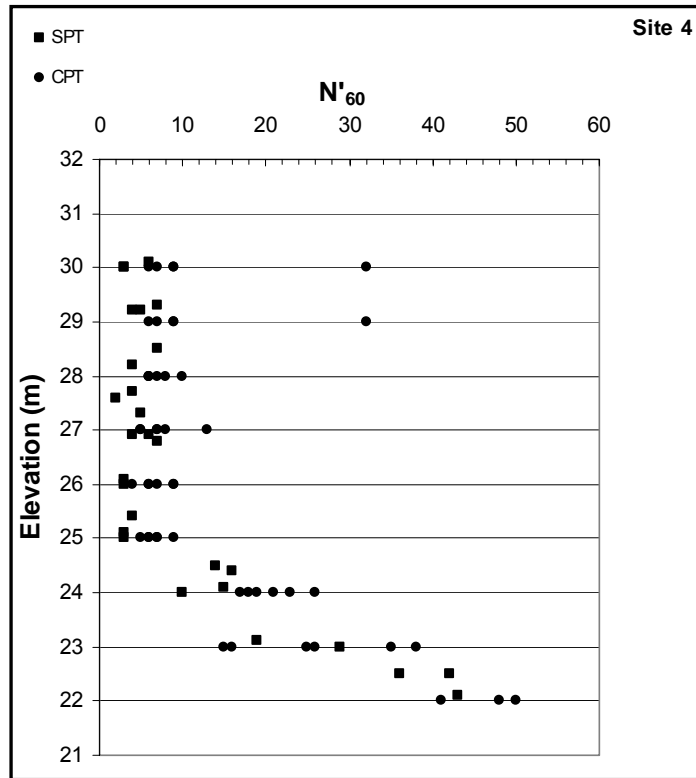


**Figure 6.13** Relationship between  $N'_{60}$  and Elevation for Site 4

For the first 5 meters in all sites, blow numbers are around 6-8. It indicates the existence of soft clay or loose sand. There is a stiff/dense layer underlies the soft / loose layer. For the layer, blow numbers sometimes reaches up to 50.

A detailed list to identify the soil type is given in table 6.9, proposed by Turkish Seismic Code.

**Table 6.9** Soil groups based on standard penetration test values

Description of Soil Group	Stand. Penetr. (N/30)
Very dense, sand, gravel	>50
Hard clay, silty clay	>32
Dense sand, gravel	30-50
Very stiff clay, silty clay	16-32
Medium dense sand and gravel	10-30
Stiff clay, silty clay	8-16
Loose sand	<10
Soft clay, silty clay	<8

Both the SPT blow numbers and the numbers provided from CPT are used to compute shear wave velocity. There are various Vs-N correlations in the literature. In this study, the empirical correlation proposed by Imai and Tonuchi (1982) was used to estimate the shear wave velocity values for the required points.

$$V_s = 97.0N_{SPT}^{0.314} \quad (6.3)$$

where Vs is in the units of m/s. Shear wave velocity values for the specific point in the sites are listed in tables 6.10 to 6.13.

**Table 6.10** Shear wave velocity values (m/sec) for site 1

Elevation (m)	CPT101	CPT102	CPT103	CPT104	CPT105	CPT106	SPT101	SPT102	SPT103	SPT104	SPT105	SPT106	SPT107
30,0		161	171			171				161		137	
29,0	161	161	150	150	206	161	150		137	150	137	121	137
28,0	150	171	150	171	161	150	137		161	161	121	241	
27,0	187	223	194	187	171	194	137	212		187			206
26,0	200	200	171	245	187	187	179	161	212		171		206
25,0	218	228	330	179	200	212		267	330		346		328
24,0	316	171	232	307		171		187			171		288
23,0	316	194	232			200		171	288				187
22,0	194	194	245			187							218
21,0	179	228	200			187		260	253				

There is no observation for the points painted as dark. The shear wave velocity is used for the following analysis as input parameter.

**Table 6.11a** Shear wave velocity values (m/sec) for site 2

Elevation (m)	CPT201	CPT202	CPT203	CPT204	CPT205	CPT206	CPT207	CPT208	CPT209
30,0	161	161	137	161		161	150	161	137
29,0	121	187	179	187	137	171	194	171	179
28,0	223	179	171	194	187	171	200	187	161
27,0	179	171	161	171	212	161	171	171	200
26,0	206	194	232	223	228	228	179	223	212
25,0	267	277	237	228	228	206	249	277	249
24,0	249	237	241	257	194	223	237	245	237
23,0	194	187	286	237	232	200	187	223	264
22,0	200	223	194	232	194	218	206	206	212
21,0	200	200	171	187	280	241	218	200	212

**Table 6.11b** Shear wave velocity values (m/sec) for site 2

Elevation (m)	CPT210	CPT211	SPT201	SPT202	SPT203	SPT204	SPT205	SPT206	SPT207
30,0	161	187			137	137	150		171
29,0	187	200	150		171	179	194	218	171
28,0	171	187	223	200	194	194	171		171
27,0	161	194	161		187	171	179		218
26,0	218	228	257	194		249	228	194	245
25,0	260	245	260	302		309	212	245	237
24,0	228	218	223			237	218		228
23,0	241	277	212			200	187	194	223
22,0	223	206		212			194		212
21,0	200	232				277			206

**Table 6.12** Shear wave velocity values (m/sec) for site 3

Elevation (m)	CPT301	CPT302	CPT303	CPT304	CPT305	CPT306	CPT307	CPT308	SPT301	SPT302	SPT303	SPT304
31,0	200	212	218	200	171	179	150	171	194	232	150	161
30,0	200	187	218	218	212	212	200	200	187	200	187	179
29,0	161	171	187	150	171	161	150	179	161	161	161	179
28,0	161	171	187	161	161	206	171	179			161	170
27,0	237	257	232	249	253	232	206	228	212	267	267	212
26,0	342	334	332	330	316	321	307	314	312		312	309
25,0		348	357	294	257	338	355	338	312		245	302
24,0		223	314	171	245	283	194	253	223		232	232
23,0		218	232	171	218	237	194	212				

**Table 6.13** Shear wave velocity values (m/sec) for site 4

Elevation (m)	CPT401	CPT402	CPT403	CPT404	CPT405	CPT406	SPT401	SPT402	SPT403	SPT404
30,0		194	171	288	194	179	150	171	137	
29,0	179	171	171	200	187	171	179	187	171	
28,0	171	171	171	150	187	171	161	187	137	
27,0	179	179	161	187	161	218	179	161	206	187
26,0	171	194	194	150	179	171		150		150
25,0	194	179	171	161	179	171	171	150	150	
24,0	270	253	241	260	237	245	241	249	212	249
23,0	228	267	297	304	232	270		307		291
22,0		332	312			328	332	330	312	

## **6.2 Statistical Analysis of Shear Wave Velocity**

Although there are some observations at specific points in the field, there is always a possibility to face a different value. Statistical analysis is one of the methods to evaluate uncertainty of soil properties.

The site is considered as a population, the entire group of individuals that we want information about and the values observed at the points are defined as a sample, the part of the population that we actually examine in order to gather information. Here the shear wave velocity computed in the exploratory points is the sample and all the analysis will be done on the sample to model the population.

In this section, graphical and quantitative analysis are discussed for the variability of shear wave velocity in order to estimate the general behavior of the soil.

### **6.2.1 Graphical Analysis of Shear Wave Velocity**

The main purpose of the graphical analysis is to have a general idea on the sample. Histograms, frequency plots and cumulative histograms are the tools to examine the first step of the statistical analysis.

The shear wave velocity is computed in specific points as a preliminary step for statistical analysis. For computation purposes, a notation is assigned for each layer. As an example, S1A could be expressed as the top layer for the elevations 30.0m to 27.0m in site 1. It covers the shear wave velocities for the corresponding layers already computed in section 6.1.3.

Histogram is the basic plot for graphical analysis. In 4 sites for 12 layers, histograms are plotted. As an example, S3B is plotted in figure 6.14.

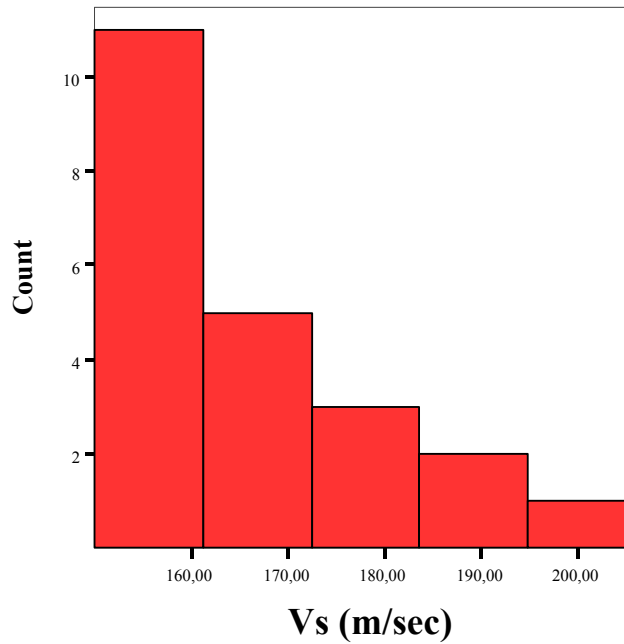


**Figure 6.14** Histogram plot for S3B

Number of the variables in the layer at B in site 3 is 22. By using the equation 2.1 the size for interval is computed as 5. Upper and lower limits of each interval are found by dividing the range to the interval size. The average value for shear wave velocity is 169.14 m/s.

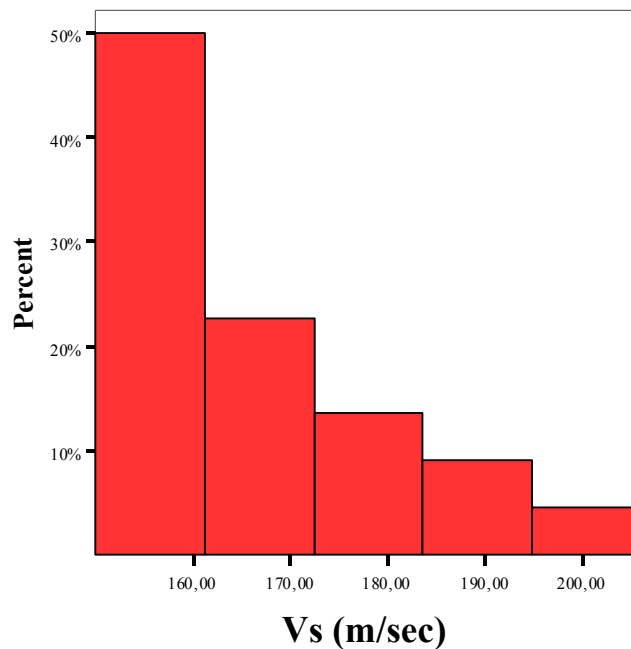


**Figure 6.15** Frequency plot for Vs variable in S3B

Another important graph is frequency plot. Comparing to histogram, there is percent value in stead of count in y axis for frequency plot; meanwhile, the shape is same.

(Figure 6.15) It is pointed in the figure that a probability, to obtain shear wave velocity between 172 and 182 m/s, is about 13%.

The last graphical analysis for variability is the cumulative histogram. It defines the total percentage up to the observation. Cumulative histogram for S3B is plotted in figure 6.16

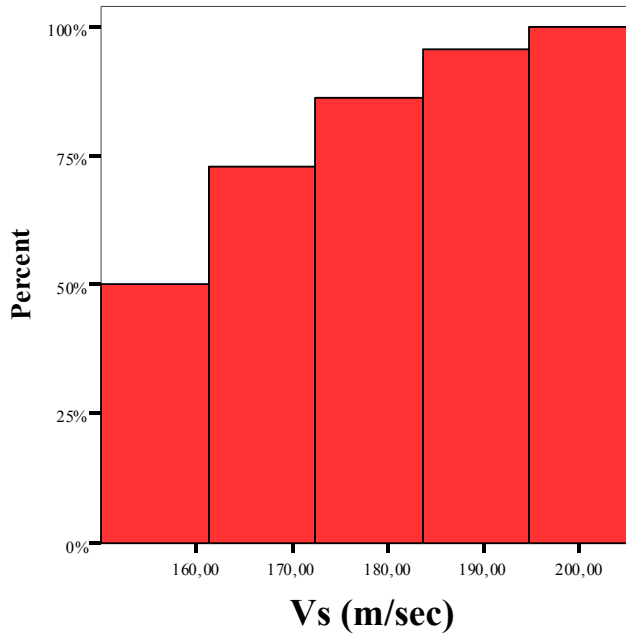


**Figure 6.16** Cumulative Histogram for Vs variable in S3B

As depicted in figure 6.15, the probability to get a shear wave velocity value equal or less than the range 172 to 182 m/s is about 85%. Likewise, the probability to obtain a value equal or less than 206 m/s is 100%, covering the whole data set.

### 6.2.2 Quantitative Analysis of Shear Wave Velocity

In addition to the graphical analysis, the variability in a data set can also be analyzed quantitatively. Quantitative analysis includes computation of mean, variance, standard deviation, skewness and kurtosis for selected data set and also discusses the number of observation, range maximum and minimum values. The outcome of the computation is used to decide the distribution characteristics of the variable.

In 4 sites for 12 layers, the quantitative analysis are performed and listed in table 6.14. For the data set S3B, number of observations, N, is 22. The shear wave velocity values vary in a range from 150 to 206 minimum to maximum, respectively. Mean of the Vs variable is 169.14 m/s which is the arithmetic average, the sum divided by the

number of cases. Standard deviation, the square root of the variance, is a measure of dispersion around the mean. It is computed as 13.16. It is an important parameter for normal distribution, 68% of cases fall within one standard deviation of the mean and 95% of cases fall within two standard deviations. Coefficient of variation, the standard deviation divided by mean, is the indicator to decide the dimension of dispersion around the mean.

Skewness is a measure of the asymmetry of a distribution. The normal distribution is symmetric and has a skewness value of 0.0. Positive skewness has a long right tail whereas, negative has a long left tail. For the S3B the skewness is measured as 1.048 which highlighted the presence of right tail. Other parameter related to the moments is kurtosis, a measure of the extent to which observations cluster around a center point. The normal distribution has a kurtosis value of 0.0. Positive kurtosis indicates that the observations cluster more and have longer tails than those in the normal distribution, and negative kurtosis indicates that the observations cluster less and have shorter tails. For the S3B, the kurtosis is measured as 1.570, highlighting that the observations cluster more and have longer tails.

Besides the statistical values, standard errors have significant role on the analysis. Standard error of the mean, a measure of how much the value of the mean may vary from sample to sample taken from the same distribution is used widely in central tendency analysis. It can be used to roughly compare the observed mean to a hypothesized value (that is, you can conclude the two values are different if the ratio of the difference to the standard error is less than -2 or greater than +2). For the data set S3B, the values in the range from 163.53 to 174.75 verify the tested mean.

**Table 6.14** Descriptive Statistics for Shear Wave Velocity in 4 Sites

	N	Range	Minimum	Maximum	Mean		Std. Deviation	Coefficient of Variation	Skewness		Kurtosis	
	Statistic	Statistic	Statistic	Statistic	Statistic	Std. Error	Statistic	Statistic	Statistic	Std. Error	Statistic	Std. Error
S1A	28	120	121	241	156.64	4.47	23.66	0.15	1.805	0.441	5.589	0.858
S1B	31	209	137	346	214.68	9.46	52.69	0.25	1.428	0.421	1.36	0.821
S1C	26	162	161	323	224.69	9.84	50.18	0.22	0.777	0.456	-0.572	0.887
S2A	64	102	121	223	175.31	2.73	21.82	0.12	0.017	0.299	0.114	0.59
S2B	49	130	179	309	234.65	3.71	25.99	0.11	0.544	0.34	1.094	0.668
S2C	43	115	171	286	215.86	4.21	27.58	0.13	1.133	0.361	0.775	0.709
S3A	24	82	150	232	193.25	4.46	21.83	0.11	-0.449	0.472	-0.348	0.918
S3B	22	56	150	206	169.14	2.8	13.16	0.08	1.048	0.491	1.57	0.953
S3C	50	186	171	357	267.58	7.4	52.3	0.20	0.088	0.337	-1.201	0.662
S4A	53	151	137	288	175.64	3.16	22.99	0.13	2.182	0.327	10.128	0.644
S4B	18	95	212	307	258.5	6.41	27.18	0.11	0.431	0.536	-0.595	1.038
S4C	6	20	312	332	324.33	3.95	9.67	0.03	-0.87	0.845	-1.891	1.741

Standard error of skewness is another important parameter. The ratio of skewness to its standard error can be used as a test of normality (normality could be rejected if the ratio is less than -2 or greater than +2). Likewise, standard error for kurtosis is an indicator of normality. If the ratio of kurtosis to its standard error is less than -2 or greater than +2, the hypothesis should be rejected.

Standard errors for skewness and kurtosis are computed as 0.491 and 0.953, respectively. The skewness error is out of limits. So, it is suggested to reject the normality on the basis of standard error analysis although standard error for kurtosis supports the hypothesis. Whether the hypothesis by the method of errors is accepted, it should be supported by the parametric or non-parametric tests.

To analyze the distribution pattern of the data set, S3B it is recommended to draw a curve on the graphical analysis. The curve will tell the shape of the distribution. Figure 6.17 shows the frequency plot of the S3B and fitted normal curve

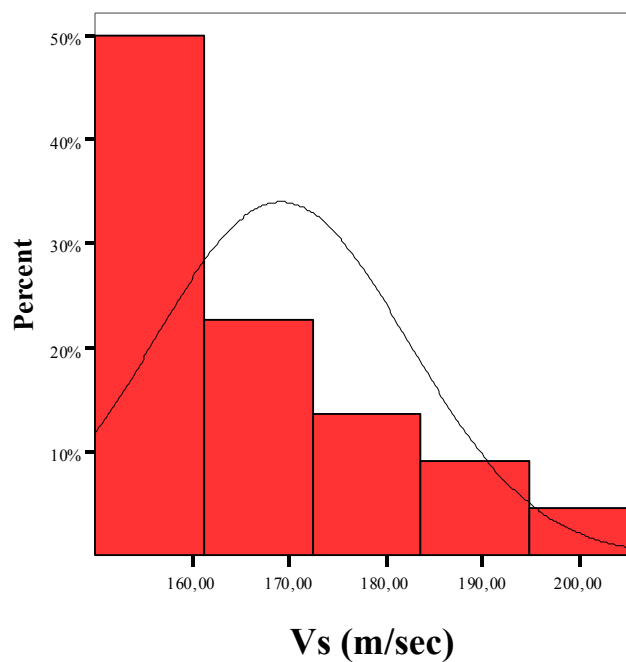


**Figure 6.17** Frequency plot for Vs variable in S3B with fitted normal curve

As depicted in figure 6.17, It is clear that there is a right long tail in other words a positive skewness. Most of the data clustered on the left side of the distribution. Therefore, the shear wave velocity variable is assumed to have a log-normal distribution in the site 3 for the layer B.

Each variable is converted to the logarithmic scale. Hence following analysis are done on the basis of log-normal distribution. New histogram is plotted in figure 6.18.

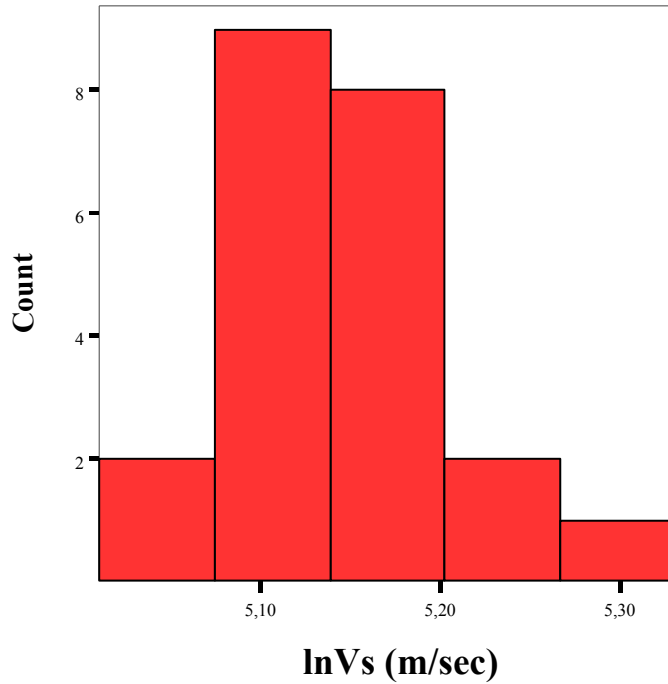


**Figure 6.18** Histogram plot for lnVs variable in S3B

The shape of the histogram, plotted in figure 6.18 is nearly a bell shape curve. So it is assumed as normal distribution on the basis of lnVs variable.

For the 12 layers already examined the proposed distributions are listed in table 6.15.

**Table 6.15** Proposed distributions for 12 layers in the area of interest

Layer	Distribution
S1A	Lognormal Distribution
S1B	Lognormal Distribution
S1C	Gamma Distribution
S2A	Normal Distribution
S2B	Normal Distribution
S2C	Gamma Distribution
S3A	Gamma Distribution
S3B	Lognormal Distribution
S3C	Normal Distribution
S4A	Lognormal Distribution
S4B	Gamma Distribution
S4C	N/A

For the layer S4C the data is not enough to estimate a distribution so it is given as N/A The distribution parameters are computed and listed in table 6.16

**Table 6.16** Distribution Parameters for the layers investigated

Layer	Distribution	Mean	Standard Deviation	Mean (ln)	Standard Deviation (ln)	Alpha	Beta	Lambda
S1A	Lognormal Distribution	156.64	23.66	5.04	0.14	-	-	-
S1B	Lognormal Distribution	214.68	52.69	5.34	0.22	-	-	-
S1C	Gamma Distribution	224.69	50.18	-	-	20.05	11.24	0.09
S2A	Normal Distribution	175.31	21.82	-	-	-	-	-
S2B	Normal Distribution	234.65	25.99	-	-	-	-	-
S2C	Gamma Distribution	215.86	27.58	-	-	61.25	3.52	0.28
S3A	Gamma Distribution	193.25	21.83	-	-	78.35	2.47	0.41
S3B	Lognormal Distribution	169.14	13.16	5.13	0.08	-	-	-
S3C	Normal Distribution	267.58	52.30	-	-	-	-	-
S4A	Lognormal Distribution	175.64	22.98	5.16	0.12	-	-	-
S4B	Gamma Distribution	258.50	27.18	-	-	90.43	2.86	0.35

To check the validity of the hypothesis, goodness of fit tests should be performed. In this study, Kolmogorov-Smirnov Test (K-S Test) is used in analysis. The test generally compares the cumulative distributions of variability for theoretical and empirical value. For the layer S3B the cumulative distributions both for theoretical and empirical are plotted and maximum differences pointed in figure 6.19

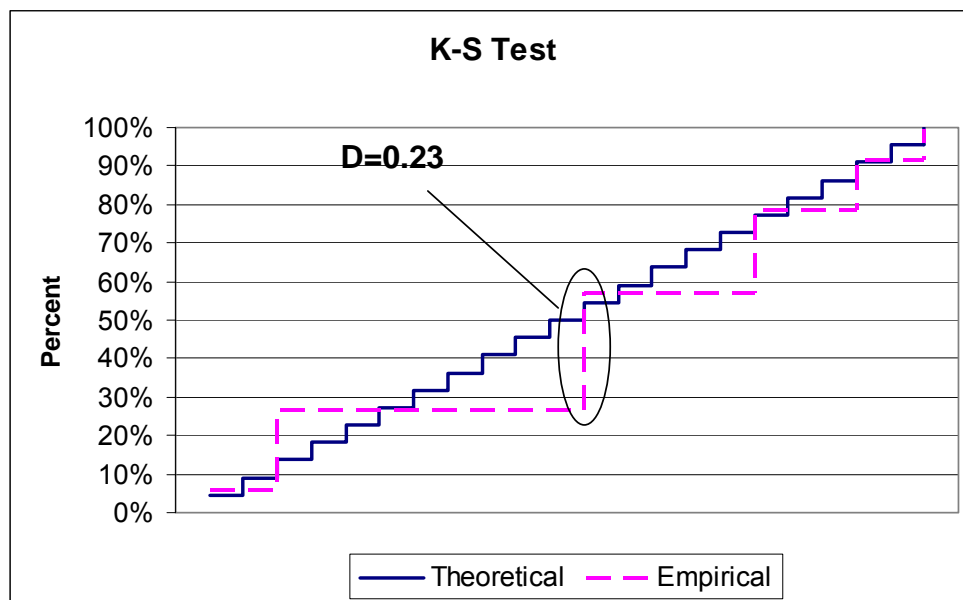


**Figure 6.19** K-S Test application to S3B data set

**Table 6.17** Results for K-S Test

	N	Absolute Difference	Critical Value
S1A	28	0.26	0.22
S1B	31	0.24	0.19
S1C	26	0.27	0.17
S2A	64	0.17	0.13
S2B	49	0.19	0.11
S2C	43	0.20	0.14
S3A	24	0.27	0.13
S3B	22	0.28	0.23
S3C	50	0.19	0.12
S4A	53	0.19	0.15
S4B	14	0.34	0.15
S4C	*	*	*

\* the number of observations for S4C is too few. So there is no estimation for the distribution at layer C in site 4.

Result of K-S test for S3B shows the absolute difference between the cumulative distributions is 0.23. The D value should be in limits to accept the hypothesis. Critical value for the difference should be taken from table 2.5. The C value is 0.23, since it is larger than the computed difference, the hypothesis is approved. K-S test results are given in table 6.17.

Gamma distribution has two main parameters; one is for scale and the other for shape characteristics. Both parameters are computed by using the mean and standard deviation of the data set. For the following analysis,  $\alpha$  is defined as shape parameter and  $\beta$  is scale parameter. In literature, sometimes in stead of  $\beta$  a new scale parameter  $\lambda$ , inverse of  $\beta$ , is used. The parameters are found by using the formulas below;

$$\mu = \alpha\beta \quad (6.4)$$

$$\sigma^2 = \alpha\beta^2 \quad (6.5)$$

$$\lambda = 1/\beta \quad (6.6)$$

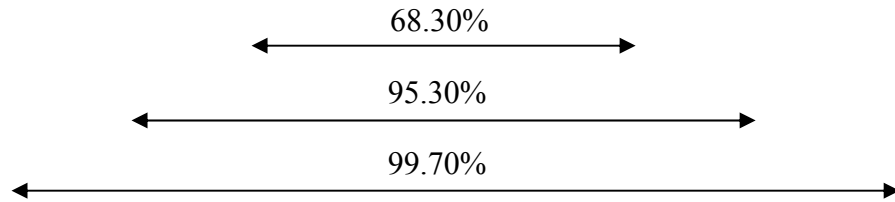
As mentioned in section 2.4.2, gamma distribution could be used as general probability distribution if skewness exists.

Alpha and Beta parameters are computed for the layers. The parameters corresponds to the case III in section 2.4.2 which indicated that, the distribution assumed as a unimodal but skewed shape and since the alpha parameter is relatively high, the skewness of the distribution is reduced.

For proposed distributions, with the computed parameters, it can be determined that 68.3% of scores will fall within 1 standard deviation above and below the mean, 95.4% of scores will fall within 2 standard deviations above and below the mean and that 99.7% of scores will fall within 3 standard deviations below or above the mean. Table 6.18 shows the limits of the probability of occurrence. The boundaries are computed by using bootstrap method (Davison and Hinkley, 1997). For the layer S3B, shear wave velocity population varies between 134.56 and 212.30. there is no chance to observe any value out of limits under the assumption. Similarly, the values in the site is accepted to distribute between 156.65 and 182.36 with the probability of 68.3%

**Table 6.18** Shear wave velocity (m/sec) distribution and probability to observe for each layer

Layer	3 <sup>rd</sup> boundary	2 <sup>nd</sup> boundary	1 <sup>st</sup> boundary	Mean	1 <sup>st</sup> boundary	2 <sup>nd</sup> boundary	3 <sup>rd</sup> boundary
S1A	101.49	116.75	134.29	156.64	177.68	204.38	235.1
S1B	107.77	134.29	167.34	214.68	259.82	323.76	403.43
S1C	110.12	135.24	174.02	224.69	273.93	333.82	387.54
S2A	109.85	131.67	153.49	175.31	197.13	218.95	240.77
S2B	156.68	182.67	208.66	234.65	260.64	286.63	312.62
S2C	147.61	165.04	190.03	215.86	245.86	276.48	300.05
S3A	137.02	149.76	168.90	193.25	212.35	235.24	252.6
S3B	134.56	145.18	156.65	169.14	182.36	196.76	212.30
S3C	110.68	162.98	215.28	267.58	319.88	372.18	424.48
S4A	121.51	137.00	154.47	175.64	196.37	221.41	249.64
S4B	187.92	207.56	231.03	258.50	285.86	314.64	338.78



Turkish Seismic Code classifies the soils due to the shear wave velocity values already observed in the layer (Table 6.19). Critical values are 200, 300, 400 and 700 m/sec. Because of the boundaries defined in the code, it is required to estimate the soil class by the computed probability.

**Table 6.19** Soil groups based on shear wave velocities (m/sec)

Description of Soil Group	Shear Wave Velocity (m/sec)
Very dense, sand, gravel	>700
Hard clay, silty clay	>700
Dense sand, gravel	400-700
Very stiff clay, silty clay	300-700
Medium dense sand and gravel	200-400
Stiff clay, silty clay	200-300
Loose sand	<200
Soft clay, silty clay	<200

**Table 6.20** Probability to observe shear wave velocity below the given limits

layer	Distribution	Shear Wave Velocity (m/sec)		
		<200	<300	<400
S1A	Lognormal Distribution	96.80%	100.00%	100.00%
S1B	Lognormal Distribution	42.50%	95.10%	99.90%
S1C	Gamma Distribution	33.90%	92.70%	99.80%
S2A	Normal Distribution	87.10%	100.00%	100.00%
S2B	Normal Distribution	9.20%	99.40%	100.00%
S2C	Gamma Distribution	26.20%	99.80%	100.00%
S3A	Gamma Distribution	66.60%	100.00%	100.00%
S3B	Lognormal Distribution	58.70%	77.30%	87.10%
S3C	Normal Distribution	9.80%	73.20%	99.30%
S4A	Lognormal Distribution	87.50%	100.00%	100.00%
S4B	Gamma Distribution	1.10%	93.30%	100.00%

For the layer S3B, the shear wave velocity values are expected to be below 200 m/sec with a possibility of 58.7%. The probability to face a value between 200 and 300 m/sec is 18.6% and with the probability 12.9% the shear wave velocity values are in the range of 300 to 400 m/sec.

### 6.3 Geostatistical Analysis of Shear Wave Velocity

Geostatistical data, also termed random filed data consist of measurements taken at fixed locations. Specifically, this section discusses the variogram analysis and kriging.

The main idea of geostatistical method is to relate the spatial variation to the distance lag for a population. As examined in previous sections, shear wave velocity is computed by using empirical formula at specific points. Geostatistics deals with the coordinates of the each shear wave velocity variable and create a function in order to describe the variation.

The first and most important step in evaluation process is defining the coordinates of the points. Although the boring logs are shown in the site maps in section 6.1.2, there should be more comprehensive investigations for the computation process.

### 6.3.1 Line description for Geostatistical Analysis

The need to define coordinate scale for geostatistical analysis leads to define a new order for the boring locations. For each site, one imaginary line, covers most of the boring location in the site is appointed. The lines and distances between the performed test are shown in figure 6.20 to figure 6.23

Name	Distance from CPT104 (m)
CPT104	0
SPT103	5
SPT104	15
SPT105	20
CPT105	22
SPT106	25
SPT107	35
CPT106	40

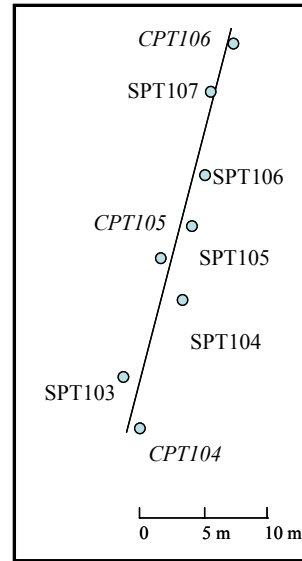


**Figure 6.20** Line 1 defined for geostatistical analysis in site 1

Name	Distance from CPT201 (m)
CPT201	0
SPT201	15
CPT202	20
SPT202	30
SPT203	35
SPT204	40

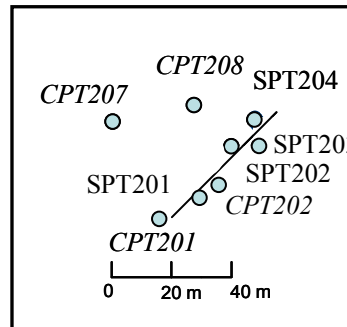


**Figure 6.21** Line 2 defined for geostatistical analysis in site 2

Name	Distance from CPT301 (m)
CPT301	0
SPT301	10
CPT302	15
SPT302	16
CPT303	20
CPT304	25

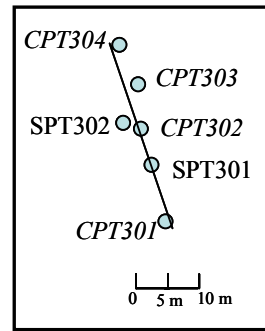
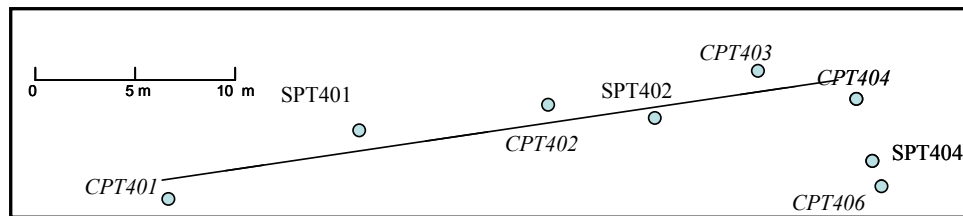


**Figure 6.22** Line 3 defined for geostatistical analysis in site 3



Name	Distance from CPT401 (m)
CPT401	0
SPT401	10
CPT402	20
SPT402	25
CPT403	30
CPT404	35

**Figure 6.23** Line 4 defined for geostatistical analysis in site 4

Shear wave velocity values for each exploratory depth is shown in figure 6.24 to figure 6.27. In order to get first comment on data set statistical analysis for line 1 is computed. There are 46 observations varying in a range from 121 to 345 m/s. Mean value and standard deviation for the variable are 198.24 and 56.94, respectively. It has a positive skewness, 1.168 which shows the cluster on the left in pdf.

To be a preliminary research for geostatistical evaluation for line 2 the descriptive statistics parameters are examined. For 52 computed shear wave velocity values, minimum and maximum observations are 137 and 285 m/s, respectively. Average is 202.06 m/s and standard deviation is 33.45. The observations are plotted in figure 6.24

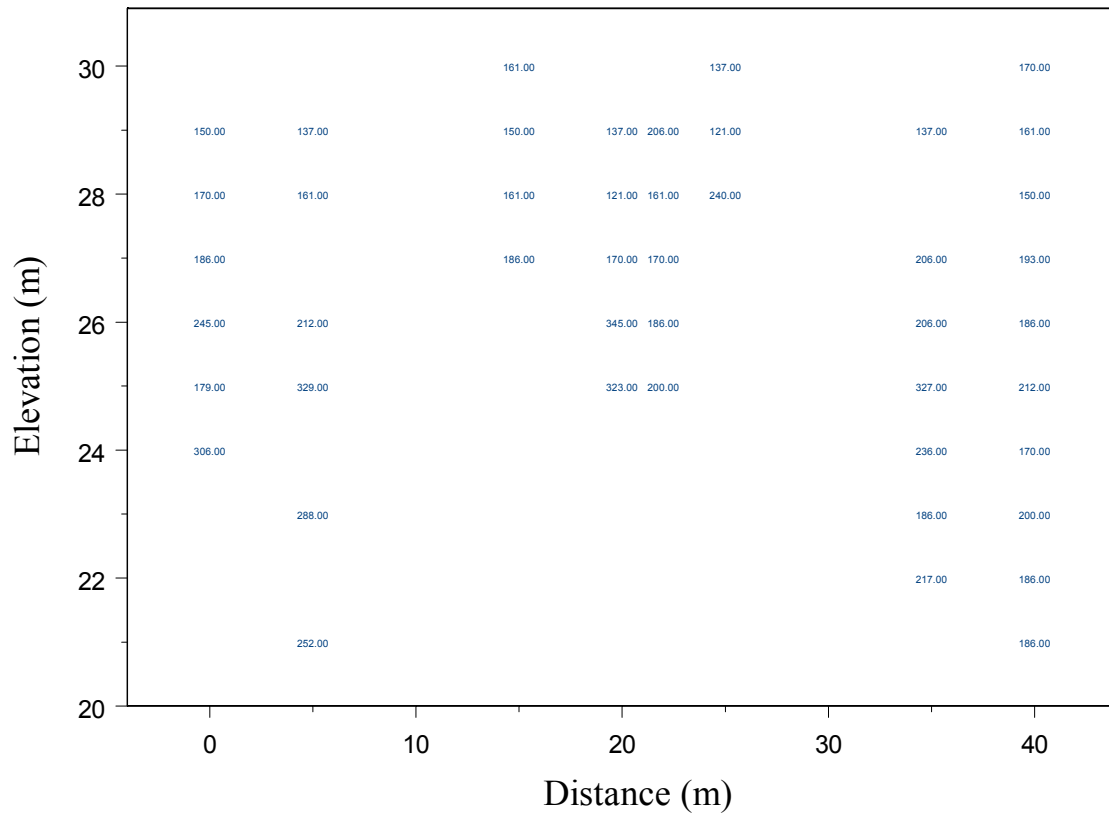


Figure 6.24 Shear wave velocity values (m/sec) shown in elevation distance map for line 1

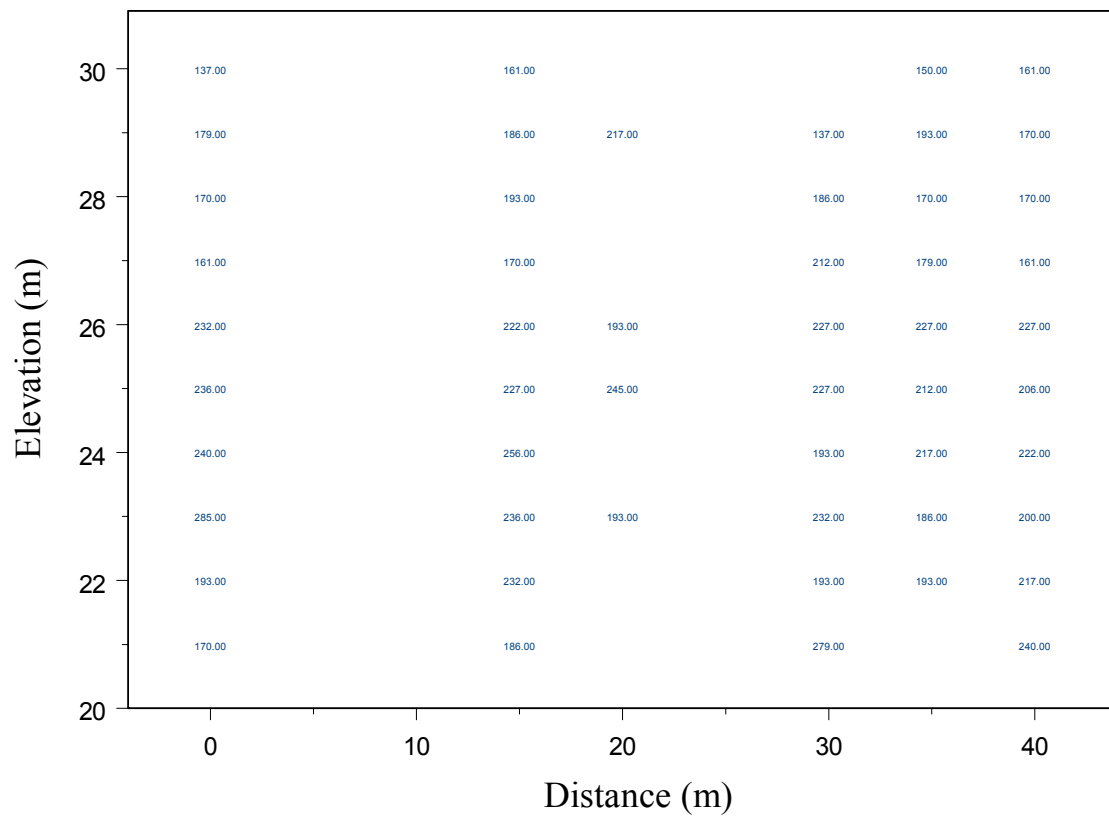


Figure 6.25 Shear wave velocity values (m/sec) shown in elevation distance map for line 2

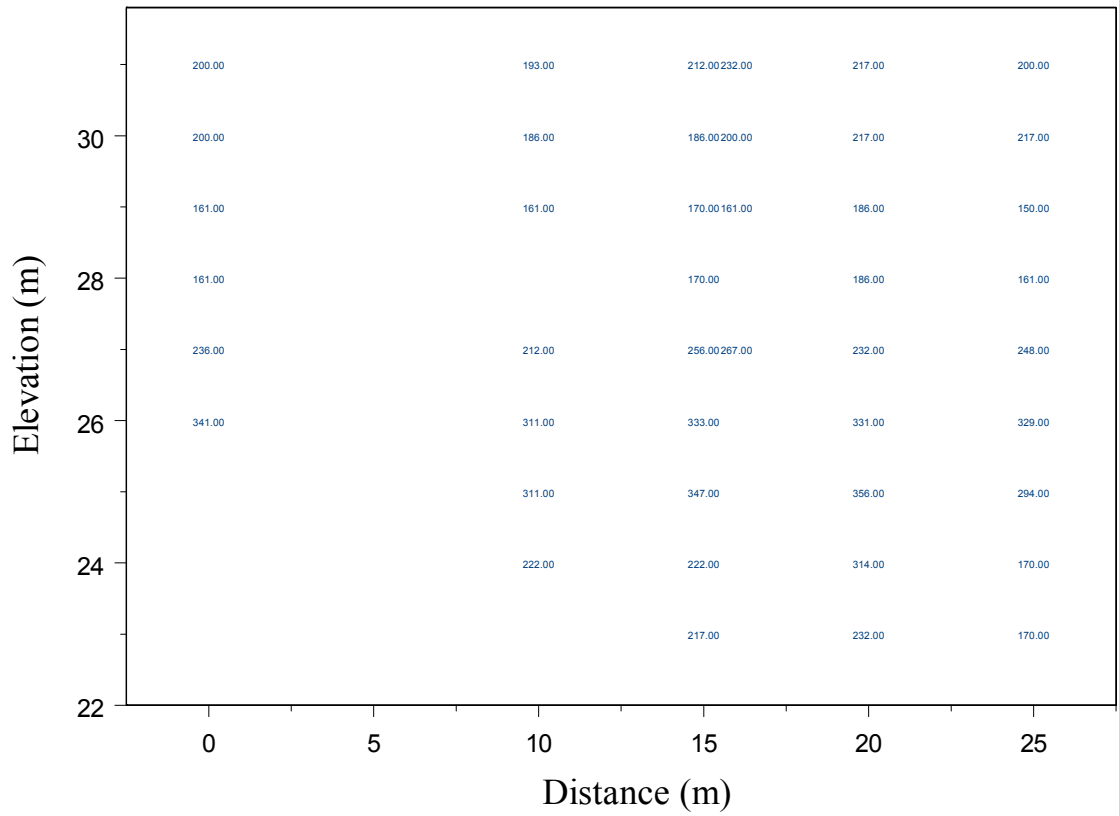


Figure 6.26 Shear wave velocity values (m/sec) shown in elevation distance map for line 3

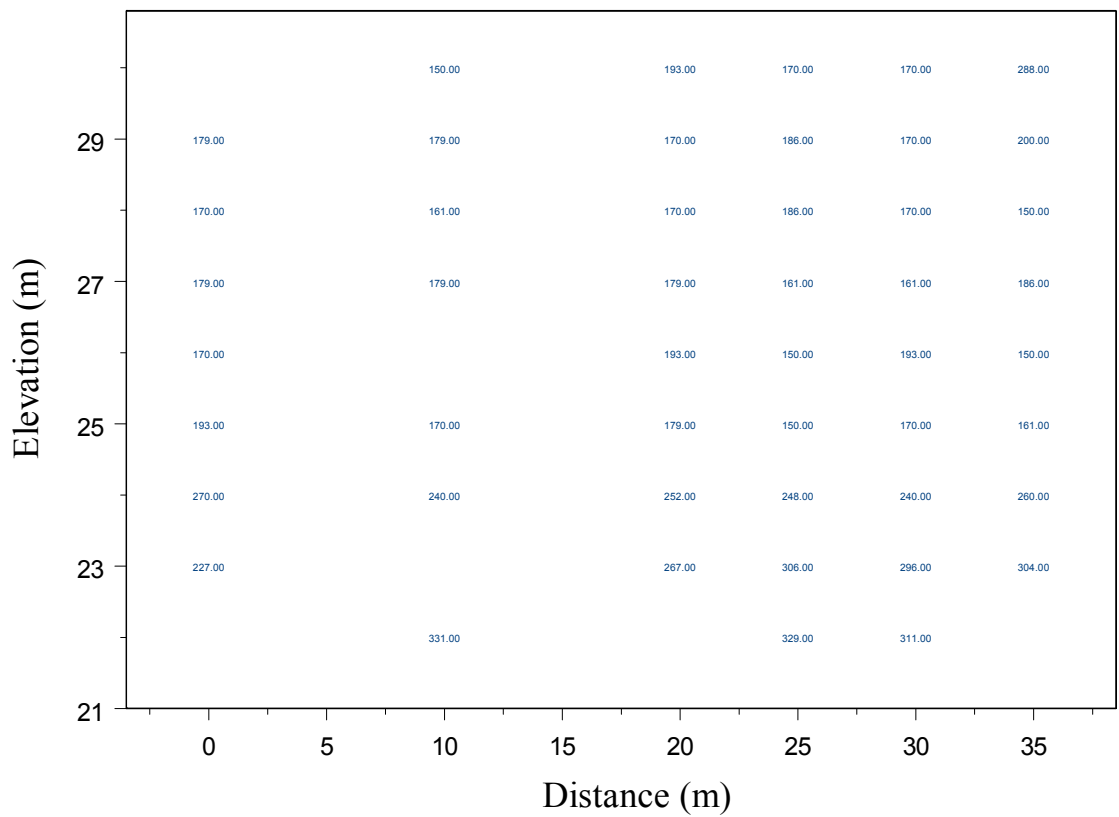


Figure 6.27 Shear wave velocity values (m/sec) shown in elevation distance map for line 4

Shear wave velocity is varies in a range of 150 to 356 m/s for 44 observations for line 3. Two significant parameters are computed in order to define statistical behavior of variable. Mean is 229.05 m/s and standard deviation is 60.60. Dispersion around the mean is relatively high where the coefficient of variation is 0.265. Data set for line 3 is shown in figure 6.26

Line 4 is the focus of interest for geostatistical analysis in site 4. In order to have an idea on the variability of shear wave velocity in the site, descriptive statistical parameters are computed. Minimum and maximum observations are 150 and 331 m/s respectively, whereas mean and standard deviation is found out as 205.57 m/s and 53.90. Figure 6.27 presents the locations of each shear wave velocity values in line 4.

### **6.3.2 Variogram Estimation for Shear Wave Velocity**

For the defined lines in the previous section, it is required to determine variogram in order to model the shear wave velocity profile. The existence of the variogram is based on the assumption of intrinsic stationarity of the random function. Actually, the intrinsic stationarity implies a process with a constant mean and with a variance for shear wave velocity values defined only through the magnitude of  $h$ .

The first step to obtain a variogram from a data set is to plot variogram cloud. Variogram cloud is a tool, used to assess variability with increasing distance. It is the distribution of variance between all pairs of points at all possible distance,  $h$ . Squared differences cloud which is used to define variance function of interest, results in a plot of  $(X_{i+h} - X_i)^2 / 2$  versus  $h$ . The variability at small distances appears a bit less than that for larger distances. The squared-differences variogram cloud for line 1 is illustrated in figure 6.28.

As depicted in figures 6.24 the difference between the columns is generally 5m. In the same way, difference between the rows is 1m. That is the reason why the points clustered on integer distances. Maximum distance for the variogram analysis indicates the maximum reliable distance. So, reliable distance should be decided by the evaluation of the whole analysis. Decrease on the distance provides a clear plot in order to analyze. In figure 6.28 for the analysis of line 1 the reliable distance is chosen as 20 m.

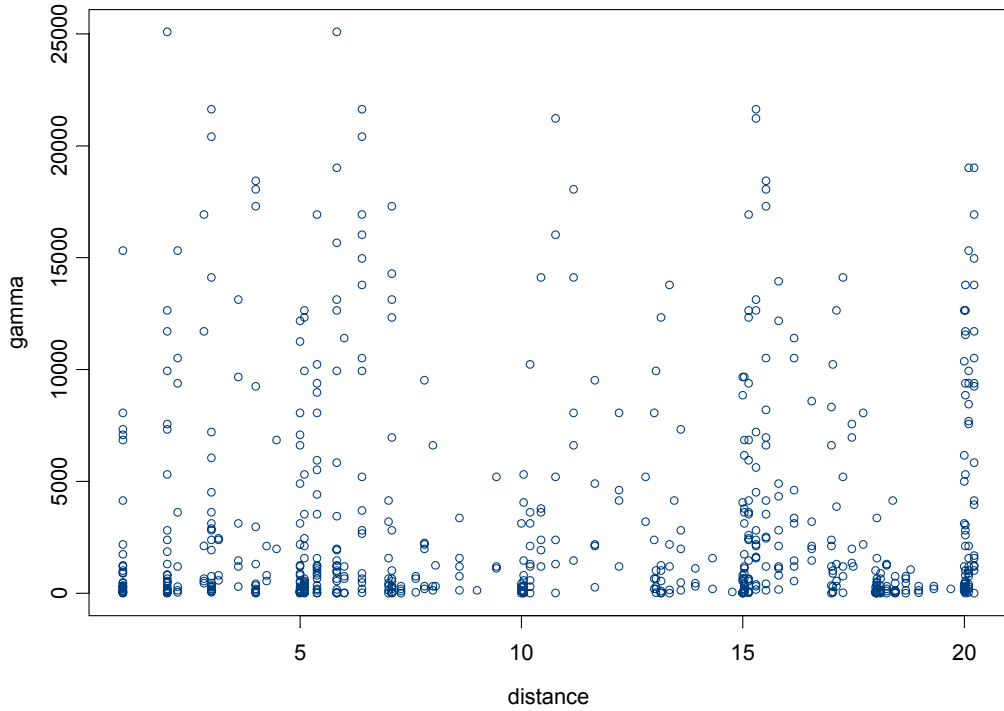


**Figure 6.28** Squared-differences variogram cloud for line 1

The experimental variogram is the second step for geostatistical analysis. It provides a description of how the data is correlated with distance. The variogram function, as given in equation 6.7, is used to compute the Experimental variogram values.

$$\gamma(h) = \frac{1}{2N(h)} \sum_{i=1}^{N(h)} [X_i - X_{i+h}]^2 \quad (6.7)$$

where,  $X_{i+h}$ ,  $X_i$  are the variables at the points  $x_{i+h}$  and  $x_i$ , respectively.  $N(h)$  is the number of pairs for selected distance. As mentions in previous section,  $(X_{i+h} - X_i)^2 / 2$  defines the variogram cloud. So, the result of variogram function is average of the variogram cloud for related distance.

To plot the Experimental variogram, some parameters already defined in literature should be described. Number of pairs is mentioned, difference between the pairs is same for defined lag distance. Lag distance or shortly, lag is the computed distance which is expressed by  $h$ . Number of lags is used to characterize the area of interest. It has a relationship between maximum distance in other words, reliable distance. Number of lags is computed by dividing maximum distance to the lag distance. Lag tolerance is a numerical value defines the tolerance for the lag distance.

Computed direction is important in variogram analysis. The variable could change in different directions. For the shear wave velocity values, since it is investigated in one direction as a line, it is assumed to have no effect of anisotropy. If the direction exists, the effect is considered with the parameter azimuth.

Third step for geostatistical analysis is to model the experimental variogram. It is necessary to define a model in order to use in kriging section. Since the variance of the predicted values is positive the experimental variogram must be replaced with a theoretical variogram. Most common theoretical variogram models are exponential, spherical and gaussian as bounded variogram functions and linear and power as unbounded functions. All of the theoretical functions require specification of a distance factor. The exponential, gaussian and spherical models also requires a range value whereas, linear and power models use slope as parameter.

For the shear wave velocity values arranged on a line, Experimental variograms are plotted and theoretical models are fitted to the variograms. As an example, variogram for line 1 is plotted and discussed. Other results for variograms are given in appendix III

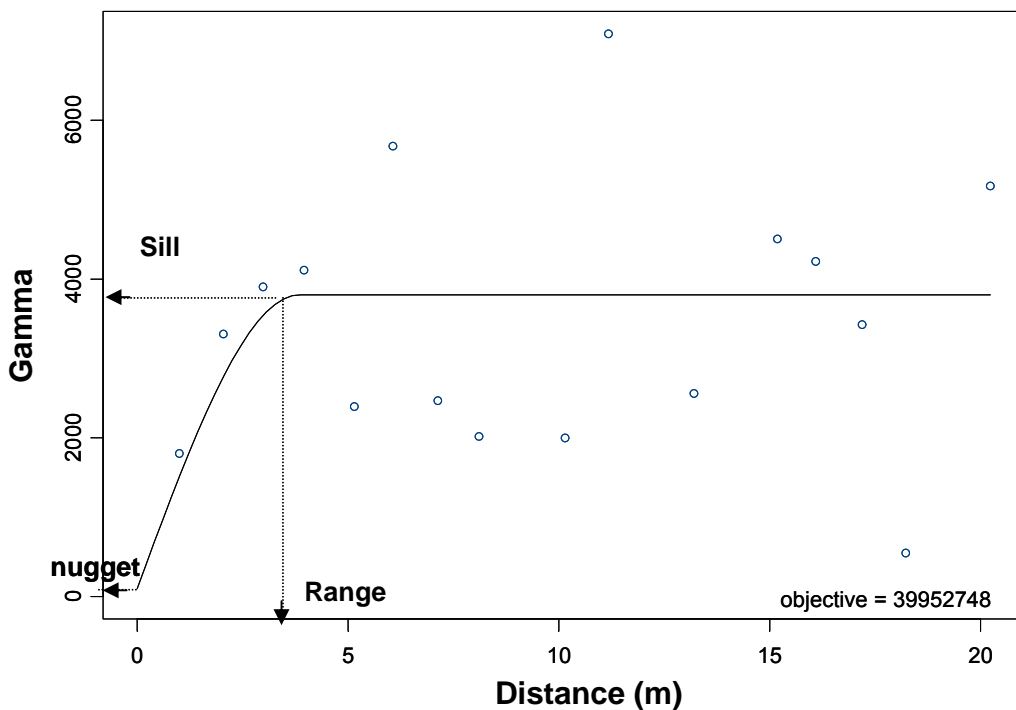


**Figure 6.29** Experimental Variogram and Model fitting for line 1

Objective value for the graph is a relative measure to indicate the fitness of the sum of the differences between the square of experimental and theoretical gamma values. For the lines including the shear wave velocity values the best theoretical models are searched and fitted. Experimental and model variogram for line 1 is shown in figure 6.29.

The values pointed in the variogram graph are the average values of gamma values for corresponding distance in variogram cloud. Table 6.21 is the list of points already plotted in figure 6.29. Distance column is the difference between the coordinates for each regionalized variable, here it is shear wave velocity. There are 34 number of pairs which has 1.00 m distance among the points. Azimuth is selected zero since there is no direction effect for the analysis.

**Table 6.21** Experimental variogram result for line 1

Distance	Gamma	N.Pairs	Azimuth
1.00	1801.68	34	0
2.04	3308.04	42	0
2.99	3900.28	34	0
3.96	4111.80	27	0
5.15	2391.78	86	0
6.07	5673.68	48	0
7.13	2466.16	34	0
8.11	2014.94	17	0
10.15	1995.66	34	0
11.18	7087.75	16	0
13.20	2558.28	32	0
15.18	4504.16	92	0
16.09	4220.50	23	0
17.20	3425.10	30	0
18.23	545.82	48	0
20.23	5172.81	116	0

In order to decide the type and parameters of the model variogram, the objective value is used as an indicator. Best estimate for the selected experimental variogram is spherical variogram with the parameters; range=3.85m, sill=3700 and nugget=100. There is no correlation for the shear wave velocity values along the line if the lag distance is more than 3.85m. It is clear that the dispersion on the right of the range value is definitely couldn't ignored in figure 6.29

Variance of the shear wave velocity along the line is equal to the sill value. Standard deviation is computed as 60.83 for line 1. Nugget effect is the initial effect including measurement errors and short distance variation. With a standard deviation of 10, the small dispersion effect is taken into account.

The model variograms and parameters of the models are listed in table 6.22.

**Table 6.22** Parameters for the model variogram for defined lines

	Line 1	Line 2	Line 3	Line 4
Number of Data Points	46	52	44	48
Model	Spherical	Spherical	Spherical	Spherical
Range	3.85	3.50	3.20	7.00
Sill	3700	1150	4050	4500
Nugget	100	500	0	250
Standard Deviation for Vs	60.83	25.50	63.64	67.08
Standard Deviation for Initial Effect	10.00	22.36	0.00	15.81

Range of the model is the distance at which data are no longer correlated. For the lines already defined, a minimum distance 3.20m is computed as the correlation distance in line 3, whereas the maximum is in line 4 with a value 7.00m. Sill value is the variance of the regionalized variable. Standard deviations for the line 1, line 2, line 3 and line 4 are 60.83, 25.50, 63.64 and 67.08, respectively. The computed standard deviations are slightly different from the values calculated by the statistical analysis. That is why, the reliable distance limits size of the data. Missing in the data could change the dispersion around the mean. Nugget effect is generally described as the micro-scale variation or measurement error. There is a significant effect on line 2 where the variance is nearly equal to the nugget.

The results of model variogram is used in interpolation techniques, here it is called as kriging.

### 6.3.3 Kriging for Shear Wave Velocity

Kriging is an interpolation technique that satisfies values for unknown locations from observations at known locations. It uses the variogram model as input and with the matrix, mentioned in section 3.7 attains to the value at required point. Theoretical covariance functions, obtained from the bounded variogram models; exponential,



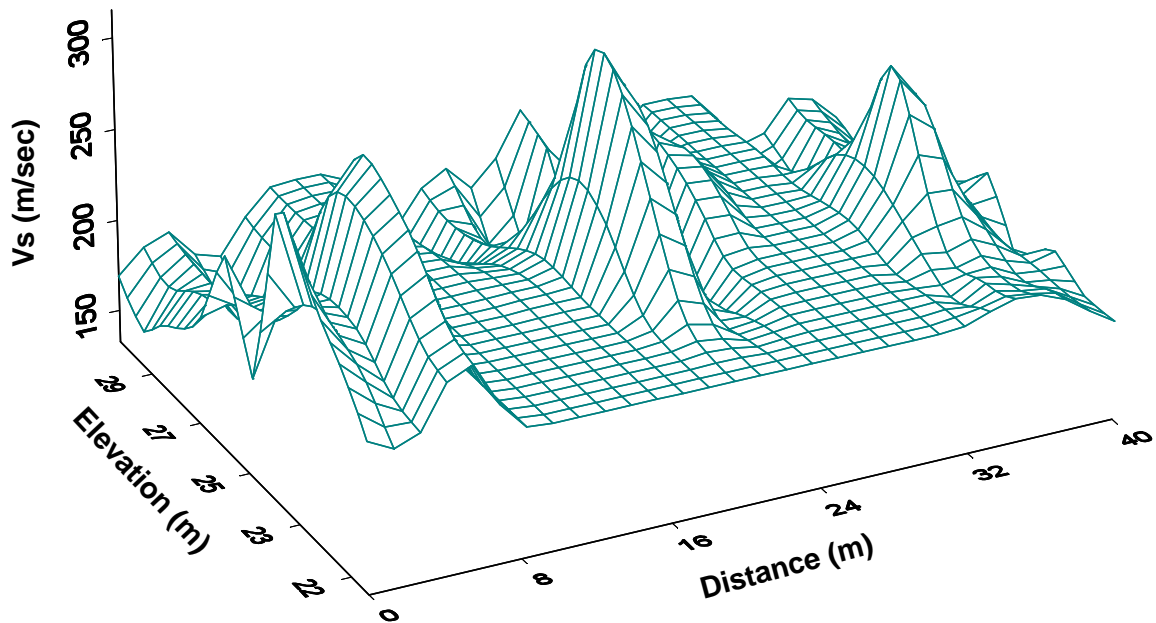


**Figure 6.31** 3-D Surface Map for kriging of line 1

By using the kriging technique the soil is modeled for shear wave velocity variable. The range is found out 3.85 for line 1. So, further site investigations should be done with the consideration of correlation distance.

Geostatistical Analysis used to define the correlation between each variable. In other words, shear wave velocity values are defined as regionalized variable in stead of random variable. By using limited observations, 46 points for the line 1, kriging technique predicts 900 data for the shear wave velocity profiles for the defined coordinates.

Computed shear wave velocity profiles is used for the seismic behavior of the soil profile in the following section.

#### **6.4. Site Response of Adapazari Soil Deposits**

Field study and laboratory research, performed after the Kocaeli earthquake on Adapazari soil deposits are the initial point in this study. By using standard penetration test and cone penetration test results for 4 sites, soil profiles were determined. In order to examine variability of shear wave velocity in the sites, SPT-

Vs correlations are used. Statistical and geostatistical analysis methods were applied for shear wave velocities in the sites. The soil was modeled for shear wave velocities along 4 different lines. (See figures, 6.21, 6.22, 6.23 and 6.24)

In this section, response analysis of the modeled soil profiles are studied.

#### 6.4.1. Input Motion

For the site response analysis for the modeled soils in Adapazari basin, SKR ground motion record observed in 1999 Kocaeli earthquake is used as input motion. The acceleration time history of the record is given in figure 6.32.

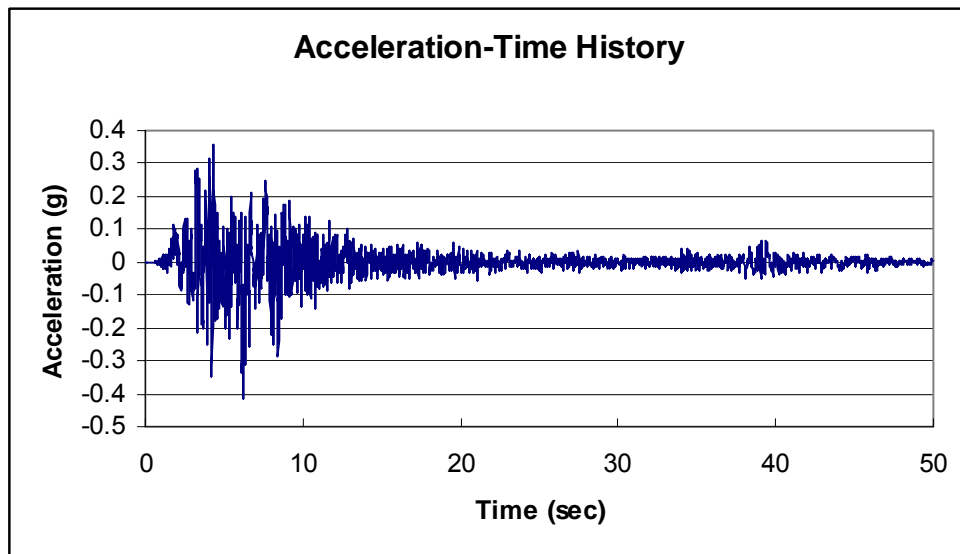


**Figure 6.32** SKR Station, E-W record from 1999 Kocaeli Earthquake used as input motion

The only record obtained from the station is for transverse direction. A peak acceleration of 0.41g is the maximum observed value obtained from the ground motion stations during the earthquake. As an input parameter, it is necessary to modify the peak acceleration to outcrop record. From the many analysis performed by one dimensional response analysis with the numerical tool Proshake indicated that the outcrop record can be chosen as 0.24g.

#### 6.4.2. Soil Profile

In previous chapters, soil is modeled both with statistical and geostatistical analysis. Models herewith are converted to the finite element meshes in order to perform in site response analysis.

For the statistical analysis, mean value of shear wave velocity variable for each soil layer is taken as  $V_s$  value. For geostatistical analysis in order to take into account the kriging maps, it is necessary to assign grids and divide the soil profile to the clusters. For the best estimates, the dimensions of each cluster were 1m vertically and 5m horizontally.

In this thesis, the top 10 m of the soil profile are discussed. However it is necessary to reach bedrock in order to input earthquake record. Therefore, the boring log suggested by Bray et al(2004) given in figure 4.7 is used for the analysis from 10m till bedrock.

Defined finite element mesh by statistical and geostatistical analysis for line 1 are given in figure 6.33 and 6.34.

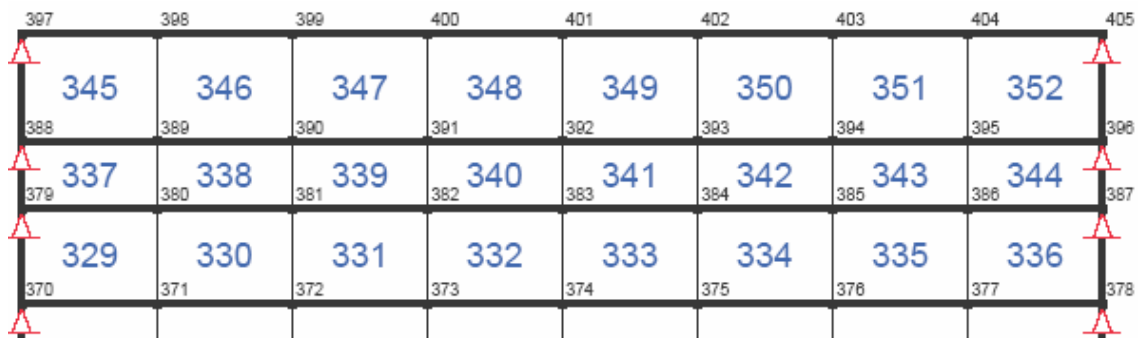


**Figure 6.33** Finite element mesh for top 10 m for statistically modeled soil profile (line 1)

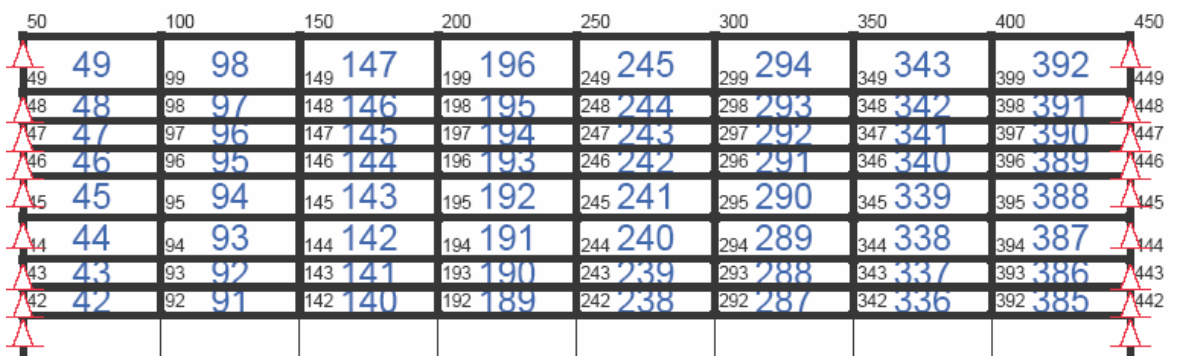


**Figure 6.34** Finite element mesh for top 10 m for geostatistically modeled soil profile (line 1)

For statistically modeled profile there are 3 materials, 352 elements and 405 nodes describing the existing situation for line 1, whereas, 64 materials 450 nodes and 392 elements are used for geostatistically modeled soil profile for line 1. The mesh used in analysis including the imported profile from figure 4.7 is given in figure 6.35



**Figure 6.35** Finite element mesh used in analysis including the imported soil profile from Bray et al (2004) (line 1)

Input parameters used in the analysis are Vs values computed by statistical and geostatistical analysis, poisson's ratio and unit weight of the soil. Shear wave velocity values for materials are given in tables 6.23 and 6.24

**Table 6.23** Vs values computed based on geostatistical analysis for line 1

Layer*	Relative Distance**	Material ID	Vs (m/s)	Layer*	Relative Distance**	Material ID	Vs (m/s)
1	0	17	173	6	0	12	258
1	5	25	166	6	5	20	235
1	10	33	190	6	10	28	202
1	15	41	170	6	15	36	221
1	20	49	176	6	20	44	209
1	25	57	184	6	25	52	202
1	30	65	187	6	30	60	213
1	35	73	175	6	35	68	205
2	0	16	172	7	0	11	245
2	5	24	185	7	5	19	225
2	10	32	190	7	10	27	202
2	15	40	161	7	15	35	204
2	20	48	163	7	20	43	201
2	25	56	197	7	25	51	202
2	30	64	184	7	30	59	202
2	35	72	168	7	35	67	197
3	0	15	183	8	0	10	226
3	5	23	190	8	5	18	218
3	10	31	195	8	10	26	202
3	15	39	176	8	15	34	202
3	20	47	189	8	20	42	202
3	25	55	210	8	25	50	202
3	30	63	194	8	30	58	204
3	35	71	182	8	35	66	197
4	0	14	203	9	0	9	250
4	5	22	201	10	0	8	300
4	10	30	200	11	0	7	325
4	15	38	214	12	0	6	325
4	20	46	207	13	0	5	350
4	25	54	213	14	0	4	400
4	30	62	205	15	0	3	600
4	35	70	201	16	0	2	600
5	0	13	218	17	0	1	750
5	5	21	226				
5	10	29	202				
5	15	37	240				
5	20	45	220				
5	25	53	206				
5	30	61	224				
5	35	69	218				

\* layers are assigned from top to bottom with an increasing order

\*\* relative distance indicates the distance of each material to the left boundary.

**Table 6.24** Vs values computed based on statistical analysis for line 1

Layer	Relative Distance	Material ID	Vs (m/s)
1	0	12	157
2	0	11	215
3	0	10	225
4	0	9	250
5	0	8	300
6	0	7	325
7	0	6	325
8	0	5	350
9	0	4	400
10	0	3	600
11	0	2	600
12	0	1	750

Equivalent linear model is selected as the constitutive model. Variations of shear modulus and damping ratio with shear strain for clays and for sand are used in equivalent linear model and listed in table 6.25, figure 6.36 and figure 6.37

**Table 6.25** Modulus reduction curves and damping curves for analysis

Soil	Modulus Reduction Curve	Damping Curve
Clay	Seed and Sun, 1989	Idriss, 1990
Sand	Seed and Idriss, 1970	Idriss, 1991

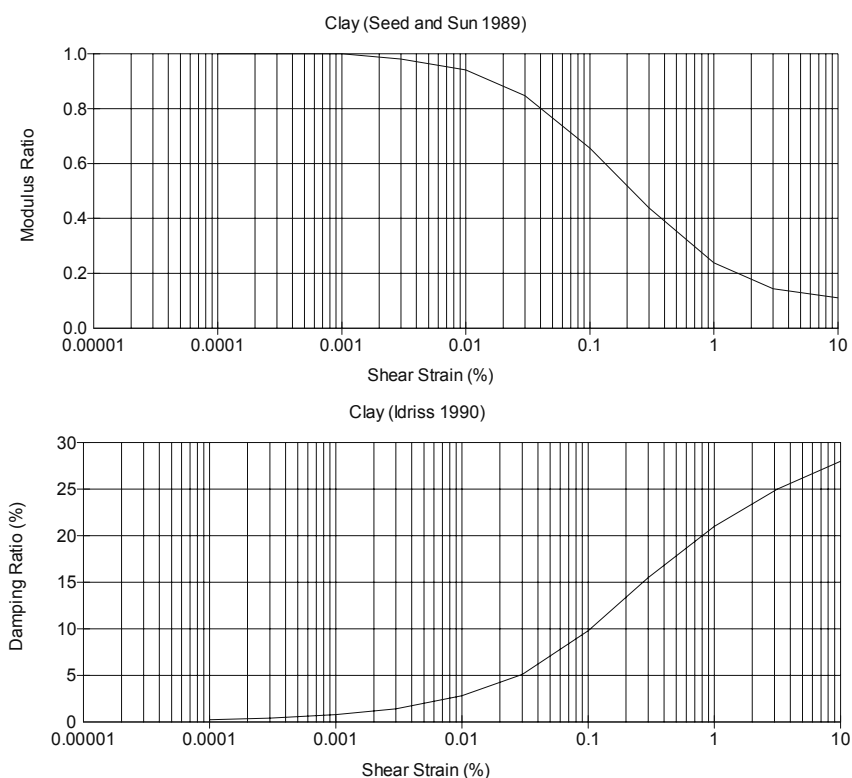


**Figure 6.36** Modulus Reduction and Damping Curves for Clay

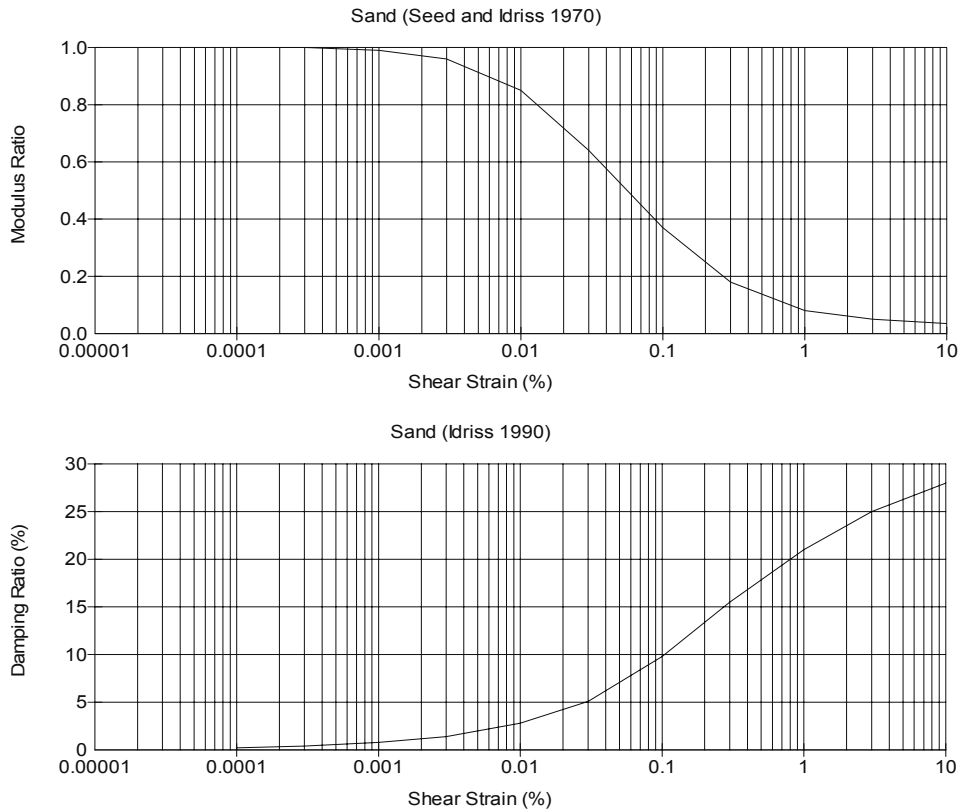


**Figure 6.37** Modulus Reduction and Damping Curves for Sand

### 6.4.3. Results of Analyses

Site response analyses are performed for both statistically and geostatistically modeled soil profiles.

#### *Statistically Modeled Soil Profile*

The soil model used in analysis for the first 10 m (for line 1) is given in figure 6.38



**Figure 6.38** Statistically modeled soil profile (line 1)

Statistically modeled soil profile has 3 materials for 10 m below ground surface. So, three shear wave velocity values represent the selected model.

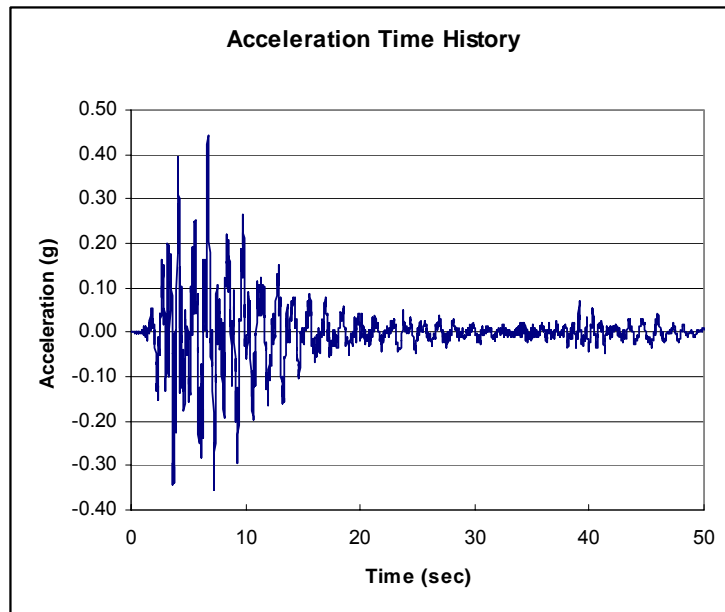


**Figure 6.39** Acceleration time history at ground surface for statistically modeled soil profile (line 1)

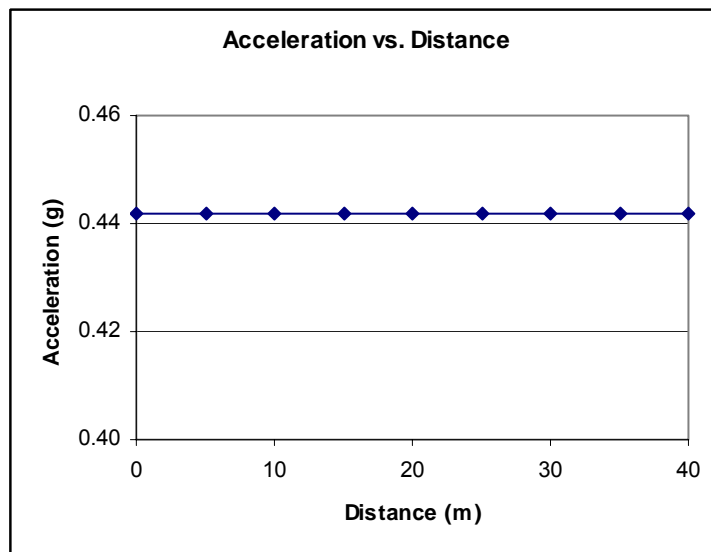


**Figure 6.40** Peak acceleration vs distance, computed at ground surface for statistically modeled soil profile (line 1).

Peak Acceleration is computed at ground surface with the value 0.4422 g. Distribution of acceleration for soil profile is given in figure 6.41.

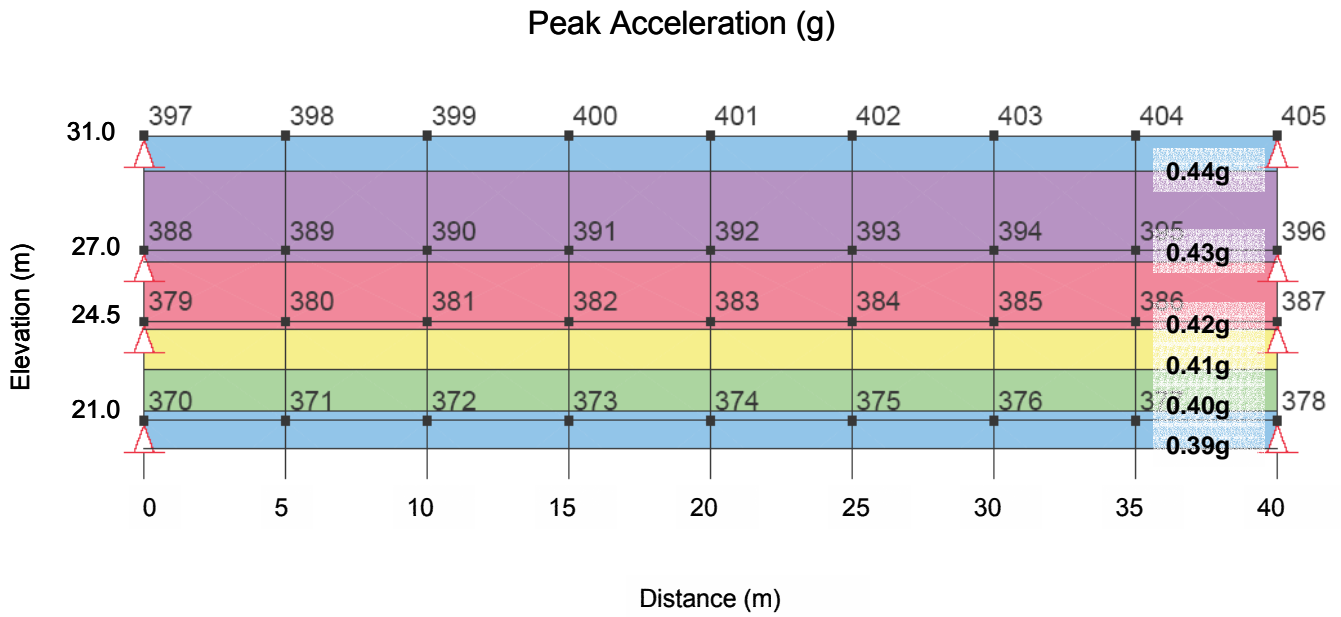


**Figure 6.41** Peak Acceleration distribution for statistically modeled soil (line 1).

Response spectrum (damping 5%) at elevation 31.0 is plotted in figure 6.42. The peak spectral acceleration observed 1.1875 g

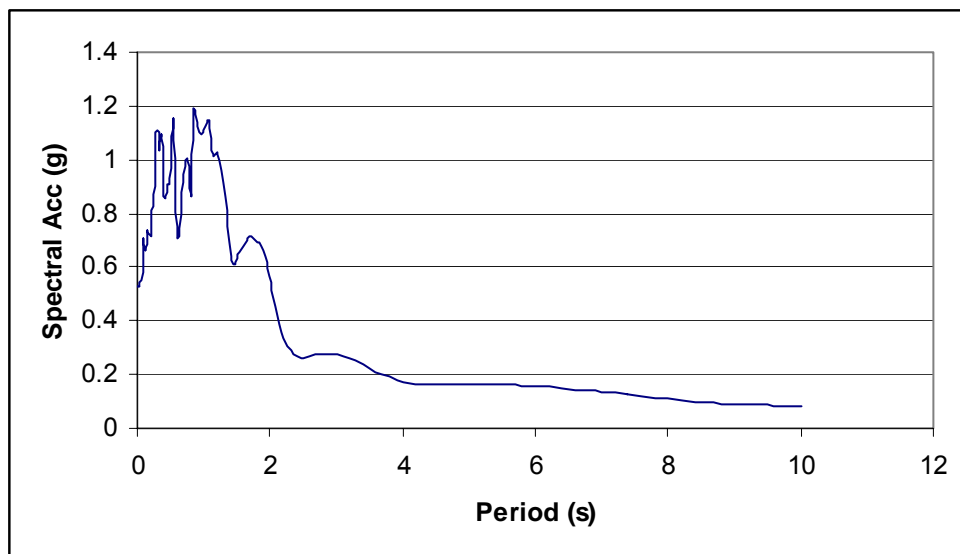


**Figure 6.42** Response Spectrum for statistically modeled profile (line 1)

### Geostatistically Modeled Soil Profile

The soil model used in analysis for 10 m below ground surface (line 1) is given in figure 6.43

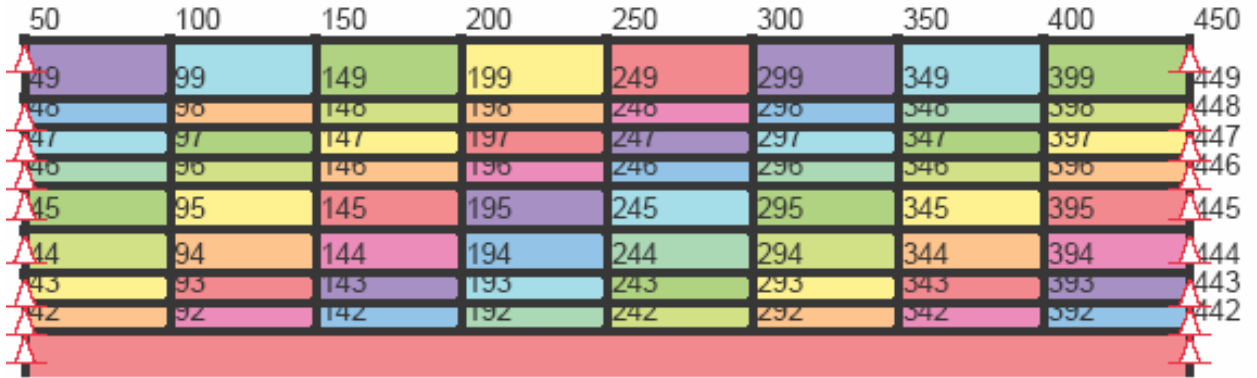
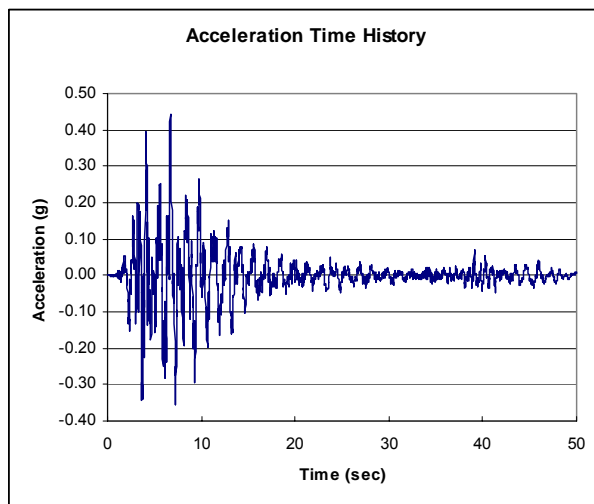


**Figure 6.43** Geostatistically modeled soil profile (line 1)

The geostatistically modeled soil profile is composed of 64 materials. Vs values vary both only in the y direction and in the x direction. Therefore, during the analysis, the soil is modeled as a two dimensional model.



	PGA(g)
Node 50 Distance 0m	0.43155
Node 100 Distance 5m	0.43151
Node 150 Distance 10m	0.43126
Node 200 Distance 15m	0.43223
Node 250 Distance 20m	0.43433
Node 300 Distance 25m	0.43579
Node 350 Distance 30m	0.43701
Node 400 Distance 35m	0.43777
Node 450 Distance 40m	0.43802

**Figure 6.44** Acceleration time history for Geostatistically modeled soil profile (line 1)

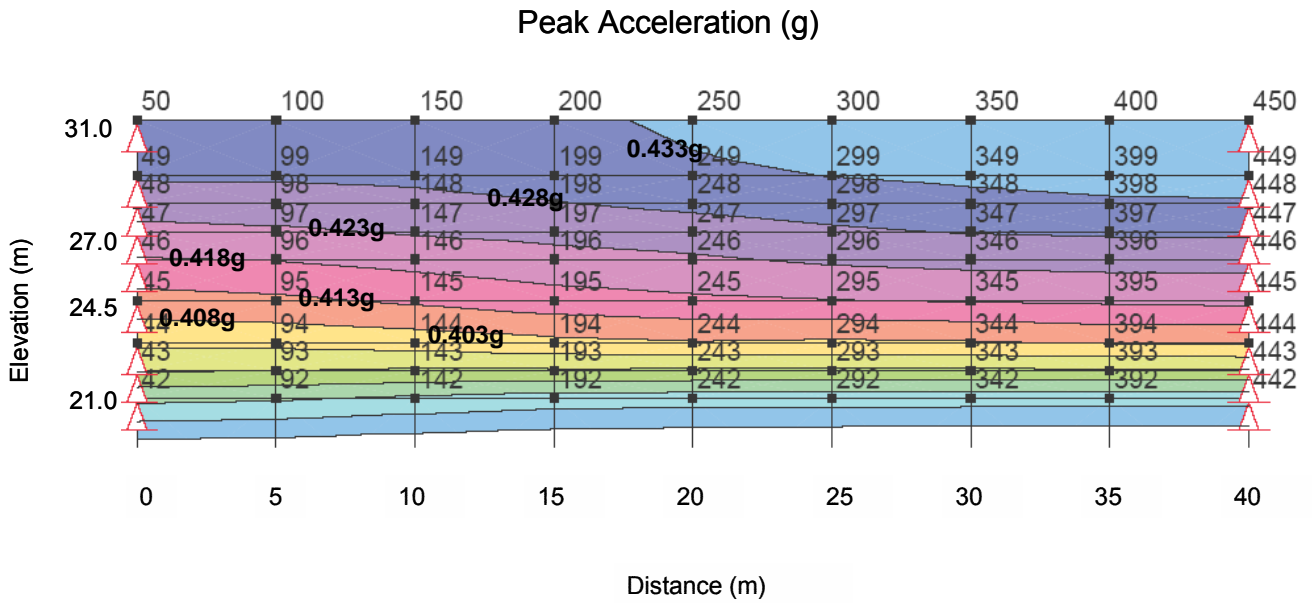


**Figure 6.45** Peak Acceleration distribution for geostatistically modeled soil (line 1).

The maximum acceleration on the ground surface is 0.4380 g whereas minimum acceleration is 0.4313 g. Peak ground acceleration for ground surface varies due to the shear wave velocity changes in the model. Acceleration change on the ground surface can be easily seen in figure 6.46.

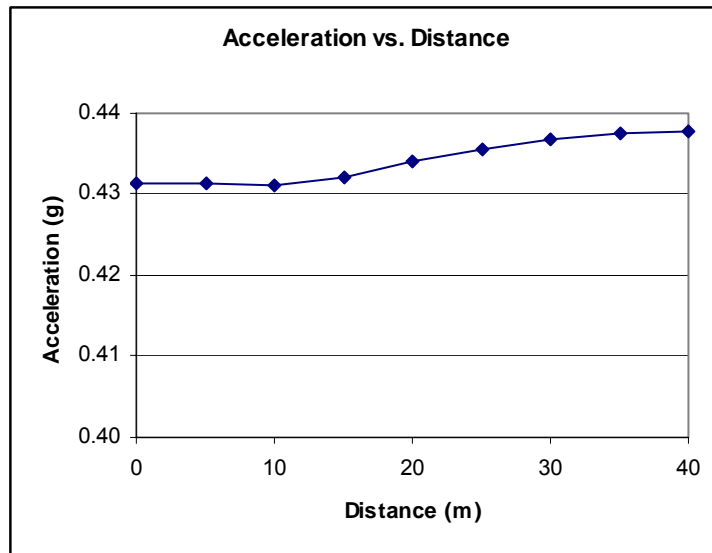
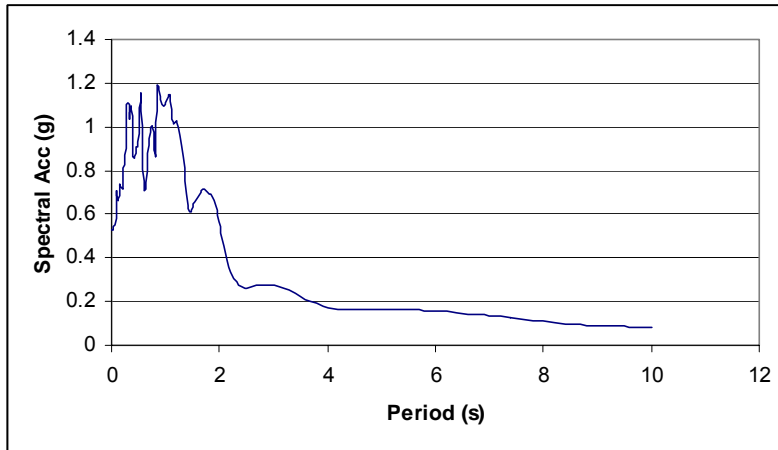


**Figure 6.46** Relationship between acceleration versus distance for the ground surface (line 1)

Response spectrum (damping 5%) at elevation 31.0 is plotted in figure 6.47. Maximum spectral acceleration is 1.1923 g whereas, minimum spectral acceleration is 1.1892 g.



	PSA(g)
Node 50 Distance 0m	1.1908
Node 100 Distance 5m	1.1905
Node 150 Distance 10m	1.1892
Node 200 Distance 15m	1.1895
Node 250 Distance 20m	1.1910
Node 300 Distance 25m	1.1915
Node 350 Distance 30m	1.1920
Node 400 Distance 35m	1.1923
Node 450 Distance 40m	1.1923

**Figure 6.47** Response Spectrum for geostatistically modeled profile (line 1)

#### *Comparison of Models*

To compare statistically modeled and geostatistically modeled soil profiles for line 1, figure 6.48 is plotted.

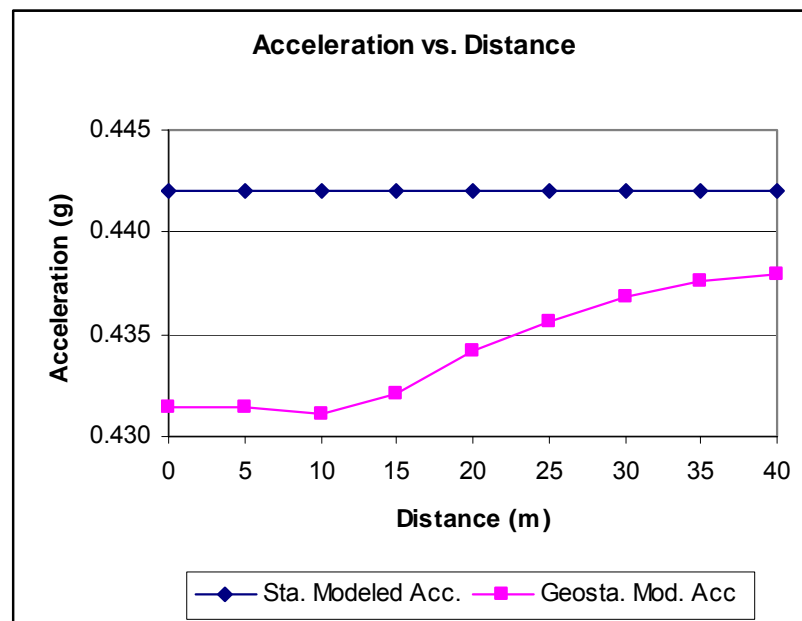


**Figure 6.48.** Acceleration (g) and distance (m) at the ground surface (line 1)

For statistically modeled soil profile (line 1) the acceleration is constant and about 0.44 g on the contrary, geostatistically modeled profile (line 1) has different values and the values are increasing due to increase on distance, and converges to 0.44 g.

For 4 different lines, the soil models are solved under earthquake loading. The results are given in table 6.26. Soil models and output files for lines are presented in the appendix part D.

**Table 6.26** Site response analysis results for 4 lines

	Peak Ground Acceleration (g)			Peak Spectral Acceleration (g)		
	Statistical Analysis	Geostatistical Analysis		Statistical Analysis	Geostatistical Analysis	
		Maximum	Minimum		Maximum	Minimum
Line 1	0.44215	0.43802	0.43126	1.1875	1.1923	1.1892
Line 2	0.46003	0.45543	0.45452	1.2471	1.2266	1.2255
Line 3	0.43510	0.42924	0.42868	1.1282	1.1487	1.1479
Line 4	0.46346	0.45984	0.45724	1.2100	1.2077	1.2045

The statistically modeled soil profiles response to earthquake loading is larger than the geostatistically modeled soil profiles by about 0.01 g.

Peak ground accelerations are given on figure 6.49.

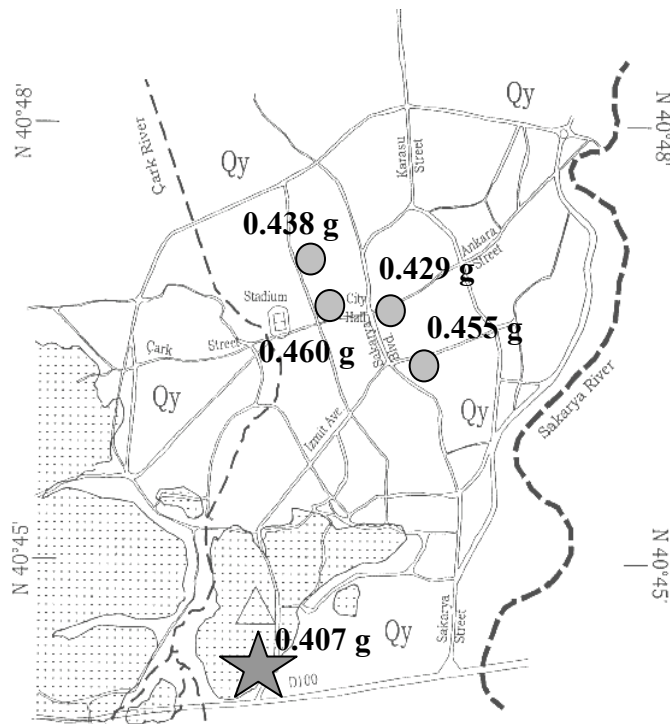


**Figure 6.49** Computed peak accelerations on sites in Adapazari

To evaluate the results according to recommendations in Turkish seismic code, the design acceleration for Adapazari basin is 0.40 g and peak spectral acceleration is 1.0 g. Both analysis are above the limits whereas, due to results of the analysis statistically modeled soils needs to have greater design acceleration than geostatistically modeled soils.

Spectral accelerations obtained from the line analysis are compared to the soil groups defined in the Turkish Seismic Code. Figure 6.50 shows the response spectrum for the lines and corresponding soil groups in the code.

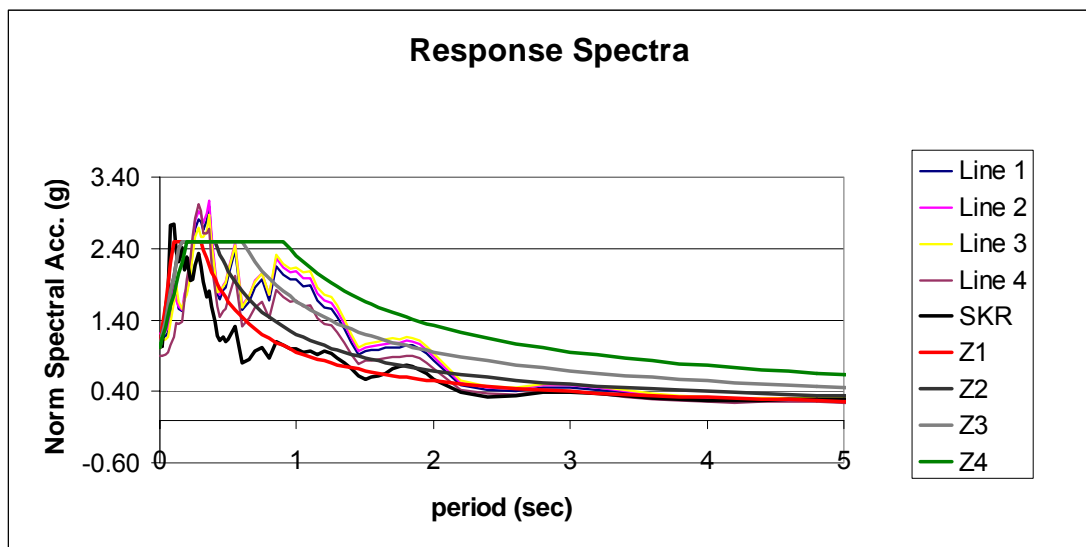


**Figure 6.50** Normalized Spectral Acceleration for the lines and soil classes defined in Turkish Seismic Code

Soil group Z4 covers all response spectrums obtained from sites. All the cases have greater spectral acceleration values than the values recorded in SKR station.

## 7. Conclusions

This research addresses the effect of spatial variability of soils. The research methodology is based on geostatistical analysis. Soil models defined by analysis and used as input parameter in order to characterize site response analysis.

Geostatistics deals with spatial data and it is assumed that there is some connection between location and data value. From known values at sampled locations geostatistical analysis can be used to predict spatial distributions.

As a case study, field test results performed in Adapazari city center after the 1999 Kocaeli earthquake are used. By using empirical correlations shear wave velocity values are computed and used as input for the statistical and geostatistical analysis.

For the research areas, descriptive statistics for shear wave velocity are computed. For 11 layers in 4 sites, coefficient of variation of shear wave velocity is about 0.13. So it can be used as a parameter in future analysis.

As a result of analysis, shear wave velocity can be modeled as normal (28%), log-normal (36%) and gamma (36%) distribution. By using random number generators for each distribution, with corresponding distribution parameters, it is easier to create shear wave velocity values for using in site response analysis.

There must be sufficient number of data in order to perform the analysis, since one of the layers during statistical analysis could not be modeled with six parameters.

Shear wave velocity values are below 200 m/sec for top layers (varies from 2.7 to 6.0 m in 4 sites) in each site indicated with soft clay / loose sand content about 84.5%

During the analysis, probability to observe shear wave velocity values equal to and greater than 400 m/sec is 1.2% for the 10m below ground surface of Adapazari soil deposits.

As a result of the geostatistical analysis, range values are 3.20-7.00 m, whereas 75% of values are clustered at 3.50 m. There is no correlation between the values if the

distance is greater than 3.50 m, vertically and horizontally. This information can be used for site investigations regarding shear wave velocity to take values at a maximum distance, 7.0 m.

All the variograms are modeled as spherical variograms. Therefore, it is suggested to use spherical variograms for modeling the experimental variogram.

With a probability of 75% a nugget effect is observed in the analysis. It is the indicator of measurement errors and short distance variation. Coefficient of variation for short distance effect and also measurement errors for relatively close shear wave velocity values is about 0.07.

During the geostatistical analysis, there are limited number of values which are 44-52. On the contrary, after the kriging analysis, 900 values are predicted and used in order to model the soil profile and use in finite element analysis.

Ansal(2004b) pointed that one dimensional wave propagation analysis cannot explain the recorded earthquake motions in the existence of complex site conditions. In addition, Baise(2004) noticed that “The resulting site characterization is generally sparse; therefore, uncertainty enters the problem at multiple points in the soil characterization and spatial representation of soil. Many site response studies are deterministic and one-dimensional relying on a single boring log to characterize the site geology. These existing methods do not appropriately account for the spatial variability”. A research on computational models for dynamic analysis stated that for the last 40 years a large number of models have been developed and the most successful models have been the suite of programs based on the equivalent linear soil model (Finn, 2004). So, based on recommendations on site response analysis statistically modeled and geostatistically modeled soil profiles performed by using the equivalent linear soil model on two dimensional analyses performed to reach more reliable results; how the shaking is felt on sites.

As a result of site response analysis performed in Adapazari city center, the maximum peak acceleration is about 0.429 g to 0.460 g. Acceleration time history recorded at SKR station which is on stiff soil and located 4.5 km to the sites investigated, is 0.407 g . Maximum peak acceleration obtained from the strong ground motion stations is 0.407g. Since it is below the computed values on sites, it doesn't characterize the real situation in Adapazari city center. Similarly, Kudo et

al(2002) determined the peak accelerations in the Adapazari basin at different sites and suggested that the value is in the range of 0.38 g – 0.50 g and that values can be used as lower and upper bounds in the analysis.

Statistically modeled and geostatistically modeled soil profiles are studied for site response analysis. 3 different materials are used for statistically modeled profile whereas 64 different materials are used for geostatistically modeled profile. Peak accelerations obtained from the statistically modeled profile are relatively higher (0.01 g) than the geostatistically modeled profile. In reality, it is expected to have different values at the ground surface as the distance increases.

Statistics generally analyzes and interprets the uncertainty by limiting sampling. However, there is no information regarding the location of the data where the higher values are grouped. On the other hand, geostatistics interprets statistical distributions and also spatial relationships.

Advantages of geostatistical analysis can be listed as follows

- Powerful and simple tool in order to describe soil heterogeneity

- Optimization of the location of sampling

- Reliable data including location parameter

- Digital maps and contours in order to model soil parameters

Geostatistical analysis is a new tool in geotechnical engineering investigations. Evaluation of soil heterogeneity, minimizing the uncertainty for geotechnical analysis is a basic issue in design process. Geostatistical analysis, as it is about the spatial distribution of soil variables, is an alternative solution to evaluate the variation in soil profile.

In dynamic geotechnical analysis, discussing the response of soil under dynamic loading requires large and reliable data. Instead of assigning a single deterministic soil property, models performed by using geostatistical analysis could be used. Geostatistical analysis is a new powerful tool for the future.

## REFERENCES

- Ansal, A. et. al**, 2004, Site Characterization and Site Amplification for a Seismic Microzonation Study in Turkey, Proceedings of the 11<sup>th</sup> International Conference on Soil Dynamics&Earthquake Engineering (11<sup>th</sup> ICSDEE)& the 3<sup>rd</sup> International Conference on Earthquake Geotechnical Engineering (3<sup>rd</sup> ICEGE), January 7-9, Berkeley, CA, pp. 53-60.
- Ansal, A., Bardet, J.P., Bray, J., Cetin, K.O., Durgunoglu, T., Erdik, M., Kaya, A., Ural, D., Yilmaz, T. , Youd, L.**, 2000 Initial Geotechnical Observations of the August 17, 1999, Izmit Earthquake, *U.C. Berkeley, Earthquake Engineering Research Institute (EERI) Report*, 2000.
- Ansal A.**, 2004, Non-Linear Soil Models for Site Response; European Experience, *International Workshop on the Uncertainties in Nonlinear Soil Properties and their Impact on Modeling Dynamic Soil Response, March 18-19, 2004, California, USA*
- Atkinson P. M. and Tate N.J.**, 2000, Spatial Scale Problems and Geostatistical Solutions: A Review, *Professional Geographer*, 52(4), 607-623
- Baise, L.**, 2004, Opinion Paper, PEER Workshop on Uncertainties in Nonlinear Soil Properties and their Impact on Modeling Dynamic Soil Response
- Barka A.**, 1992, The North Anatolian Fault Zone, *Annales Tectonicae*, Special Issue, VI, 164-195
- Bakir, B.S., Yilmaz, T., M., Yakut, A., and Gülkan, P.**, 2005, Re-examination of damage distribution in Adapazari: Geotechnical Considerations, *Engineering Structures*, 27, 1002-1013
- Bardet, J.P.**, 2000, Kocaeli and Taiwan Earthquake, *International Journal for Housing and Its Applications*, 24(1), 13-23
- Baturay M. B., Bray J.D., Durgunoglu T., Sancio R. B., Stewart J. P. and Ural D.**, 2000. Damage Patterns and Foundation Performance in Adapazari, *Earthquake Spectra*, Vol. 16A, pp.163-189
- Bardet, J.P., Cetin, K.O., Lettis, W., Rathje, E., Rau, G., Seed R.B. and Ural, D.**, 2000, Soil Liquefaction, Landslides and Subsidences, *Earthquake Spectra*, Vol. 16A, pp.141-162,
- Bayazit, M.**, 1996, Probability and Statistics, Birsen Publishing, Istanbul (in Turkish)

- Bray, J.D., et al.**, 2004, Subsurface Characterization at Ground Failure Sites in Adapazari, Turkey, *Journal of Geotechnical and Geoenvironmental Engineering*, ASCE, 130(7), 673-685
- Bowles, J.E.**, 1996, *Foundation Analysis and Design*, Mc Graw Hill Co., NY
- Celebi, M., Toprak, S. and Holzer, T.**, 2000, Strong Motion, Site Effects and Hazard Issues in Rebuilding Turkey. *International Journal for Housing and Its Applications*, 24(1), 25-37
- Christian, J.T.**, 2004, Geotechnical engineering reliability: How well do we know what we are doing? *Journal of Geotechnical and Geoenvironmental Engineering*, ASCE, 130(10), 985-1003
- Cox, B., R.**, 2001, Shear Wave Velocity Profiles at Sites Liquefied by the 1999 Kocaeli, Turkey Earthquake, *Master Thesis*, Utah State University, Logan, Utah, USA
- Cranswick, E. et al**, 1999, Earthquake Damage, Site Response, and Building Response in Avcilar, West of Istanbul, Turkey, *International Conference on the Kocaeli Earthquake: A Scientific Assessment and Recommendations for Re-Building*, ITU-IAHS, Istanbul
- Cressie, N. A. C.**, 1993, *Statistics for Spatial Data*, John Willey & Sons, New York, USA
- Christian, J. T., Ladd, C. C., and Baecher, G. B.**, 1994, Reliability applied to slope stability analysis. *Journal of Geotechnical and Geoenvironmental Engineering*, ASCE, 120(12), 2180-2207.
- Davis, J. C.**, 2002, *Statistics and Data Analysis in Geology*, J Willey, New York, USA
- Davison, A. C., and Hinkley, D. V.**, 1997, *Bootstrap Methods and Their Applications*, Cambridge University Press
- Duncan, J. M.**, 2000, Factors of Safety and Reliability in Geotechnical Engineering, *Journal of Geotechnical and Geoenvironmental Engineering*, 126(4) 307–316.
- Erdik, M.**, 1999, Report on Kocaeli and Düzce Earthquakes, *Bogazici University Department of Earthquake Engineering*, Istanbul
- Erken A., Gülerce, Ü., Balkaya, M., Hatipoglu, M., Dündar, S. and Kaya, Z.**, 2004a, An Example for the Effects of Soil Conditions on Structural Behavior in Adapazari, 6<sup>th</sup> *International Congress on Advances in Civil Engineering*, Istanbul, Turkey, October 6-8

- Erken, A., Kaya, Z., Ulker, M. B. C.**, 2004b, Liquefaction in Adapazari during 1999 Kocaeli Earthquake, *6<sup>th</sup> International Congress on Advances in Civil Engineering*, Istanbul, Turkey, October 6-8
- Fenton, G. A.**, 1999, Estimation for stochastic soil models. *Journal of Geotechnical and Geoenvironmental Engineering*, ASCE., 125(6), 470–485.
- Finn, L. W. D.**, 2004, Nonlinear Soil Properties and their Use in Dynamic Analysis, *International Workshop on the Uncertainties in Nonlinear Soil Properties and their Impact on Modeling Dynamic Soil Response, March 18-19, 2004, California, USA*
- Geo-Slope**, 2002, Quake/W Geo-Slope Office, Manual Book, Alberta, Canada
- Gibert B.R.**, 1997, Basic Random Variables, Probabilistic Methods in Geotechnical Engineering, ASCE *GeoLogan '97 Conference*, Logan, Utah, 14-37
- Imai, T. and Tonuchi, K.**, 1982, Correlation of N-SPT Value with S-Wave Velocity and Shear Modulus, *Proceedings of the 2<sup>nd</sup> European Symposium on Penetration Testing*, Amsterdam, 24–27 May.
- Issaks, E. H. and Srivastava, R. M.**, 1989. An Introduction to Applied Geostatistics, Oxford University Press
- Jones A. L., Kramer S. L. and Arduino P.**, 2002, Estimation of uncertainty in geotechnical properties for performance-based earthquake engineering, *Pacific Earthquake Engineering Research Center Report 2002/16*, University of California, Berkeley
- Journel, A. G. and Huijbregts, C. J.**, 1978, Mining Geostatistics, Academic Press. USA
- Kaya, Ş., Curran, P.J., Llewellyn, G.**, 2005. Post-earthquake building collapse: A comparison of government statistics and estimates derived from SPOT HRVIR data, *International Journal of Remote Sensing*, 26(13), 2731-2740
- Kim, H.**, 2005, Spatial Variability in Soils: Stiffness and Strength, *PhD Thesis*, Georgia Institute of Technology, Atlanta, USA
- Krahn., J.**, 2004, Dynamic Modeling with Quake/W, An Engineering Methodology, Geo-Slope International LTD., Canada
- Kramer, S. L.**, 1996, Geotechnical Earthquake Engineering, Prentice Hall Publishing Inc., USA
- Kramer, S. L., and Paulsen S., B.**, 2004, Practical Use of Geotechnical Site Response Models, *International Workshop on the Uncertainties in Nonlinear Soil Properties and their Impact on Modeling Dynamic Soil Response, March 18-19, 2004, California, USA*

- Kudo, K., Kanna T., Okada, H., Ozel, O., Erdik, M., Sasatani, T., Higashi, S., Takahashi, M., and Yoshida, K., (2002)**, 2002, Site Specific Issues for Strong Ground Motion during The Kocaeli Turkey Earthquake of 17 August 1999, as Inferred from Array Observations of Microtremors and Aftershocks. *Bulletin of the Sesimological Society of America*, Vol 92/1 pp 448-465
- Lacasse and Nadim**, 1996, Uncertainties in characterizing soil properties, Uncertainty in the Geologic Environment, From Theory to Practice, *Proceeding of Uncertainty '96*, Geotechnical Special Publication No. 58.
- Makdisi, F., I. and Wang., Z., L.,** 2004, Non linear Site Response, *International Workshop On The Uncertainties In Nonlinear Soil Properties And Their Impact On Modelling Dynamic Soil Response*, March 18-19
- Matheron, G.**, 1963, Principles of geostatistics, *Economic Geology*, 58, 1246-1266
- Midorikawa, S.**, 1987, Prediction of Iseismic Map in the Kanto Plain due to Hypothetical Earthquake, *Journal of Structural Engineering*, 33(B), 43-48
- Omonode, R. A.**, 2001, Soil Spatial Variability: Structures, Models and Their Effects on Crop Yield Variability in Central Illinois, *PhD Thesis*, University of Illinois at Urbana-Champaign, Urbana, IL
- Özmen, B.**, 2000, Aftermath of Izmit Bay Earthquake with Numerical Analysis, Turkish Earthquake Foundation, Istanbul (in Turkish)
- Proshake Manual v.1.1**, 2001, EduPro Civil Systems, USA
- R Language**, 2005, R Foundation for Statistical Computing, Australia
- Ramaswamy, S.D. et al**, 1982, Pressuremeter Correlations with Standard Penetration and Cone Penetration Tests. *Proceedings of the 2<sup>nd</sup> European Symposium on Penetration Testing*, Amsterdam, 24-27 May
- Rathje, E.**, 2000, Strong Ground Motions and Site Effects, *Earthquake Spectra*, 16(S1), 65-96
- Rathje, E. M., Stokoe, K. H. and Rosenblad, B.**, 2003, Strong Motion Station Characterization and Site Effects During the 1999 Earthquakes in Turkey, *Earthquake Spectra*, 19(3), 653-675
- Robertson, P. K. and Wride, C. E.**, 1997, Cyclic Liquefaction and Its Evaluation Based on the SPT and CPT: *Proceedings of the NCEER Workshop on Evaluation of Liquefaction Resistance of Soils: Technical Report NCEER-97-0022*, National Center for Earthquake Engineering Research, Buffalo, NY, 41-87
- Sancio, R. B.**, 2003, Ground Failure and Building Performance in Adapazari, Turkey, *PHD Thesis*, University of California, Berkeley, USA

- Seed, H.B., Mori, K, and Chan C.K.,** 1975, Influence of Seismic History on the Liquefaction Characteristics of Sands, *Report EERC 75-35, Earthquake Engineering Research Center, University of California, Berkeley*
- S plus 7.0 Manual,** 2005, Insightful Corporation, United Kingdom
- Spatial Stats v.1.5 Manual,** 2005, Insightful Corporation, United Kingdom
- SPSS v.14 Manual,** 2005, LEAD Tools, USA
- Stein, R. S., Barka, A. and Dieterich J. H.,** 1997, Progressive failure on the North Anatolian Fault Since 1939 by Earthquake Stress Triggering, *Geophysical Journal International*, 128, 594-604.
- Sucuoglu H.,** 2000, The Kocaeli and Düzce-Turkey Earthquakes, *Middle East Technical University, Ankara*
- Tang, W. H.,** 1984, Principles of Probabilistic Characterizations of Soil Properties. : *Bridge between Theory and Practice*, ASCE, New York, 74–89.
- Tercan E. and Sarac, C.,**1998, Geostatistical Analysis for Assessment on Ore Deposits, Turkish Chamber of Geology Engineers, Ankara, (In Turkish)
- Tezcan S., S. and Ozgirgin, F.,** 2001, Soil Amplification and Case Studies, Turkish Earthquake Foundation, Istanbul.
- Trangmar, B.B., Yost, R.S., Uehara, G.,** 1985, Application of Geostatistics, to Spatial Studies of Soil Properties, *Advances in Agronomy*, 38, 45-93
- Turkish Seismic Code,** Ministry of Public Works and Settlement Government of Republic of Turkey, Issued on: 2.9.1997, Official Gazette No.23098, Effective from: 1.1.1998, Amended on: 2.7.1998, *Official Gazette No.23390* (English translation by N. Aydinoglu, 1998).
- Tuysuz, O., and Genc, C.,** 2000, Geological Factors Controlling the Distribution of Damage During the 17<sup>th</sup> August and 12<sup>th</sup> November 1999 Earthquakes, *ITU-IAHS International Conference on the Kocaeli Earthquake 17 August 1999*, pp 19-22, Istanbul
- United States Army Corps of Engineers (USACE),** 1995, Appendix B – Introduction to probability and reliability in geotechnical engineering, Engineering Technical Letter (ETL) 1110-2-547
- United States Geological Survey,** 1999, Implications for Earthquake Risk Reduction in the United States from the Kocaeli, Turkey Earthquake of August 17,1999, *US Geological Survey Circular 1193*, Denver, CO, USA

**Ural, D., Saygili, G., Bayrak, B.,** 2003, Liquefaction Effects on Housing during the Kocaeli, Turkey Earthquake, *International Journal for Housing Science and its Applications*; Vol.27, No.4, pp 269-285

**Ural, D.,** 2001, The 1999 Kocaeli and Düzce Earthquakes: Lessons Learned and Possible Remedies to Minimize Future Losses, *A Workshop on Seismic Fault-induced Failures, University of Tokyo, Japan, January 11-12, 2001.*

**Ural, D.,** 2006, Soil Dynamics Lecture Notes, *Istanbul Technical University Geotechnical Engineering Division, Istanbul*

**Whitman, R. V.,** 2000, Organizing and Evaluating Uncertainty in Geotechnical Engineering, *Journal of Geotechnical and Geoenvironmental Engineering, ASCE, 125(6), 583-593*

**Zhang, L., Tang, W. H. H., Zhang, L. and Zheng, J.,** 2004, Reducing Uncertainty of Prediction from Empirical Correlations, *Journal of Geotechnical and Geoenvironmental Engineering.*, 130(5) 526-534.

Documenting Incidents of Ground Failure Resulting from the August 17, 1999 Kocaeli, Turkey Earthquake is available on internet (April 15,2006);

<http://peer.berkeley.edu/turkey/adapazari/>

National Information Service for Earthquake Engineering, Initial Geotechnical Observations of the August 17, 1999, Izmit Earthquake is available on internet (April 15, 2006)

<http://nisee.berkeley.edu/turkey/report.html>

PEER Strong Motion Database is available on internet (April15, 2006);

<http://peer.berkeley.edu/smcat/index.html>

United States Geological Survey Webpage, available on internet (April 15, 2006);

<http://www.usgs.gov/>

## APPENDIX – A

### In-situ Test Results Used in Analysis

UCB-BYU-UCLA  
ZETAŞ-SAU  
Joint Research

**Project Name:** Ground Failure and Building Performance in Adapazari, Turkey

**Page:** 1 of 2

**Location:** Site 1- Bölük Street, İstiklal District, Adapazari

Thesis Name: Geostatistical Analysis for Soil Dynamics

**Test Number:** CPT-101

**Type of Cone:** ELC10 CF No. 990617 (a.p. v.d. Berg)

**Elevation:** 30.56 m

**Date:** June 15, 2000 17:52

Sponsored by:

NSF, PEER

Caltrans, CEC, PG&E

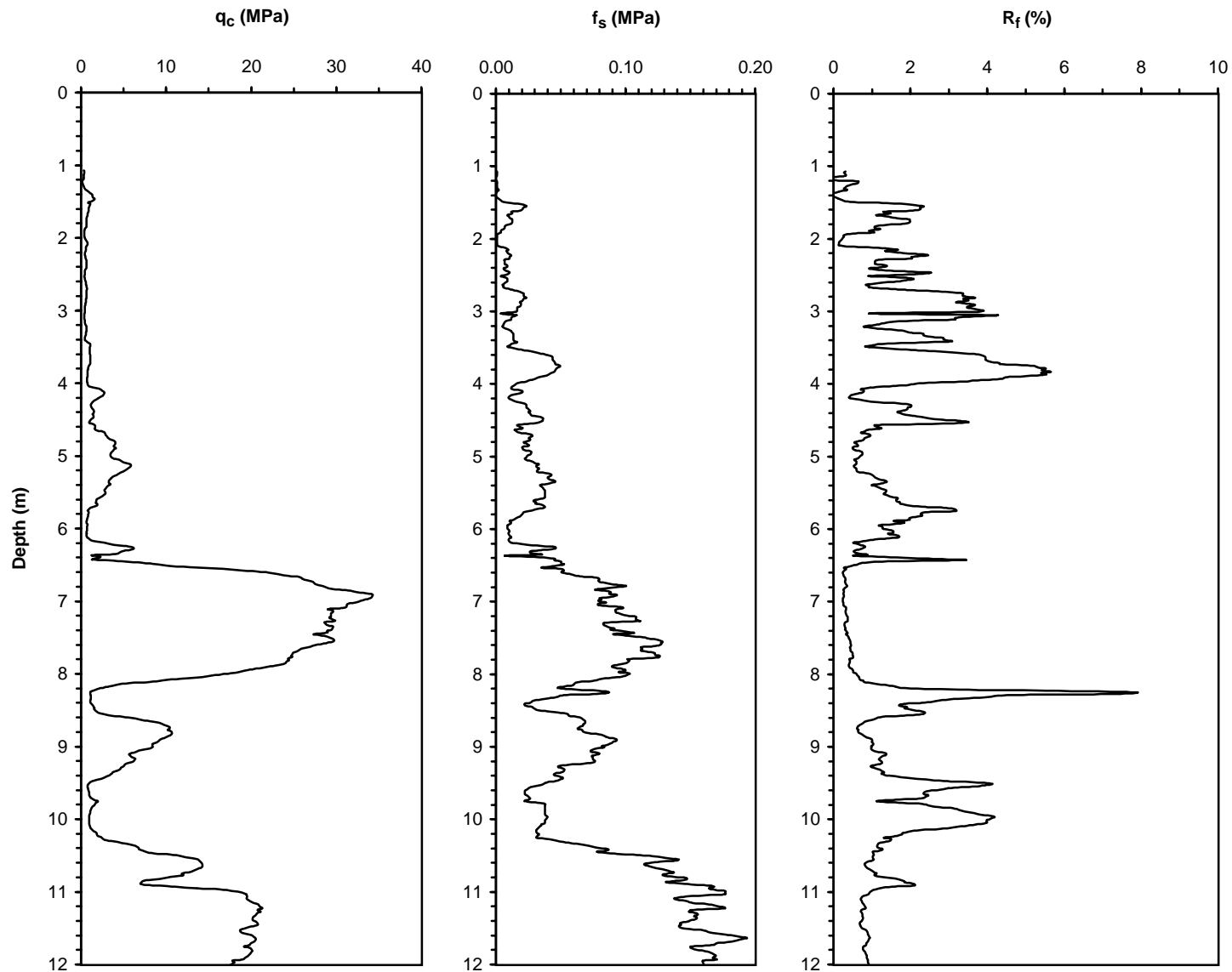
**File Name:**

**Operator:** ZETAŞ (Zemin Teknolojisi, A. Ş.)

**Water Table Elevation:** Not measured

**Responsible Engineers:** J. D. Bray and R. B. Sancio, U. C. Berkeley

**Notes:**



UCB-BYU-UCLA  
ZETAŞ-SAU  
Joint Research

**Project Name:** Ground Failure and Building Performance in Adapazari, Turkey

**Page:** 2 of 2

**Location:** Site 1 - Bölük Street, İstiklal District, Adapazari

Thesis Name: Geostatistical Analysis for Soil Dynamics

**Test Number:** CPT-101

**Elevation:** 30.56 m

**Type of Cone:** ELC10 CF No. 990617 (a.p. v.d. Berg)

**Date:** June 15, 2000 17:52

Sponsored by:

**File Name:** .

**Water Table Elevation:** Not measured

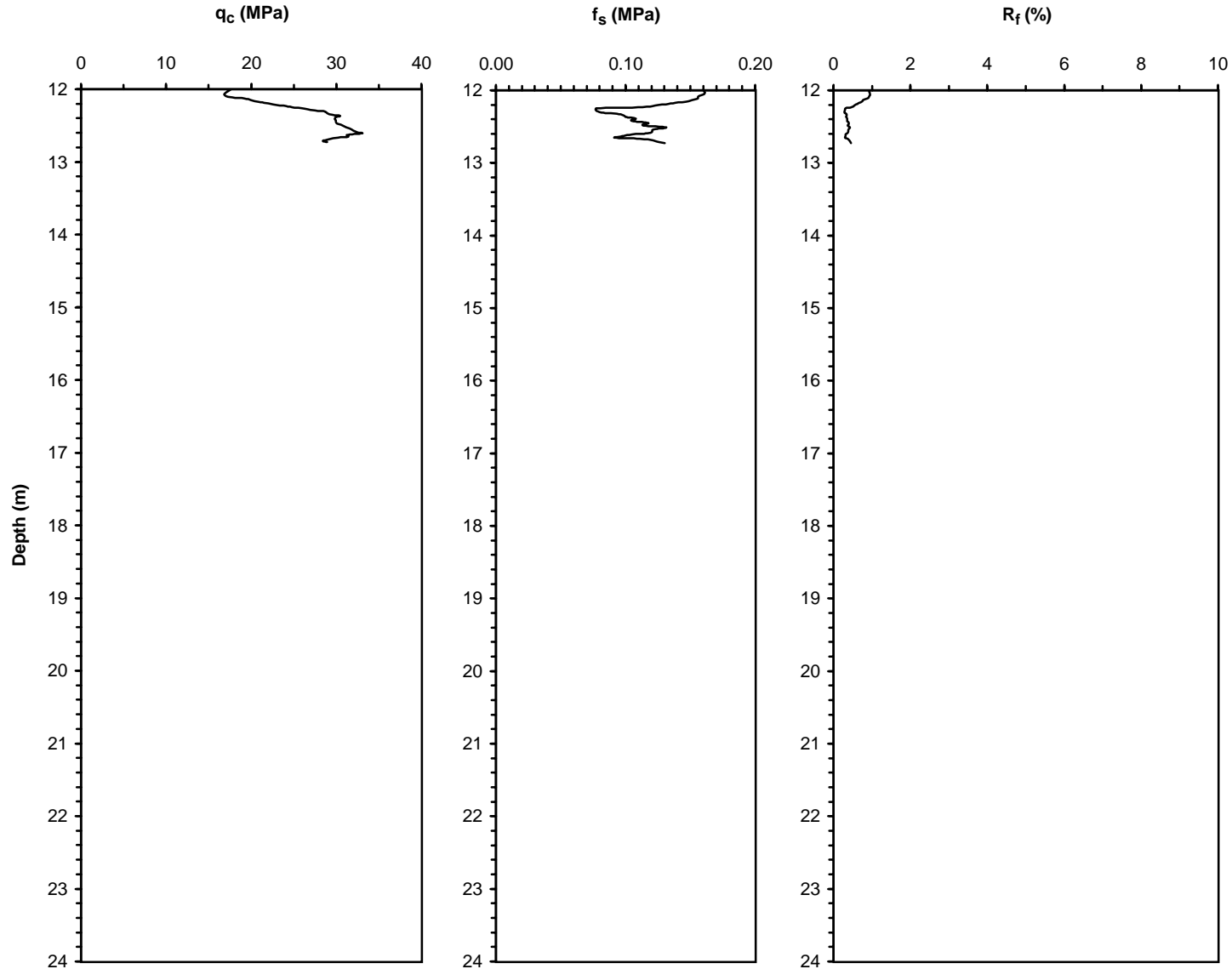
NSF, PEER

**Operator:** ZETAŞ (Zemin Teknolojisi, A. Ş.)

**Responsible Engineers:** J. D. Bray and R. B. Sancio, U. C. Berkeley

Caltrans, CEC, PG&E

**Notes:**



UCB-BYU-UCLA  
ZETAŞ-SAU  
Joint Research

**Project Name:** Ground Failure and Building Performance in Adapazari, Turkey

**Page:** 1 of 1

**Location:** Site 1 - Bölük Street, İstiklal District, Adapazari

**Thesis Name:** Geostatistical Analysis for Soil Dynamics

**Test Number:** CPT-102

**Elevation:** 30.78 m

**Type of Cone:** ELC10 CFPS No. 991232 (a.p. v.d. Berg)

**Date:** June 15, 2000

Sponsored by:

**File Name:** .

**Water Table Elevation:** Not measured

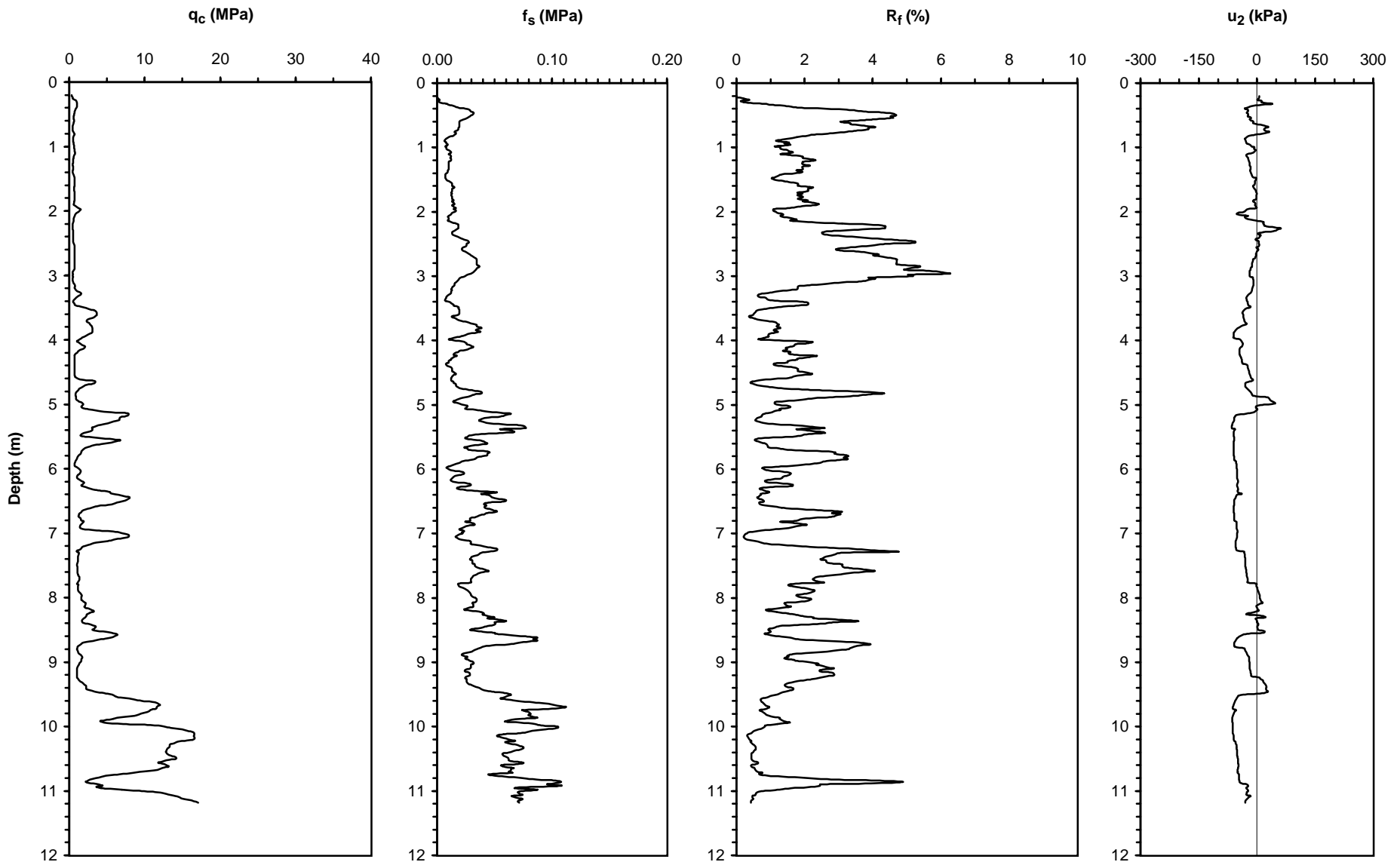
NSF, PEER

**Operator:** ZETAŞ (Zemin Teknolojisi, A. Ş.)

**Responsible Engineers:** J. D. Bray and R. B. Sancio, U. C. Berkeley

Caltrans, CEC, PG&E

**Notes:**



UCB-BYU-UCLA  
ZETAŞ-SAU  
Joint Research

**Project Name:** Ground Failure and Building Performance in Adapazari, Turkey

**Page:** 1 of 1

**Location:** Site 1 - Bölük Street, İstiklal District, Adapazari

Thesis Name: Geostatistical Analysis for Soil Dynamics

**Test Number:** CPT-103

**Elevation:** 30.78 m

**Type of Cone:** ELC10 CFPS No. 991232 (a.p. v.d. Berg)

**Date:** June 16, 2000

Sponsored by:

**File Name:** .

**Water Table Elevation:** Not measured

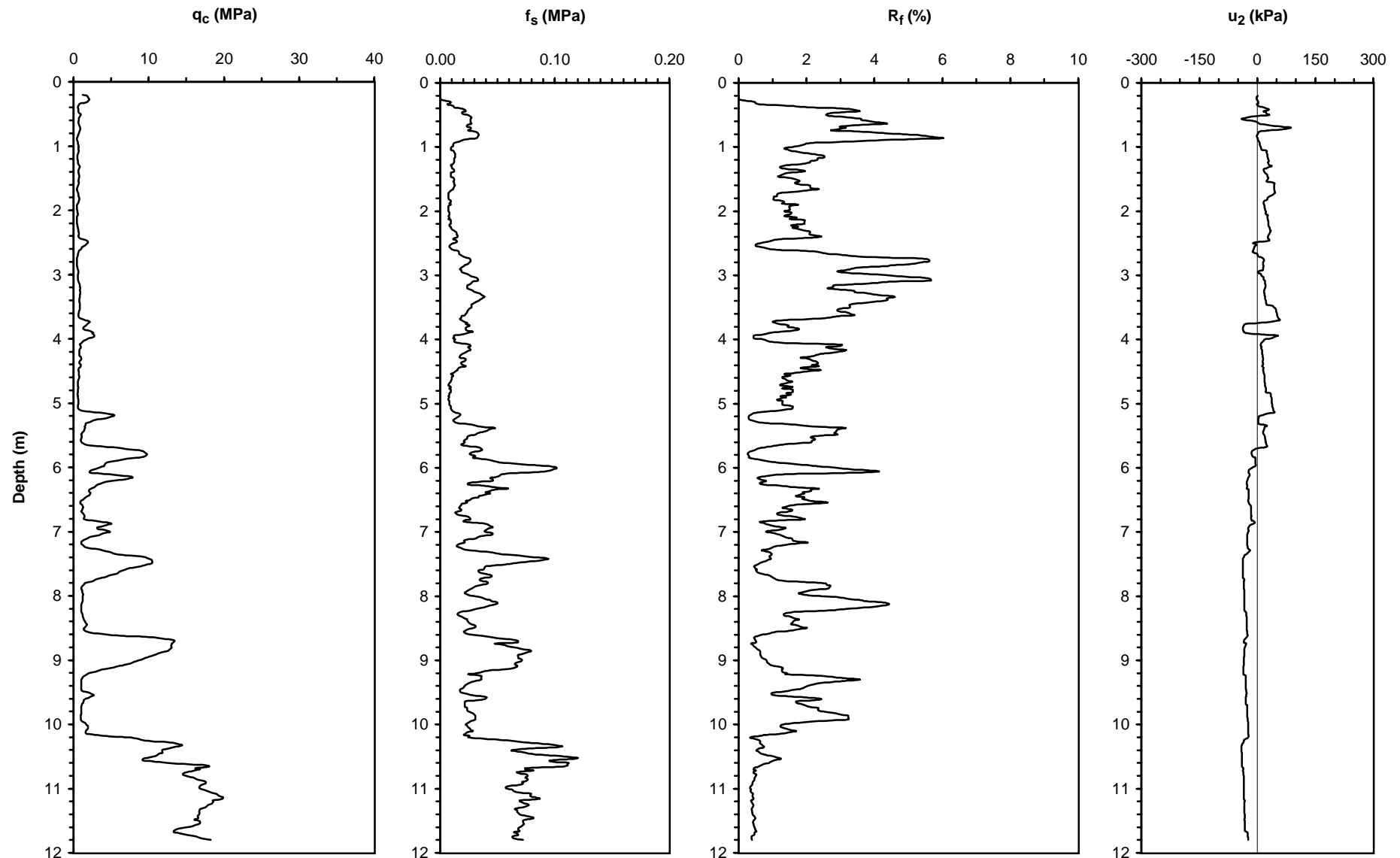
NSF, PEER

**Operator:** ZETAŞ (Zemin Teknolojisi, A. Ş.)

**Responsible Engineers:** J. D. Bray and R. B. Sancio, U. C. Berkeley

Caltrans, CEC, PG&E

**Notes:**



UCB-BYU-UCLA  
ZETAŞ-SAU  
Joint Research

**Project Name:** Ground Failure and Building Performance in Adapazari, Turkey

**Page:** 1 of 1

**Location:** Site 1 - Bölük Street, İstiklal District, Adapazari

Thesis Name: Geostatistical Analysis for Soil Dynamics

**Test Number:** CPT-104

**Elevation:** 30.63 m

**Type of Cone:** ELC10 CFPS No. 991232 (a.p. v.d. Berg)

**Date:** June 14, 2000

Sponsored by:

**File Name:**

**Water Table Elevation:** Not measured

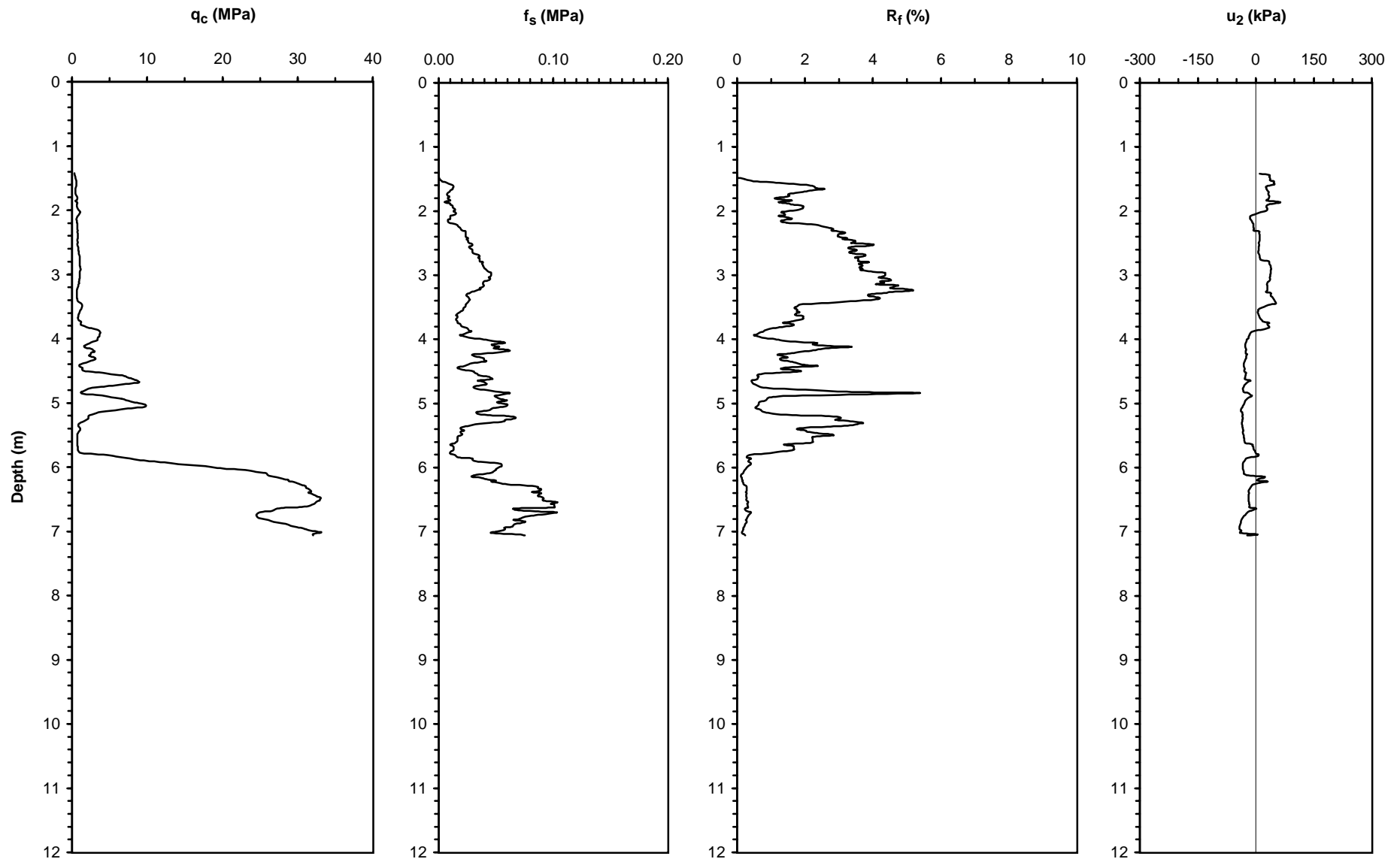
NSF, PEER

**Operator:** ZETAŞ (Zemin Teknolojisi, A. Ş.)

**Responsible Engineers:** J. D. Bray and R. B. Sancio, U. C. Berkeley

Caltrans, CEC, PG&E

**Notes:**



UCB-BYU-UCLA  
ZETAŞ-SAU  
Joint Research

**Project Name:** Ground Failure and Building Performance in Adapazari, Turkey

**Page:** 1 of 2

**Location:** Site 1 - Bölük Street, İ stiklal District, Adapazari

Thesis Name: Geostatistical Analysis for Soil Dynamics

**Test Number:** CPT-105

**Elevation:** 30.66 m

**Type of Cone:** ELC10 CF No. 990617 (a.p. v.d. Berg)

**Date:** June 15, 2000 12:04

Sponsored by:

**File Name:** .

**Water Table Elevation:** Not measured

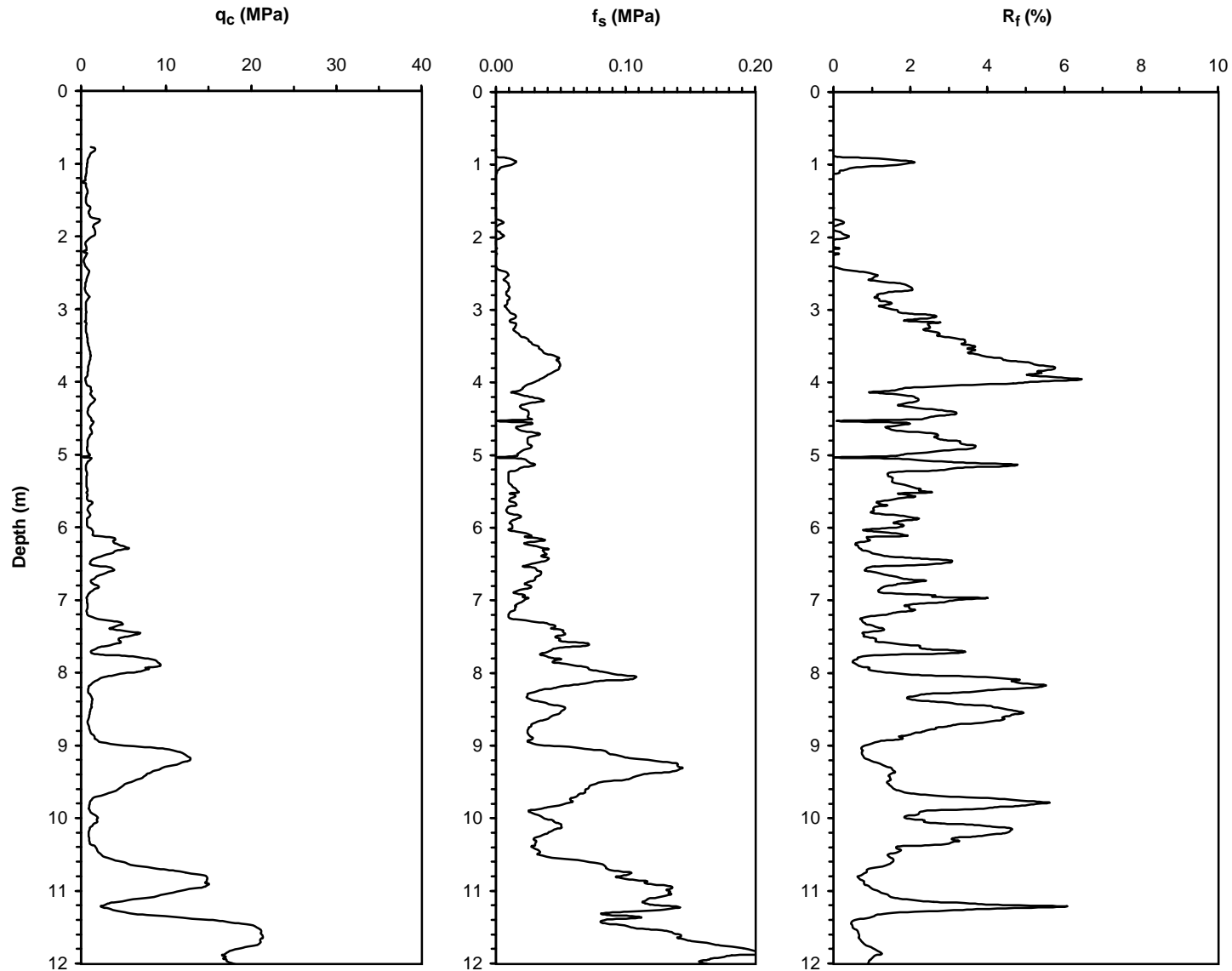
NSF, PEER

**Operator:** ZETAŞ (Zemin Teknolojisi, A. Ş.)

**Responsible Engineers:** J. D. Bray and R. B. Sancio, U. C. Berkeley

Caltrans, CEC, PG&E

**Notes:**



UCB-BYU-UCLA  
ZETAŞ-SAU  
Joint Research

**Project Name:** Ground Failure and Building Performance in Adapazari, Turkey

**Page:** 2 of 2

**Location:** Site 1 - Bölük Street, İstiklal District, Adapazari

Thesis Name: Geostatistical Analysis for Soil Dynamics

**Test Number:** CPT-105

**Elevation:** 30.66 m

**Type of Cone:** ELC10 CF No. 990617 (a.p. v.d. Berg)

**Date:** June 15, 2000 12:04

Sponsored by:

**File Name:**

**Water Table Elevation:** Not measured

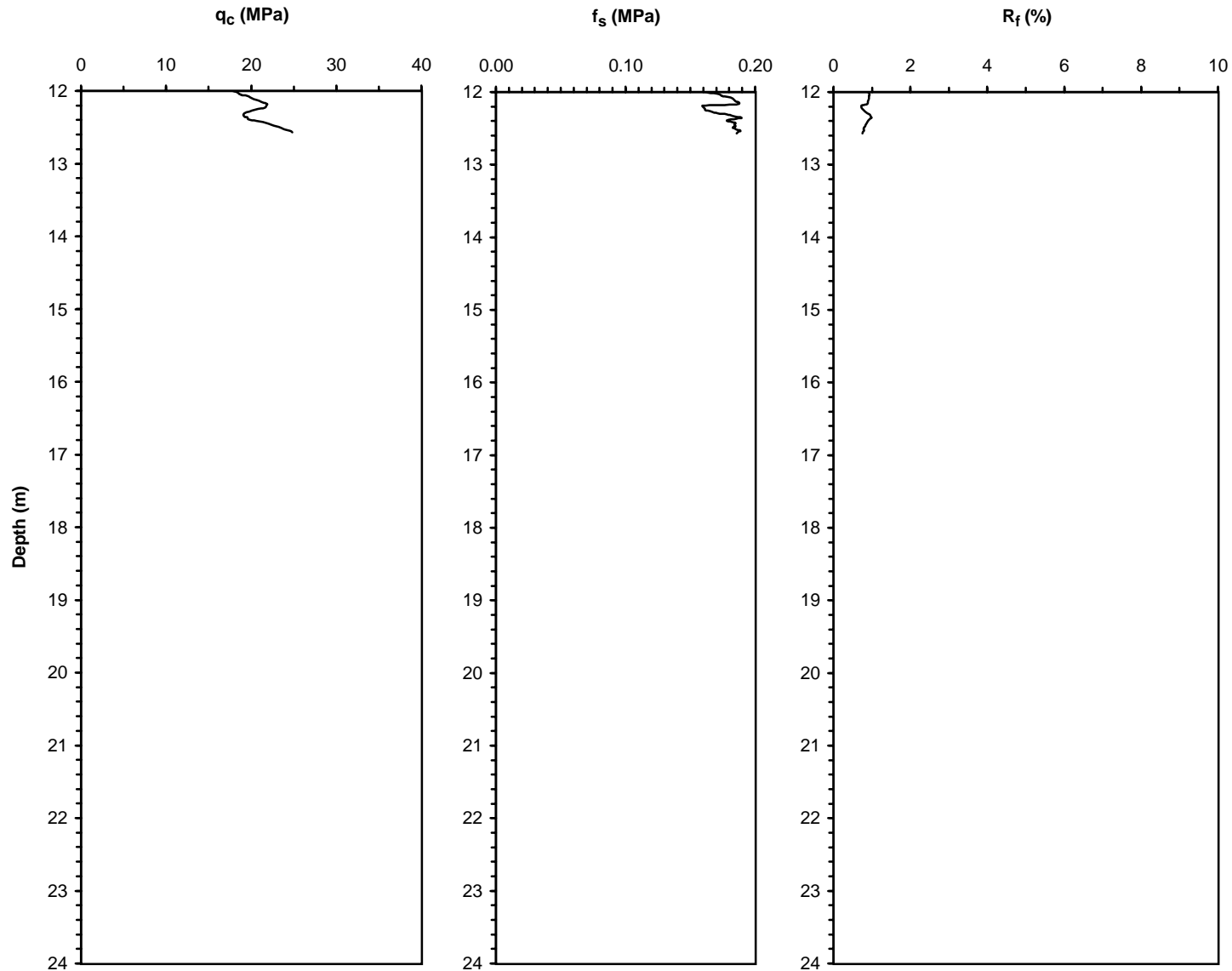
NSF, PEER

**Operator:** ZETAŞ (Zemin Teknolojisi, A. Ş.)

**Responsible Engineers:** J. D. Bray and R. B. Sancio, U. C. Berkeley

Caltrans, CEC, PG&E

**Notes:**



UCB-BYU-UCLA  
ZETAŞ-SAU  
Joint Research

**Project Name:** Ground Failure and Building Performance in Adapazari, Turkey

**Page:** 1 of 1

**Location:** Site 1 - Bölük Street, İstiklal District, Adapazari

Thesis Name: Geostatistical Analysis for Soil Dynamics

**Test Number:** CPT-106

**Elevation:** 30.69 m

**Type of Cone:** ELC10 CFPS No. 991232 (a.p. v.d. Berg)

**Date:** June 15, 2000

Sponsored by:

**File Name:**

**Water Table Elevation:** Not measured

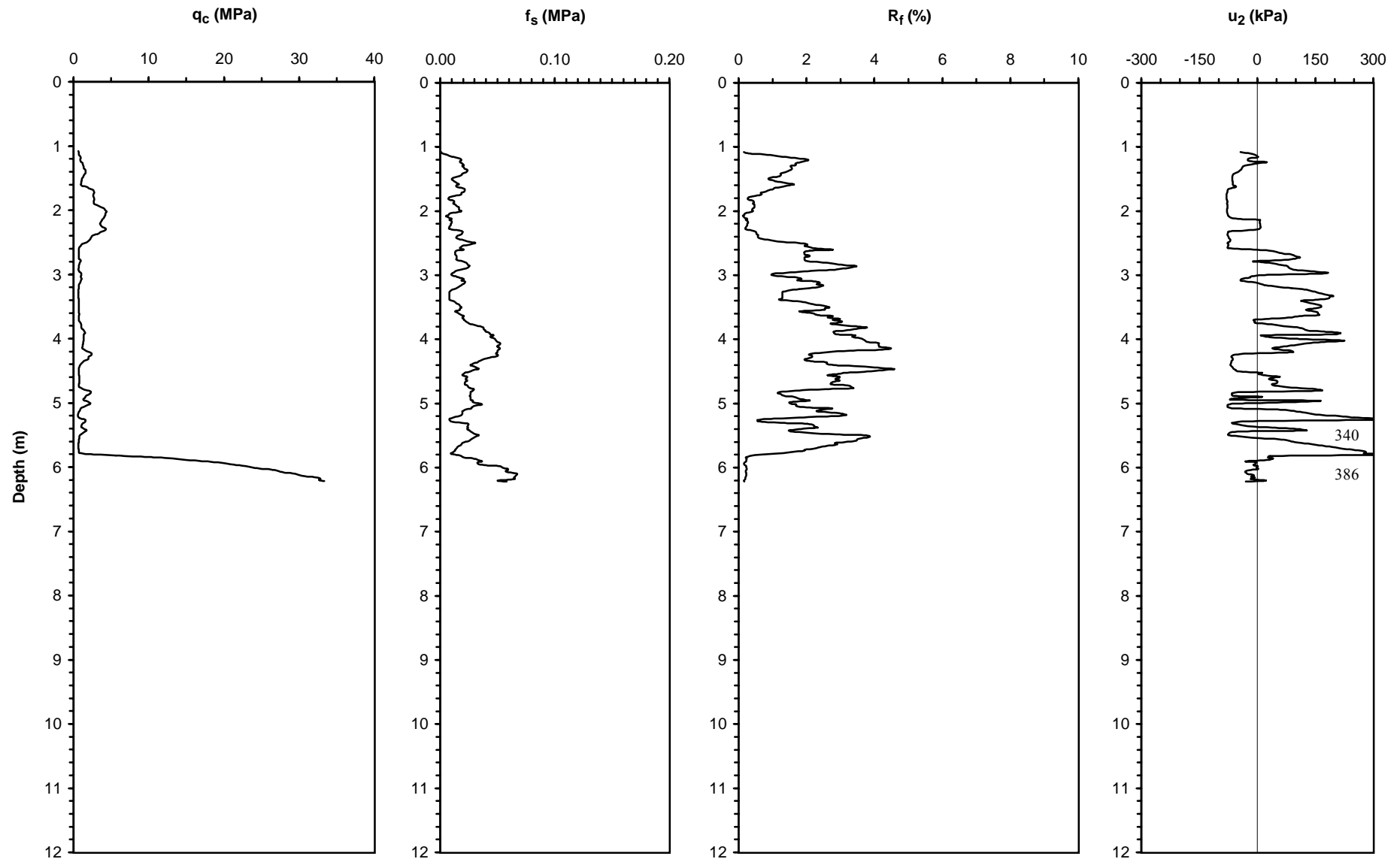
NSF, PEER

**Operator:** ZETAŞ (Zemin Teknolojisi, A. Ş.)

**Responsible Engineers:** J. D. Bray and R. B. Sancio, U. C. Berkeley

Caltrans, CEC, PG&E

**Notes:**



UCB-BYU-UCLA  
ZETAŞ-SAU  
Joint Research

**Project Name:** Ground Failure and Building Performance in Adapazari, Turkey

**Page:** 1 of 1

**Location:** Site 2 - Ç1 rak Street, Yenigün District, Adapazari

Thesis Name: Geostatistical Analysis for Soil Dynamics

**Test Number:** CPT-201

**Elevation:** 31.11 m

**Type of Cone:** ELC10 CFPS No. 991232 (a.p. v.d. Berg)

**Date:** June 19, 2000

Sponsored by:

**File Name:**

**Water Table Elevation:** Not measured

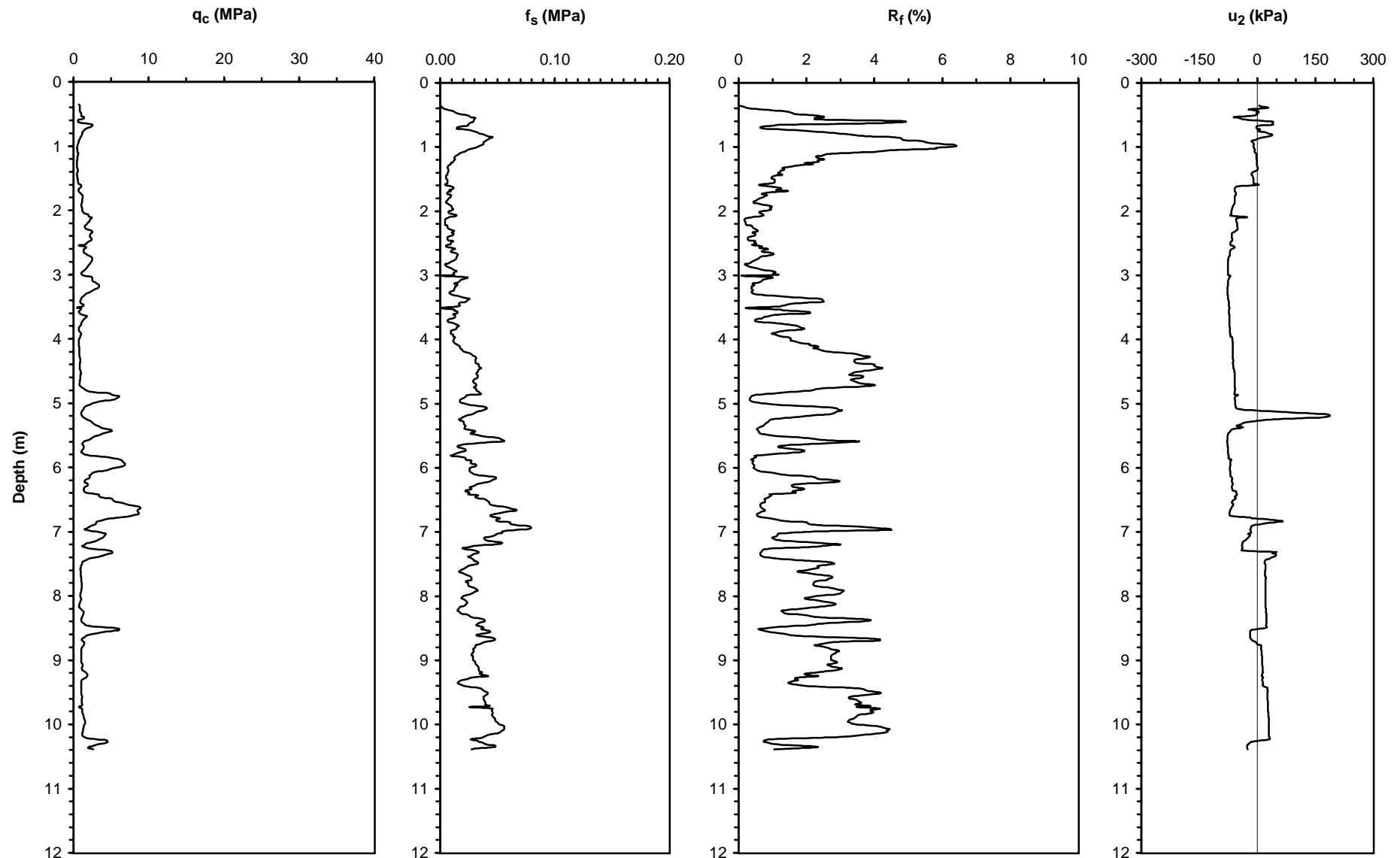
NSF, PEER

**Operator:** ZETAŞ (Zemin Teknolojisi, A. Ş.)

**Responsible Engineers:** J. D. Bray and R. B. Sancio, U. C. Berkeley

Caltrans, CEC, PG&E

**Notes:**



UCB-BYU-UCLA  
ZETAŞ-SAU  
Joint Research

**Project Name:** Ground Failure and Building Performance in Adapazari, Turkey

**Page:** 1 of 1

**Location:** Site 2 - Çırak Street, Yenigün District, Adapazari

Thesis Name: Geostatistical Analysis for Soil Dynamics

**Test Number:** CPT-202

**Type of Cone:** ELC10 CF No. 990617 (a.p. v.d. Berg)

**Elevation:** 31.09 m

**Date:** June 19, 2000 15:11

Sponsored by:

**File Name:**

**Water Table Elevation:** Not measured

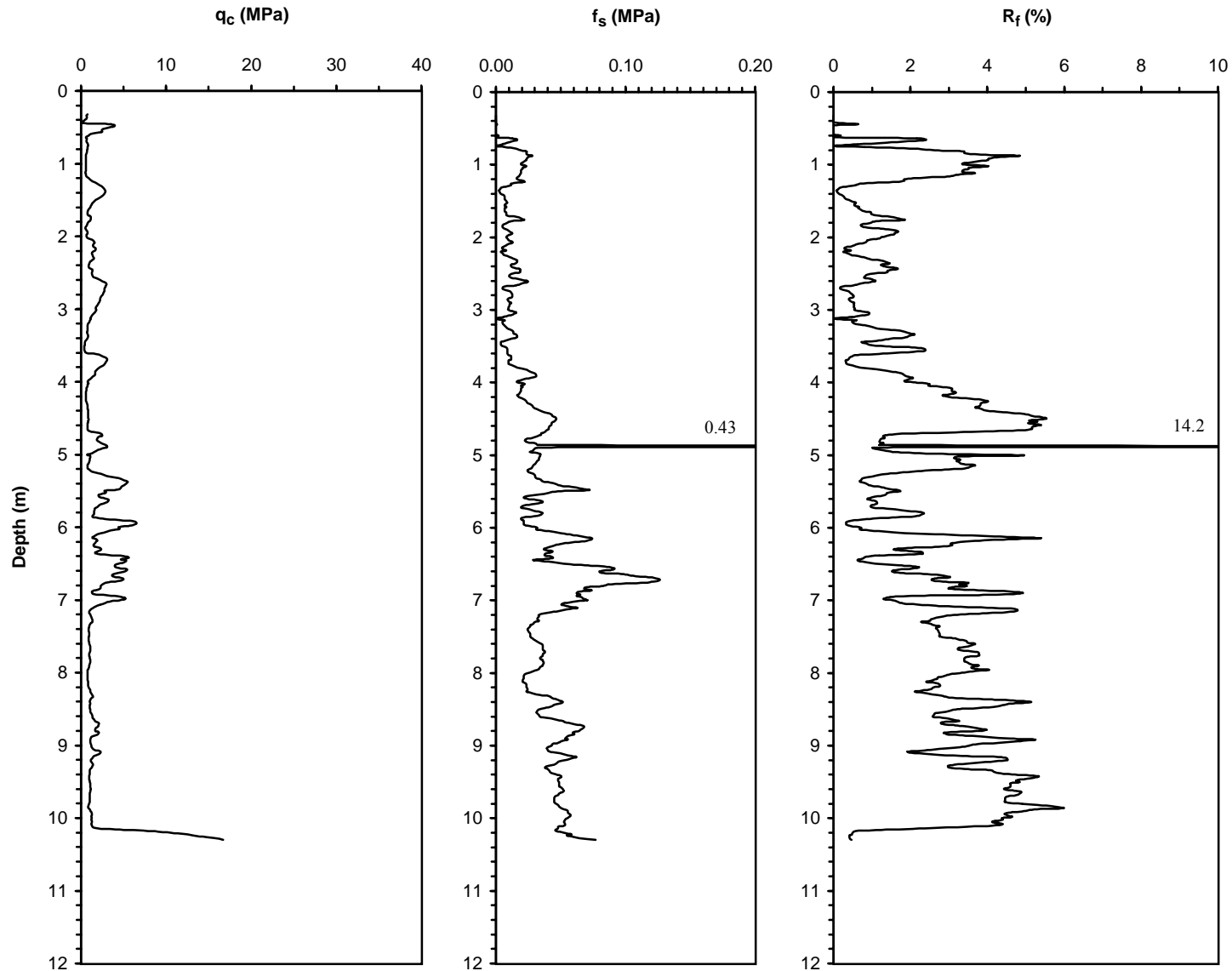
NSF, PEER

**Operator:** ZETAŞ (Zemin Teknolojisi, A. Ş.)

**Responsible Engineers:** J. D. Bray and R. B. Sancio, U. C. Berkeley

Caltrans, CEC, PG&E

**Notes:**



UCB-BYU-UCLA  
ZETAŞ-SAU  
Joint Research

**Project Name:** Ground Failure and Building Performance in Adapazari, Turkey

**Page:** 1 of 1

**Location:** Site 2 - Hasırcılar Street, Yenigün District, Adapazari

Thesis Name: Geostatistical Analysis for Soil Dynamics

**Test Number:** CPT-203

**Elevation:** 30.98 m

**Type of Cone:** ELC10 CF No. 990618 (a.p. v.d. Berg)

**Date:** June 21, 2000 15:21

Sponsored by:

**File Name:**

**Water Table Elevation:** Not measured

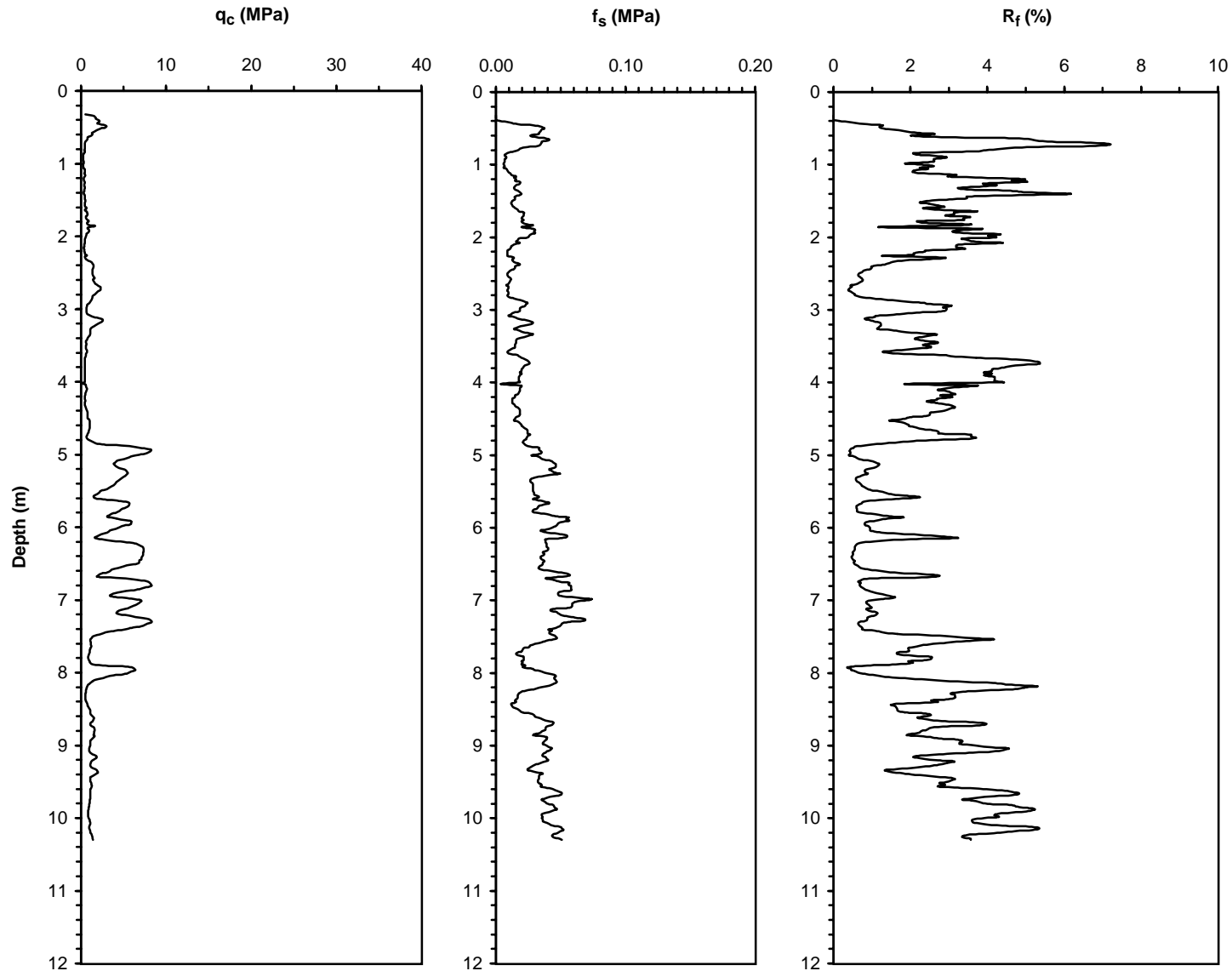
NSF, PEER

**Operator:** ZETAŞ (Zemin Teknolojisi, A. Ş.)

**Responsible Engineers:** J. D. Bray and R. B. Sancio, U. C. Berkeley

Caltrans, CEC, PG&E

**Notes:**



UCB-BYU-UCLA  
ZETAŞ-SAU  
Joint Research

**Project Name:** Ground Failure and Building Performance in Adapazari, Turkey

**Page:** 1 of 3

**Location:** Site 2 - Hası rclar Street, Yenigün District, Adapazari

Thesis Name: Geostatistical Analysis for Soil Dynamics

**Test Number:** CPT-204

**Elevation:** 31.09 m

**Type of Cone:** ELC10 CFPS No. 991232 (a.p. v.d. Berg)

**Date:** June 21, 2000

Sponsored by:

**File Name:**

**Water Table Elevation:** Not measured

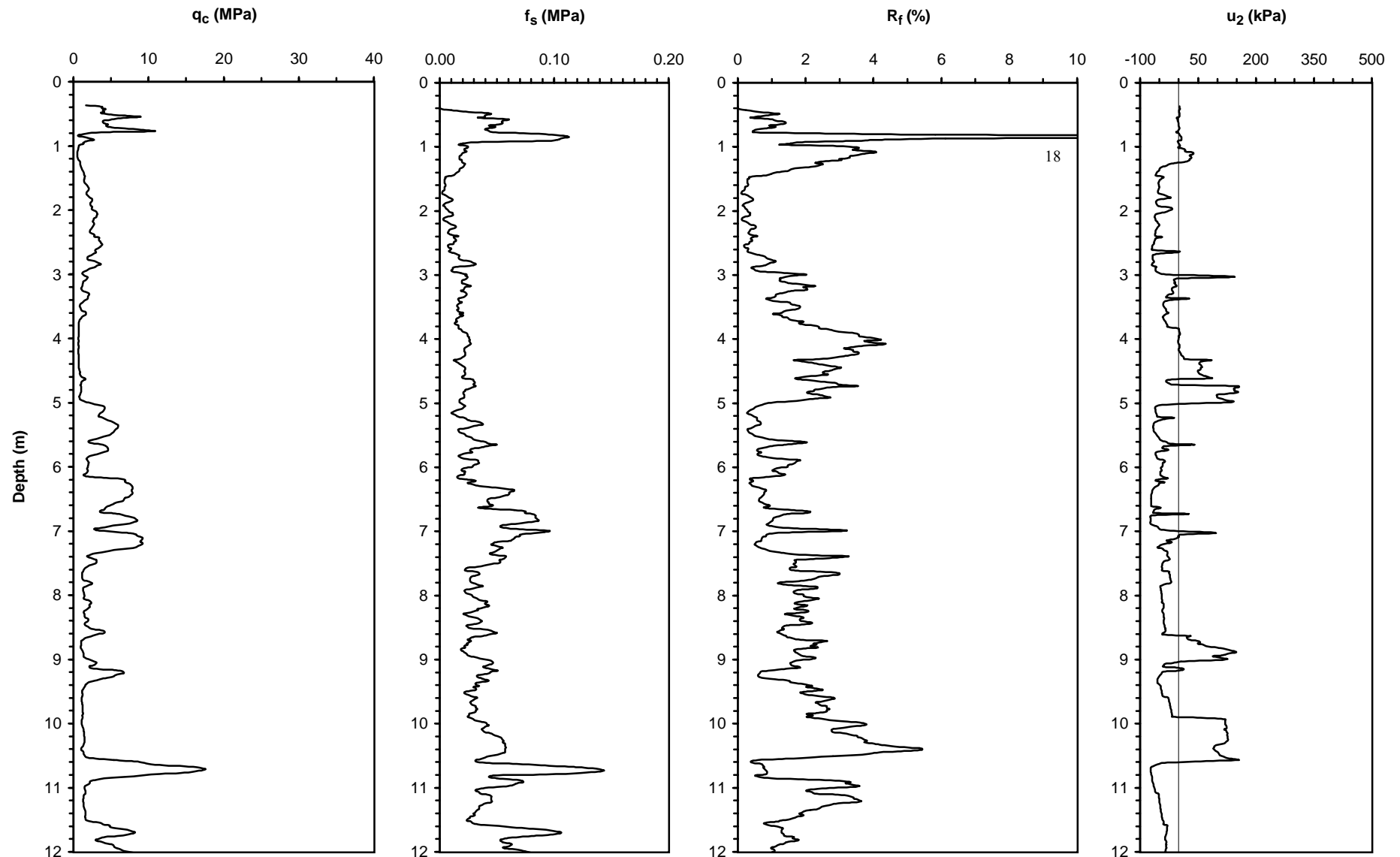
NSF, PEER

**Operator:** ZETAŞ (Zemin Teknolojisi, A. Ş.)

**Responsible Engineers:** J. D. Bray and R. B. Sancio, U. C. Berkeley

Caltrans, CEC, PG&E

**Notes:**



UCB-BYU-UCLA  
ZETAŞ-SAU  
Joint Research

**Project Name:** Ground Failure and Building Performance in Adapazari, Turkey

**Page:** 2 of 3

**Location:** Site 2 - Hasırcılar Street, Yenigün District, Adapazari

Thesis Name: Geostatistical Analysis for Soil Dynamics

**Test Number:** CPT-204

**Elevation:** 31.09 m

**Type of Cone:** ELC10 CFPS No. 991232 (a.p. v.d. Berg)

**Date:** June 21, 2000

Sponsored by:

**File Name:**

**Water Table Elevation:** Not measured

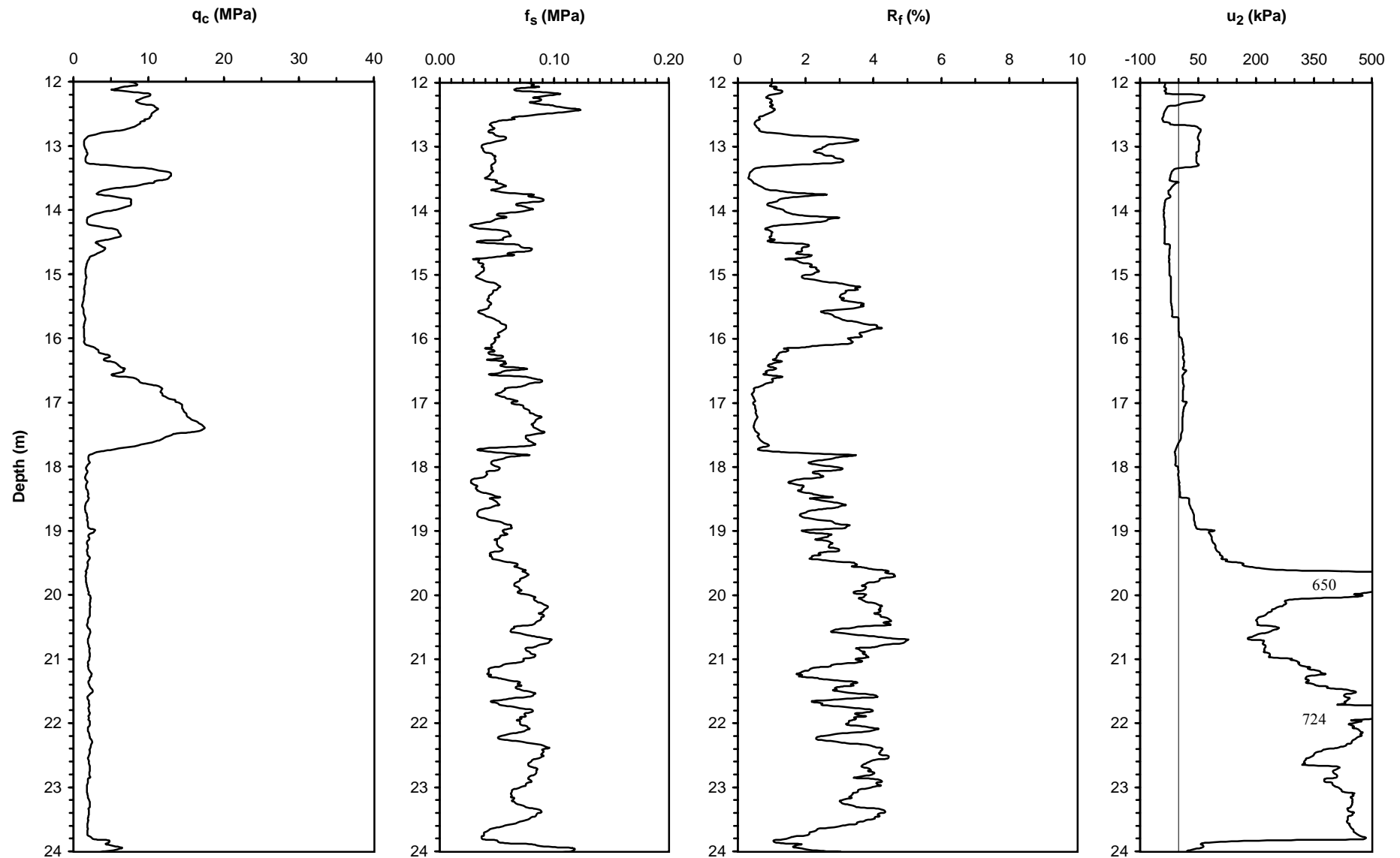
NSF, PEER

**Operator:** ZETAŞ (Zemin Teknolojisi, A. Ş.)

**Responsible Engineers:** J. D. Bray and R. B. Sancio, U. C. Berkeley

Caltrans, CEC, PG&E

**Notes:**



UCB-BYU-UCLA  
ZETAŞ-SAU  
Joint Research

**Project Name:** Ground Failure and Building Performance in Adapazari, Turkey

**Page:** 3 of 3

**Location:** Site 2 - Hası rclar Street, Yenigün District, Adapazari

Thesis Name: Geostatistical Analysis for Soil Dynamics

**Test Number:** CPT-204

**Elevation:** 31.07 m

**Type of Cone:** ELC10 CFPS No. 991232 (a.p. v.d. Berg)

**Date:** June 21, 2000

Sponsored by:

**File Name:**

**Water Table Elevation:** Not measured

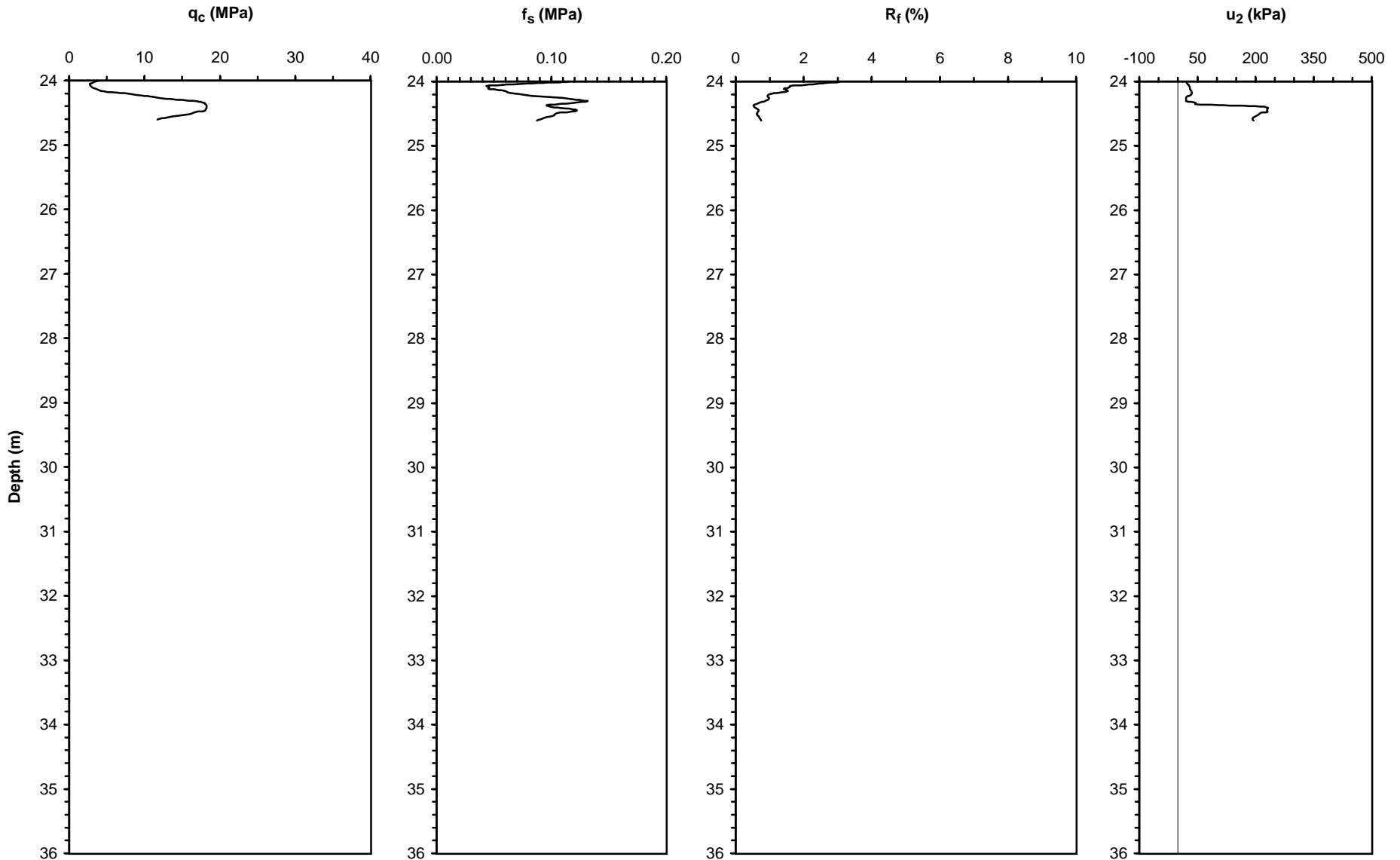
NSF, PEER

**Operator:** ZETAŞ (Zemin Teknolojisi, A. Ş.)

**Responsible Engineers:** J. D. Bray and R. B. Sancio, U. C. Berkeley

Caltrans, CEC, PG&E

**Notes:**



UCB-BYU-UCLA  
ZETAŞ-SAU  
Joint Research

**Project Name:** Ground Failure and Building Performance in Adapazari, Turkey

**Page:** 1 of 1

**Location:** Site 2 - Hasırcılar Street, Yenigün District, Adapazari

Thesis Name: Geostatistical Analysis for Soil Dynamics

**Test Number:** CPT-205

**Elevation:** 31.07 m

**Type of Cone:** ELC10 CF No. 990618 (a.p. v.d. Berg)

**Date:** July 14, 2000 08:57

Sponsored by:

**File Name:**

**Water Table Elevation:** Not measured

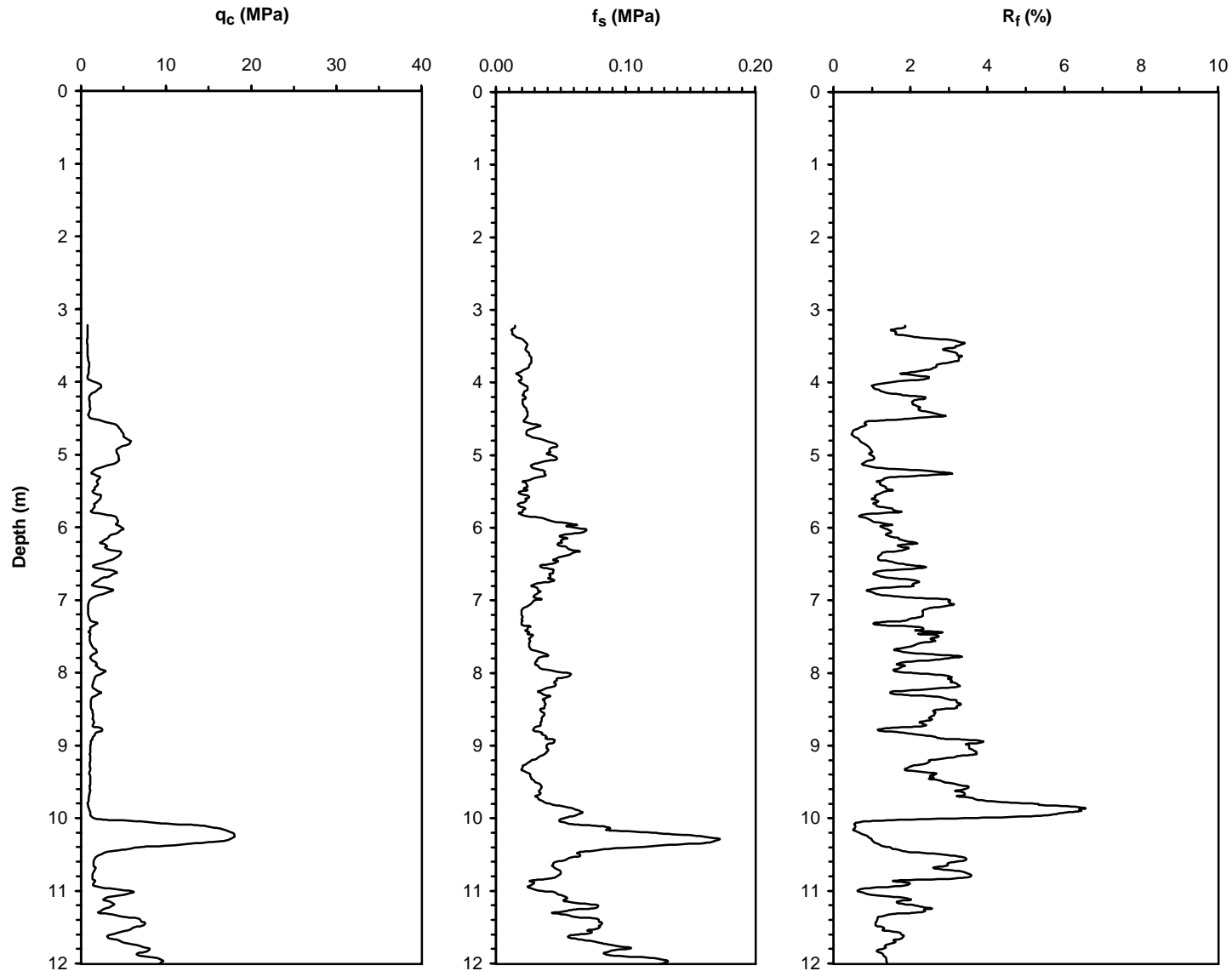
NSF, PEER

**Operator:** ZETAŞ (Zemin Teknolojisi, A. Ş.)

**Responsible Engineers:** J. D. Bray and R. B. Sancio, U. C. Berkeley

Caltrans, CEC, PG&E

**Notes:** Pre-drilled 3.2 m with auger. A casing was inserted up to 2.12 m



UCB-BYU-UCLA  
ZETAŞ-SAU  
Joint Research

**Project Name:** Ground Failure and Building Performance in Adapazari, Turkey

**Page:** 1 of 1

**Location:** Site 2 - Hasırcılar Street, Yenigün District, Adapazari

Thesis Name: Geostatistical Analysis for Soil Dynamics

**Test Number:** CPT-206

**Elevation:** 31.07 m

**Type of Cone:** ELC10 CFPS No. 991232 (a.p. v.d. Berg)

**Date:** June 21, 2000

Sponsored by:

**File Name:**

**Water Table Elevation:** Not measured

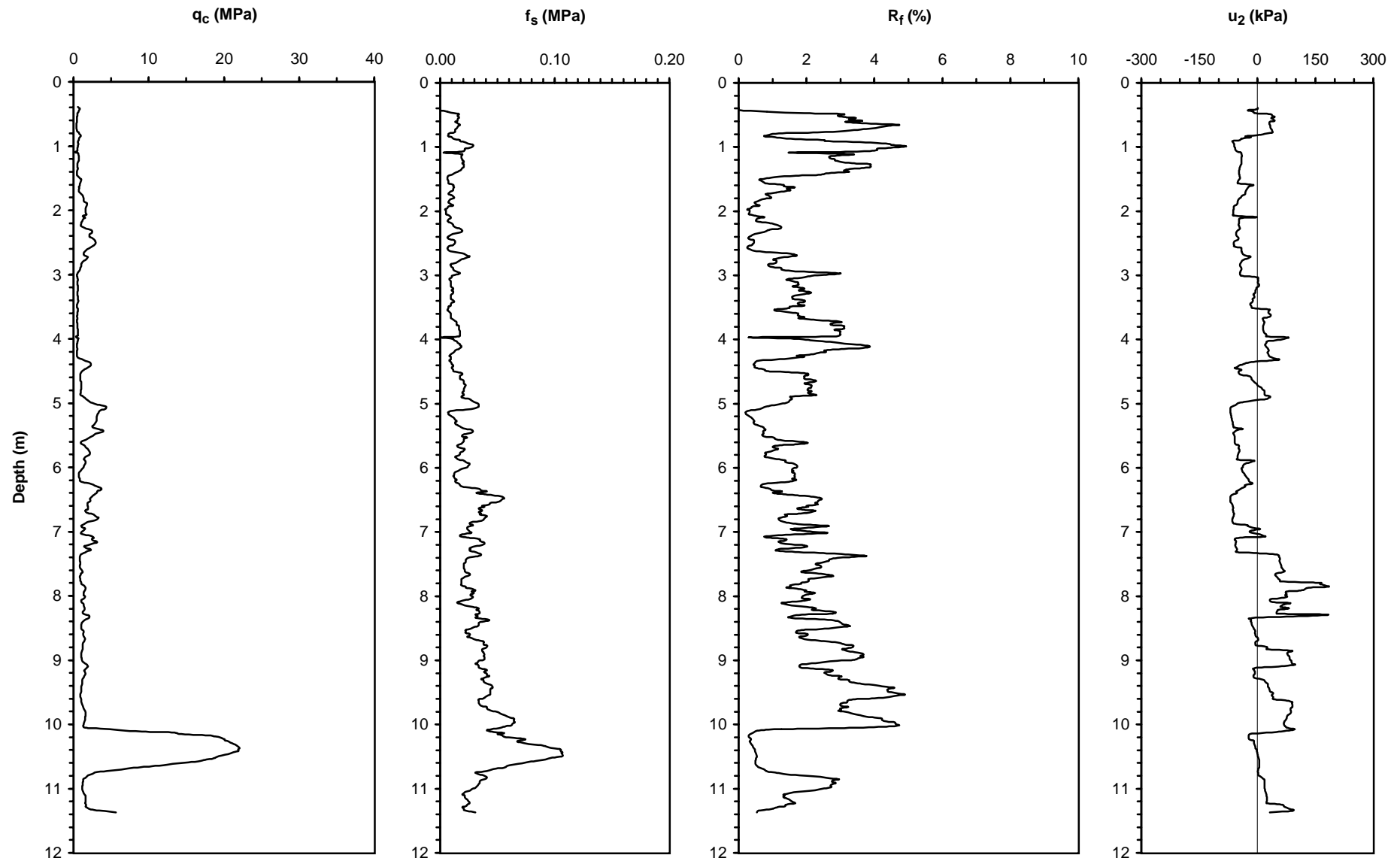
NSF, PEER

**Operator:** ZETAŞ (Zemin Teknolojisi, A. Ş.)

**Responsible Engineers:** J. D. Bray and R. B. Sancio, U. C. Berkeley

Caltrans, CEC, PG&E

**Notes:**



UCB-BYU-UCLA  
ZETAŞ-SAU  
Joint Research

**Project Name:** Ground Failure and Building Performance in Adapazari, Turkey

**Page:** 1 of 3

**Location:** Site 2 - Ç1 rak Street, Yenigün District, Adapazari

Thesis Name: Geostatistical Analysis for Soil Dynamics

**Test Number:** CPT-207

**Elevation:** 31.19 m

**Type of Cone:** ELC10 CF No. 990617 (a.p. v.d. Berg)

**Date:** June 17, 2000 16:34

Sponsored by:

**File Name:**

**Water Table Elevation:** Not measured

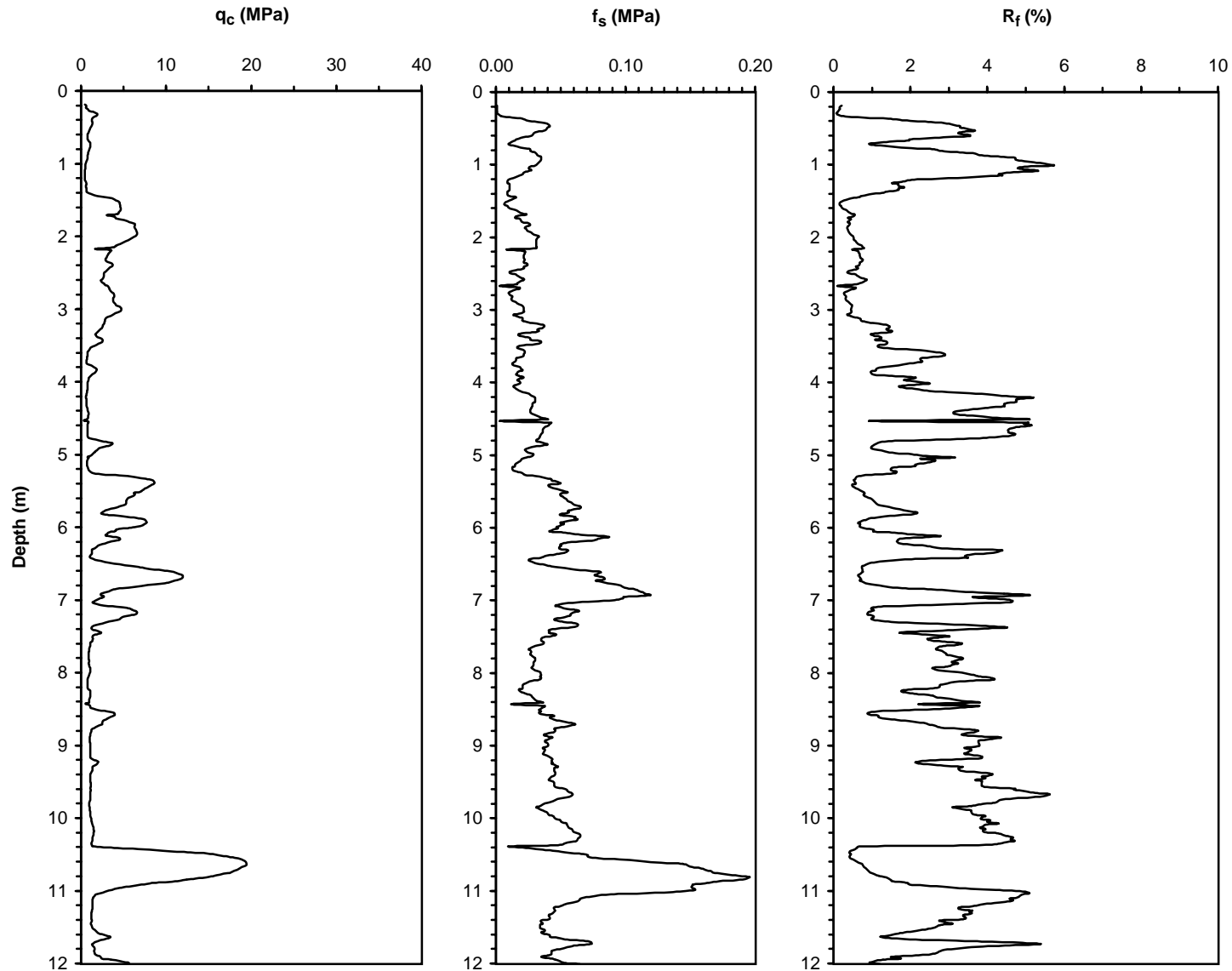
NSF, PEER

**Operator:** ZETAŞ (Zemin Teknolojisi, A. Ş.)

**Responsible Engineers:** J. D. Bray and R. B. Sancio, U. C. Berkeley

Caltrans, CEC, PG&E

**Notes:**



UCB-BYU-UCLA  
ZETAŞ-SAU  
Joint Research

**Project Name:** Ground Failure and Building Performance in Adapazari, Turkey

**Page:** 2 of 3

**Location:** Site 2 - Ç1 rak Street, Yenigün District, Adapazari

**Thesis Name:** Geostatistical Analysis for Soil Dynamics

**Test Number:** CPT-207

**Elevation:** 31.09 m

**Type of Cone:** ELC10 CF No. 990617 (a.p. v.d. Berg)

**Date:** June 17, 2000 16:34

Sponsored by:

**File Name:**

**Water Table Elevation:** Not measured

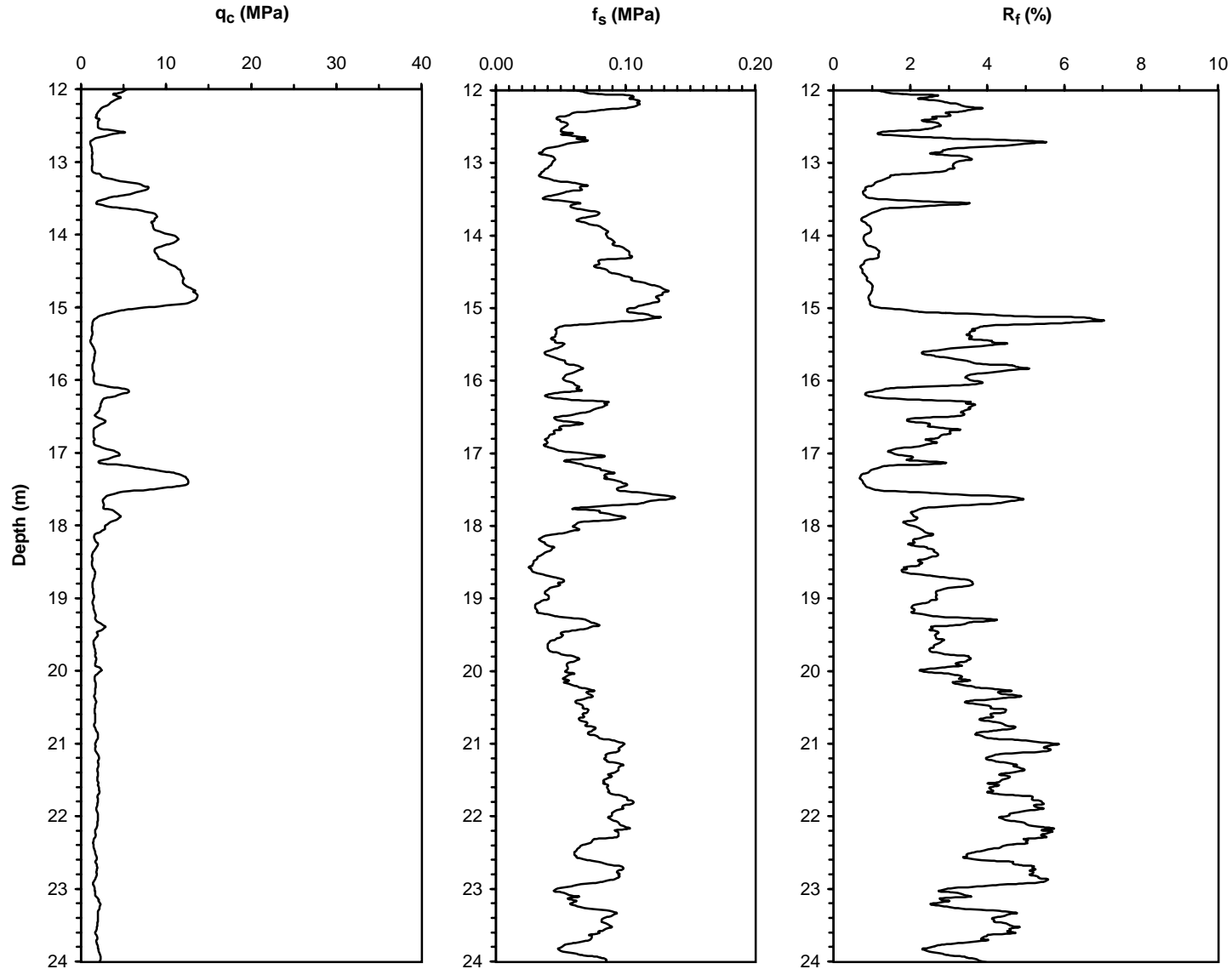
NSF, PEER

**Operator:** ZETAŞ (Zemin Teknolojisi, A. Ş.)

**Responsible Engineers:** J. D. Bray and R. B. Sancio, U. C. Berkeley

Caltrans, CEC, PG&E

**Notes:**



UCB-BYU-UCLA  
ZETAŞ-SAU  
Joint Research

**Project Name:** Ground Failure and Building Performance in Adapazari, Turkey

**Page:** 3 of 3

**Location:** Site 2 - Ç1 rak Street, Yenigün District, Adapazari

Thesis Name: Geostatistical Analysis for Soil Dynamics

**Test Number:** CPT-207

**Elevation:** 31.19 m

**Type of Cone:** ELC10 CF No. 990617 (a.p. v.d. Berg)

**Date:** June 17, 2000 16:34

Sponsored by:

**File Name:**

**Water Table Elevation:** Not measured

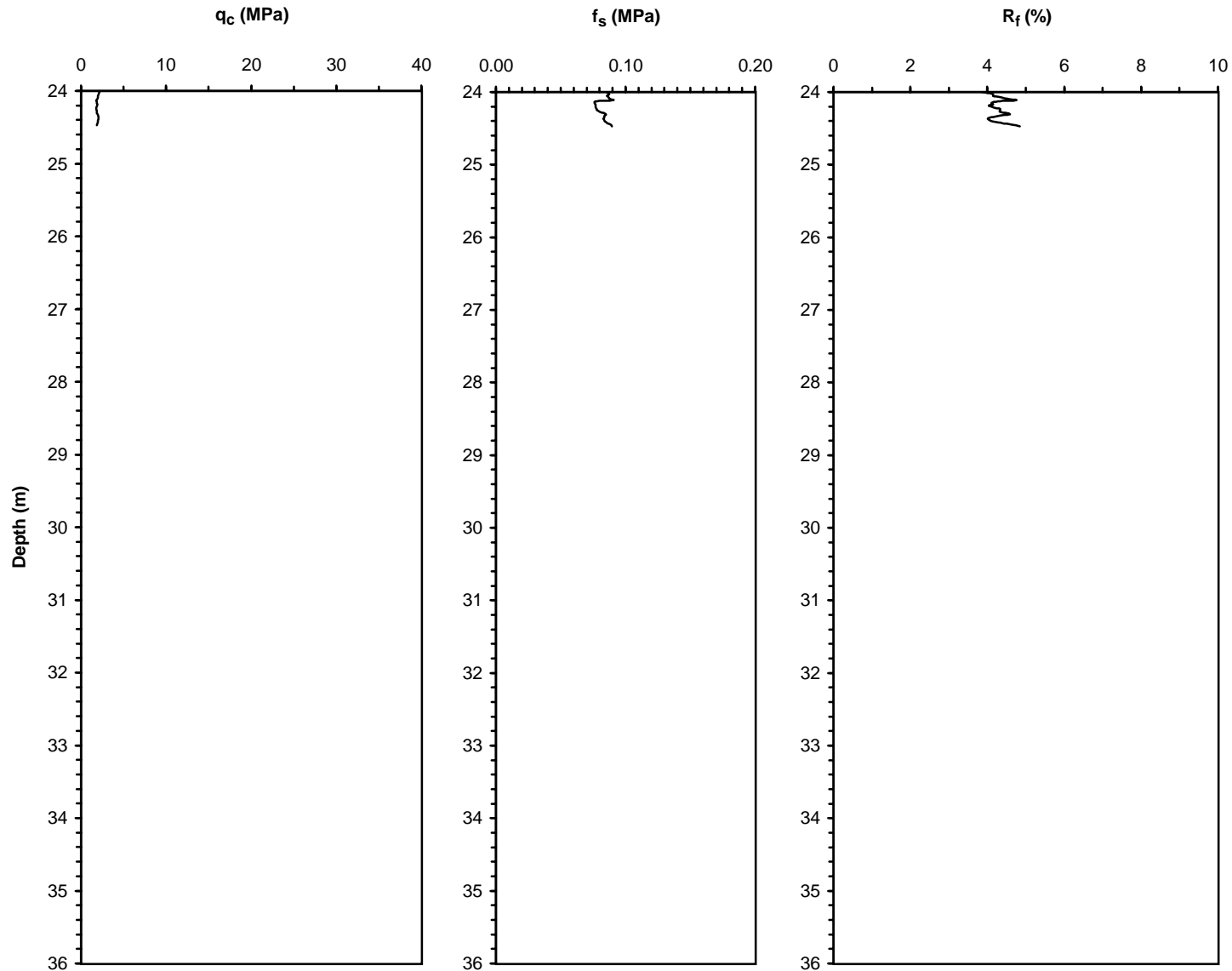
NSF, PEER

**Operator:** ZETAŞ (Zemin Teknolojisi, A. Ş.)

**Responsible Engineers:** J. D. Bray and R. B. Sancio, U. C. Berkeley

Caltrans, CEC, PG&E

**Notes:**



UCB-BYU-UCLA  
ZETAŞ-SAU  
Joint Research

**Project Name:** Ground Failure and Building Performance in Adapazari, Turkey

**Page:** 1 of 3

**Location:** Site 2 - Ç1 rak Street, Yenigün District, Adapazari

Thesis Name: Geostatistical Analysis for Soil Dynamics

**Test Number:** CPT-208

**Elevation:** 31.09 m

**Type of Cone:** ELC10 CFPS No. 991232 (a.p. v.d. Berg)

**Date:** June 19, 2000

Sponsored by:

**File Name:**

**Water Table Elevation:** Not measured

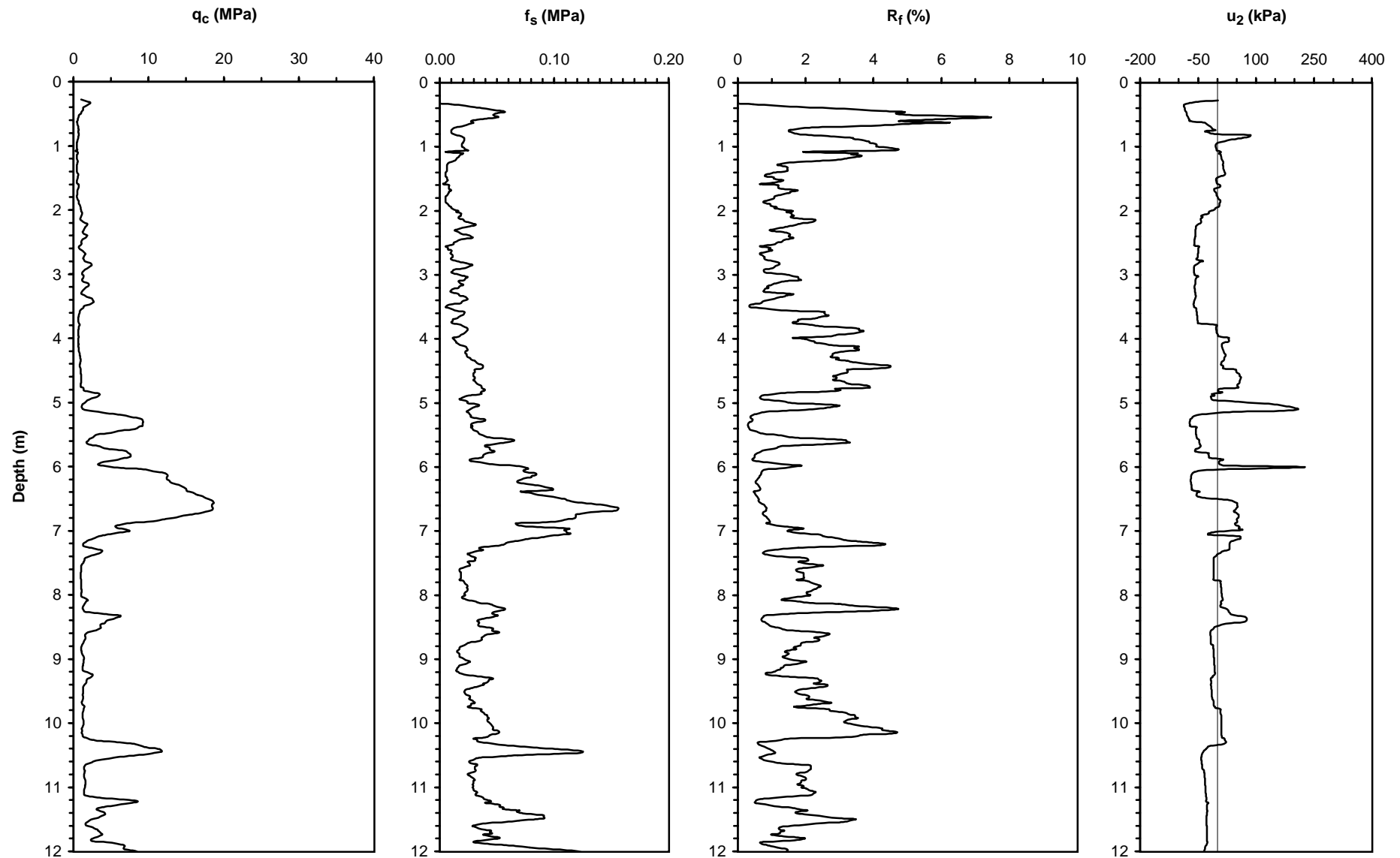
NSF, PEER

**Operator:** ZETAŞ (Zemin Teknolojisi, A. Ş.)

**Responsible Engineers:** J. D. Bray and R. B. Sancio, U. C. Berkeley

Caltrans, CEC, PG&E

**Notes:**



UCB-BYU-UCLA  
ZETAŞ-SAU  
Joint Research

**Project Name:** Ground Failure and Building Performance in Adapazari, Turkey

**Page:** 2 of 3

**Location:** Site 2- Ç1 rak Street, Yenigün District, Adapazari

Thesis Name: Geostatistical Analysis for Soil Dynamics

**Test Number:** CPT-208

**Elevation:** 31.09 m

**Type of Cone:** ELC10 CFPS No. 991232 (a.p. v.d. Berg)

**Date:** June 19, 2000

Sponsored by:

**File Name:**

**Water Table Elevation:** Not measured

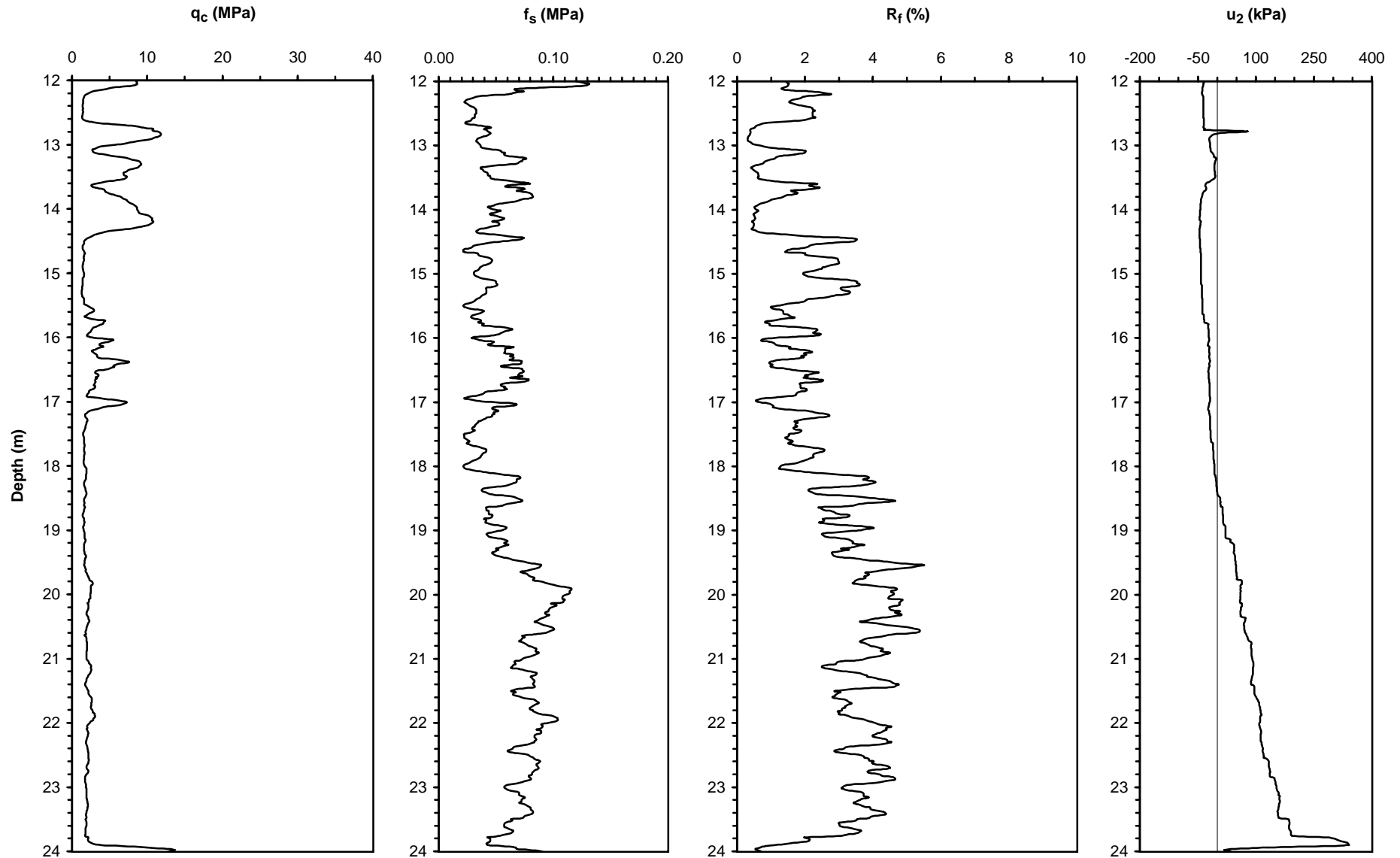
NSF, PEER

**Operator:** ZETAŞ (Zemin Teknolojisi, A. Ş.)

**Responsible Engineers:** J. D. Bray and R. B. Sancio, U. C. Berkeley

Caltrans, CEC, PG&E

**Notes:**



UCB-BYU-UCLA  
ZETAŞ-SAU  
Joint Research

**Project Name:** Ground Failure and Building Performance in Adapazari, Turkey

**Page:** 3 of 3

**Location:** Site 2- Ç1 rak Street, Yenigün District, Adapazari

Thesis Name: Geostatistical Analysis for Soil Dynamics

**Test Number:** CPT-208

**Elevation:** 31.09 m

**Type of Cone:** ELC10 CFPS No. 991232 (a.p. v.d. Berg)

**Date:** June 19, 2000

Sponsored by:

**File Name:**

**Water Table Elevation:** Not measured

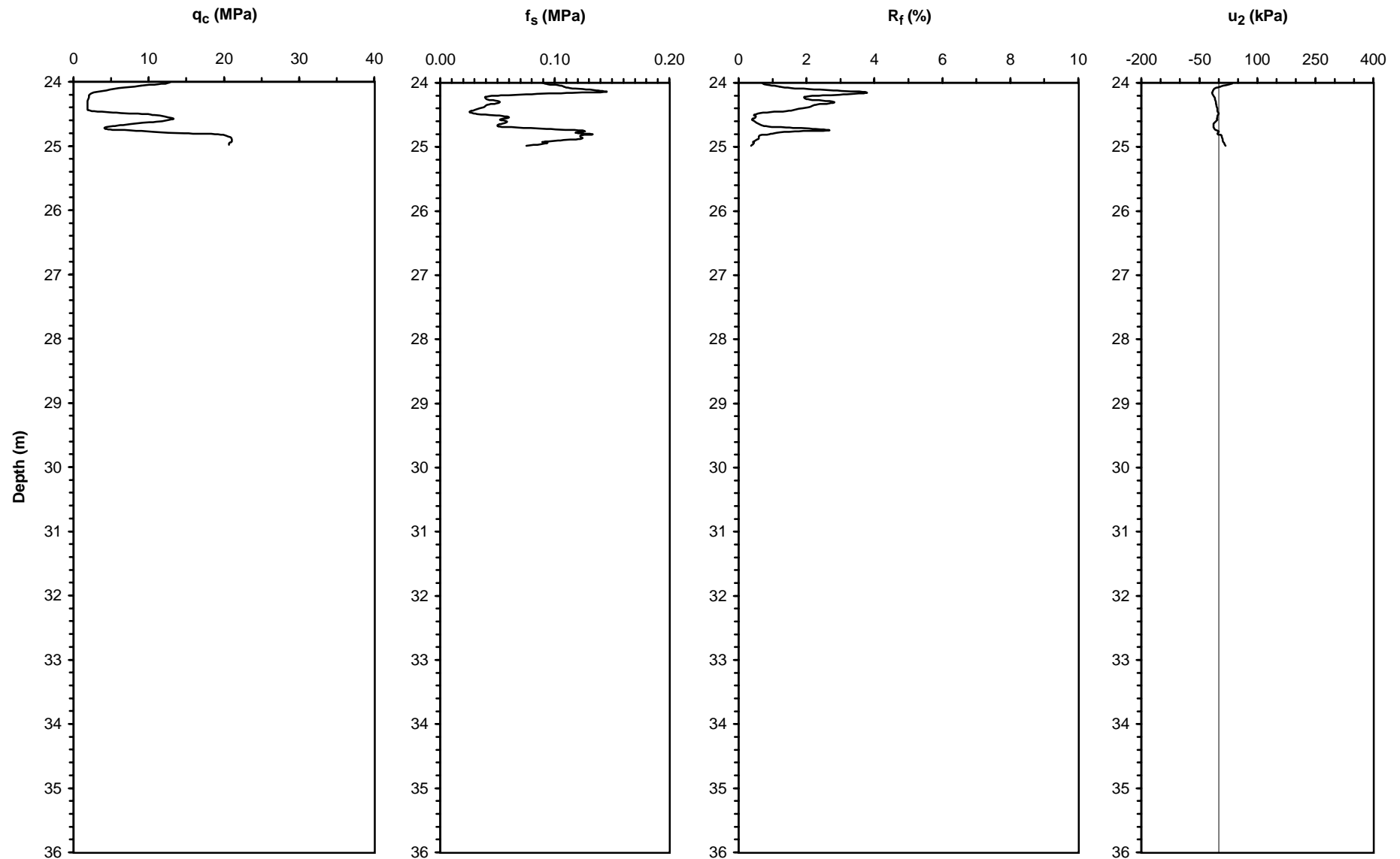
NSF, PEER

**Operator:** ZETAŞ (Zemin Teknolojisi, A. Ş.)

**Responsible Engineers:** J. D. Bray and R. B. Sancio, U. C. Berkeley

Caltrans, CEC, PG&E

**Notes:**



UCB-BYU-UCLA  
ZETAŞ-SAU  
Joint Research

**Project Name:** Ground Failure and Building Performance in Adapazari, Turkey

**Page:** 1 of 1

**Location:** Site 2 - Sönmez Street, Yenigün District, Adapazari

Thesis Name: Geostatistical Analysis for Soil Dynamics

**Test Number:** CPT-209

**Elevation:** 30.97 m

**Type of Cone:** ELC10 CF No. 990618 (a.p. v.d. Berg)

**Date:** July 14, 2000 14:40

Sponsored by:

**File Name:**

**Water Table Elevation:** Not measured

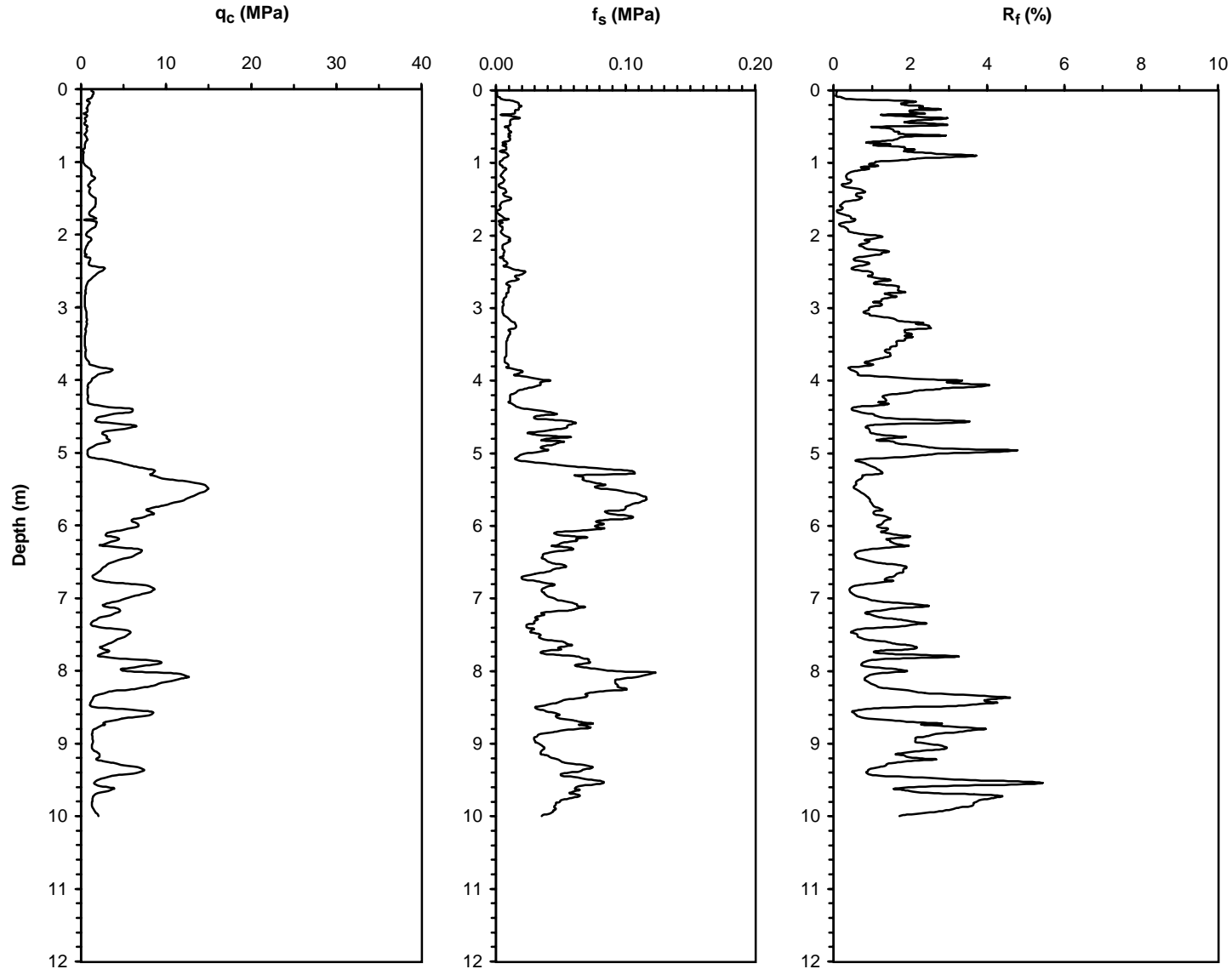
NSF, PEER

**Operator:** ZETAŞ (Zemin Teknolojisi, A. Ş.)

**Responsible Engineers:** J. D. Bray and R. B. Sancio, U. C. Berkeley

Caltrans, CEC, PG&E

**Notes:**



UCB-BYU-UCLA  
ZETAŞ-SAU  
Joint Research

**Project Name:** Ground Failure and Building Performance in Adapazari, Turkey

**Page:** 1 of 1

**Location:** Site 2 - Sönmez Street, Yenigün District, Adapazari

Thesis Name: Geostatistical Analysis for Soil Dynamics

**Test Number:** CPT-210

**Elevation:** 31.39 m

**Type of Cone:** ELC10 CF No. 990618 (a.p. v.d. Berg)

**Date:** July 14, 2000 16:02

Sponsored by:

**File Name:**

**Water Table Elevation:** Not measured

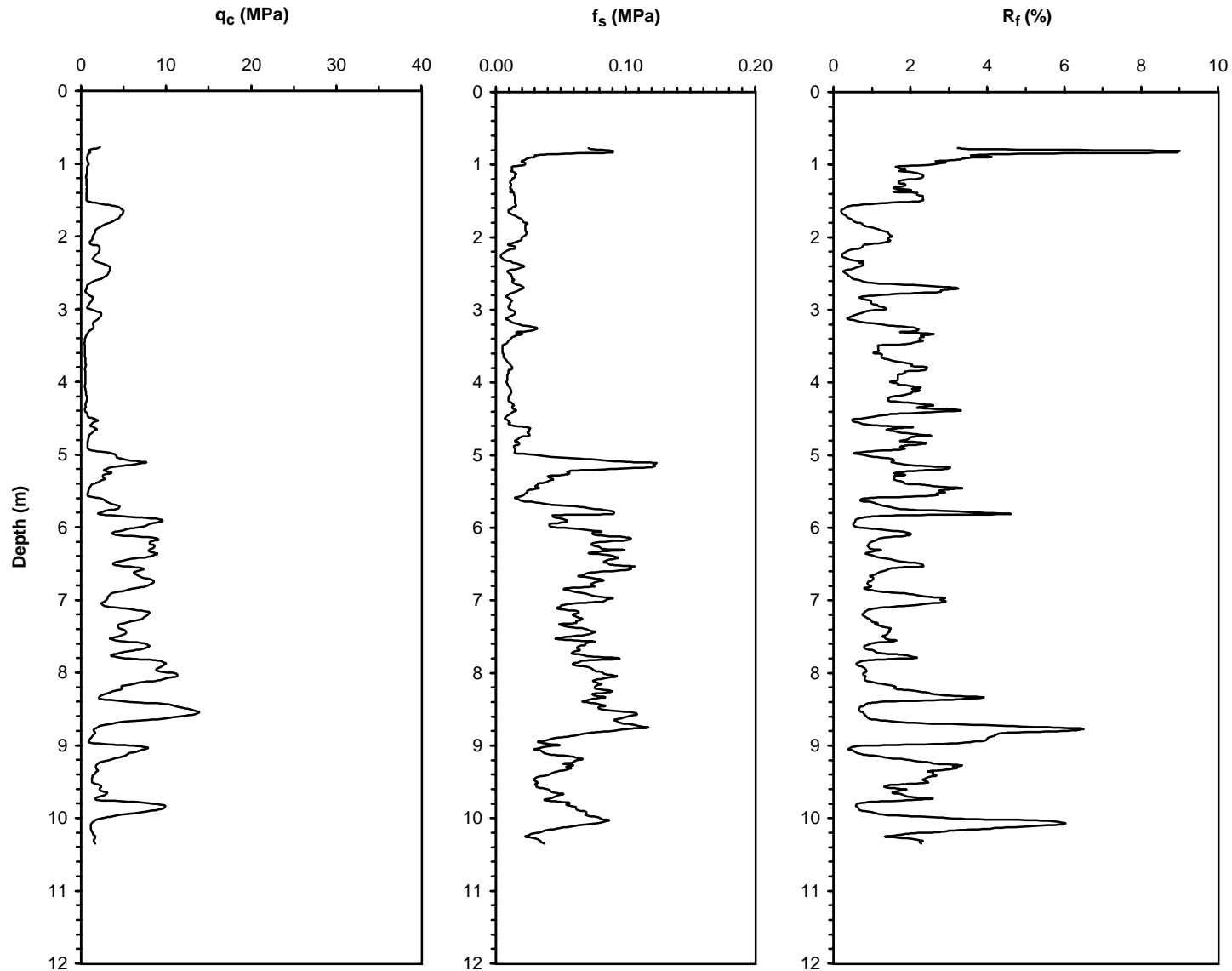
NSF, PEER

**Operator:** ZETAŞ (Zemin Teknolojisi, A. Ş.)

**Responsible Engineers:** J. D. Bray and R. B. Sancio, U. C. Berkeley

Caltrans, CEC, PG&E

**Notes:** Probed with percussion hammer 75 cm to check for utilities



UCB-BYU-UCLA  
ZETAŞ-SAU  
Joint Research

**Project Name:** Ground Failure and Building Performance in Adapazari, Turkey  
**Location:** Site 2 - Sönmez Street, Yenigün District, Adapazari

**Page:** 1 of 3

**Thesis Name:** Geostatistical Analysis for Soil Dynamics

**Test Number:** CPT-211

**Elevation:** 31.12 m

**Type of Cone:** ELC10 CFPS No. 991232 (a.p. v.d. Berg)

**Date:** July 14, 2000

Sponsored by:

**File Name:**

**Water Table Elevation:** Not measured

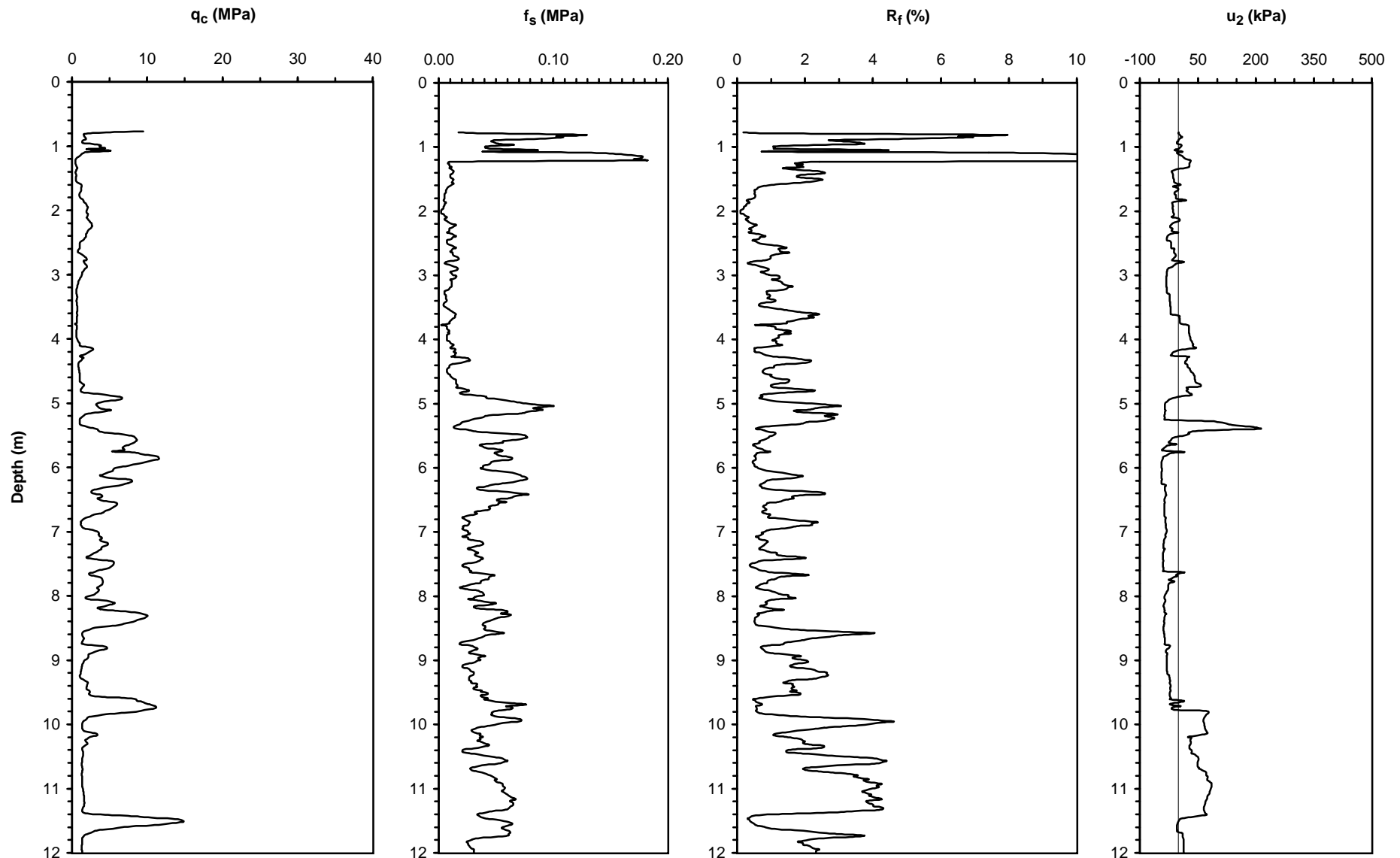
NSF, PEER

**Operator:** ZETAŞ (Zemin Teknolojisi, A. Ş.)

**Responsible Engineers:** J. D. Bray and R. B. Sancio, U. C. Berkeley

Caltrans, CEC, PG&E

**Notes:** Probed with percussion hammer 75 cm to check for utilities



UCB-BYU-UCLA  
ZETAŞ-SAU  
Joint Research

**Project Name:** Ground Failure and Building Performance in Adapazari, Turkey

**Page:** 2 of 3

**Location:** Site 2 - Sönmez Street, Yenigün District, Adapazari

Thesis Name: Geostatistical Analysis for Soil Dynamics

**Test Number:** CPT-211

**Elevation:** 31.12 m

**Type of Cone:** ELC10 CFPS No. 991232 (a.p. v.d. Berg)

**Date:** July 14, 2000

Sponsored by:

**File Name:**

**Water Table Elevation:** Not measured

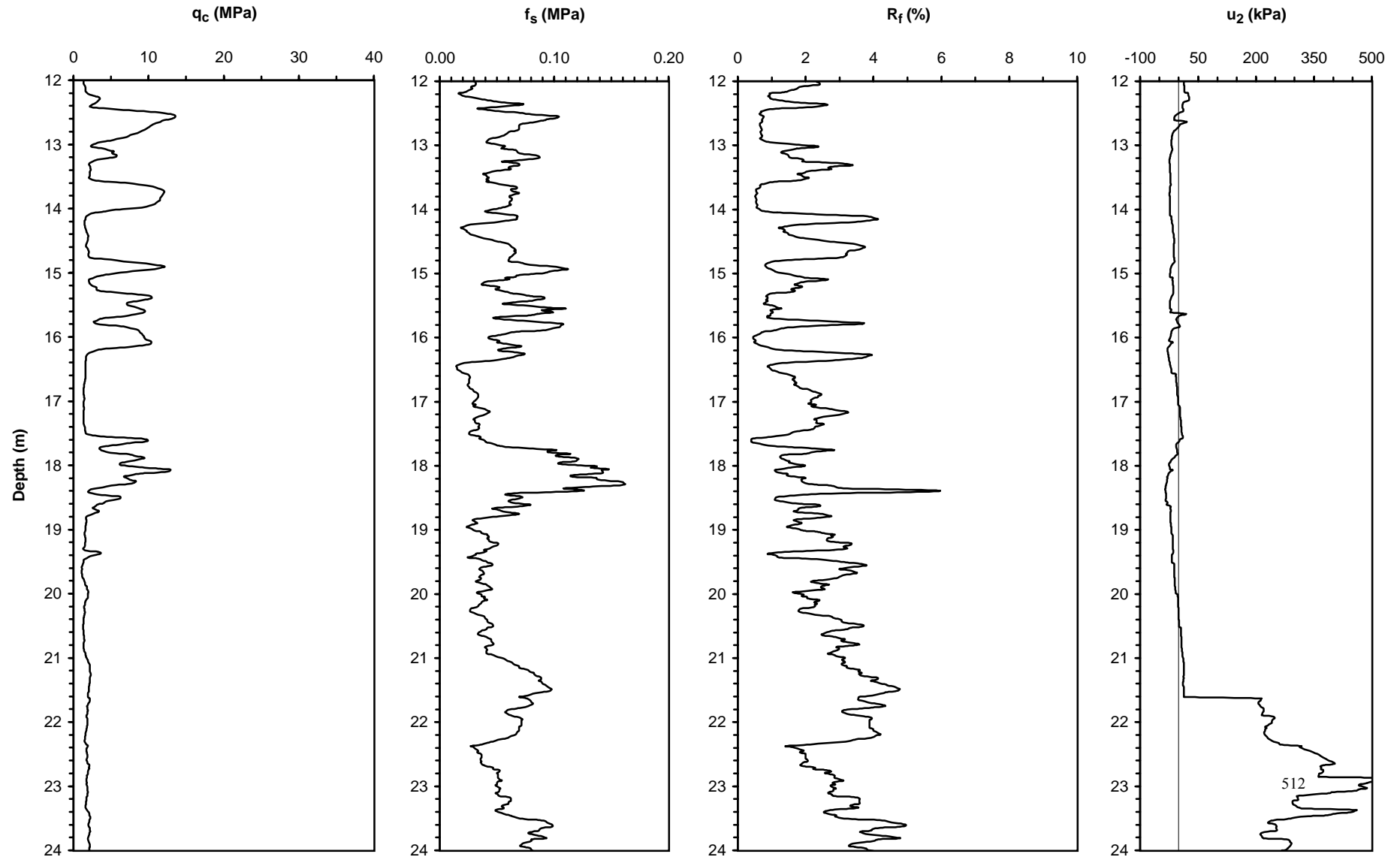
NSF, PEER

**Operator:** ZETAŞ (Zemin Teknolojisi, A. Ş.)

**Responsible Engineers:** J. D. Bray and R. B. Sancio, U. C. Berkeley

Caltrans, CEC, PG&E

**Notes:** Probed with percussion hammer 75 cm to check for utilities



UCB-BYU-UCLA  
ZETAŞ-SAU  
Joint Research

**Project Name:** Ground Failure and Building Performance in Adapazari, Turkey

**Page:** 3 of 3

**Location:** Site 2 - Sönmez Street, Yenigün District, Adapazari

Thesis Name: Geostatistical Analysis for Soil Dynamics

**Test Number:** CPT-211

**Elevation:** 31.12 m

**Type of Cone:** ELC10 CFPS No. 991232 (a.p. v.d. Berg)

**Date:** July 14, 2000

Sponsored by:

**File Name:**

**Water Table Elevation:** Not measured

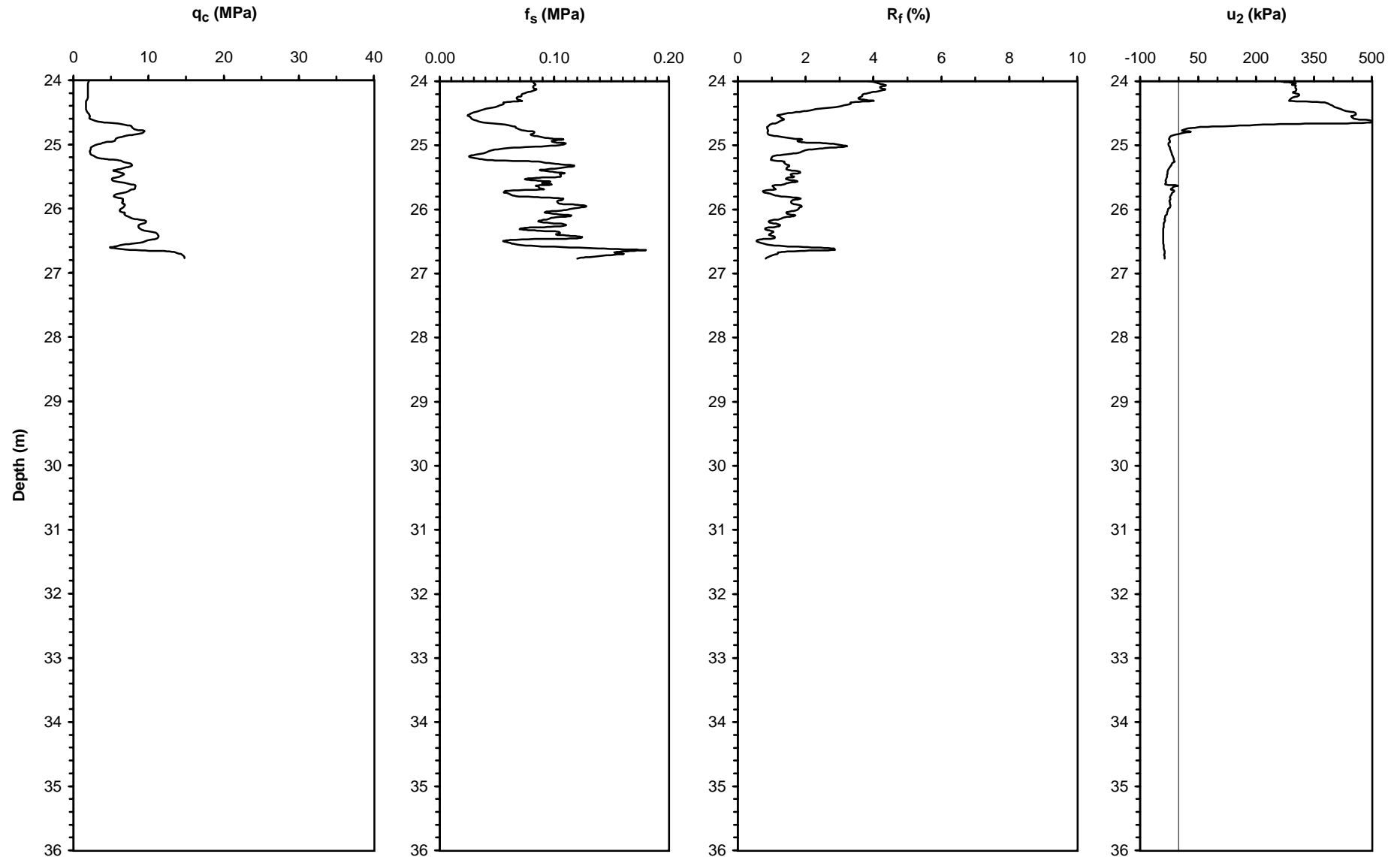
NSF, PEER

**Operator:** ZETAŞ (Zemin Teknolojisi, A. Ş.)

**Responsible Engineers:** J. D. Bray and R. B. Sancio, U. C. Berkeley

Caltrans, CEC, PG&E

**Notes:** Probed with percussion hammer 75 cm to check for utilities



UCB-BYU-UCLA  
ZETAŞ-SAU  
Joint Research

**Project Name:** Ground Failure and Building Performance in Adapazari, Turkey

**Page:** 1 of 1

**Location:** Site 3 - Kavaklar Avenue, T1 ğcılar District, Adapazari

Thesis Name: Geostatistical Analysis for Soil Dynamics

**Test Number:** CPT-301

**Elevation:** 32.87 m

**Type of Cone:** ELC10 CFPS No. 991232 (a.p. v.d. Berg)

**Date:** June 20, 2000

Sponsored by:

**File Name:**

**Water Table Elevation:** Not measured

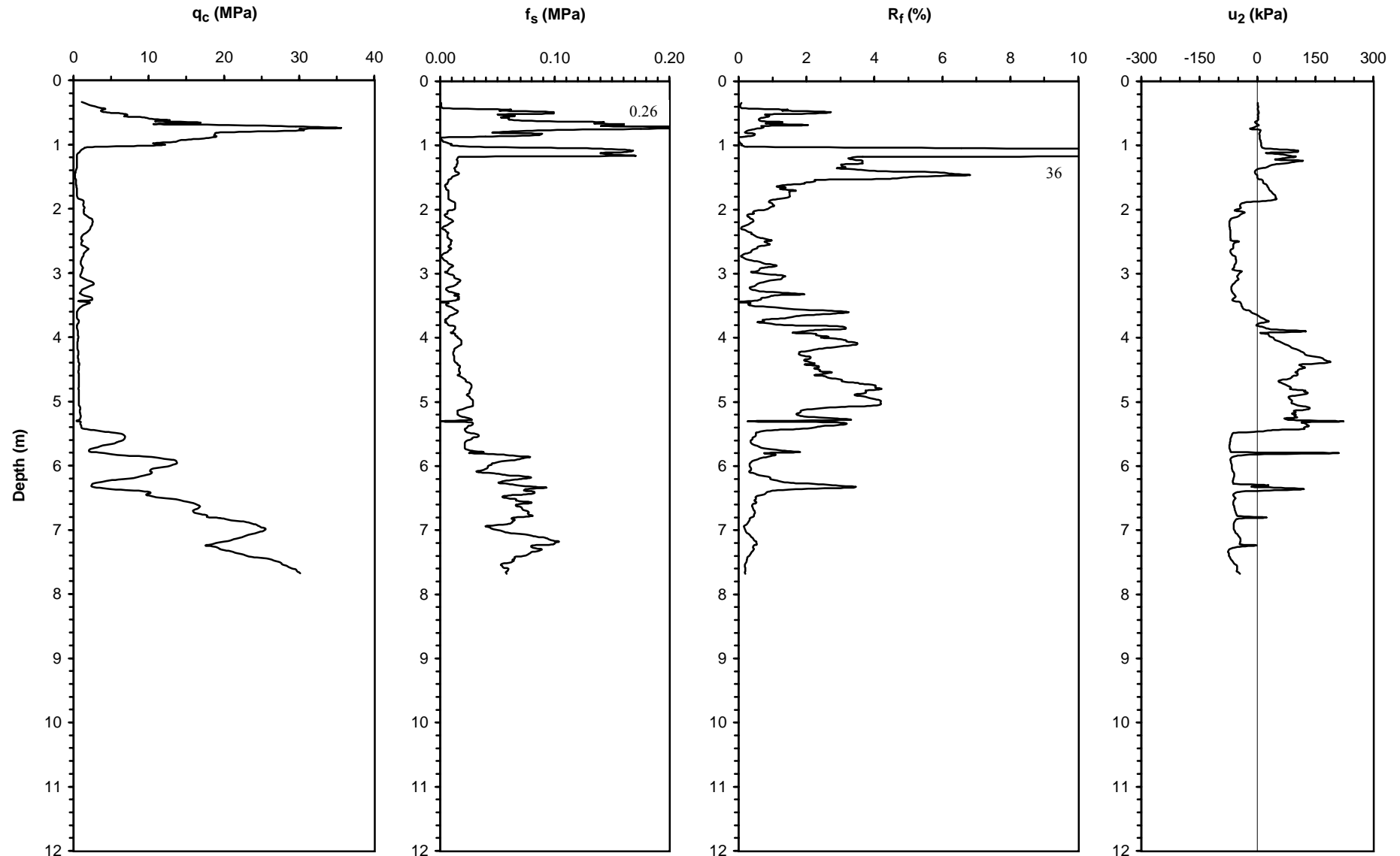
NSF, PEER

**Operator:** ZETAŞ (Zemin Teknolojisi, A. Ş.)

**Responsible Engineers:** J. D. Bray and R. B. Sancio, U. C. Berkeley

Caltrans, CEC, PG&E

**Notes:**



UCB-BYU-UCLA  
ZETAŞ-SAU  
Joint Research

**Project Name:** Ground Failure and Building Performance in Adapazari, Turkey

**Page:** 1 of 3

**Location:** Site 3 - Kavaklar Avenue, T1 cılar District, Adapazari

Thesis Name: Geostatistical Analysis for Soil Dynamics

**Test Number:** CPT-302

**Elevation:** 32.92 m

**Type of Cone:** ELC10 CFPS No. 991232 (a.p. v.d. Berg)

**Date:** June 20, 2000

Sponsored by:

**File Name:**

**Water Table Elevation:** 28 cm

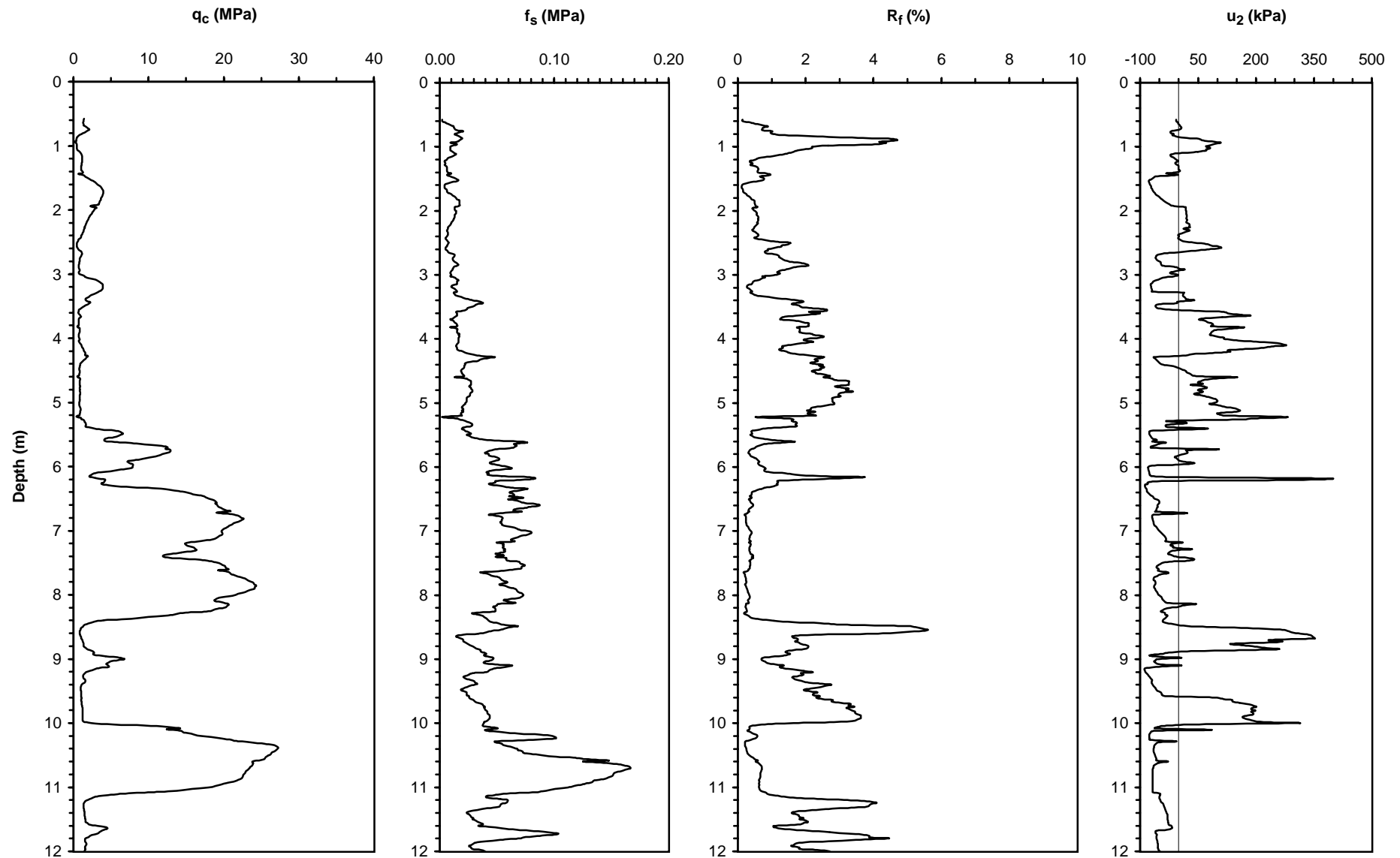
NSF, PEER

**Operator:** ZETAŞ (Zemin Teknolojisi, A. Ş.)

**Responsible Engineers:** J. D. Bray and R. B. Sancio, U. C. Berkeley

Caltrans, CEC, PG&E

**Notes:**



UCB-BYU-UCLA  
ZETAŞ-SAU  
Joint Research

**Project Name:** Ground Failure and Building Performance in Adapazari, Turkey

**Page:** 2 of 3

**Location:** Site 3 - Kavaklar Avenue, T1 cılar District, Adapazari

Thesis Name: Geostatistical Analysis for Soil Dynamics

**Test Number:** CPT-302

**Elevation:** 32.92 m

**Type of Cone:** ELC10 CFPS No. 991232 (a.p. v.d. Berg)

**Date:** June 20, 2000

Sponsored by:

**File Name:**

**Water Table Elevation:** 28 cm

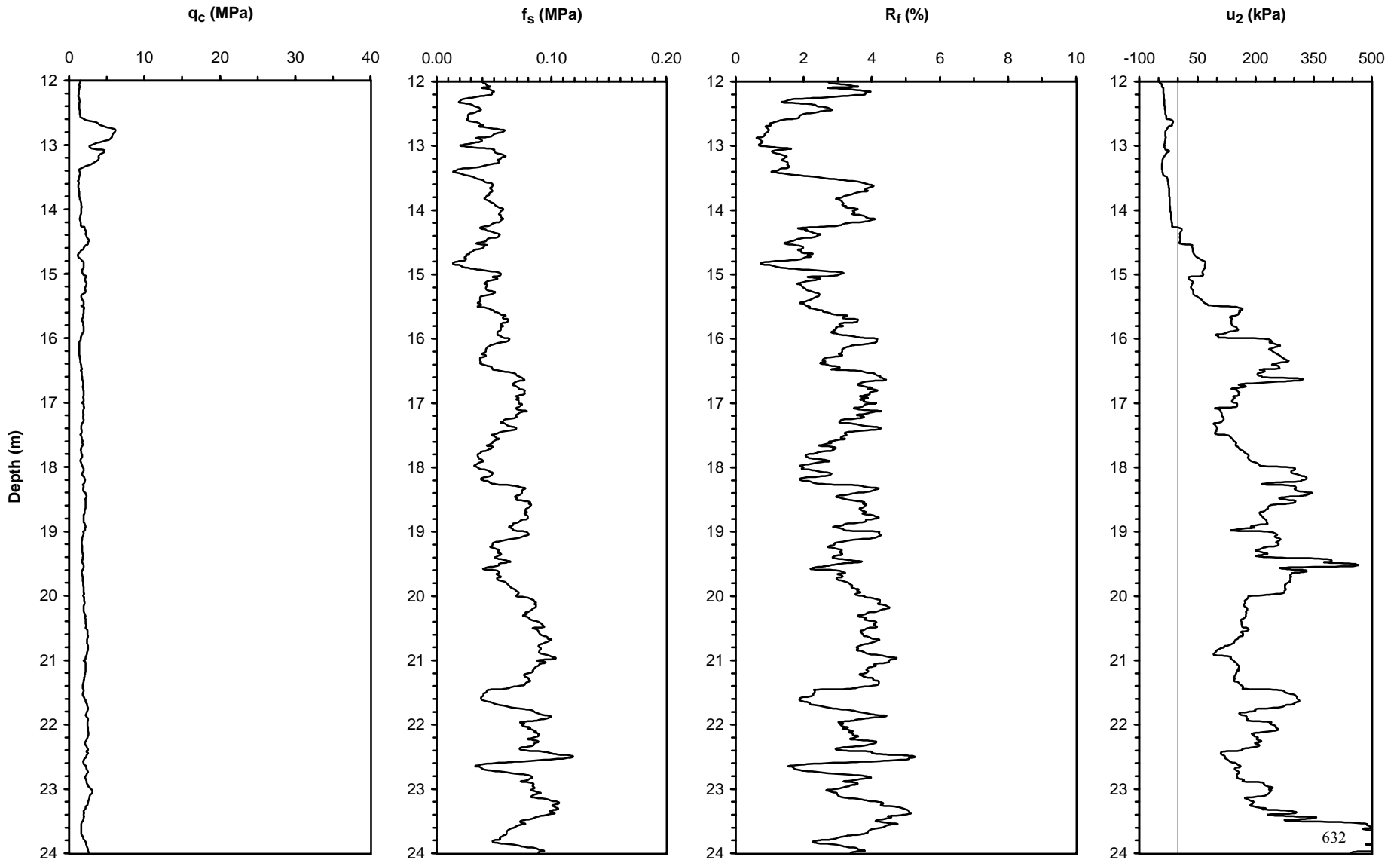
NSF, PEER

**Operator:** ZETAŞ (Zemin Teknolojisi, A. Ş.)

**Responsible Engineers:** J. D. Bray and R. B. Sancio, U. C. Berkeley

Caltrans, CEC, PG&E

**Notes:**



UCB-BYU-UCLA  
ZETAŞ-SAU  
Joint Research

**Project Name:** Ground Failure and Building Performance in Adapazari, Turkey

**Page:** 3 of 3

**Location:** Site 3 - Kavaklar Avenue, T1 ğcılar District, Adapazari

Thesis Name: Geostatistical Analysis for Soil Dynamics

**Test Number:** CPT-302

**Elevation:** 32.92 m

**Type of Cone:** ELC10 CFPS No. 991232 (a.p. v.d. Berg)

**Date:** June 20, 2000

Sponsored by:

**File Name:**

**Water Table Elevation:** 28 cm

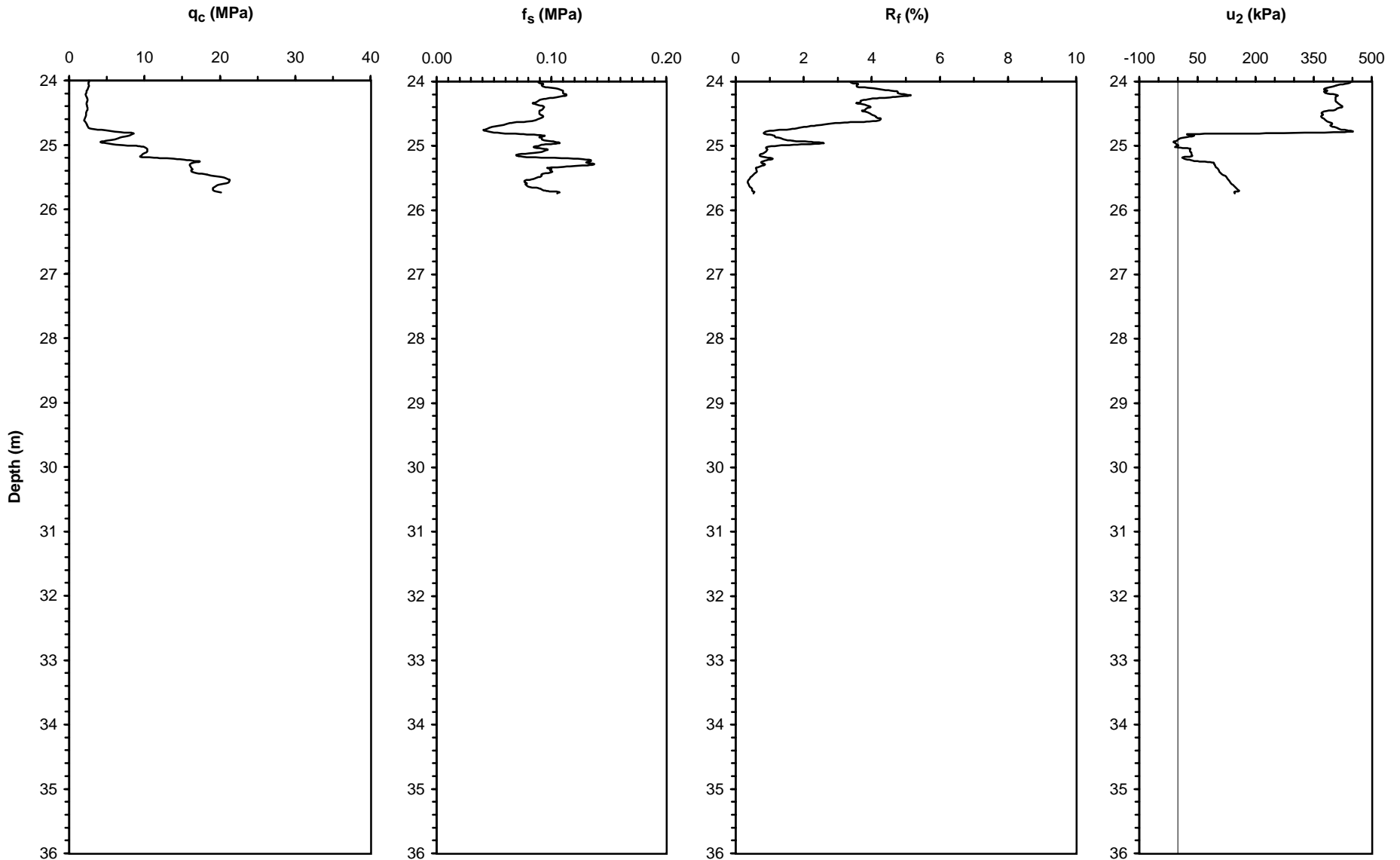
NSF, PEER

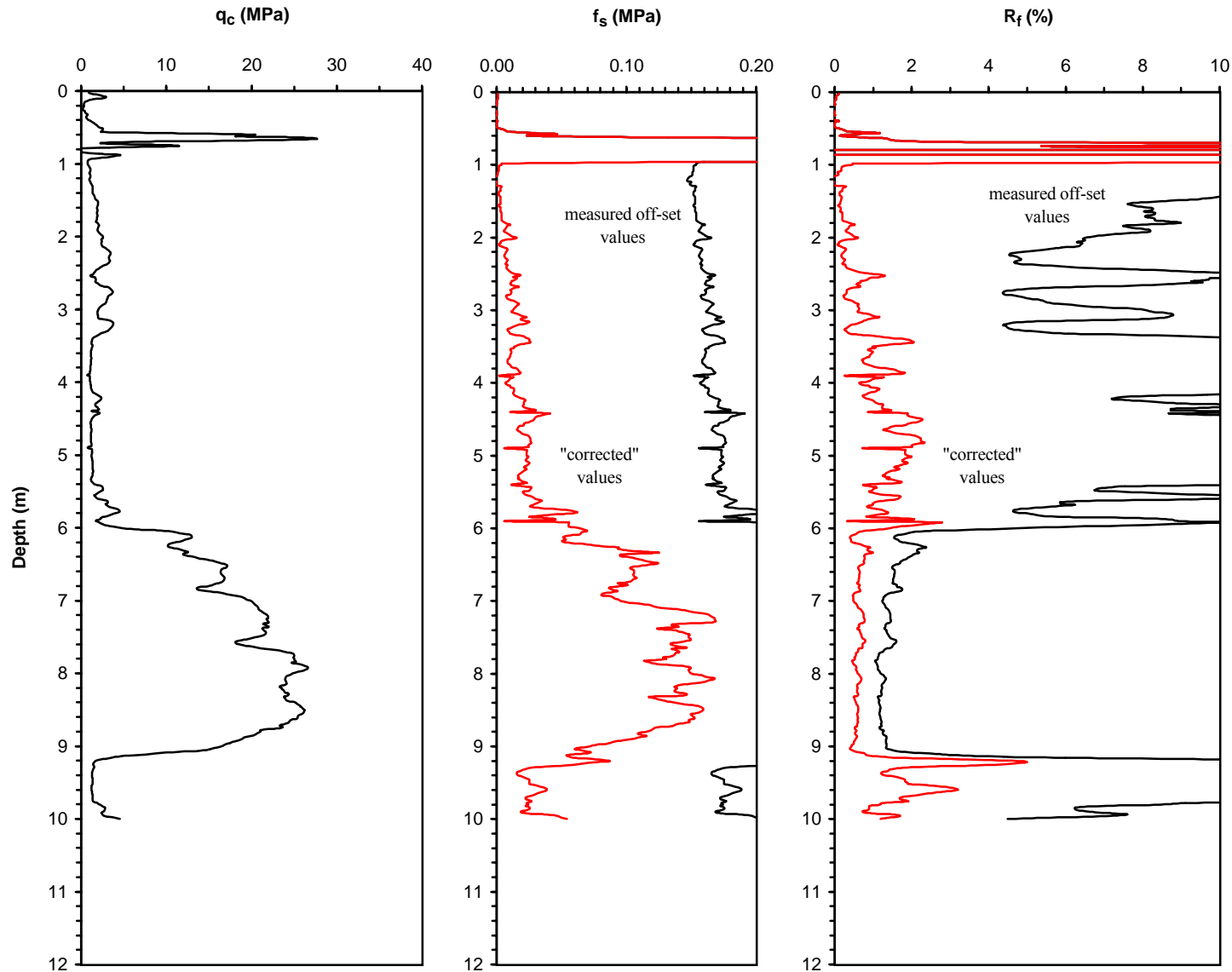
**Operator:** ZETAŞ (Zemin Teknolojisi, A. Ş.)

**Responsible Engineers:** J. D. Bray and R. B. Sancio, U. C. Berkeley

Caltrans, CEC, PG&E

**Notes:**





UCB-BYU-UCLA  
ZETAŞ-SAU  
Joint Research

**Project Name:** Ground Failure and Building Performance in Adapazari, Turkey

**Page:** 1 of 1

**Location:** Site 3 - Kavaklar Avenue, T1 cılar District, Adapazari

Thesis Name: Geostatistical Analysis for Soil Dynamics

**Test Number:** CPT-304

**Elevation:** 32.98 m

**Type of Cone:** ELC10 CF No. 990618 (a.p. v.d. Berg)

**Date:** July 18, 2000 10:30

Sponsored by:

**File Name:**

**Water Table Elevation:** Not measured

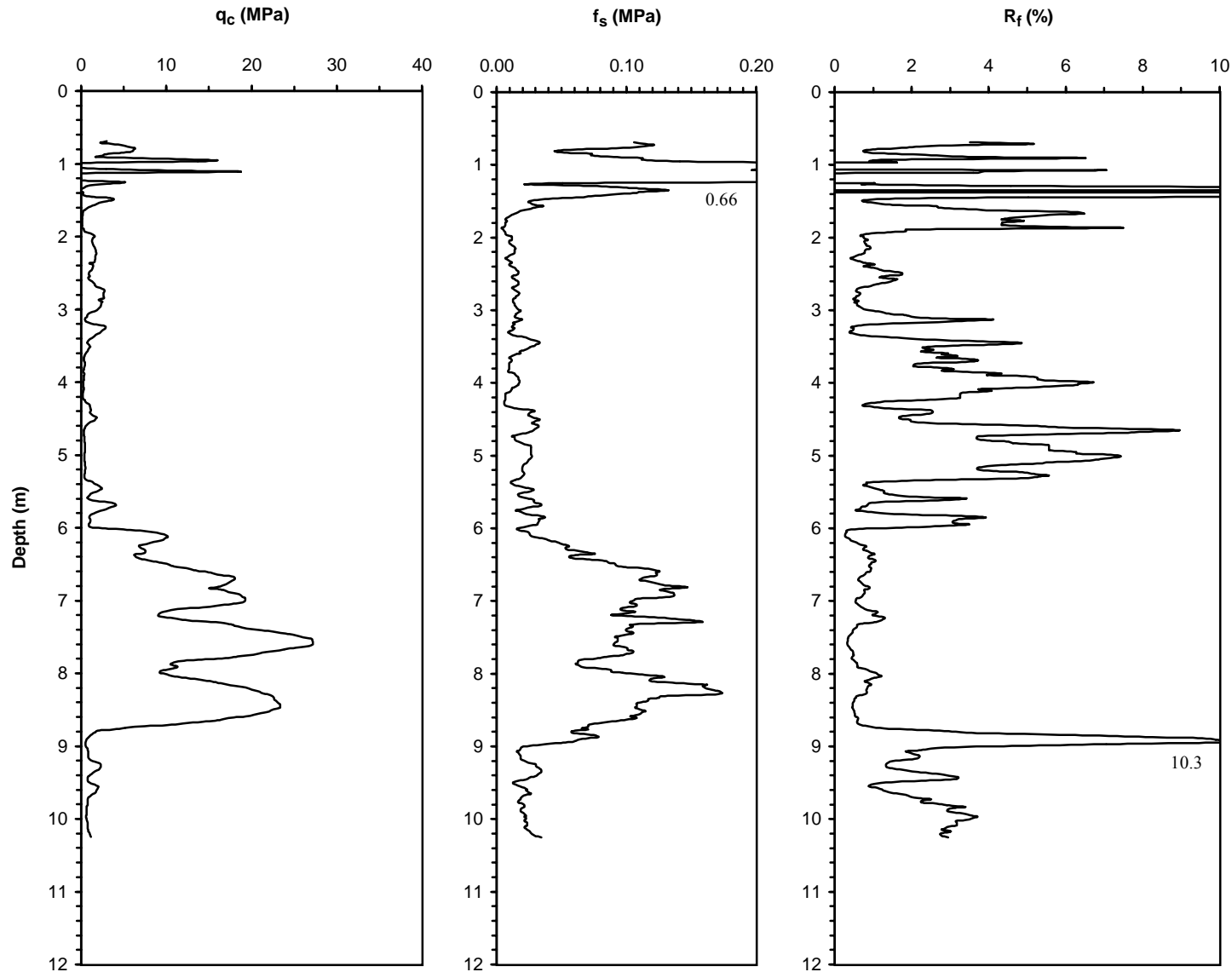
NSF, PEER

**Operator:** ZETAŞ (Zemin Teknolojisi, A. Ş.)

**Responsible Engineers:** J. D. Bray and R. B. Sancio, U. C. Berkeley

Caltrans, CEC, PG&E

**Notes:** Probed with percussion hammer 68 cm to check for utilities



UCB-BYU-UCLA  
ZETAŞ-SAU  
Joint Research

**Project Name:** Ground Failure and Building Performance in Adapazari, Turkey  
**Location:** Site 3 - Kavaklar Avenue, T1 ğılar District, Adapazari  
Thesis Name: Geostatistical Analysis for Soil Dynamics

**Page:** 1 of 1

**Test Number:** CPT-305  
**Type of Cone:** ELC10 CF No. 990618 (a.p. v.d. Berg)

**Elevation:** 32.61 m

**Date:** July 18, 2000 18:09

Sponsored by:

**File Name:**

**Water Table Elevation:** Not measured

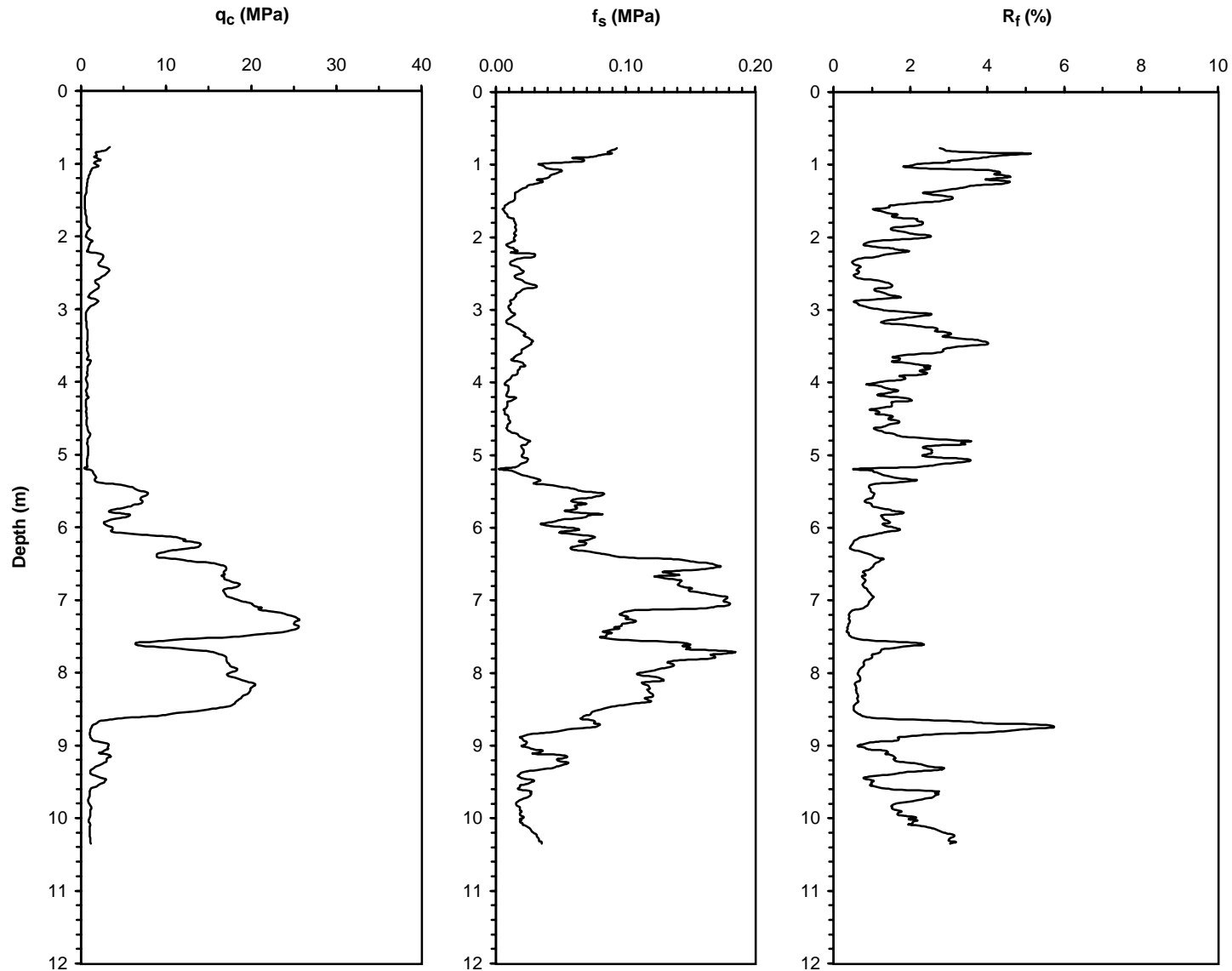
NSF, PEER

**Operator:** ZETAŞ (Zemin Teknolojisi, A. Ş.)

**Responsible Engineers:** J. D. Bray and R. B. Sancio, U. C. Berkeley

Caltrans, CEC, PG&E

**Notes:** Probed with percussion hammer 75 cm to check for utilities



UCB-BYU-UCLA  
ZETAŞ-SAU  
Joint Research

**Project Name:** Ground Failure and Building Performance in Adapazari, Turkey  
**Location:** Site 3 - Kavaklar Avenue, T1 ğılar District, Adapazari  
Thesis Name: Geostatistical Analysis for Soil Dynamics

Page: 1 of 1

**Test Number:** CPT-306  
**Type of Cone:** ELC10 CFP No. 000605 (a.p. v.d. Berg)

**Elevation:** 32.64 m

**Date:** July 19, 2000

Sponsored by:

**File Name:**

**Water Table Elevation:** Not measured

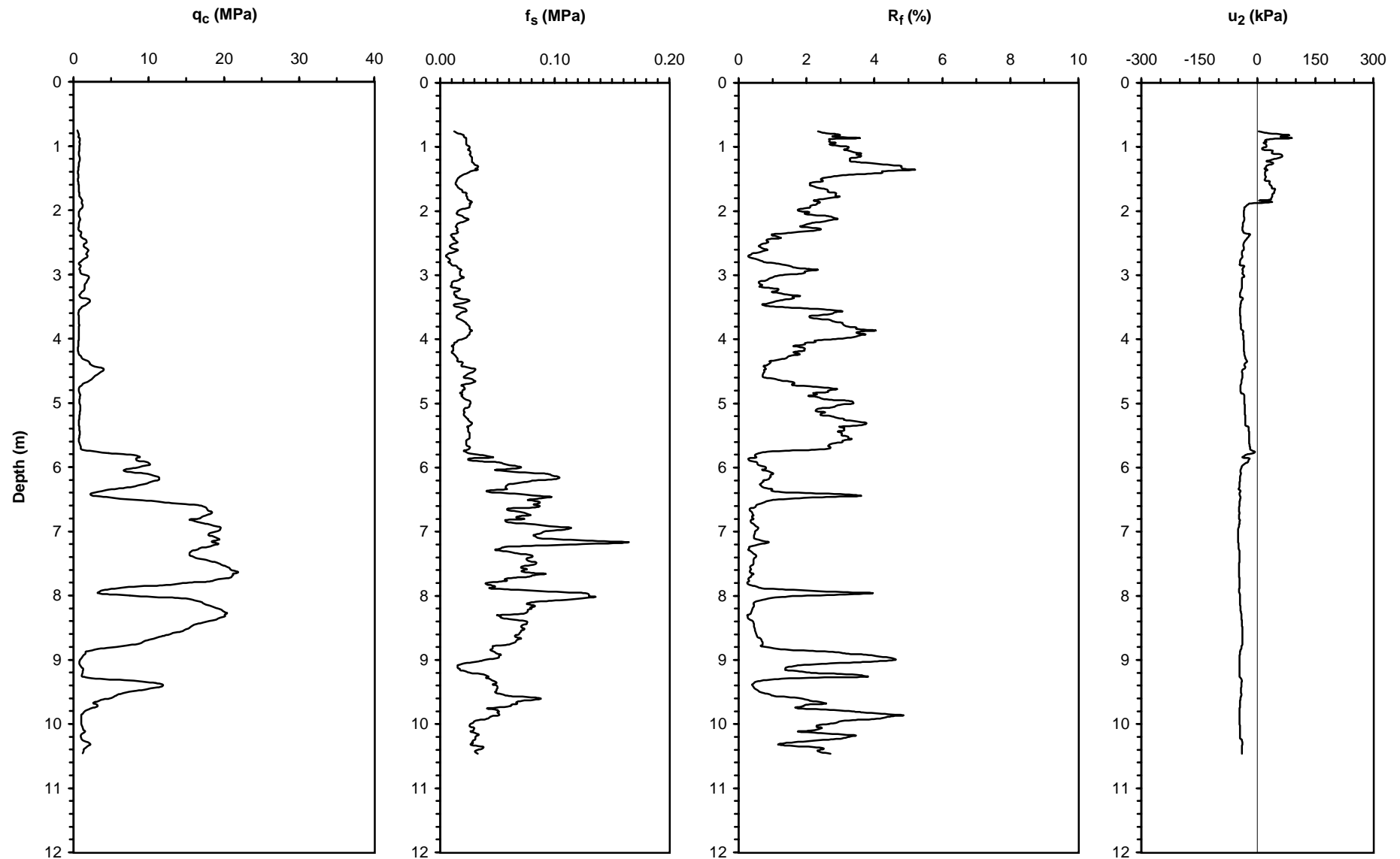
NSF, PEER

**Operator:** ZETAŞ (Zemin Teknolojisi, A. Ş.)

**Responsible Engineers:** J. D. Bray and R. B. Sancio, U. C. Berkeley

Caltrans, CEC, PG&E

**Notes:** Probed with percussion hammer 75 cm to check for utilities



UCB-BYU-UCLA  
ZETAŞ-SAU  
Joint Research

**Project Name:** Ground Failure and Building Performance in Adapazari, Turkey

**Page:** 1 of 1

**Location:** Site 3 - Ankara Avenue, Orta District, Adapazari

Thesis Name: Geostatistical Analysis for Soil Dynamics

**Test Number:** CPT-307

**Elevation:** 32.61 m

**Type of Cone:** ELC10 CF No.990618 (a.p. v.d. Berg)

**Date:** July 18, 2000 08:30

Sponsored by:

**File Name:**

**Water Table Elevation:** Not measured

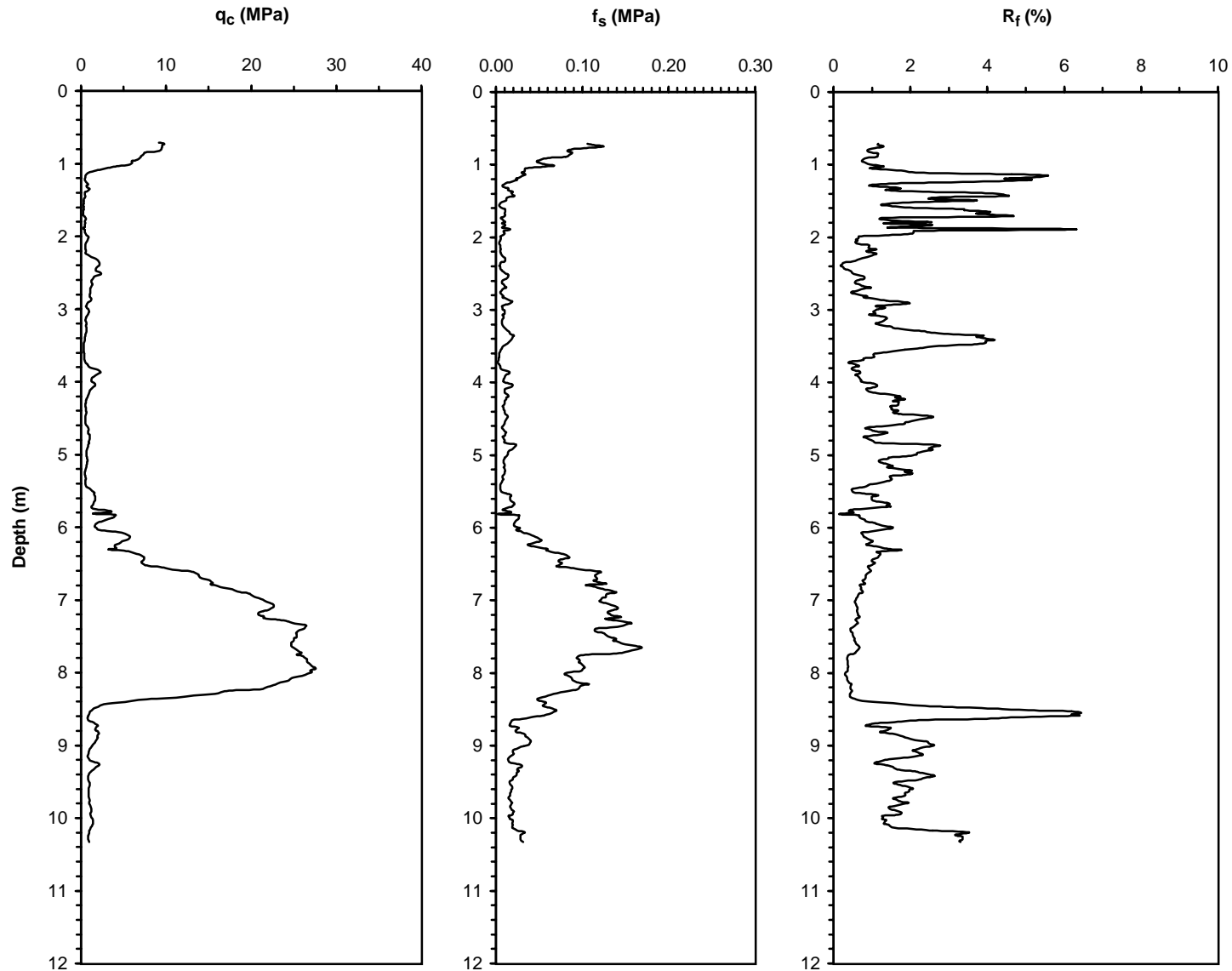
NSF, PEER

**Operator:** ZETAŞ (Zemin Teknolojisi, A. Ş.)

**Responsible Engineers:** J. D. Bray and R. B. Sancio, U. C. Berkeley

Caltrans, CEC, PG&E

**Notes:** Probed with percussion hammer 70 cm to check for utilities



UCB-BYU-UCLA  
ZETAŞ-SAU  
Joint Research

**Project Name:** Ground Failure and Building Performance in Adapazari, Turkey  
**Location:** Site 3 - Ankara Avenue, Orta District, Adapazari  
Thesis Name: Geostatistical Analysis for Soil Dynamics

**Page:** 1 of 1

**Test Number:** CPT-308  
**Type of Cone:** ELC10 CF No.990618 (a.p. v.d. Berg)

**Elevation:** 32.58 m

**Date:** July 6, 2000 08:36

Sponsored by:

**File Name:**

**Water Table Elevation:** Not measured

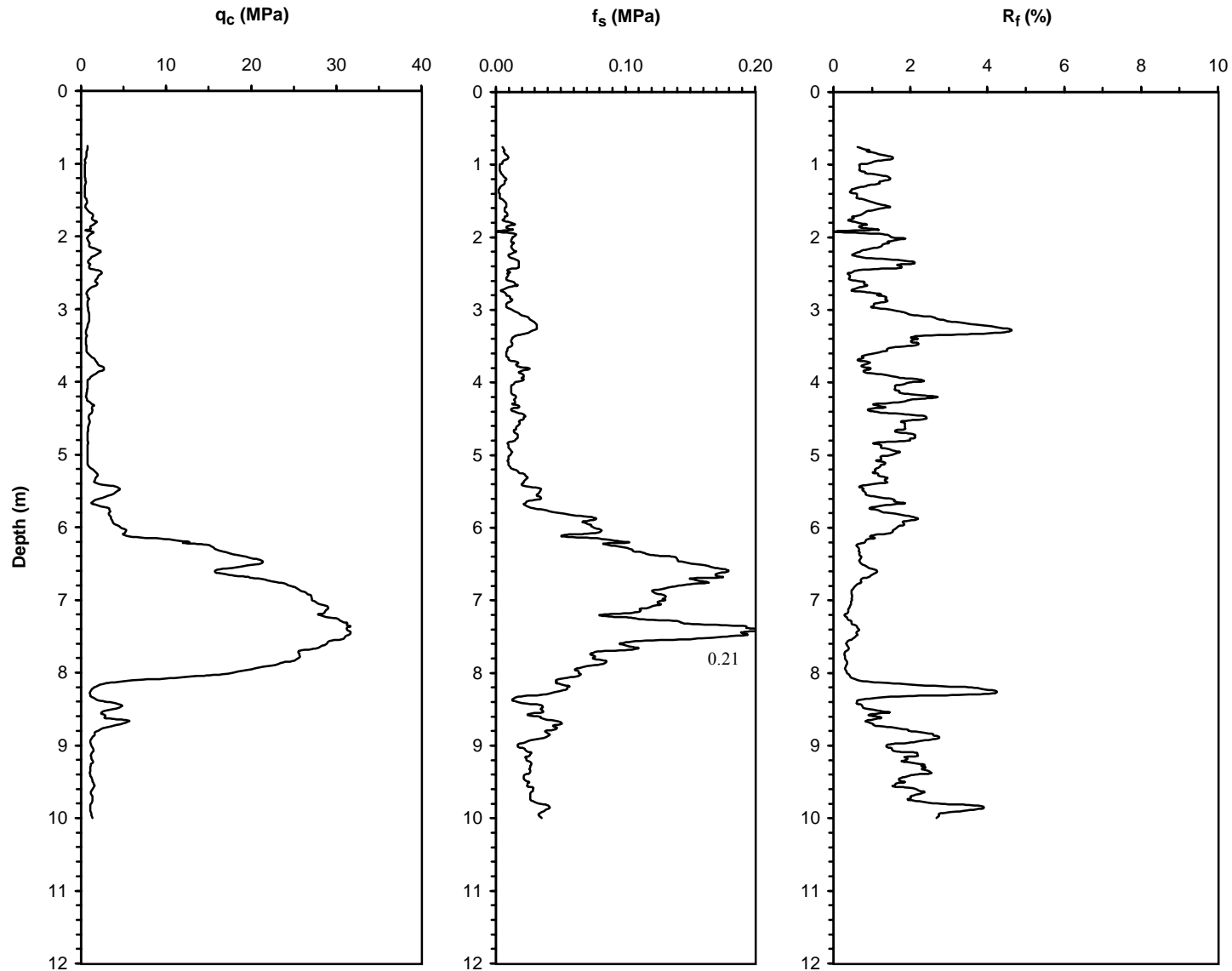
NSF, PEER

**Operator:** ZETAŞ (Zemin Teknolojisi, A. Ş.)

**Responsible Engineers:** T. L. Youd and C. Christensen, B. Y. U.

Caltrans, CEC, PG&E

**Notes:** Probed with percussion hammer 75 cm to check for utilities



UCB-BYU-UCLA  
ZETAŞ-SAU  
Joint Research

**Project Name:** Ground Failure and Building Performance in Adapazari, Turkey  
**Location:** Site 4 - Tül and Yakı n Streets, Cumhuriyet District, Adapazari  
Thesis Name: Geostatistical Analysis for Soil Dynamics

Page: 1 of 1

**Test Number:** CPT-401  
**Type of Cone:** ELC10 CFPS No. 991232 (a.p. v.d. Berg)

**Elevation:** 31.63 m

**Date:** June 14, 2000

Sponsored by:

NSF, PEER

**File Name:**

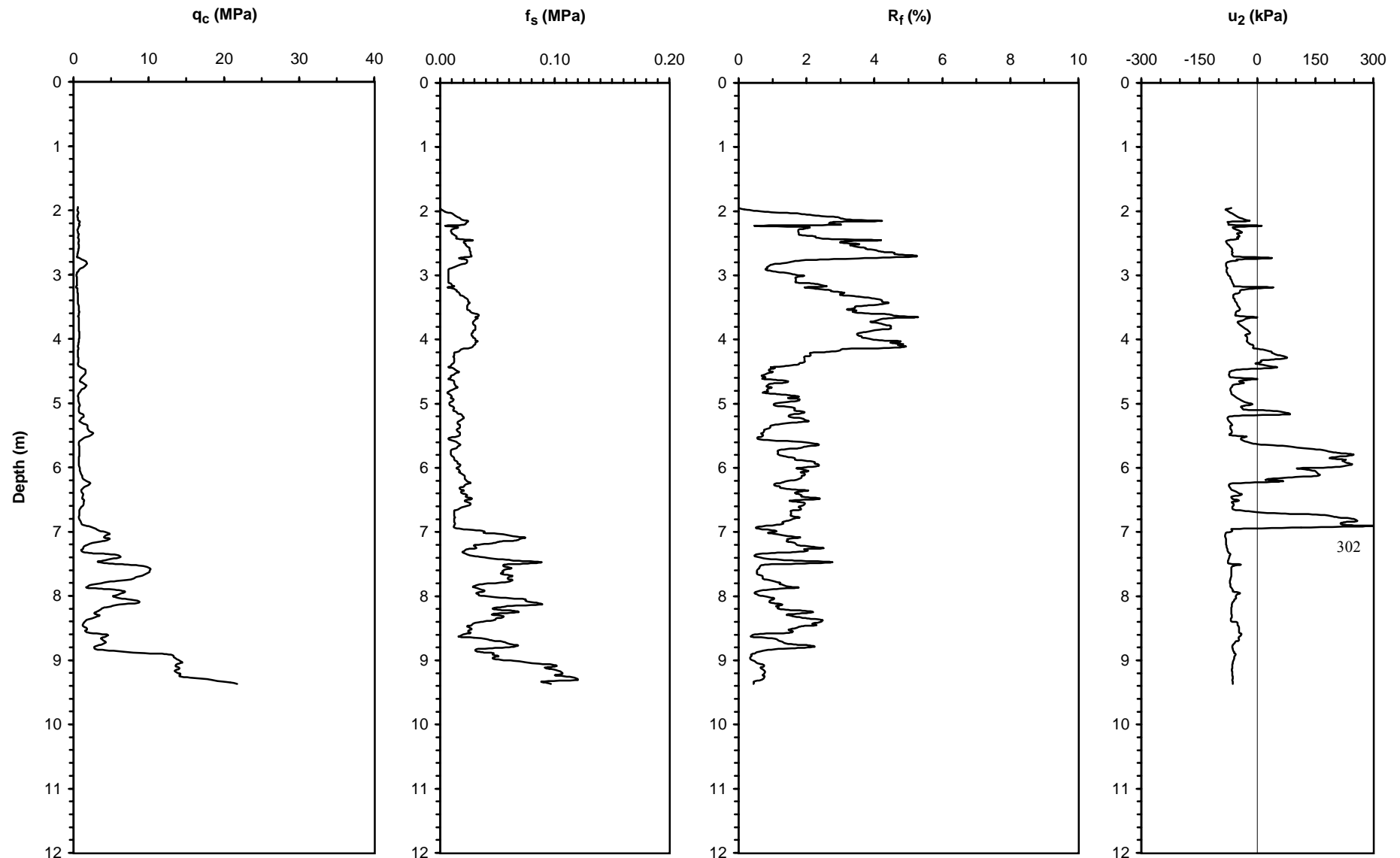
**Operator:** ZETAŞ (Zemin Teknolojisi, A. Ş.)

**Water Table Elevation:** 146 cm

**Responsible Engineers:** J. D. Bray and R. B. Sancio, U. C. Berkeley

Caltrans, CEC, PG&E

**Notes:**



UCB-BYU-UCLA  
ZETAŞ-SAU  
Joint Research

**Project Name:** Ground Failure and Building Performance in Adapazari, Turkey  
**Location:** Site 4 - Tül and Yakı n Streets, Cumhuriyet District, Adapazari  
**Thesis Name:** Geostatistical Analysis for Soil Dynamics  
**Test Number:** CPT-402  
**Type of Cone:** ELC10 CFPS No. 991232 (a.p. v.d. Berg)

Page: 1 of 1

**Elevation:** 31.09 m

**Date:** June 13, 2000

**Water Table Elevation:** Not measured

**Responsible Engineers:** J. D. Bray and R. B. Sancio, U. C. Berkeley

Sponsored by:

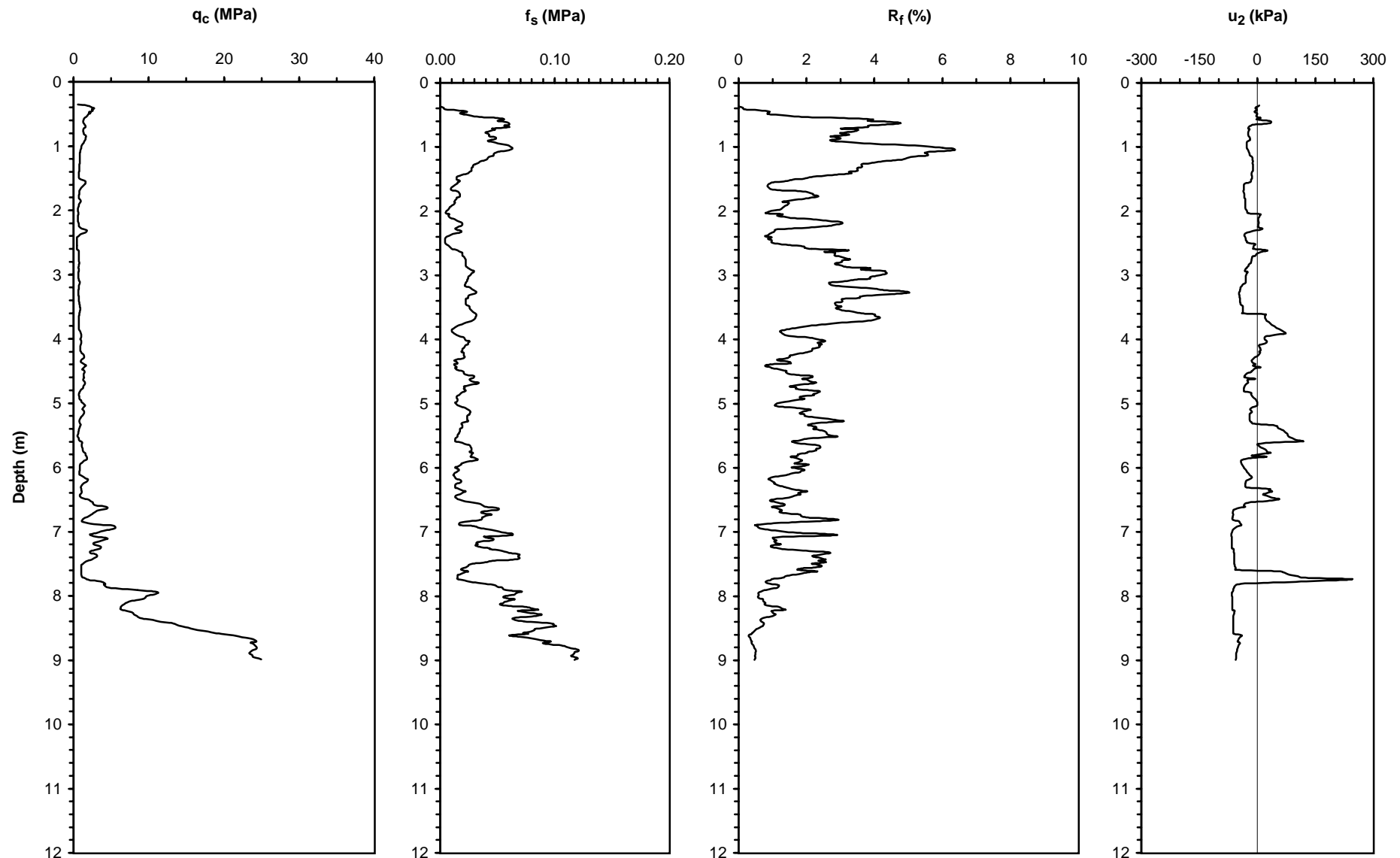
NSF, PEER

Caltrans, CEC, PG&E

**File Name:**

**Operator:** ZETAŞ (Zemin Teknolojisi, A. Ş.)

**Notes:**



UCB-BYU-UCLA  
ZETAŞ-SAU  
Joint Research

**Project Name:** Ground Failure and Building Performance in Adapazari, Turkey  
**Location:** Site 4 - Tül and Yakı n Streets, Cumhuriyet District, Adapazari  
Thesis Name: Geostatistical Analysis for Soil Dynamics  
**Test Number:** CPT-403  
**Type of Cone:** ELC10 CFPS No. 991232 (a.p. v.d. Berg)

**Elevation:** 30.91 m

**Date:** July 19, 2000

**Water Table Elevation:** Not measured

**Responsible Engineers:** J. D. Bray and R. B. Sancio, U. C. Berkeley

Sponsored by:

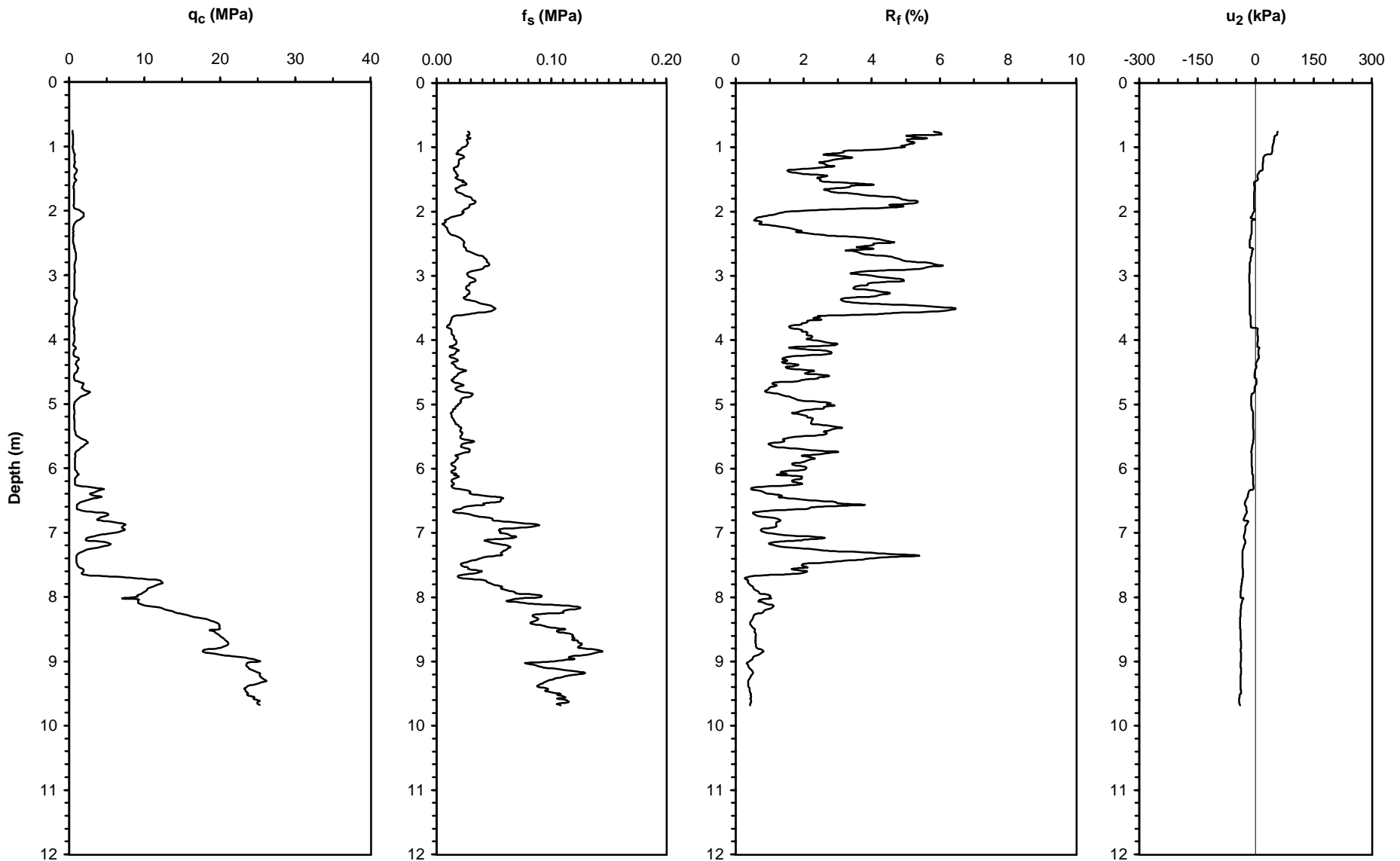
NSF, PEER

**File Name:**

**Operator:** ZETAŞ (Zemin Teknolojisi, A. Ş.)

**Notes:** Probed with percussion hammer 75 cm to check for utilities

Caltrans, CEC, PG&E



UCB-BYU-UCLA  
ZETAŞ-SAU  
Joint Research

**Project Name:** Ground Failure and Building Performance in Adapazari, Turkey  
**Location:** Site 4 - Tül and Yakı n Streets, Cumhuriyet District, Adapazari  
Thesis Name: Geostatistical Analysis for Soil Dynamics

Page: 1 of 1

**Test Number:** CPT-404  
**Type of Cone:** ELC10 CF No. 990617 (a.p. v.d. Berg)

**Elevation:** 30.95 m

**Date:** June 13, 2000 16:22

Sponsored by:

**File Name:**

**Water Table Elevation:** Not measured

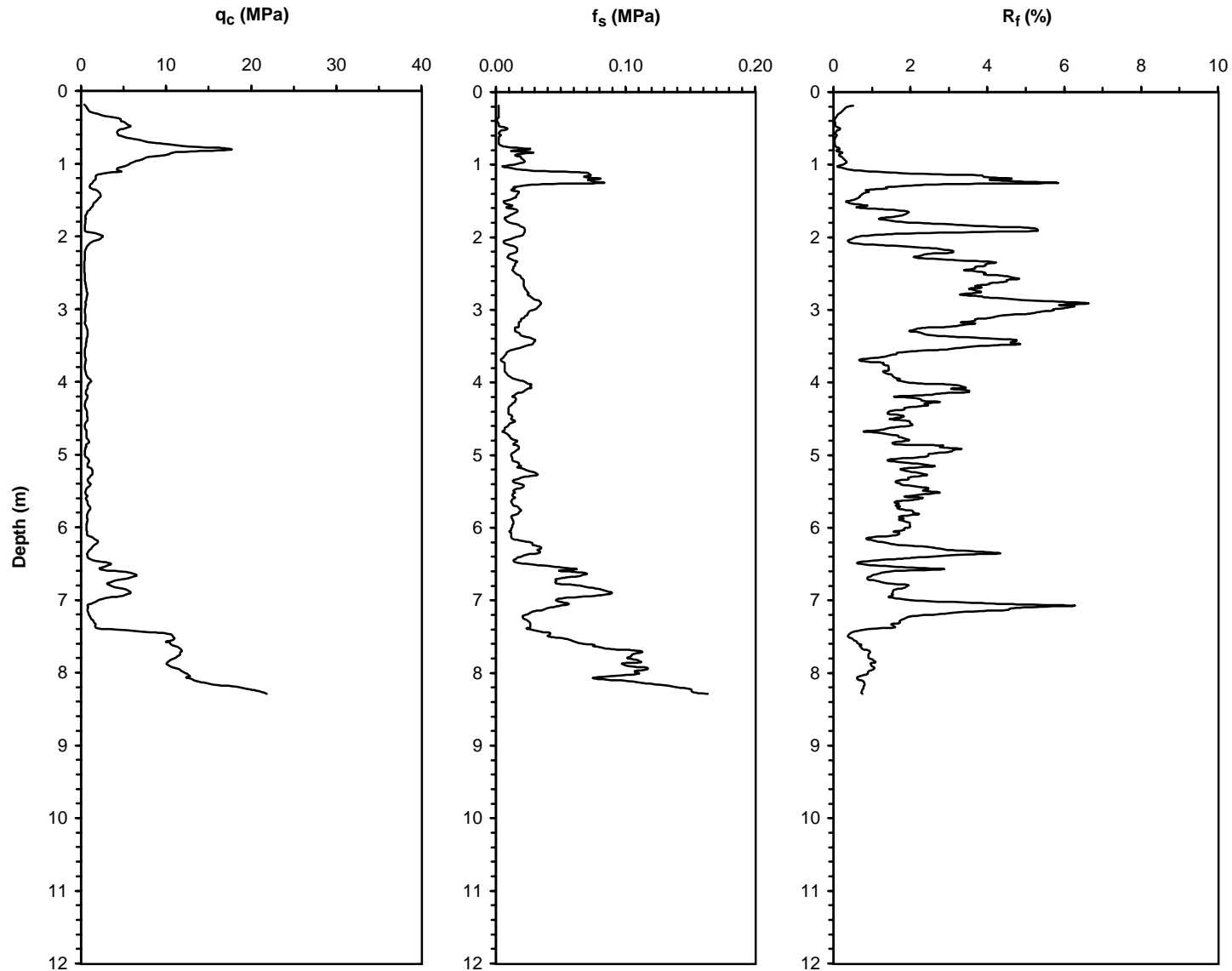
NSF, PEER

**Operator:** ZETAŞ (Zemin Teknolojisi, A. Ş.)

**Responsible Engineers:** J. D. Bray and R. B. Sancio, U. C. Berkeley

Caltrans, CEC, PG&E

**Notes:**



UCB-BYU-UCLA  
ZETAŞ-SAU  
Joint Research

**Project Name:** Ground Failure and Building Performance in Adapazari, Turkey  
**Location:** Site 4 - Tül and Yakı n Streets, Cumhuriyet District, Adapazari  
Thesis Name: Geostatistical Analysis for Soil Dynamics

**Page:** 1 of 1

**Test Number:** CPT-405  
**Type of Cone:** ELC10 CF No. 990617 (a.p. v.d. Berg)

**Elevation:** 30.99 m

**Date:** June 13, 2000 11:35

Sponsored by:

**File Name:**

**Water Table Elevation:** Not measured

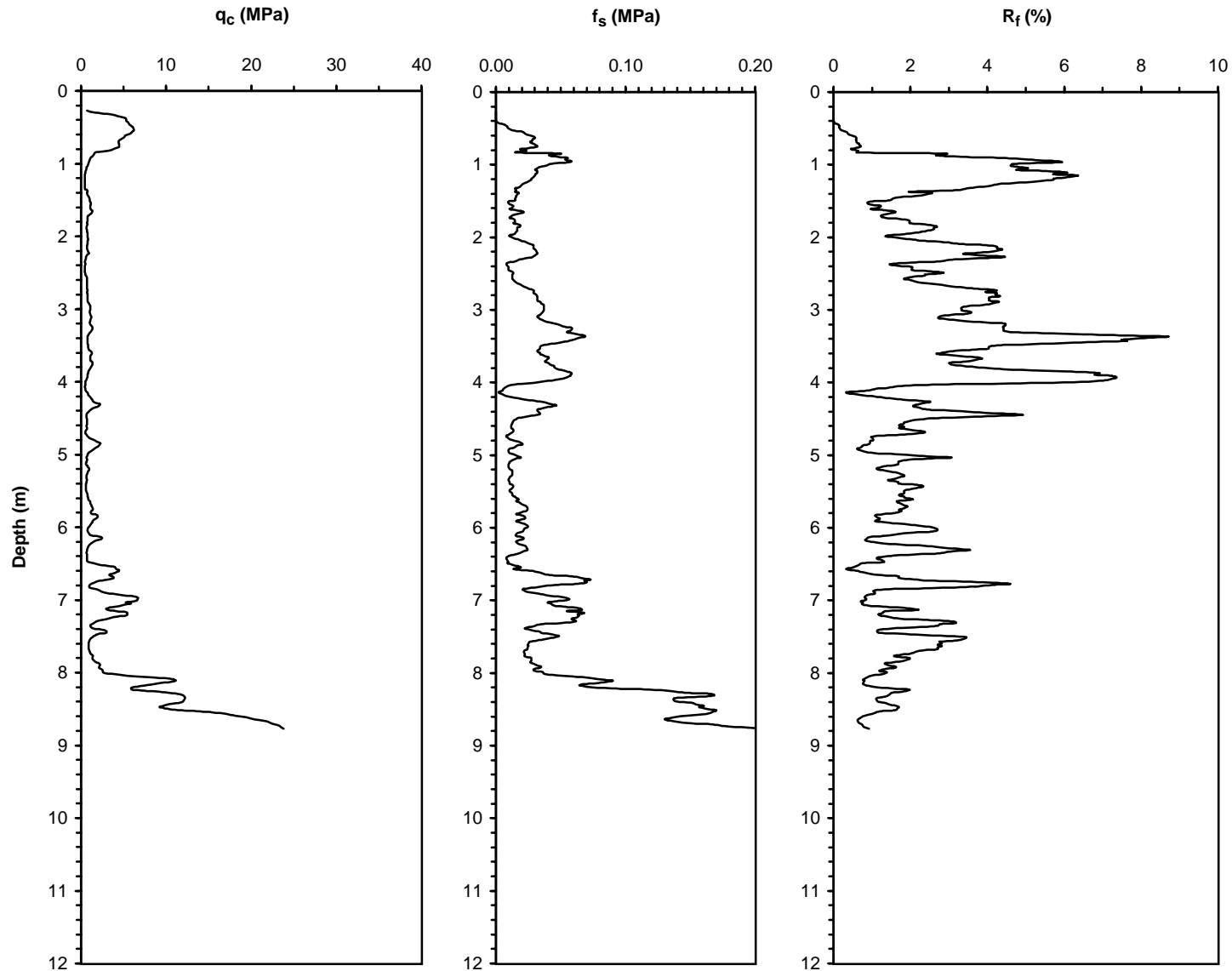
NSF, PEER

**Operator:** ZETAŞ (Zemin Teknolojisi, A. Ş.)

**Responsible Engineers:** J. D. Bray and R. B. Sancio, U. C. Berkeley

Caltrans, CEC, PG&E

**Notes:**



UCB-BYU-UCLA  
ZETAŞ-SAU  
Joint Research

**Project Name:** Ground Failure and Building Performance in Adapazari, Turkey  
**Location:** Site 4 - Tül and Yakı n Streets, Cumhuriyet District, Adapazari  
Thesis Name: Geostatistical Analysis for Soil Dynamics

Page: 1 of 1

**Test Number:** CPT-406  
**Type of Cone:** ELC10 CFPS No. 991232 (a.p. v.d. Berg)

**Elevation:** 31.03 m

**Date:** June 13, 2000 10:17

Sponsored by:

**File Name:**

**Water Table Elevation:** Not measured

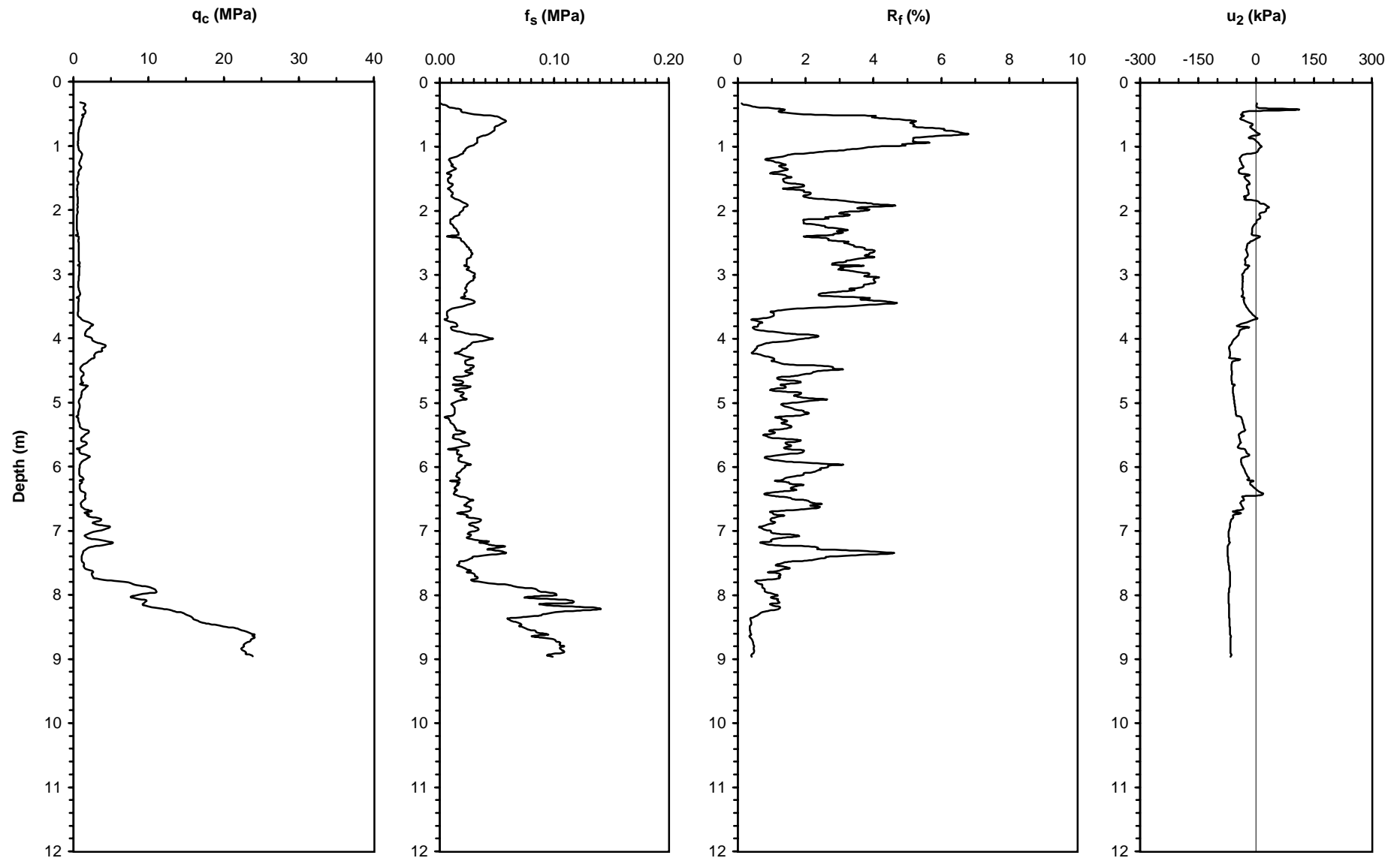
NSF, PEER

**Operator:** ZETAŞ (Zemin Teknolojisi, A. Ş.)

**Responsible Engineers:** J. D. Bray and R. B. Sancio, U. C. Berkeley

Caltrans, CEC, PG&E

**Notes:** Pre-excavated depth was not measured, 30 cm was estimated.



Depth Scale (m)	Lithology	USCS	Sample Type and No.	Recovery/Length (cm)	SPT Blows/15 cm	Casing Depth (m)	Rod Length (m)	Energy Ratio (%)	Description	q <sub>u</sub> Pocket Pen (kPa)	s <sub>u</sub> Torvane (kPa)	Moisture Content (%)	Liquid Limit	Plasticity Index	% fines < 75 µm	< 5 µm (%)	< 2 µm (%)	D <sub>50</sub> (mm)	D <sub>10</sub> (mm)	Remarks	
0									Fill: The boring was drilled through a thin (~5 cm) concrete slab on the west entrance of building C2												
1				0/45	2-1-2	1.45	4.27	48	CLAYEY SILT: Brown silty clay/clayey silt to sandy silt/silty sand												
2		CL	S-C4-1	29/45	3-1-1	2.45	5.80	47		60	31	42	45	22	99	57	46	0.003	<2µm	Sand catcher was used to aid sample recovery	
3				0/45	2-1-1	3.45	7.32	61													Sand catcher was used
4		ML	S-C4-2A	27/45	3-2-3	4.35	8.84	62		40	24	29	-	-	51	15	14	0.07	0.003		Sand catcher was used
5		ML	S-C4-2B						50		34	30	-	83	35	29	0.018	<2µm			

Depth Scale (m)	Lithology	USCS	Sample Type and No.	Recovery/Length (cm)	SPT Blows/15 cm	Casing Depth (m)	Rod Length (m)	Energy Ratio (%)	Description	q <sub>u</sub> Pocket Pen (kPa)	s <sub>u</sub> Torvane (kPa)	Moisture Content (%)	Liquid Limit	Plasticity Index	% fines < 75 µm	< 5 µm (%)	< 2 µm (%)	D <sub>50</sub> (mm)	D <sub>10</sub> (mm)	Remarks
0									Fill: The boring was drilled through a thin concrete slab on grade under which lies a gray silty sandy fill											
1									SILT: Brown silt to clayey silt with traces of fine sand interspersed with strata of brown silty sand to sandy silt											An attempt to obtain a Shelby tube sample at 1.5 m failed
2			SH-C3-1	42/42	-	2.8	-	-												
3																				
4	SM		S-C3-2	38/45	3-3-4	3.75	7.32	67		90	27	-	-	28	-	-	0.18	-		
5	CL/ML		S-C3-3	43/45	2-2-1	4.55	8.84	66		130	38	40	15	88	-	-	-	-		Traces of shells in sample S-C3-3
6	CL/ML SM		S-C3-4A S-C3-4B	38/45	3-10-8	5.45	8.84	66		125 250	34 23	45 -	20 -	97 37	13	10	0.09	0.001		
7	ML		S-C3-5	36/45	3-4-7	6.65	10.37		SM: Gray silty fine sand SILTY CLAY: Gray silty clay to clayey silt with some fine sand			31	31	83	23	16	0.027	<2µm		Traces of wood fragments in sample S-C3-5
8	CH/MH		S-C3-6	35/45	1-3-2	7.65	10.37	62	CLAY AND SILT: Gray low plasticity silt with sand interbedded with gray high plasticity clay. Red oxidation zone towards the upper portion of sample S-C3-6. The clay loses strength when remolded	70	23	42	67	36	98	-	-	-	-	
9																				
10	ML		S-C3-7	45/45	2-7-14	9.75	13.42	65		370	25	28	-	75	18	15	0.033	<2µm		

Depth Scale (m)	Lithology	USCS	Sample Type and No.	Recovery/Length (cm)	SPT Blows/15 cm	Casing Depth (m)	Rod Length (m)	Energy Ratio (%)	Description	q <sub>u</sub> Pocket Pen (kPa)	s <sub>u</sub> Torvane (kPa)	Moisture Content (%)	Liquid Limit	Plasticity Index	% fines < 75 µm	< 5 µm (%)	< 2 µm (%)	D <sub>50</sub> (mm)	D <sub>10</sub> (mm)	Remarks
0									Fill: Dark brown clayey fill											
1																				
2	ML/CL	S-C1-1	43/45	1-1-1	-	5.80	-	-	CLAY: Brown tan silty clay to clayey silt. Red oxidation points in samples indicating oxidation of ferric minerals	30	14	40	44	17	99	-	-	-	-	
3	CH	S-C1-2	35/45	1-2-2	-	5.80	47			120	32	42	64	42	99	84	67	<2µm	<2µm	
4			40/42	-	2.0	-	-			100	24									
5	ML ML	S-C1-4A S-C1-4B	33/45	2-3-5	4.15	7.32	63 63		SANDY SILT: Gray low plasticity sandy silt interbedded with gray silty clay with traces of fine sand. Thin gray clay layer at approximately 5.15 m.	180 130	23 -	35 29	36 30	8 -	98 90	- 18	- 14	- 0.027	- <2µm	
6	ML	S-C1-5	35/45	2-5-9	5.0	8.84	64			170	23	28	26	-	67	-	-	-	-	
7	ML SW-SM	S-C1-6A S-C1-6B	40/45	5-12-30	5.95	8.84	59 59		SAND: Gray sand to silty sand of variable gradation interspersed with thin layers of silty clay. Variable gravel content in samples S-C1-6B and S-C1-7 (10% - 20%)	180 -	- -	29 -	31 -	- -	53 7	14 -	11 -	0.07 1	0.001 0.11	
8	SP	S-C1-7	38/45	7-13-7	7.3	10.37	56			-	-	14	-	-	1	-	-	2.8	1	
9																				
10	ML	S-C1-8	36/45	3-3-8	9.45	11.89	71		ML: Gray low plasticity clayey silt with fine sand	-	30	30	32	-	89	42	32	0.007	<2µm	

Depth Scale (m)	Lithology	USCS	Sample Type and No.	Recovery/Length (cm)	SPT Blows/15 cm	Casing Depth (m)	Rod Length (m)	Energy Ratio (%)	Description	$q_u$ Pocket Pen (kPa)	$s_u$ Torvane (kPa)	Moisture Content (%)	Liquid Limit	Plasticity Index	% fines < 75 $\mu$ m	< 5 $\mu$ m (%)	< 2 $\mu$ m (%)	D50 (mm)	D10 (mm)	Remarks
0									Fill: Top soil and brown clayey fill in east yard of building C2											
1		ML	S-C7-1	33/45	1-1-3	0.95	4.27	50	ML: Brown low plasticity silt with sand to sandy silt. Soil has red oxidized points	70	33	34	-	84	29	23	0.017	<2 $\mu$ m		
2		ML	S-C7-2	38/45	1-2-1	1.50	5.80	51		40	33	33	-	72	22	18	0.034	<2 $\mu$ m		
3		CL/CH	S-C7-3	40/45	1-1-2	0.95	7.32	50	CLAY: Brown high plasticity silty clay w/ red oxidized points	100	17	49	28	99	58	40	0.004	<2 $\mu$ m		
		CH	S-C7-4	33/45	2-2-3	0.95	7.32	62			38	65	43	99	70	53	0.002	<2 $\mu$ m		

Depth Scale (m)	Lithology	USCS	Sample Type and No.	Recovery/Length (cm)	SPT Blows/15 cm	Casing Depth (m)	Rod Length (m)	Energy Ratio (%)	Description	$q_u$ Pocket Pen (kPa)	$s_u$ Torvane (kPa)	Moisture Content (%)	Liquid Limit	Plasticity Index	% fines < 75 $\mu$ m	< 5 $\mu$ m (%)	< 2 $\mu$ m (%)	D50 (mm)	D10 (mm)	Remarks
0									Fill: Top soil of garden area on the east side of building C2. Wash water shows a fine to coarse sub-angular to sub-rounded colorful clean sand at 1.8 m											Vane shear test at 1.25 m. First reading = 2.5 kPa, Average second reading = 3.5 kPa. Although the test was performed correctly, the first reading must be wrong
1			SH-C5-1	0/70	-	-	-	-												
2			S-C5-2	0/45	1-1-1	1.75	5.80	-	CL: Brown silty clay w/ red oxidized zones	40		41	44	24	96	50	38	0.005	<2 $\mu$ m	
3	CL		S-C5-3	27/45	1-0-1	2.85	7.32	56												
4	CL		SH-C5-4	44/50	-	4.25	-	-	CL: Gray silty clay			41	48	27	91	-	-	-	-	
5	CL		S-C5-5	38/45	1-1-3	5.05	8.84	64				40	42	18	100	70	50	0.002	<2 $\mu$ m	Sand catcher was used for S-C5-2. One blow was sufficient to drive the rods > 45 cm at 1.9 m. No sample was recovered. The sampler was reinserted at 2.3 m and driven 45 cm. No sample was recovered
6	ML		S-C5-6	40/45	6-17-23	5.95	10.37	67	SILT: Gray clayey silt			37	36	-	99	31	25	0.017	<2 $\mu$ m	
7	SP		S-C5-7	22/45	14-17-17	6.95	11.89	67	SAND: Gray fine to coarse sand with traces of gravel. Fine gravel content in S-C5-7 = 8%			14	-	-	4	-	-	0.7	0.2	

Depth Scale (m)	Lithology	USCS	Sample Type and No.	Recovery/Length (cm)	SPT Blows/15 cm	Casing Depth (m)	Rod Length (m)	Energy Ratio (%)	Description	$q_u$ Pocket Pen (kPa)	$s_u$ Torvane (kPa)	Moisture Content (%)	Liquid Limit	Plasticity Index	% fines < 75 $\mu$ m	< 5 $\mu$ m (%)	< 2 $\mu$ m (%)	D50 (mm)	D10 (mm)	Remarks
0									Fill: Top soil and brown clayey fill in east yard of building C2											
1		ML	S-C6-1	28/45	1-1-1	0.95	4.27	48	ML: Brown silt to silt with sand w/ red oxidized zones	60		13	40	-	94	30	25	0.014	<2 $\mu$ m	
2		ML	S-C6-2	41/45	1-0-1	1.50	5.80	53		60		36	31	-	87	28	20	0.015	<2 $\mu$ m	
3		CH SM	S-C6-3A S-C6-3B	35/45	2-4-6	1.50	7.32	65	CH: Brown high plasticity silty clay.	70	47	45 32	56 36	33 -	99 45	57 <15%	44 <10%	0.003 0.08	<2 $\mu$ m 0.01	
									SILTY SAND: Brown silty sand											

Depth Scale (m)	Lithology	USCS	Sample Type and No.	Recovery/Length (cm)	SPT Blows/15 cm	Casing Depth (m)	Rod Length (m)	Energy Ratio (%)	Description	$q_u$ Pocket Pen (kPa)	$s_u$ Torvane (kPa)	Moisture Content (%)	Liquid Limit	Plasticity Index	% fines < 75 $\mu$ m	< 5 $\mu$ m (%)	< 2 $\mu$ m (%)	D50 (mm)	D10 (mm)	Remarks
0									CLAYEY SILT: Dark brown clayey silt with uniform color. Moist, soft consistency.											Located near the sediment ejecta
1									CLAYEY SILT: Brown clayey silt to high plasticity silty clay. Traces of fine sand											
2	CL/ML	S-C2-1	38/45	1-1-1	4.27	54			50	20	37	40	15	97	-	-	-	-		
3	ML/CL	SH-C2-2	42/42	-	2.4	-			80	45	43	42	15	94	22	8	0.013	0.003		
4	CH	S-C2-3	35/45	2-2-4	3.2	7.32	69		170	72	41	74	45	99	-	-				
5	MH	SH-C2-4	40/42	-	4.05	-			85	53	26	73	28	99	60	41	0.003	<2 $\mu$ m		
6	ML/CL	S-C2-5	36/45	2-4-3	4.85	8.84	73		230		33	42	15	87	-	-	-	-		
7	ML SW-SM	S-C2-6A S-C2-6B	38/45	5-15-19	5.65	8.84	70				26 13	27 -	- -	71 5	34 -	24 -	0.014 0.7	<2 $\mu$ m 0.15		
8	ML	S-C2-7	36/45	2-5-6	6.45	10.37	75		300		29	34	-	92	-	-	-	-	Black fibrous wood chip at approx. 6.5 m	
9	CL/CH	S-C2-8	35/45	1-3-3	7.5	10.37	65		130		38	49	26	99	48	40	0.006	<2 $\mu$ m		
10	ML	S-C2-9	43/45	4-3-4	8.9	13.42	71		280	50	36	37	-	99	60	49	0.002	<2 $\mu$ m		

Depth Scale (m)	Lithology	USCS	Sample Type and No.	Recovery/Length (cm)	SPT Blows/15 cm	Casing Depth (m)	Rod Length (m)	Energy Ratio (%)	Description	$q_u$ Pocket Pen (kPa)	$s_u$ Torvane (kPa)	Moisture Content (%)	Liquid Limit	Plasticity Index	% fines < 75 $\mu$ m	< 5 $\mu$ m (%)	< 2 $\mu$ m (%)	D50 (mm)	D10 (mm)	Remarks
0									Fill: Electric power line burried at 0.5 m											
1									ML: Brown low plasticity clayey silt with fine sand to sandy silt. Silt layers alternate with silty clay/clayey silt	50		32	32	-	81	-	-	-	-	
2	ML		S-J2-1	32/45	1-2-1	1.75	5.80	50												
3	ML		S-J2-2	35/45	2-4-4	2.65	7.32	62		230		33	28	-	53	-	-	0.07	-	
4	CH		S-J2-3	44/45	1-1-2	4.00	7.32	56	CH: Gray high plasticity silty clay with traces of brown roots. Does not soften when remoulded	100	30	48	75	44	99	80	68	<2 $\mu$ m	<2 $\mu$ m	
5	SM		S-J2-4	36/45	3-8-7	5.15	8.84	65	SILT AND SAND: Alternating strata of gray silty fine sand and low plasticity clayey silt to sandy silt. Traces of wood at approximately 7.2 m. Seaming of gray silty clay with sandy silt in S-J2-6	310		26	-	-	39	-	-	0.09	<0.07	
6	ML		S-J2-5A	39/45	2-5-12	6.25	10.37	63		130		35	37	10	99	47	36	0.006	<2 $\mu$ m	
7	ML		S-J2-5B					63		>450		24	26	-	70	21	18	0.038	<2 $\mu$ m	
7	ML		S-J2-6	35/45	3-6-5	7.05	11.89	61		110	48	32	36	-	98	31	25	0.013	<2 $\mu$ m	
8	CH		S-J2-7A	33/45	2-6-4	8.35	11.89	65	CLAY AND SAND: Interbedded strata of high plasticity, gray silty clay and silty fine sand	120		40	66	40	100	70	55	<2 $\mu$ m	<2 $\mu$ m	

Depth Scale (m)	Lithology	USCS	Sample Type and No.	Recovery/Length (cm)	SPT Blows/15 cm	Casing Depth (m)	Rod Length (m)	Energy Ratio (%)	Description	q <sub>u</sub> Pocket Pen (kPa)	s <sub>u</sub> Torvane (kPa)	Moisture Content (%)	Liquid Limit	Plasticity Index	% fines < 75 µm	< 5 µm (%)	< 2 µm (%)	D <sub>50</sub> (mm)	D <sub>10</sub> (mm)	Remarks
0									Fill: Drilled through the concrete slab between buildings J1 and J2. Without prior knowledge, the boring was drilled through the buildings septic tank											
1																				
2			SH-J3-1	0/42 38/45		1.75 1.75			ML: Brown to gray clayey silt to silt with fine sand. Transition from brown to gray occurs at approx. 2.5 m	110										A Shelby tube sample was attempted at 1.8 m. No sample was recovered
3																				
4	ml ML		S-J3-2A S-J3-2B	36/45	2-3-3	3.45	7.32		CH: Gray high plasticity silty clay	200 70		30 28	- 30	- -	98 78	36 30	30 24	0.01 0.029	<1µm <1µm	
5	CH		S-J3-3	42/42		4.55			ML: Gray low plasticity silt with sand to sandy silt	70	40	41	95	66	98	63	46	0.003	<1µm	
6	ML		S-J3-4	41/45	4-2-4	5.45	10.37			130		32	30	-	72	-	-	-	-	
7	ML		S-J3-5	37/45	6-13-18	6.45	10.37			400		40	28	-	64	25	22	0.043	<2µm	
8									CH: Gray silty clay											
9	CH		S-J3-6	34/45	2-3-5	8.95	11.89			150	56	36	61	33	97	65	50	0.002	<2µm	

Depth Scale (m)	Lithology	USCS	Sample Type and No.	Recovery/Length (cm)	SPT Blows/15 cm	Casing Depth (m)	Rod Length (m)	Energy Ratio (%)	Description	$q_u$ Pocket Pen (kPa)	$s_u$ Torvane (kPa)	Moisture Content (%)	Liquid Limit	Plasticity Index	% fines < 75 $\mu$ m	< 5 $\mu$ m (%)	< 2 $\mu$ m (%)	D50 (mm)	D10 (mm)	Remarks
0									Fill: Borehole drilled through 5 cm-thick concrete slab behind building J1											
1	ML ML	S-J4-1A S-J4-1B	27/45	1-2-1	4.27	38	80 120	31 31	40 30	10 -	91 67	43 23	36 20	0.008 0.039	<2 $\mu$ m <2 $\mu$ m					
2	ML	S-J4-2	35/45	1-3-2	1.95	5.80	46	29	33	-	56	26	23	0.05	<2 $\mu$ m					
3	ML ML	S-J4-3A S-J4-3B	35/45	2-4-6	2.75	5.80	34	150	38 32	25 35	- -	65 87	15 22	13 17	0.041 0.02	<2 $\mu$ m <2 $\mu$ m				
4	CH/CL ML	S-J4-4A S-J4-4B	33/45	2-2-2	3.55	8.84	56	180	35	38 34	50 32	26 -	97 79	49 23	35 20	0.005 0.023	<2 $\mu$ m <2 $\mu$ m			
	MH	S-J4-5	32/45	2-2-3	4.35	8.84	60	175	75	40	72	34	99	70	46	0.002	<2 $\mu$ m			

Depth Scale (m)	Lithology	USCS	Sample Type and No.	Recovery/Length (cm)	SPT Blows/15 cm	Casing Depth (m)	Rod Length (m)	Energy Ratio (%)	Description	q <sub>u</sub> Pocket Pen (kPa)	s <sub>u</sub> Torvane (kPa)	Moisture Content (%)	Liquid Limit	Plasticity Index	% fines < 75 µm	< 5 µm (%)	< 2 µm (%)	D <sub>50</sub> (mm)	D <sub>10</sub> (mm)	Remarks
0									Fill: 5 cm-thick concrete slab followed by brown clayey sand											
1	ML/CL	S-J1-1	S-J1-1	35/45	1-1-1		4.27	44	ML: Brown to gray clayey silt with traces of fine sand to silt with sand. Red oxidized zones throughout the stratum	30		36	43	15	97	35	25	0.01	<2µm	
2	ML	S-J1-2	S-J1-2	34/45	1-2-3		5.80	52		120		36	37	10	93	-	-	-	-	
3	ML ML	S-J1-3A S-J1-3B	S-J1-3A S-J1-3B	38/45	1-3-3	2.75	5.80	59 59				35 32	35 29	7 -	92 76	- 32	- 26	- 0.02	- <2µm	
4	CH	S-J1-4	S-J1-4	38/45	1-1-1	3.55	7.32	57	CH: Gray high plasticity silty clay with traces of fine sand. Wood pieces found at approximately 3.9 m and 4.7 m	90	26	40	55	29	96	50	37	0.005	<2µm	
5	CH/MH	S-J1-5	S-J1-5	36/45	1-2-2	4.35	8.84	59		80	43	41	62	32	94	-	-	-	-	
6	SM	S-J1-6	S-J1-6	41/45	6-7-6	5.15	8.84	66	SILT AND SAND: Interbedded strata of gray low plasticity clayey silt and silty fine sand	300		25	-	-	18	-	-	0.12	<0.08	
7	ML	S-J1-7	S-J1-7	42/45	6-12-16	5.95	10.37	65		450		24	28	-	88	-	-	-	-	
8	SM ML/MH	S-J1-8A S-J1-8B	S-J1-8A S-J1-8B	43/45	5-5-7	6.75	10.37	67 67		230		28 37	- 49	- 16	14 99	- 58	- 41	0.13 0.003	<0.08 <2µm	
9	ML	S-J1-9	S-J1-9	36/45	3-4-4	8.3	11.89	66		210		31	30	-	91	18	11	0.013	0.002	
10	SM	S-J1-10	S-J1-10	40/45	9-15-12	10.15	13.42	-				23	-	-	19	-	-	0.15	<0.08	

Depth Scale (m)	Lithology	USCS	Sample Type and No.	Recovery/Length (cm)	SPT Blows/15 cm	Casing Depth (m)	Rod Length (m)	Energy Ratio (%)	Description	q <sub>u</sub> Pocket Pen (kPa)	s <sub>u</sub> Torvane (kPa)	Moisture Content (%)	Liquid Limit	Plasticity Index	% fines < 75 µm	< 5 µm (%)	< 2 µm (%)	D <sub>50</sub> (mm)	D <sub>10</sub> (mm)	Remarks
0									Fill: 20 cm of topsoil followed by a dark brown to black clayey silt with sand											
1		CL/ML	S-G1-1	33/45	1-1-2	1.45	4.27	50	CLAYEY SILT: Interbedded strata of olive brown to brown clayey silt with traces of fine sand and brown sandy silt	50	35	41	16	97	35	26	0.013	<2µm		Roots were found in sample S-G1-1
2		ML	S-G1-2	38/45	2-3-4	2.25	5.80	51		200	32	29	-	69	-	-	-	-		
3		ML	S-G1-3	32/45	2-2-2	3.05	7.32	55		60	36	33	-	95	-	-	-	-		
4		CH	S-G1-4	33/45	1-2-2	3.95	7.32	-	CLAY: High plasticity gray silty clay	100	39	38	53	33	97	50	40	0.005	<2µm	
5		CL ML	S-G1-5A S-G1-5B	36/45	2-3-6	4.75	8.84	67	SILT AND SAND: Gray silt and sandy silt to silty sand. FC varies from 22% to 90%. 4 mm red silty clay to clayey silt seam found at approx. 7.2 m	120		30 26	48 25	25 -	84 71	42 -	32 -	0.009 -	<2µm -	
6		ML SM	S-G1-6A S-G1-6B	40/45	4-3-5	5.55	10.37	61		120		34 27	34 -	- -	90 22	25 -	19 -	0.028 0.15	<2µm -	
7		ML	S-G1-7	31/45	5-4-6	6.95	11.89	62			27	27	-	67	-	-	-	-		
8		MH	S-G1-8	33/45	2-3-3	7.95	11.89	64	MH: High plasticity gray clayey silt. Softens when remoulded. Red oxidized 5 mm-thick seam at approx. 9.2 m	150	34	36	58	22	99	50	34	0.005	<2µm	
9		MH/CH	S-G1-9	30/45	2-3-4	8.95	13.42	70		120	24	34	52	22	99	-	-	-	-	

Depth Scale (m)	Lithology	USCS	Sample Type and No.	Recovery/Length (cm)	SPT Blows/15 cm	Casing Depth (m)	Rod Length (m)	Energy Ratio (%)	Description	q <sub>u</sub> Pocket Pen (kPa)	s <sub>u</sub> Torvane (kPa)	Moisture Content (%)	Liquid Limit	Plasticity Index	% fines < 75 µm	< 5 µm (%)	< 2 µm (%)	D50 (mm)	D10 (mm)	Remarks
0									Fill: Rubble from sidewalk. Black clayey sand with strong odor, probably due to a nearby septic tank											
1			S-G2-1	0/45	1-2-2	-	3.67	-	ML: Brown low plasticity silt with fine sand to sandy silt											
2			S-G2-2	35/45	3-4-5	2.45	5.80	58		75	29	25	-	-	65	22	18	0.04	<2µm	
3	ML		S-G2-2	80/90		3.25														
4	ML ML CH/MH		SH-G2-3A SH-G2-3B SH-G2-3C						CH: Gray high plasticity silty clay with traces of fine sand			15 15 15	33 37 60	7 10 30	78 77 95	14 17 68	6 9 40	0.028 0.022 0.003	0.003 0.002 <2µm	
5			S-G2-4	40/45	2-3-3	5.15	8.84	60	ML: Gray low plasticity clayey silt to silt with sand. Red clay seams from approximately 6.15 m to 6.2 m	75	34	30	-	75	-	-	-	-	-	
6	ML ML		S-G2-5A S-G2-5B	35/45	2-6-7	5.95	10.37	66		110	24	37 28	44 26	13 -	99 92	43 -	20 -	0.007 -	<2µm -	
7			SH-G2-6	41/40		7.45			CH: Soft gray, high plasticity silty clay	60	25	47	58	31	99	85	59	0.001	<1µm	
8			S-G2-7A S-G2-7B	32/45	3-4-4	8.45	11.29		ML: Gray clayey silt with traces of fine sand			36 33	36 43	- 18	89 99	21 40	18 30	0.029 0.007	<2µm <2µm	
9	ML CL/ML		S-G2-7A S-G2-7B						CLAY: Gray silty clay to clayey silt. Some shells at approx. 10.3 m											
10			SH-G2-8	42/42		9.45				120	35	39	48	24	99	45	30	0.006	<2µm	
11	CH/CL		S G2 9	37/45	2 4 5	10 95	14 94	61		200	55	31	51	30	98	61	51	0 001	<1µm	

**Legend**  
 S: Spit Spoon (SPT) SH: Shelby tube

Depth Scale (m)	Lithology	USCS	Sample Type and No.	Recovery/Length (cm)	SPT Blows/15 cm	Casing Depth (m)	Rod Length (m)	Energy Ratio (%)	Description	$q_u$ Pocket Pen (kPa)	$s_u$ Torvane (kPa)	Moisture Content (%)	Liquid Limit	Plasticity Index	% fines < 75 $\mu$ m	< 5 $\mu$ m (%)	< 2 $\mu$ m (%)	D50 (mm)	D10 (mm)	Remarks
11	CH/CL	S-G2-9	37/45	2-4-5	10.95	14.94	61			200	55	31	51	30	98	61	51	0.001	<1 $\mu$ m	
12	ML	S-G2-10A S-G2-10B	39/45	5-10-15	11.95	14.94	69		ML: Interbedded strata of gray low plasticity silt with sand and gray clayey silt. Some red clay seams	320		36 26	35 26	- -	97 76	18	15	0.021	<2 $\mu$ m	
13																				
14	ML/CL	S-G2-11	37/45	3-4-7	13.95	17.99	70			175		32	47	18	99	47	35	0.006	<2 $\mu$ m	

Depth Scale (m)	Lithology	USCS	Sample Type and No.	Recovery/Length (cm)	SPT Blows/15 cm	Casing Depth (m)	Rod Length (m)	Energy Ratio (%)	Description	$q_u$ Pocket Pen (kPa)	$s_u$ Torvane (kPa)	Moisture Content (%)	Liquid Limit	Plasticity Index	% fines < 75 $\mu$ m	< 5 $\mu$ m (%)	< 2 $\mu$ m (%)	D50 (mm)	D10 (mm)	Remarks
0									Fill: Hole is drilled through fill and rubble of the foundation of the building that was located to the north of building F1											
1		ML	S-F1-1	38/45	1-2-3	0.95	4.27	50	ML: Brown low plasticity sandy silt to silt			32	28	-	72	11	7	0.06	0.004	
2		ML	S-F1-2	32/45	3-2-2	1.75	5.80	57				28	27	-	68	11	9	0.048	0.007	
3		ML	S-F1-3	32/45	2-3-2	2.55	5.80	51				33	31	-	92	42	38	0.008	<2 $\mu$ m	
4		ML/CL	S-F1-4	32/45	2-1-2	3.45	7.32	54	CL: Brown low plasticity silty clay to clayey silt with traces of fine sand	75	28	37	47	19	97	40	27	0.008	<2 $\mu$ m	
5		CL ML	S-F1-5A S-F1-5B	36/45	2-3-6	4.45	8.84	64	SILT AND SAND: Gray sandy silt to silty sand. FC of recovered samples varies from 35% to 77%			31 28	35 30	13 -	85 77	18 18	14 14	0.019 0.041	<2 $\mu$ m <2 $\mu$ m	
6		ML	S-F1-6	35/45	5-7-7	5.35	8.84	67				27	28	-	51	8	6	0.07	0.013	
7		ML SM	S-F1-7A S-F1-7B	33/45	3-7-7	6.15	10.37	59				34 28	28 -	- -	72 35	20 -	15 -	0.05 0.1	<2 $\mu$ m -	
8		SM	S-F1-8	45/45	4-4-9	6.95	10.37	59				26	-	-	42	<15%	<10%	0.085	0.013	Thin brown organic seam at approx. 7.35 m
9		ML	S-F1-9	34/45	5-6-7	7.95	11.89	57				29	31	-	74	17	13	0.034	<2 $\mu$ m	Wood fragments were found in the sample at approx. 8.1 m
10		CH CL/ML	S-F1-10A S-F1-10B	37/45	2-4-7	8.95	11.89	61	CLAY: Gray silty clay to clayey silt with traces of fine sand. LL of recovered samples varies from 38 to 57	170	55	38 34	57 41	29 17	100 99	50 -	26 -	0.005 0.007	<2 $\mu$ m <2 $\mu$ m	
11		ML CH/MH	S-F1-11A S-F1-11B	31/45	3-4-5	9.95	13.42	70				33 23	38 58	- 29	96 100	23 40	17 22	0.019 0.007	<2 $\mu$ m <2 $\mu$ m	

**UCB-BYU-UCLA**  
**ZETAS-SaU-METU**  
 Joint Research  
 Sponsored by:  
**NSF, Caltrans**  
**CEC, PG&E**

**Project Name:** Ground Failure and Building Performance in Adapazari, Turkey  
**Location:** Site 2 - Sönmez Street, Yenigün District, Adapazari  
**Date:** July 20, 2000  
**Field Log by:** Rodolfo B. Sancio  
**Operator:** ZETAS (Zemin Teknolojisi, A. S.)  
**Drilling Method:** Rotary wash with 9 cm-diameter tricone bit  
**Water Table Elevation:** GWL = 1.64 m 07/21/00, caved in 08/04/00  
**Notes:** .

**Test ID:** SPT-207  
**Thesis Name:** Geostatistical Analysis for Soil Dynamics  
**Elevation:** 31.11 m  
**Drilling Equipment:** Custom made, equivalent to Crealius XC90H  
**Responsible Engineers:** J. D. Bray and R. B. Sancio, U. C. Berkeley  
**SPT System:** Rope, pulley and cathead method. AWJ rods.  
**Hammer Type:** Safety Hammer (per Kovacs et al. 1983)

Depth Scale (m)	Lithology	USCS	Sample Type and No.	Recovery/Length (cm)	SPT Blows/15 cm	Casing Depth (m)	Rod Length (m)	Energy Ratio (%)	Description	$q_u$ Pocket Pen (kPa)	$s_u$ Torvane (kPa)	Moisture Content (%)	Liquid Limit	Plasticity Index	% fines < 75 $\mu$ m	< 5 $\mu$ m (%)	< 2 $\mu$ m (%)	D50 (mm)	D10 (mm)	Remarks
11																				
12		ML/CL SM	S-F1-12A S-F1-12B	37/45	4-13-20	11.95	14.94	54	SM: Gray silty fine sand			29 25	38 26	12 -	90 30	21 -	14 -	0.019 0.1	0.001 -	

Depth Scale (m)	Lithology	USCS	Sample Type and No.	Recovery/Length (cm)	SPT Blows/15 cm	Casing Depth (m)	Rod Length (m)	Energy Ratio (%)	Description	q <sub>u</sub> Pocket Pen (kPa)	s <sub>u</sub> Torvane (kPa)	Moisture Content (%)	Liquid Limit	Plasticity Index	% fines < 75 μm	< 5 μm (%)	< 2 μm (%)	D <sub>50</sub> (mm)	D <sub>10</sub> (mm)	Remarks
0									Fill: Brown sandy fill with rubble (bricks and concrete) and some fines. Black clayey soil with slight smell.											
1									SP: Poorly graded, medium to fine brown clean sand											
2	SP		S-E1-1	34/45	2-2-4	1.55	4.27			-	23	-	-	2	-	-		0.51	0.2	
3	ML		S-E1-2A	36/45	2-2-3	2.85	5.80		SILT AND SAND: Interbedded strata of brown low plasticity sandy silt and clayey silt with brown medium sand	125		33	28	-	59	-	-	0.06	-	
	ML		S-E1-2B									34	33	-	90	28	20	0.014	<2μm	
4	MH/CH		S-E1-3	41/45	1-2-1	3.65	7.32		SILTY CLAY: Brown clayey silt/silty clay. Traces of organics and oxidation veins	60	30	49	52	22	99	-	-	-	-	
5	CH		SH-E1-4A	35/42	-	4.45	-			110	50		61	32	96	40	24	.007	<2μm	
	CH		SH-E1-4B									61	33	95	54	33	.004	<2μm		
	CH		SH-E1-4C									62	35	95	53	37	.005	<2μm		
6	SM		S-E1-5A	45/45	3-4-5	5.35	8.84		SAND: Gray fine to medium sand interbedded with gray low plasticity silt deposits. FC in this stratum varies from 3% to 61%	80		33	-	-	47	-	-	0.08	-	
	SP		S-E1-5B									17	-	-	7	-	-	0.4	0.1	
7	ML		S-E1-6A	41/45	5-13-19	6.35	10.37			-		25	26	-	61	16	11	0.048	<2μm	
	SW-SM		S-E1-6B							450		18	-	-	12	-	-	0.2	0.06	
8			S-E1-7	40/45	9-16-18	7.35	11.89			280										
9	SP		S-E1-8A	45/45	1-4-8	8.08	11.89			100		21	-	-	3	-	-	0.6	0.2	
	CL		S-E1-8B						CLAY: Gray clay with traces of fine sand	125		30	39	17	97	31	24	0.014	<2μm	

Depth Scale (m)	Lithology	USCS	Sample Type and No.	Recovery/Length (cm)	SPT Blows/15 cm	Casing Depth (m)	Rod Length (m)	Energy Ratio (%)	Description	q <sub>u</sub> Pocket Pen (kPa)	s <sub>u</sub> Torvane (kPa)	Moisture Content (%)	Liquid Limit	Plasticity Index	% fines < 75 μm	< 5 μm (%)	< 2 μm (%)	D <sub>50</sub> (mm)	D <sub>10</sub> (mm)	Remarks
0									Fill: Bricks from the foundation of the collapsed building. Maybe a septic tank as evidenced by the dark color of the wash water.											
1		SP-SM	S-E2-1	33/45	4-5-7	1.55	4.13	55	SP: Poorly graded fine to medium brown sand. FC <= 5%		24	-	-	5	-	-	0.28	0.1		
2		SP ML	S-E2-2A S-E2-2B	40/45	3-2-1	2.3	4.13	52	ML: Brown silt to sandy silt with red oxidized points	60	13 35	- 31	- -	2 94	- 22	- 17	0.56 0.018	0.18 <2μm		
3		ML	S-E2-3	40/45	3-3-3	3.05	5.65	64	CLAY: Gray silty clay	110	34	20	-	59	14	11	0.053	0.001		
4		CH CL	S-E2-4A S-E2-4B	37/45	2-1-2	3.95	7.17	62			52 39	62 44	34 21	99 99	70 58	51 48	0.002 0.003	<2μm <2μm		
5		CL ML SM/ML	S-E2-5A S-E2-5B S-E2-5C	40/45	5-6-11	5.35	8.70	67	SILT AND SAND: Gray silt with sand to sandy silt/silty sand	80 120	36 31 27	43 34 22	22 -	98 89 49	58 33 18	45 26 15	0.003 0.01 0.075	<2μm <2μm <2μm		

Depth Scale (m)	Lithology	USCS	Sample Type and No.	Recovery/Length (cm)	SPT Blows/15 cm	Casing Depth (m)	Rod Length (m)	Energy Ratio (%)	Description	q <sub>u</sub> Pocket Pen (kPa)	s <sub>u</sub> Torvane (kPa)	Moisture Content (%)	Liquid Limit	Plasticity Index	% fines < 75 μm	< 5 μm (%)	< 2 μm (%)	D <sub>50</sub> (mm)	D <sub>10</sub> (mm)	Remarks
0									Fill: Clayey fill											
1	CL	S-K1-1	26/45	1-1-2	1.05	4.27	51		CLAY AND SILT: Brown low plasticity clayey silt/silty clay with traces of fine sand. S-K1-1 is dark gray and has a light odor, probably due to a nearby septic tank. Transition to gray color occurs at approx. 5.5 m	70	26	39	46	23	99	54	40	0.004	<2μm	
2		S-K1-2	0/45	1-2-2	2.05	5.80	53													
3	ML	S-K1-3	38/45	2-2-3	2.95	7.32	53			30		34	35	9	85	29	25	0.028	<2μm	
4	ML/CL	S-K1-4	38/45	1-2-1	3.75	7.32	55			40	24	36	41	14	95	17	9	0.019	0.002	
5	CL	S-K1-5	34/45	2-1-2	4.55	8.84	62			70	36	39	46	21	98	60	47	0.003	<2μm	
6	ML SM	S-K1-6A S-K1-6B	38/45	2-9-11	5.45	8.84	59		SILTY SAND: Gray silty sand to sand with silt			33 24	37 -	11 -	89 34	30 -	21 -	0.02 0.1	<2μm <0.07	
7	SP-SM	S-K1-7	40/45	10-13-17	5.5	10.37	65					23	-	-	8	-	-	0.024	0.08	
8	SM	S-K1-8	43/45	2-6-8	8.0	11.89	70					31	-	-	25	-	-	0.1	<0.07	
9	ML	S-K1-9A	34/45	4-8-5	9.0	13.42	66		ML: Gray low plasticity silt to sandy silt	190	36	29	37	10	81	50	41	0.005	<2μm	

Depth Scale (m)	Lithology	USCS	Sample Type and No.	Recovery/Length (cm)	SPT Blows/15 cm	Casing Depth (m)	Rod Length (m)	Energy Ratio (%)	Description	q <sub>u</sub> Pocket Pen (kPa)	s <sub>u</sub> Torvane (kPa)	Moisture Content (%)	Liquid Limit	Plasticity Index	% fines < 75 μm	< 5 μm (%)	< 2 μm (%)	D <sub>50</sub> (mm)	D <sub>10</sub> (mm)	Remarks
0									Fill: Pavement and bricks followed by sand subgrade and black to gray clayey silt with fine sand and some gravel											
1		CL	S-L1-1	16/45	3-2-2	0.95	4.27	49		180	40	40	46	24	77	40	30	0.009	<2μm	
2		ML	S-L1-2	28/45	3-3-2	2.15	5.80	57				31	26	-	74	<15%	<10%	0.06	0.028	
3		ML/CL	S-L1-3	0/45	2-1-1	3.0	7.32	54	CLAYEY SILT: Brown low plasticity silt with sand to sandy silt interspersed with brown low plasticity silty clay. Samples exhibit red oxidation areas. FC varies from 57% to 97%			44	41	15	93	56	41	0.003	<2μm	A piece of gravel got stuck in the sampler and no sample was recovered at 3.05 m (S-L1-3). When rods were reinserted in the hole, they reached the same depth and they were pushed to obtain a representative sample
4		ML ML	S-L1-4A S-L1-4B	37/45	4-3-2	3.75	7.32	52		50		31 38	28 37	- 9	79 97	<15% 22	<10% 10	0.059 0.01	0.02 0.002	
5		ML CL	S-L1-5A S-L1-5B	38/45	2-2-2	4.45	8.84	58		150	45	33 35	31 42	- 21	57 93	10 39	6 30	0.063 0.01	0.005 <2μm	
6		ML	S-L1-6	38/45	3-3-6	5.45	8.84	59		160		34	33	6	87	12	4	0.03	0.004	
7		SM SP-SM	S-L1-7A S-L1-7B	37/45	16-15-18	6.45	10.37	57	SILTY SAND: Brown (S-L1-7) to gray (S-L1-8) silty sand to sand with silt. Approx. 5% fine gravel in S-L1-8			22 22	22 -	- -	45 11	9 -	1 -	0.08 0.27	0.007 0.07	
8		SP-SM	S-L1-8	39/45	10-13-18	7.45	11.89					17	-	-	8	-	-	0.43	0.1	
		MH/CH	S-L1-9A	32/45	3-8-6	8.45	11.89	61	CLAYEY SILT: Gray clayey silt interbedded with silt with sand	50	28	39	51	22	98	32	18	0.01	<2μm	

Depth Scale (m)	Lithology	USCS	Sample Type and No.	Recovery/Length (cm)	SPT Blows/15 cm	Casing Depth (m)	Rod Length (m)	Energy Ratio (%)	Description	q <sub>u</sub> Pocket Pen (kPa)	s <sub>u</sub> Torvane (kPa)	Moisture Content (%)	Liquid Limit	Plasticity Index	% fines < 75 μm	< 5 μm (%)	< 2 μm (%)	D <sub>50</sub> (mm)	D <sub>10</sub> (mm)	Remarks
0									Fill: Asphalt, subgrade and fill consisting of dark brown clayey gravelly sand.											
1		-	S-A3-1	0/45	2-1-2		4.27	47												
2	CH		S-A3-2	25/45	1-2-3		5.80	55	CH: Brown, high plasticity silty clay. At about 2 m there is a layer of brown fine sandy silt	170	61	39	61	33	99	-	-	-	-	
3	CH		S-A3-3	28/45	1-2-2		5.80	43		150	47	38	59	33	99	50	35	0.005	<2μm	
4	ML		S-A3-4A S-A3-4B	34/45	2-3-2		7.32	56	ML: Gray low plasticity clayey silt with fine sand.	70	12	30	31	6	79	-	-	-	-	A 3 cm-thick fine sand seam at 20 cm above the tip of the sampler
5	ML		SH-A3-5	42/42	-	4.45	-	-		80	18	39	38	9	91	13	3	0.024	0.004	
6	ML		S-A3-6	38/45	2-2-2	5.55	8.84	62		40	30	42	43	15	96	-	-	-	-	
7	ML		S-A3-7	38/45	3-4-10	6.45	10.37	61		170	-	31	37	8	88	-	-	-	-	
8			SP-SM	35/45	7-18-24	8.45	11.89	65	SAND: Gray poorly graded sand with silt and traces (8%) of fine rounded gravel	360	-	23	-	-	9	-	-	0.22	0.08	

Depth Scale (m)	Lithology	USCS	Sample Type and No.	Recovery/Length (cm)	SPT Blows/15 cm	Casing Depth (m)	Rod Length (m)	Energy Ratio (%)	Description	q <sub>u</sub> Pocket Pen (kPa)	s <sub>u</sub> Torvane (kPa)	Moisture Content (%)	Liquid Limit	Plasticity Index	% fines < 75 μm	< 5 μm (%)	< 2 μm (%)	D <sub>50</sub> (mm)	D <sub>10</sub> (mm)	Remarks
0									ASPH: Boring performed through asphalt and subgrade of Tul street											
1	ML	S-A1-1	18/45	1-3-3	4.27	37			FILL: Materials transition from a brown to gray gravelly sand to red silty clay of hard consistency			38	41	13	90					
2	MH/CH	S-A1-2	40/45	3-2-5	5.80	46			CH: Brown, moist, sticky, high plasticity silty clay without visible sand particles. S-A1-4 shows darker tones and some fine to medium sand content		28	39	53	23	94					
3	CH	S-A1-3	31/45	2-3-4	5.80	42				140	50	39	65	35	100	61	36	0.0035	<2μm	
4	CL	S-A1-4	36/45	1-2-2	7.32	57				80	22	37	46	23	87					
5	ML/ML-CL	S-A1-5	40/45	2-2-2	7.32	53			ML: Gray silt with sand. Field description: ML	70	23	29	29	6	74	16	>10%	0.045	0.003	
6	CH	S-A1-6	45/45	1-2-1	8.84	55			ML: Brown, low plasticity silt with fine sand and some red clay points	80	25	44	55	28	92					
7	CL/ML	S-A1-7	39/45	1-1-2	8.84	50			CH: High plasticity gray clay with low sand content (traces). At 5.3 m a thin fine sand seam was identified. Sample A1-7 exhibits some sand seams	75	26	39	47	20	97	31	18	0.012	<2μm	
8	ML	S-A1-8	37/45	6-6-9	10.37	65			ML: Gray sandy silt. Increasing sand content with depth	450		27	30		70	15	10	0.057	0.002	
9	ML	S-A1-9	41/45	6-9-10	11.89	75				275		27	29		58					
9	SP	S-A1-10	41/45	11-20-23	11.89	64			SP: Medium to fine poorly graded gray sand	300		24			5			0.29	0.12	

Depth Scale (m)	Lithology	USCS	Sample Type and No.	Recovery/Length (cm)	SPT Blows/15 cm	Casing Depth (m)	Rod Length (m)	Energy Ratio (%)	Description	q <sub>u</sub> Pocket Pen (kPa)	s <sub>u</sub> Torvane (kPa)	Moisture Content (%)	Liquid Limit	Plasticity Index	% fines < 75 μm	< 5 μm (%)	< 2 μm (%)	D <sub>50</sub> (mm)	D <sub>10</sub> (mm)	Remarks
0									ASPH: Asphalt of Yakin Street.											
0.5									Fill											
1	ML/CL	S-A2-1	28/45	1-2-1	-	4.27	37	37	ML: Brown clayey silt to silty clay with some red oxidation points and some fine sand	150	10	37	31	8	74	-	-	-	-	
2	ML	S-A2-2	42/45	1-2-2	-	5.80	53	53	CH: Brown high plasticity silty clay to clayey silt. Some fine to medium sand in a silty clay matrix was observed in the wash water	75	18	36	35	8	86	-	-	-	-	
3	CH/MH	SH-A2-3	42/42		2.55	-	-	-	ML: Brown/gray clayey silt with traces of fine sand	-	48	44	51	23	100	75	57	0.001	<2μm	
4	CL/CH	S-A2-4	40/45	2-1-1	3.35	7.32	52	52	CH: Gray silty clay of medium to high plasticity. Sticky to the fingers. Softens when remoulded	120	53	37	49	25	85	-	-	-	-	
5	ML	S-A2-5	28/45	2-3-4	4.15	7.32	65	65	ML: Gray clayey silt with some fine sand	160	35	34	35	7	93	18	12	0.018	0.001	
6	CL	SH-A2-6	42/42		4.95	-	-	-	SP-SM: Poorly graded gray fine sand with silt. Gravel content ~ 8% in sample S-A2-10	-	31	44	43	20	95	-	-	-	-	
7	MH/CH	S-A2-7	39/45	1-1-2	5.95	8.84	65	65	ML: Gray clayey silt with some fine sand	75	37	43	51	22	99	42	30	0.007	<2μm	
8	ML	S-A2-8	32/45	3-5-5	6.95	10.37	60	60	SP-SM: Poorly graded gray fine sand with silt. Gravel content ~ 8% in sample S-A2-10	170	36	33	39	11	85	20	13	0.026	0.001	At approximately 7.15 m, an 8-cm thick stratum of black, fibrous material (Peat) was identified in the sample
9	SP-SM	S-A2-9	38/45	12-20-16	8.45	11.89	61	61		380	-	33	-	-	8	-	-	0.12	0.08	
10	SP-SM	S-A2-10	38/45	7-10-15	9.95	12.82	-	-		320	-	22	-	-	6	-	-	0.33	0.1	

Depth Scale (m)	Lithology	USCS	Sample Type and No.	Recovery/Length (cm)	SPT Blows/15 cm	Casing Depth (m)	Rod Length (m)	Energy Ratio (%)	Description	q <sub>u</sub> Pocket Pen (kPa)	s <sub>u</sub> Torvane (kPa)	Moisture Content (%)	Liquid Limit	Plasticity Index	% fines < 75 μm	< 5 μm (%)	< 2 μm (%)	D <sub>50</sub> (mm)	D <sub>10</sub> (mm)	Remarks
0									FILL: Asphalt, pavement and fill on Yakin Street											
1																				
2	CL/ML	CL/ML	SH-A4-1A SH-A4-1B	39/42	-	1.2	-	-	CL: Low to high plasticity, brown silty clay to clayey silt with traces of fine sand. Soil is highly inhomogeneous, showing variable FC	75 75	41 41	24 33	34 42	11 17	80 94	35 45	24 34	0.017 0.006	<2μm <2μm	Shear Vane @ 1.65 m. Peak = 16 kPa, Residual = 4 kPa
3	CL		SH-A4-2	33/42	-	1.2	-	-		60	32	35	48	24	99	32	25	0.02	<2μm	Shear Vane @ 2.45 m. Peak = 29 kPa, Residual = 9 kPa
4			SH-A4-3	41/42	-	1.2	-	-		70	26	-	-	-	-	-	-	-	-	
5	ML		S-A4-4	30/45	3-3-3	4.05	7.32	51	ML: Brown low plasticity silt with traces of fine sand	-	-	32	36	10	97	24	18	0.017	<2μm	Shear Vane @ 3.45 m. Peak = 15 kPa, Residual = 5 kPa
6	CL/MH		S-A4-5	28/45	3-1-2	4.95	8.84	53	CL: Low to high plasticity gray silty clay to clayey silt with traces of fine sand	75	27	39	49	22	98	56	42	0.004	<2μm	
7	CL		S-A4-6	-	6-5-11	6.45	10.37	59		-	-	37	38	14	92	43	37	0.007	<2μm	Initially no sample was recovered at a depth of 6.5 m. In a second attempt, a sample was obtained at 6.6 m with the aid of a sand catcher.
8	ML		S-A4-7	33/45	11-12-17	7.95	11.89	60	SANDY SILT: Gray low plasticity sandy silt	440	-	25	25	-	66	35	32	0.018	<2μm	
9																				
10	SP-SM		S-A4-8	40/45	24-38-36	9.45	12.82	-	SAND: Gray poorly to well graded sand with silt. 22% gravel content in S-A4-9, very low (< 5%) in other samples.	-	-	18	-	-	8	-	-	0.3	0.185	
11	SW SM		S A4 9	39/45	14 18 20	10 95	14 94	54												

**Legend**  
 S: Spit Spoon (SPT) SH: Shelby tube

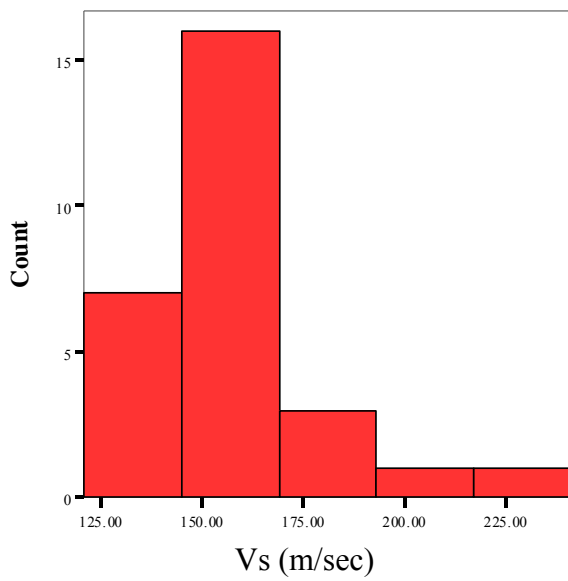
Depth Scale (m)	Lithology	USCS	Sample Type and No.	Recovery/Length (cm)	SPT Blows/15 cm	Casing Depth (m)	Rod Length (m)	Energy Ratio (%)	Description	$q_u$ Pocket Pen (kPa)	$s_u$ Torvane (kPa)	Moisture Content (%)	Liquid Limit	Plasticity Index	% fines < 75 $\mu$ m	< 5 $\mu$ m (%)	< 2 $\mu$ m (%)	D50 (mm)	D10 (mm)	Remarks
11		SW-SM	S-A4-9	39/45	14-18-20	10.95	14.94	54		-	-	17	-	-	10	-	-	0.61	0.074	
12		SP-SM	S-A4-10	33/45	14-17-18	12.45	16.46	62		-	-	16	-	-	7	-	-	0.5	0.1	
13																				
14									CH: Gray, high plasticity stiff clay.											
15		CH	S-A4-11	26/45	4-4-7	14.95	17.92	62		250	53	37	69	45	100	86	73	<2 $\mu$ m	<2 $\mu$ m	BW rods were used for the SPT at 15 m

APPENDIX – B

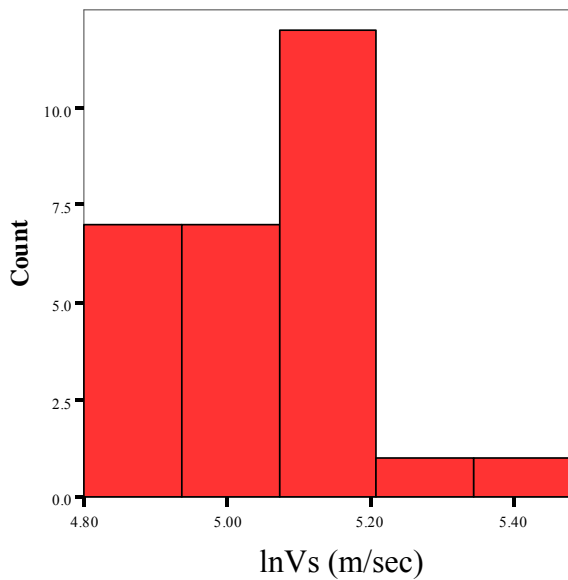
Statistical Analysis Results

**Table B-1** Descriptive Statistics for Layers already investigated

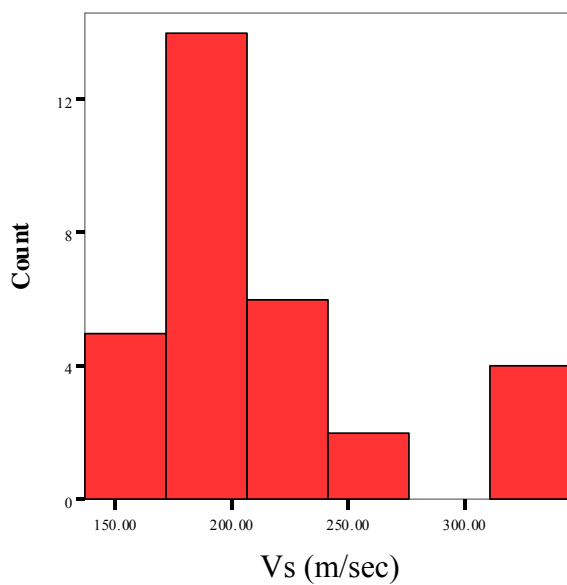
	N	Range	Minimum	Maximum	Mean		Std. Deviation	Coefficient of Variation	Skewness		Kurtosis	
	Statistic	Statistic	Statistic	Statistic	Statistic	Std. Error	Statistic	Statistic	Statistic	Std. Error	Statistic	Std. Error
S1A	28	120	121	241	156.64	4.47	23.66	0.15	1.805	0.441	5.589	0.858
S1B	31	209	137	346	214.68	9.46	52.69	0.25	1.428	0.421	1.36	0.821
S1C	26	162	161	323	224.69	9.84	50.18	0.22	0.777	0.456	-0.572	0.887
S2A	64	102	121	223	175.31	2.73	21.82	0.12	0.017	0.299	0.114	0.59
S2B	49	130	179	309	234.65	3.71	25.99	0.11	0.544	0.34	1.094	0.668
S2C	43	115	171	286	215.86	4.21	27.58	0.13	1.133	0.361	0.775	0.709
S3A	24	82	150	232	193.25	4.46	21.83	0.11	-0.449	0.472	-0.348	0.918
S3B	22	56	150	206	169.14	2.8	13.16	0.08	1.048	0.491	1.57	0.953
S3C	50	186	171	357	267.58	7.4	52.3	0.2	0.088	0.337	-1.201	0.662
S4A	53	151	137	288	175.64	3.16	22.99	0.13	2.182	0.327	10.128	0.644
S4B	18	95	212	307	258.5	6.41	27.18	0.11	0.431	0.536	-0.595	1.038
S4C	6	20	312	332	324.33	3.95	9.67	0.03	-0.87	0.845	-1.891	1.741



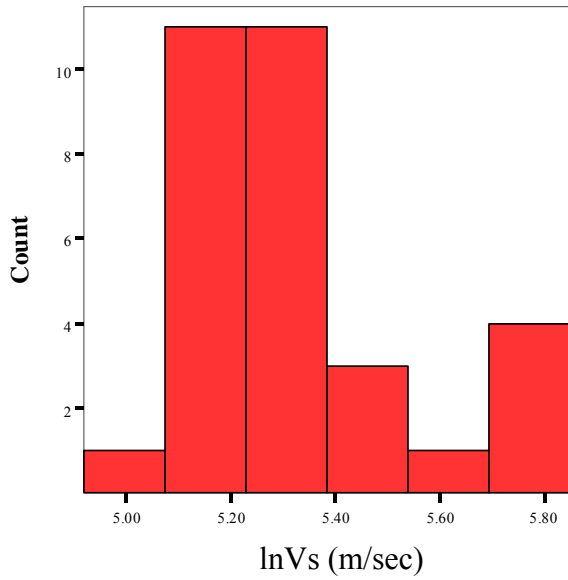
Layer: S1A  
 N: 28  
 Mean : 156.64  
 Standard Deviation: 23.66  
 Distribution: Lognormal



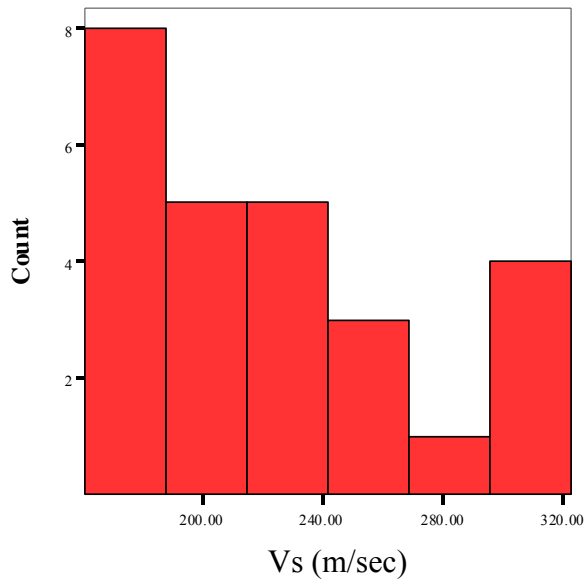
Layer: S1A  
 N: 28  
 Mean : 5.04  
 Standard Deviation: 0.14  
 Distribution: Lognormal



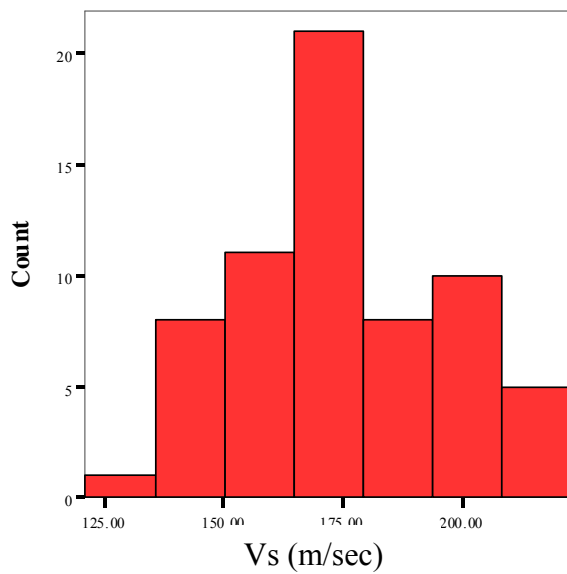
Layer: S1B  
 N: 31  
 Mean : 214.68  
 Standard Deviation: 52.69  
 Distribution: Lognormal



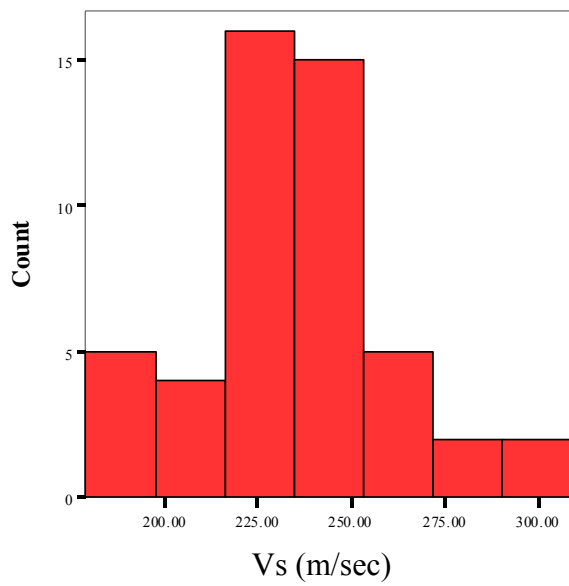
Layer: S1B  
 N: 31  
 Mean : 5.34  
 Standard Deviation: 0.22  
 Distribution: Lognormal



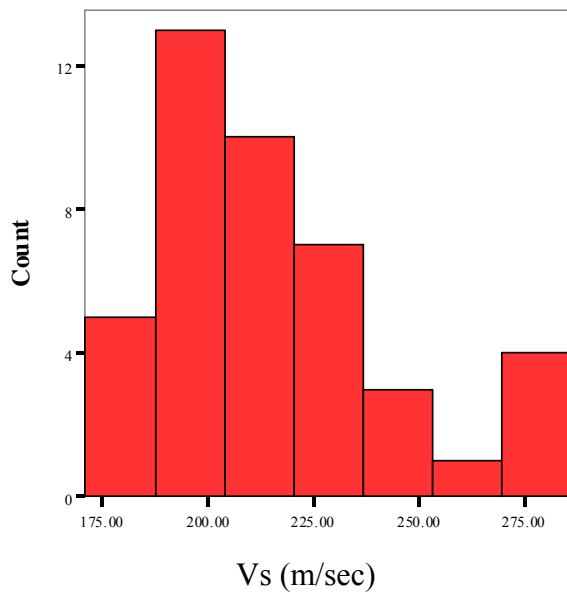
Layer: S1C  
 N: 26  
 Mean : 224.69  
 Standard Deviation: 50.18  
 Distribution: Gamma



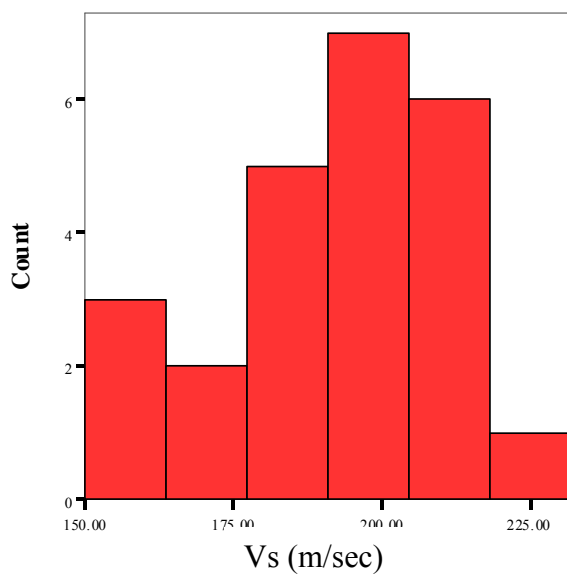
Layer: S2A  
 N: 64  
 Mean : 175.31  
 Standard Deviation: 21.82  
 Distribution: Normal



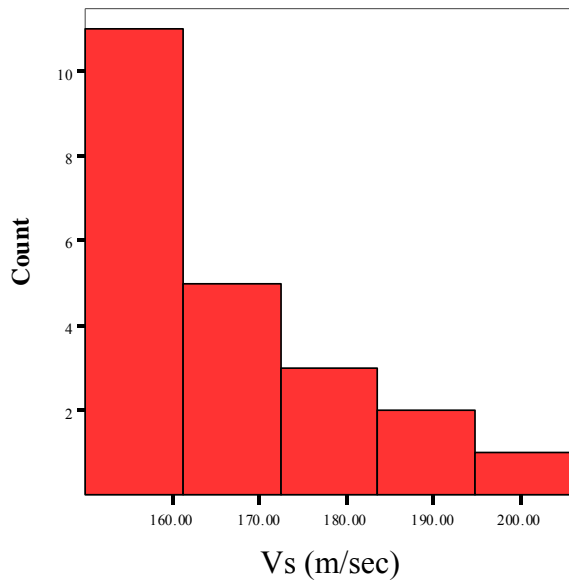
Layer: S2B  
 N: 49  
 Mean : 234.65  
 Standard Deviation: 25.99  
 Distribution: Normal



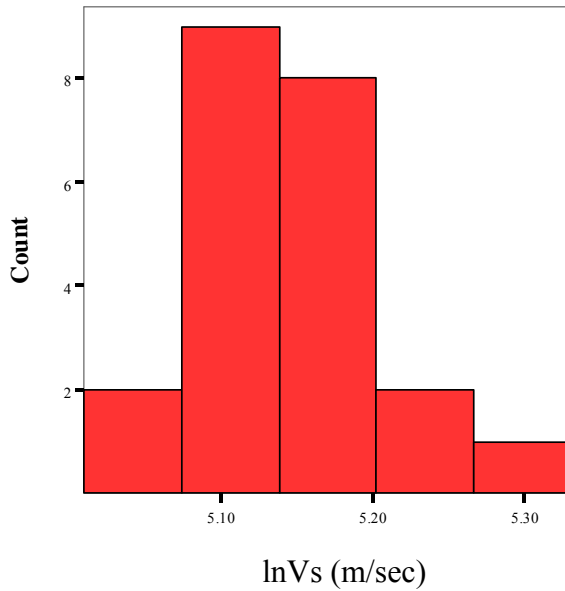
Layer: S2C  
 N: 43  
 Mean : 215.86  
 Standard Deviation: 27.58  
 Distribution: Gamma



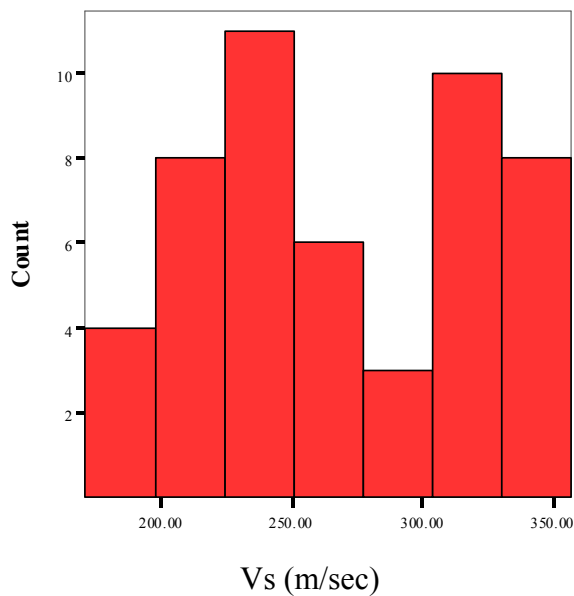
Layer: S3A  
 N: 24  
 Mean : 193.25  
 Standard Deviation: 21.83  
 Distribution: Gamma



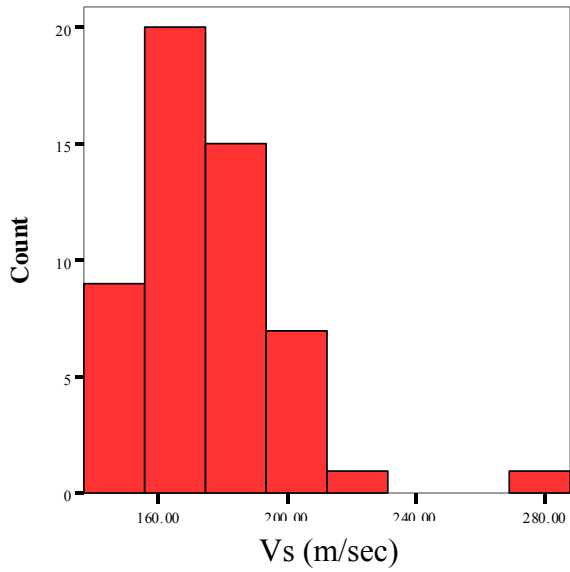
Layer: S3B  
 N: 22  
 Mean : 169.14  
 Standard Deviation: 13.16  
 Distribution: Lognormal



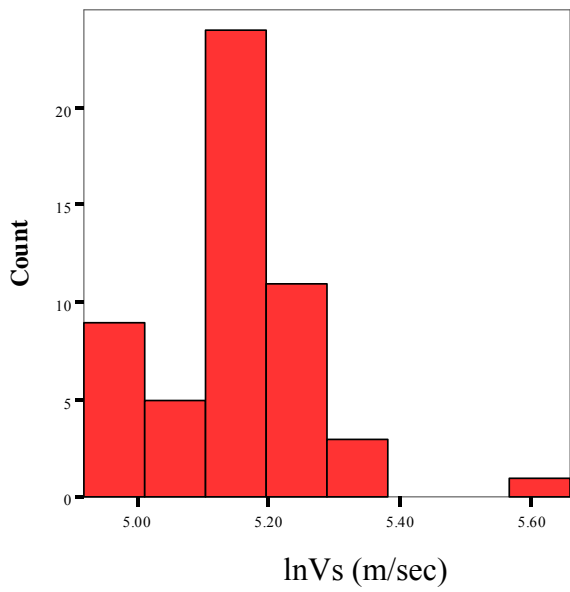
Layer: S3B  
 N: 22  
 Mean : 5.13  
 Standard Deviation: 0.08  
 Distribution: Lognormal



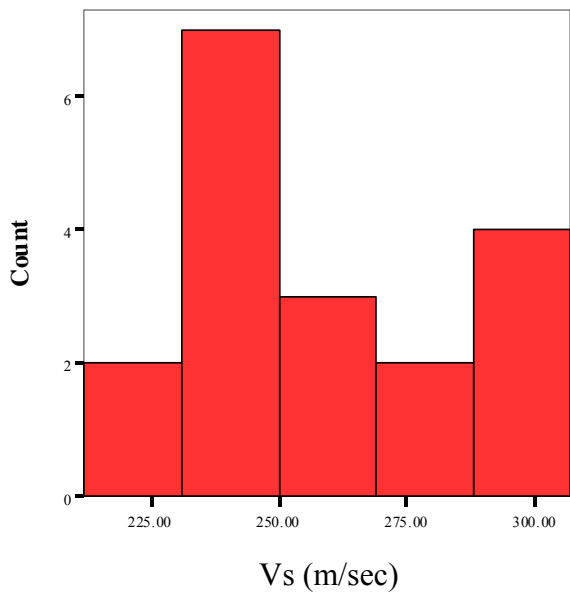
Layer: S3C  
 N: 50  
 Mean : 267.58  
 Standard Deviation: 52.30  
 Distribution: Normal



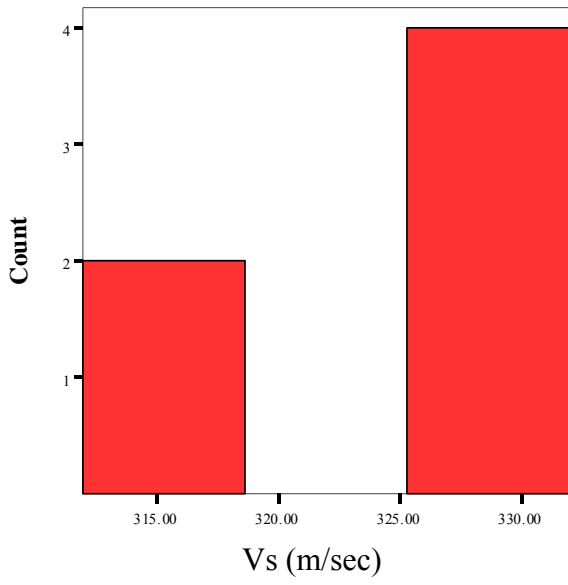
Layer: S4A  
 N: 53  
 Mean : 175.64  
 Standard Deviation: 22.98  
 Distribution: Lognormal



Layer: S4A  
 N: 53  
 Mean : 5.16  
 Standard Deviation: 0.12  
 Distribution: Lognormal



Layer: S4B  
 N: 18  
 Mean : 258.50  
 Standard Deviation: 27.18  
 Distribution: Gamma



Layer: S4C  
N: 6  
Mean : 324.33  
Standard Deviation: 9.67  
Distribution: undefined

## APPENDIX – C

### Geostatistical Analysis Results

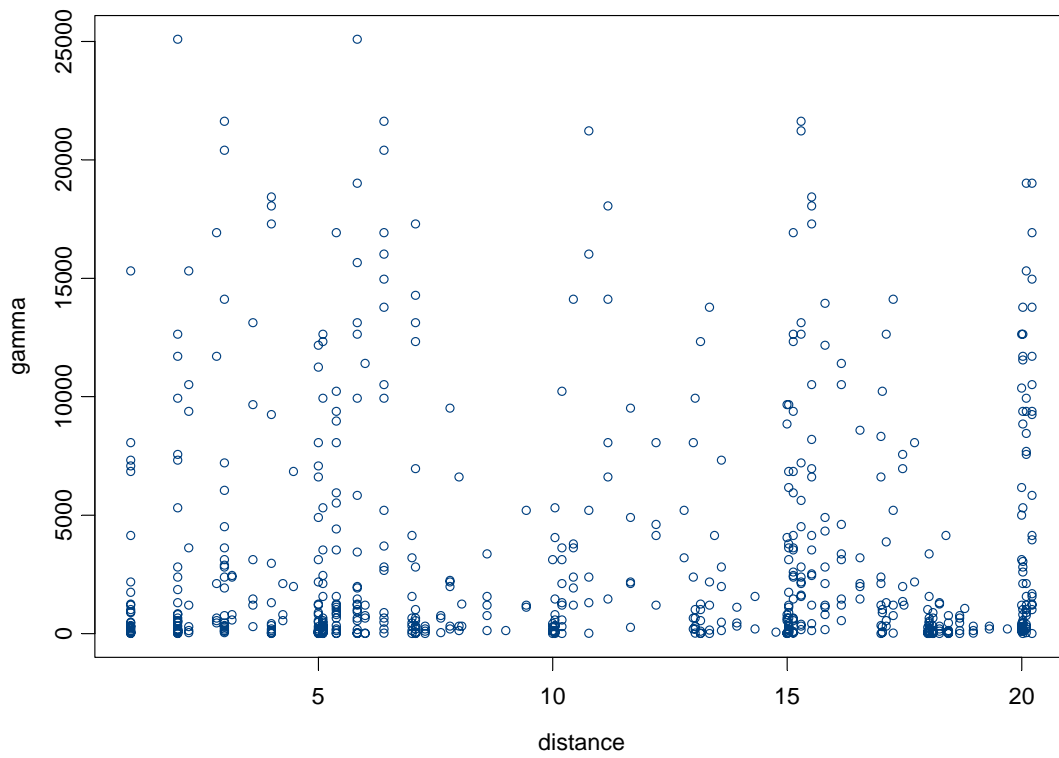


**Figure C-1** Variogram clouds of shear wave velocity for line 1

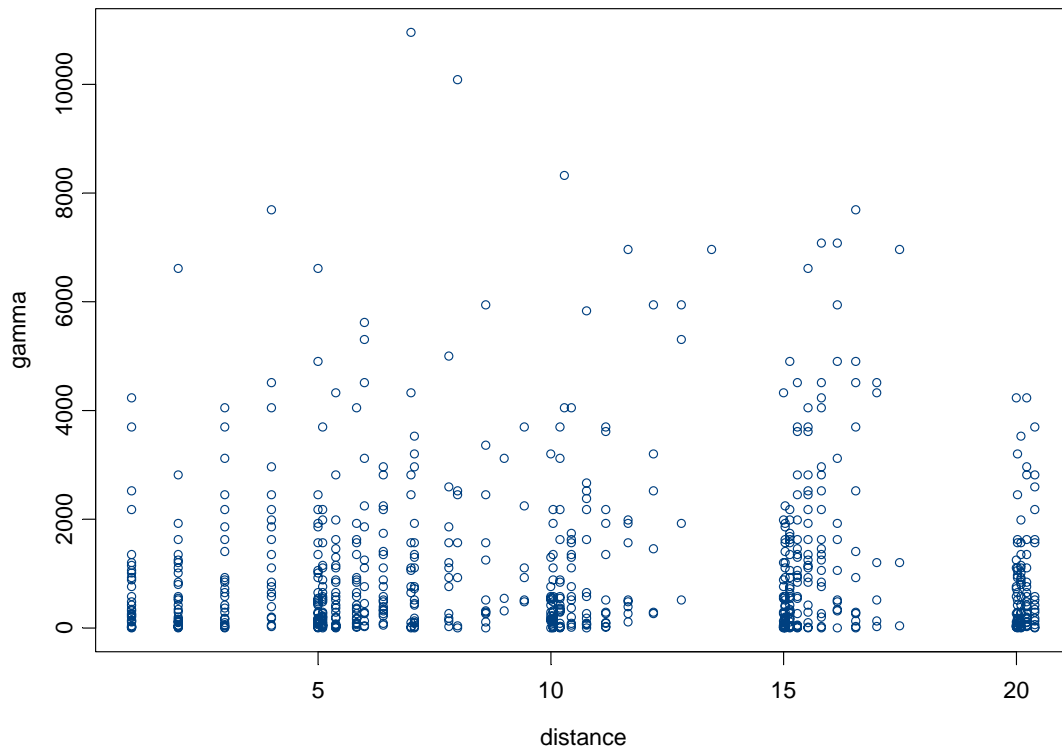


**Figure C-2** Variogram clouds of shear wave velocity for line 2

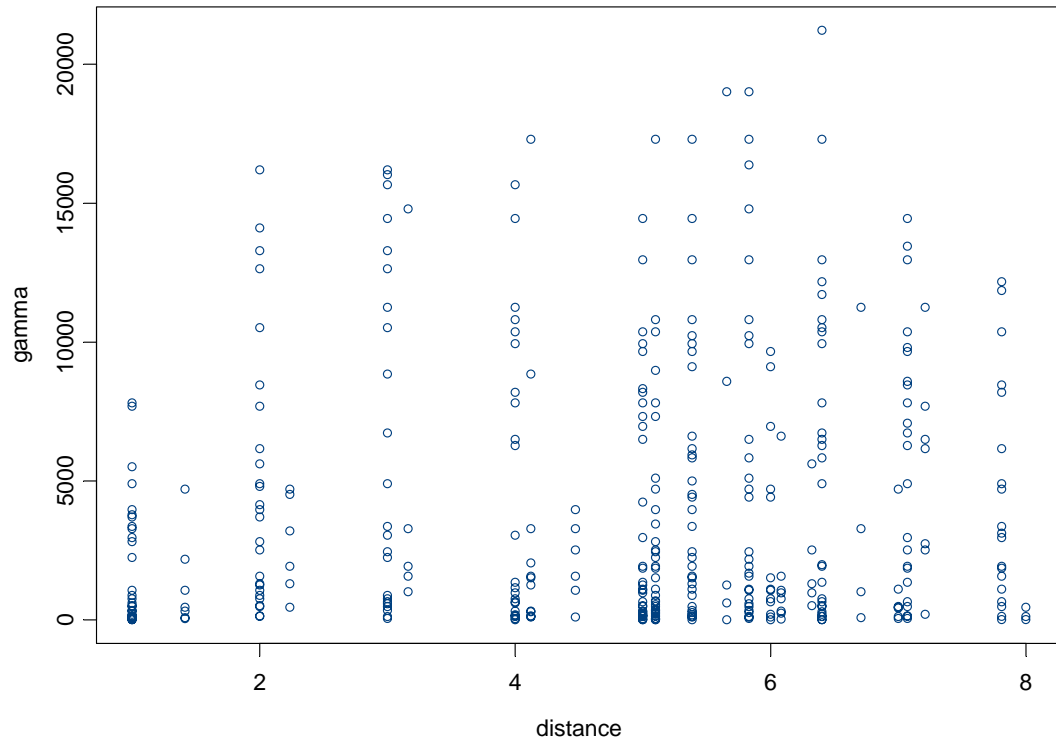


**Figure C-3** Variogram clouds of shear wave velocity for line 3

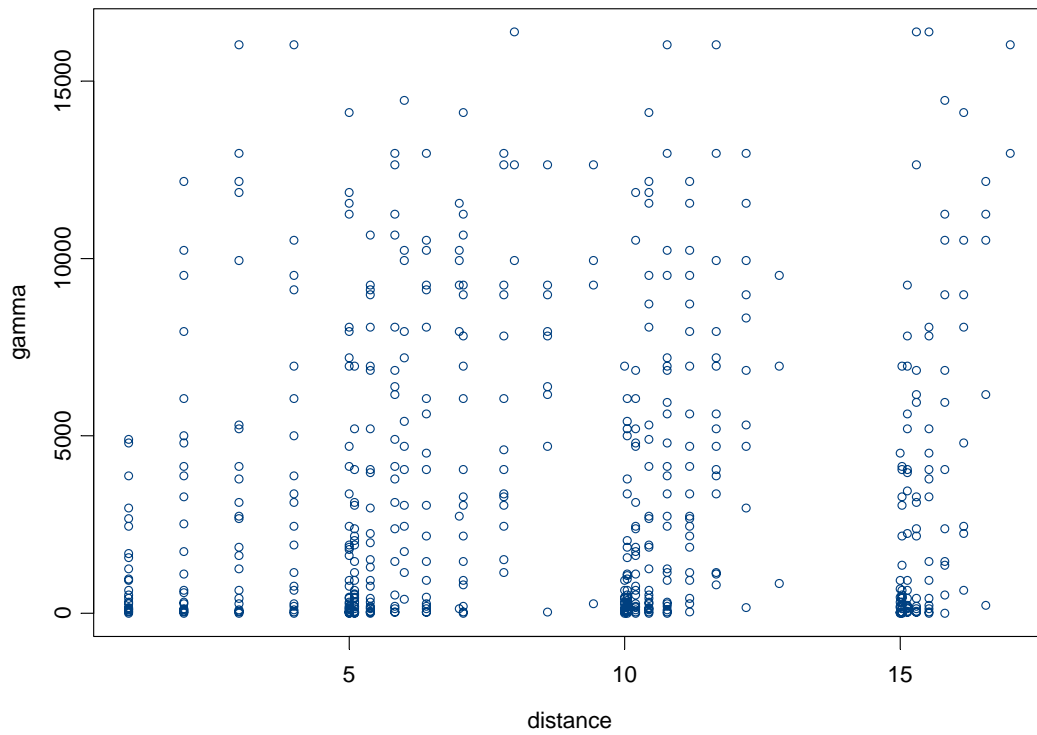


**Figure C-4** Variogram clouds of shear wave velocity for line 4

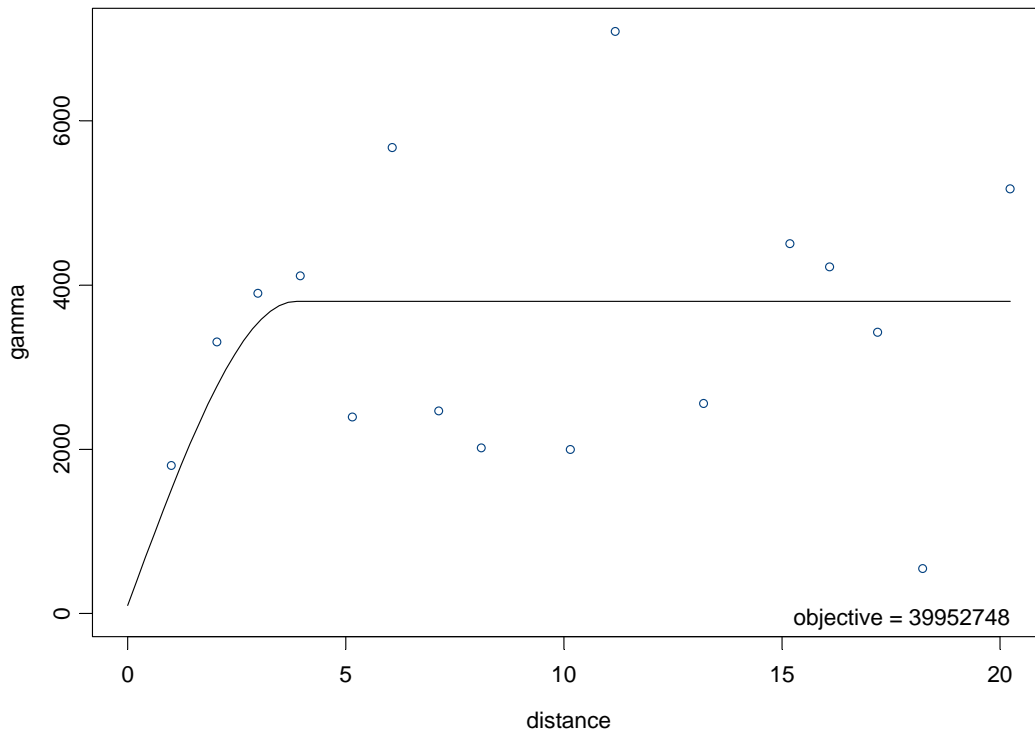


**Figure C-5** Experimental Variogram and Model fitting for line 1

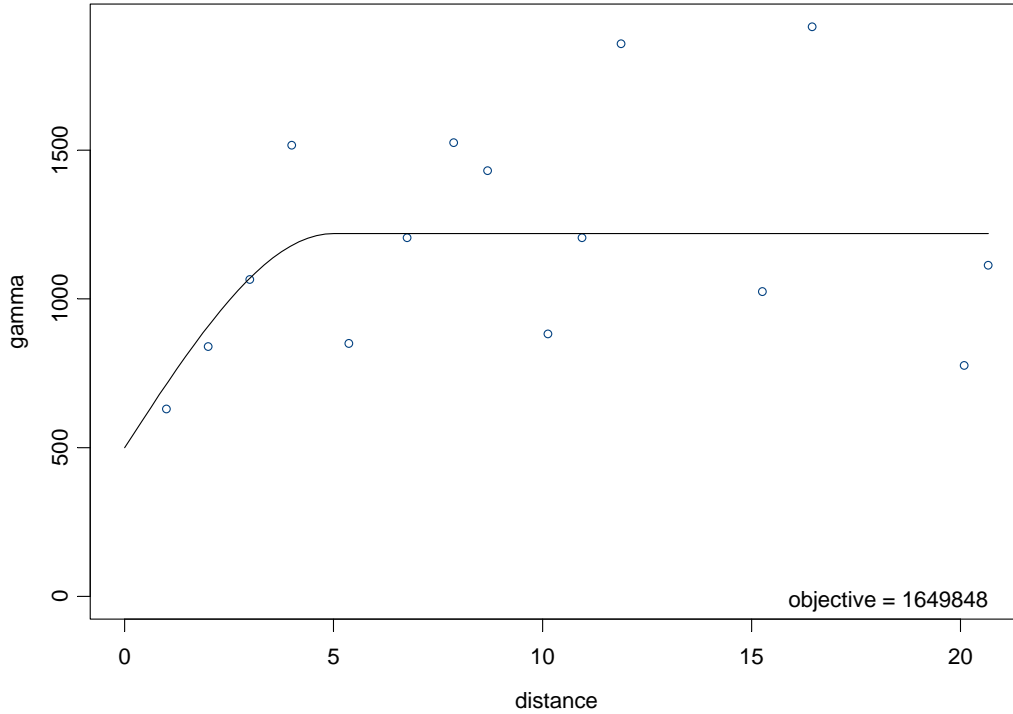


**Figure C-6** Experimental Variogram and Model fitting for line 2

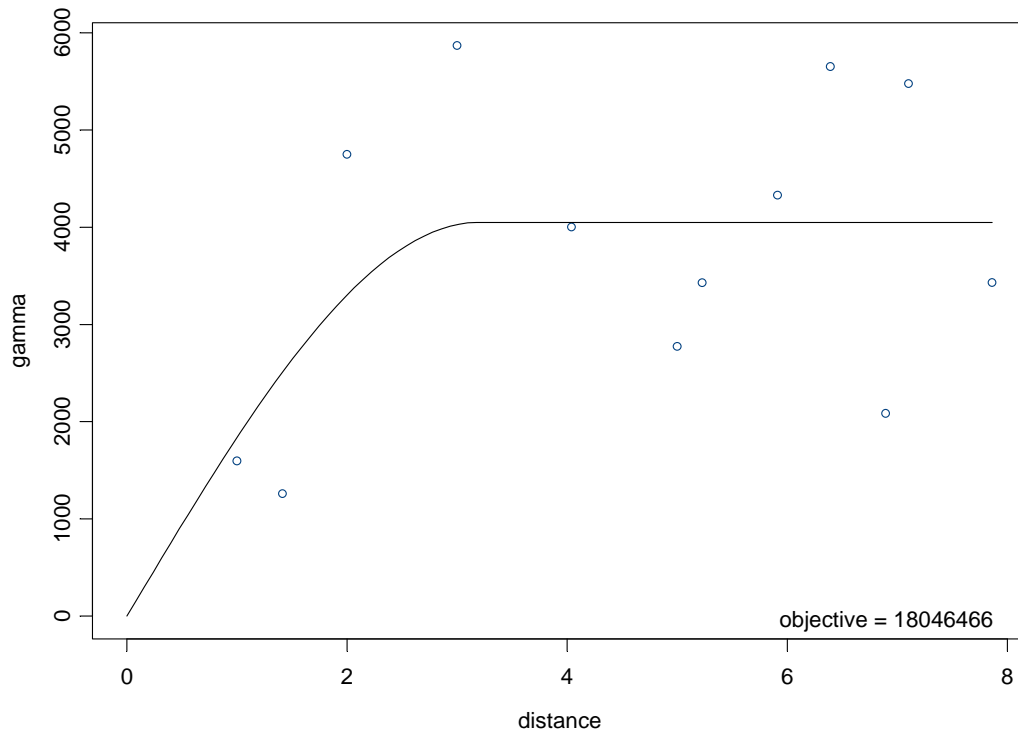


**Figure C-7** Experimental Variogram and Model fitting for line 3

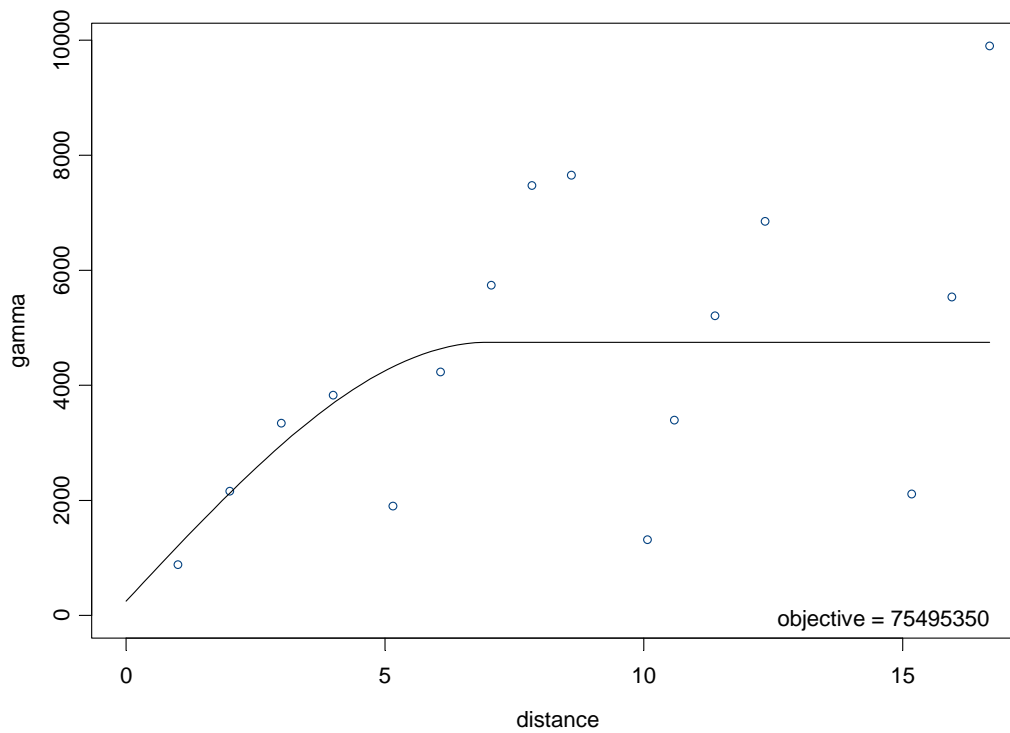


**Figure C-8** Experimental Variogram and Model fitting for line 4

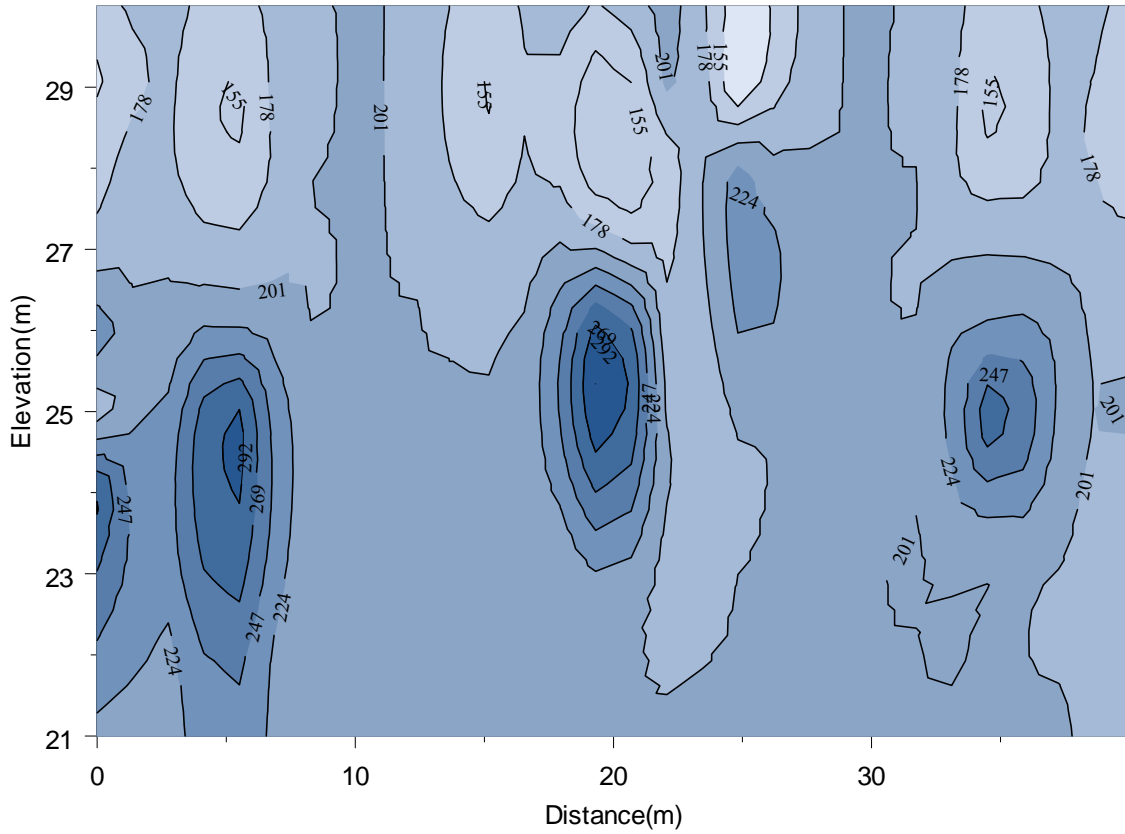


**Figure C-9** 2-D Kriging map of shear wave velocity (m/sec) for line 1

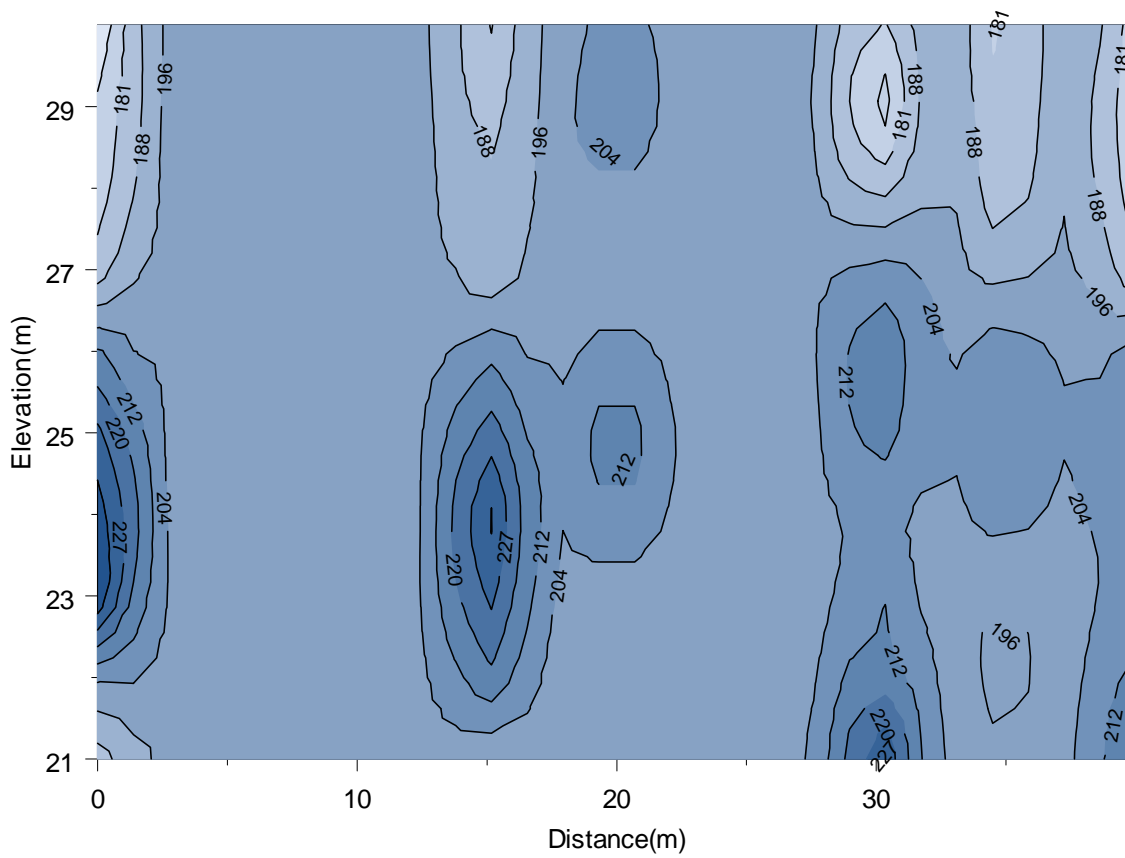


**Figure C-10** 2-D Kriging map of shear wave velocity (m/sec) for line 2

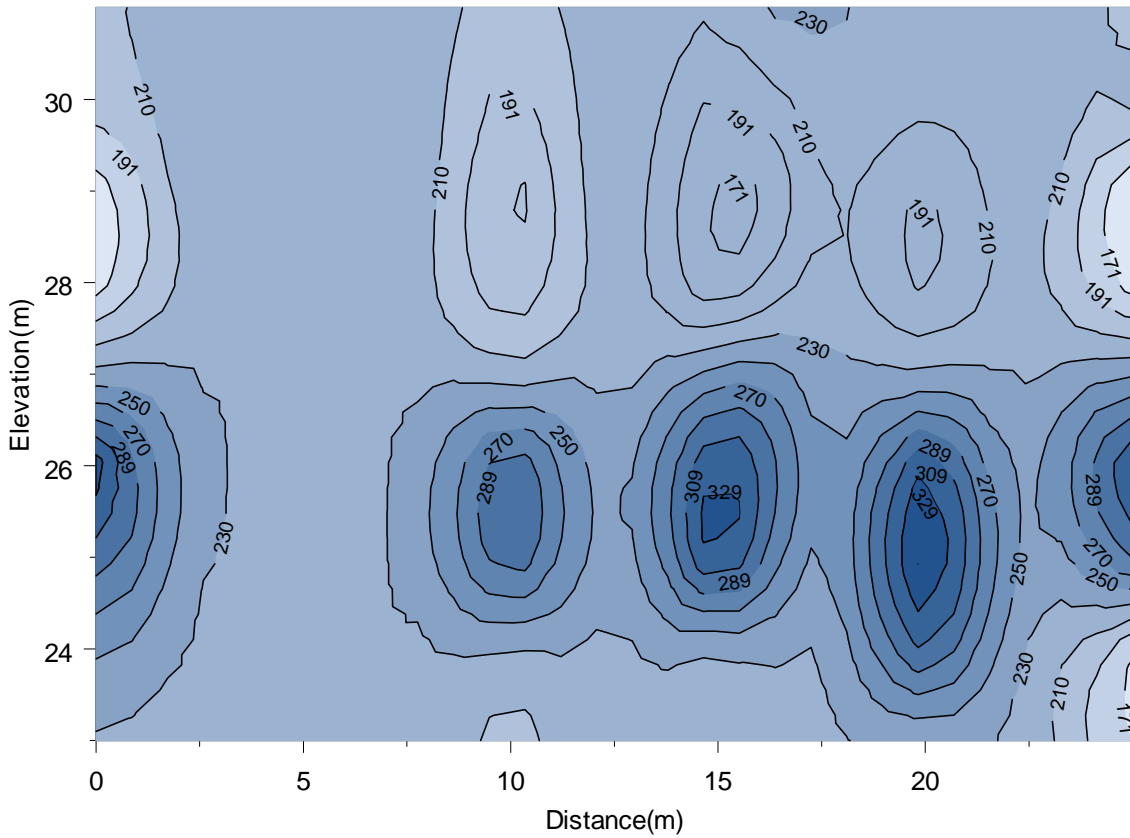


**Figure C-11** 2-D Kriging map of shear wave velocity (m/sec) for line 3

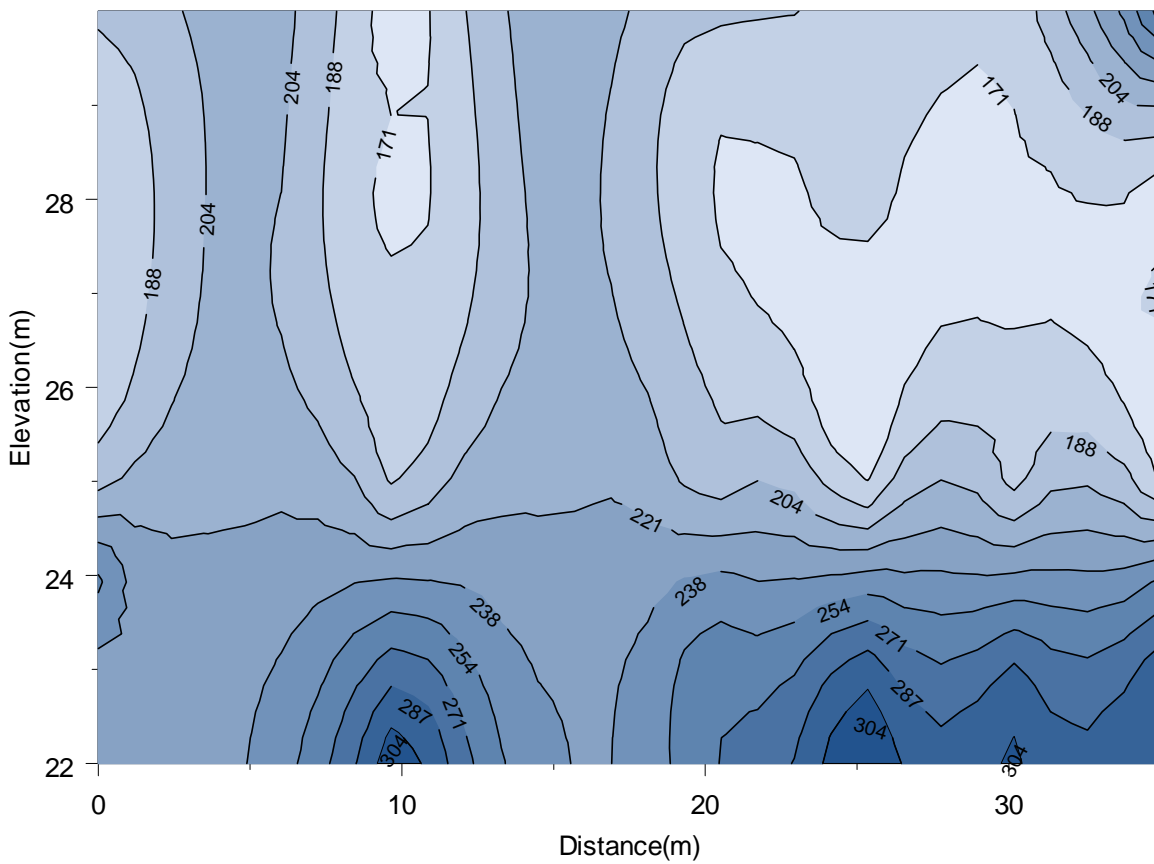


**Figure C-12** 2-D Kriging map of shear wave velocity (m/sec) for line 4

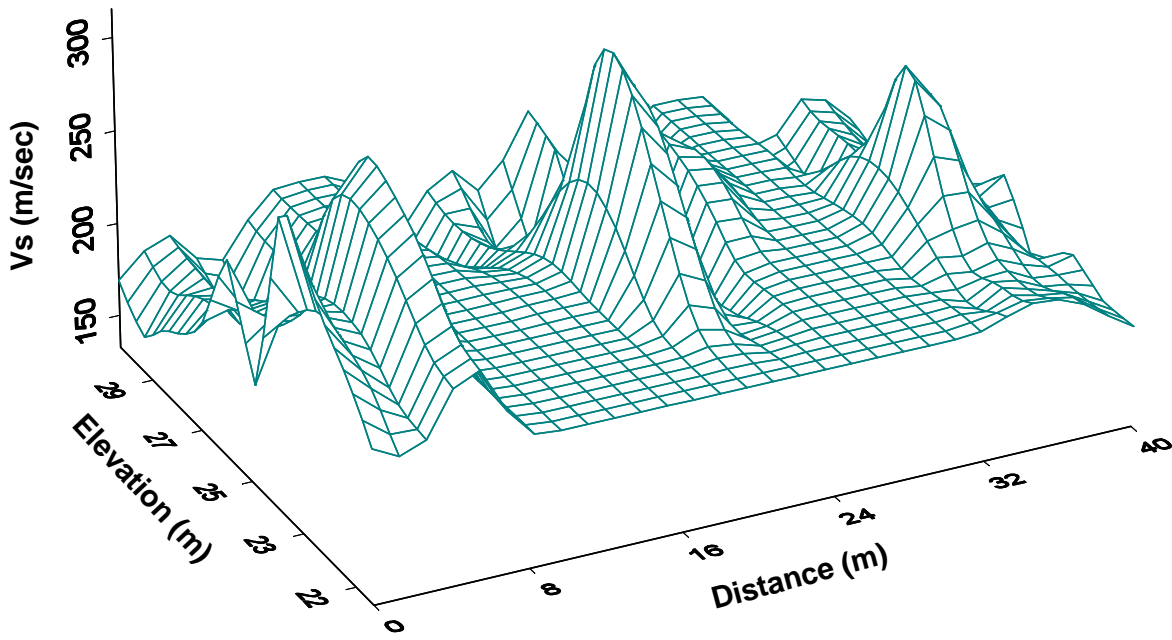


Figure C-13 3-D Kriging map of shear wave velocity (m/sec) for line 1

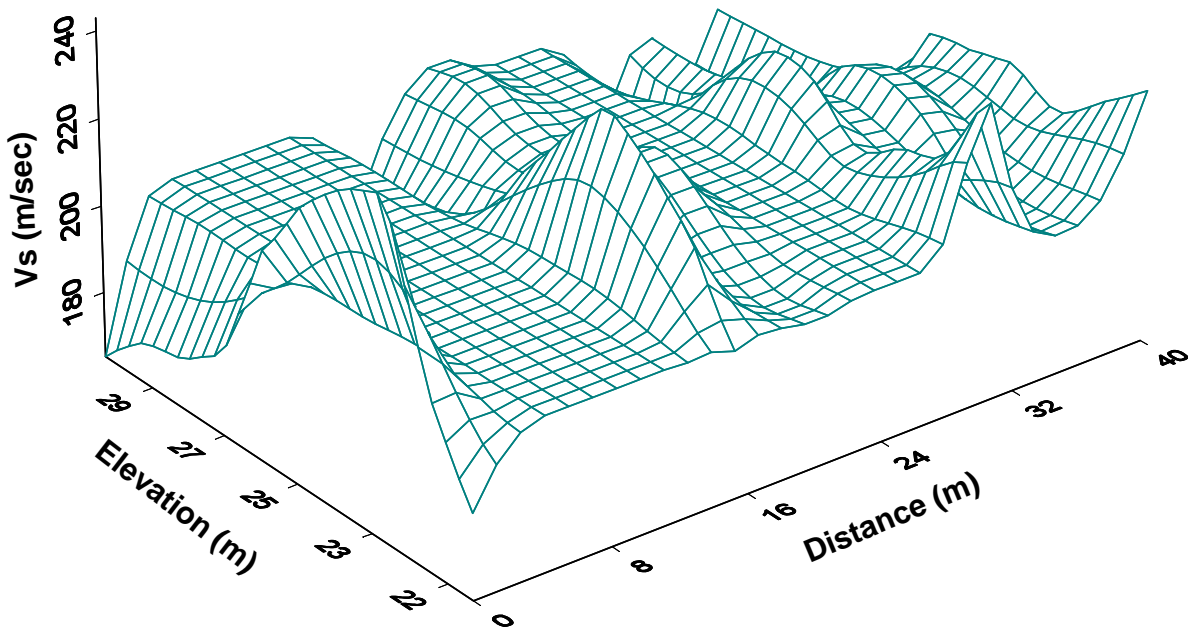


Figure C-14 3-D Kriging map of shear wave velocity (m/sec) for line 2

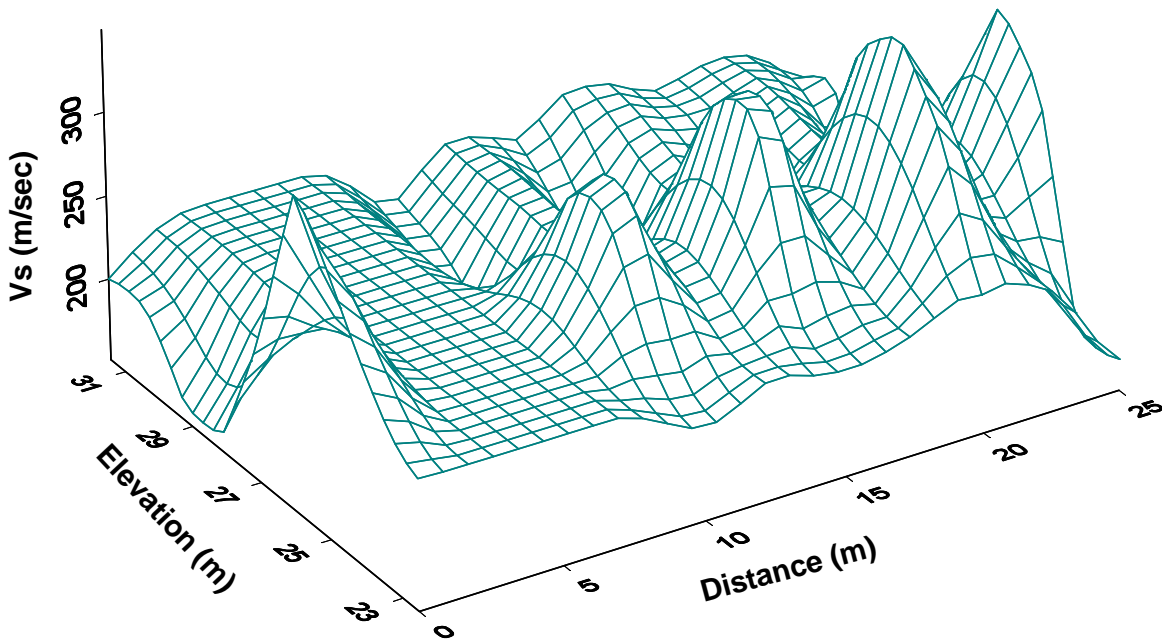


Figure C-15 3-D Kriging map of shear wave velocity (m/sec) for line 3

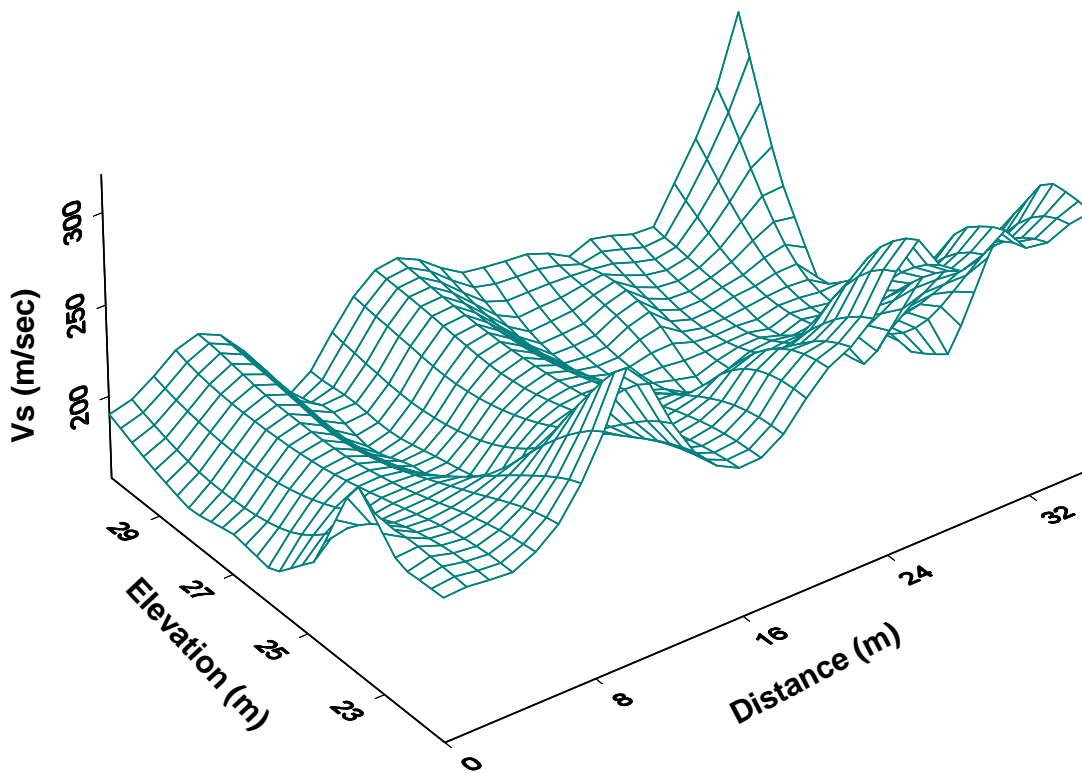
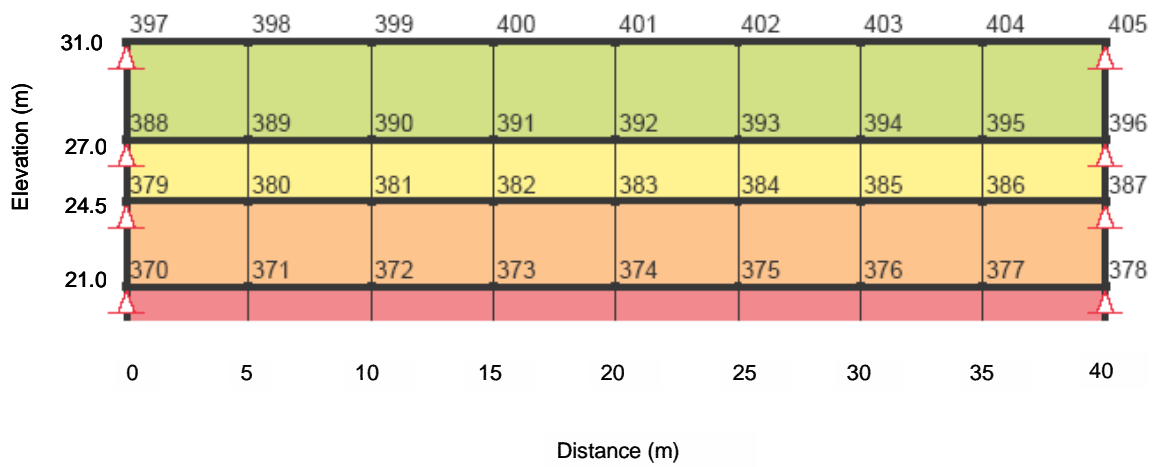


Figure C-16 3-D Kriging map of shear wave velocity (m/sec) for line 4

## APPENDIX – D

### Site Response Analysis Results



**Figure D -1** Statistically Modeled soil profile for line 1

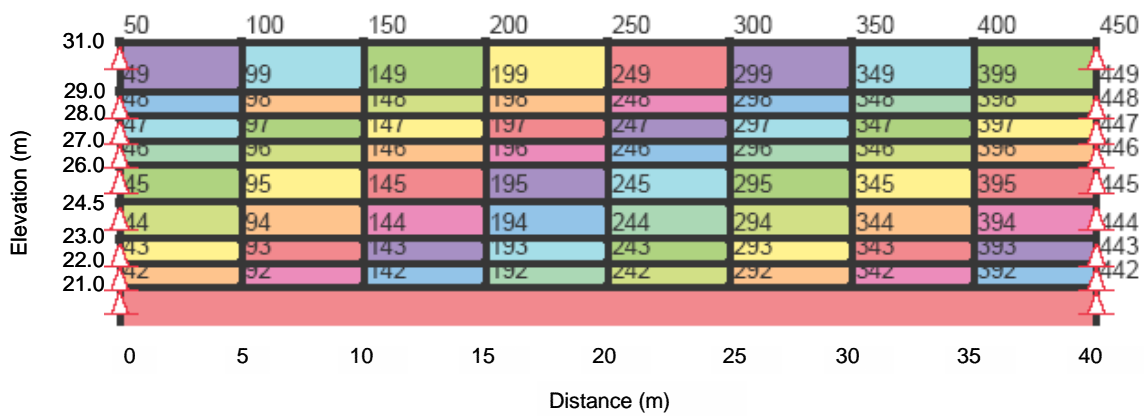


**Figure D-2** Geostatistically Modeled soil profile for line 1

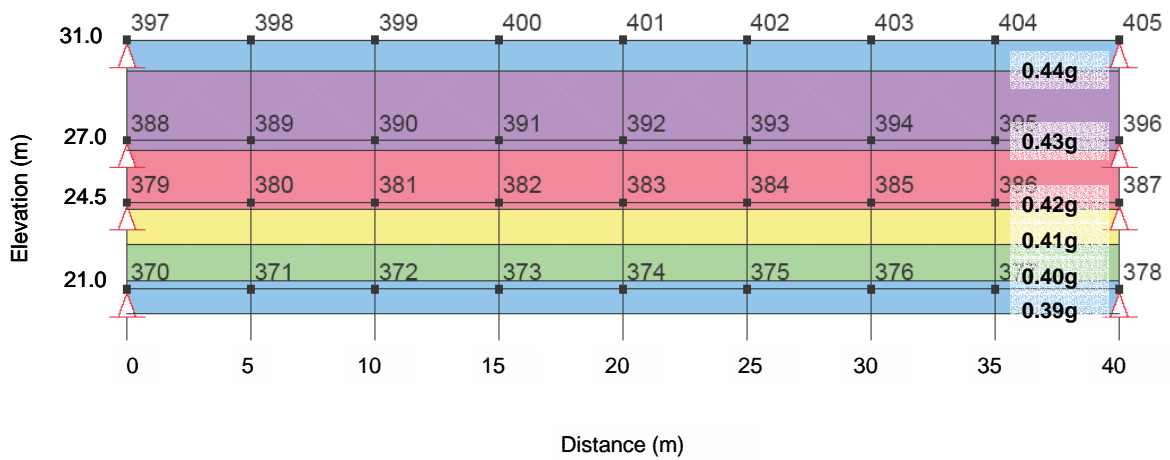


**Figure D-3** Peak acceleration distribution for statistically Modeled soil profile for line 1

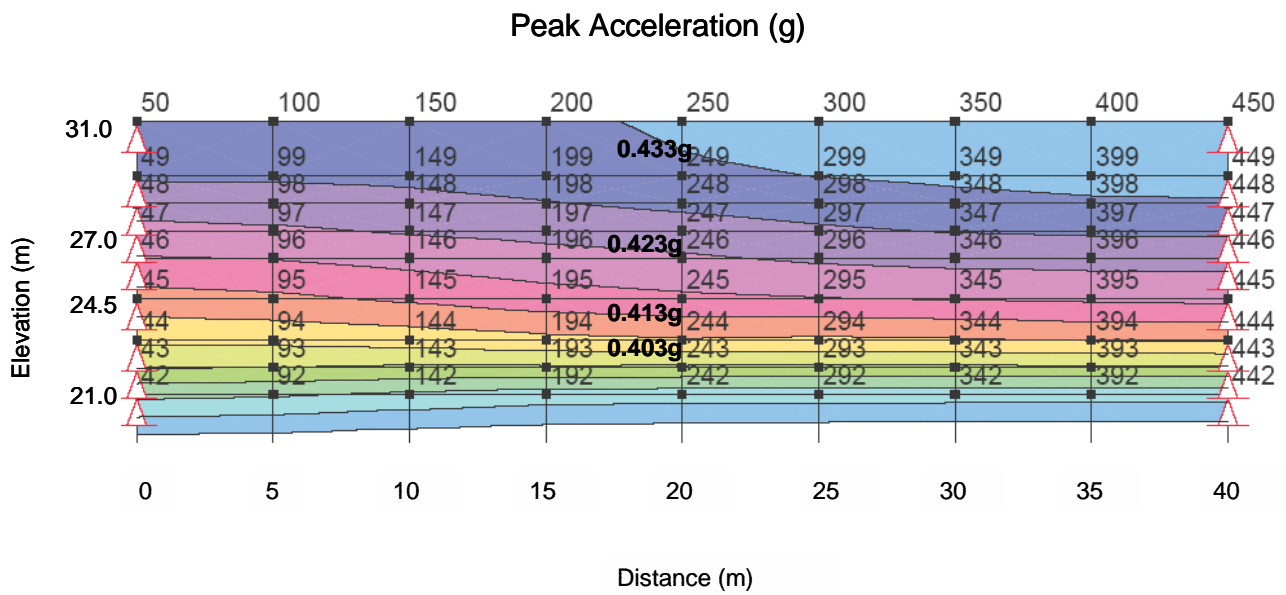


**Figure D-4** Peak acceleration distribution for geostatistically Modeled soil profile for line 1

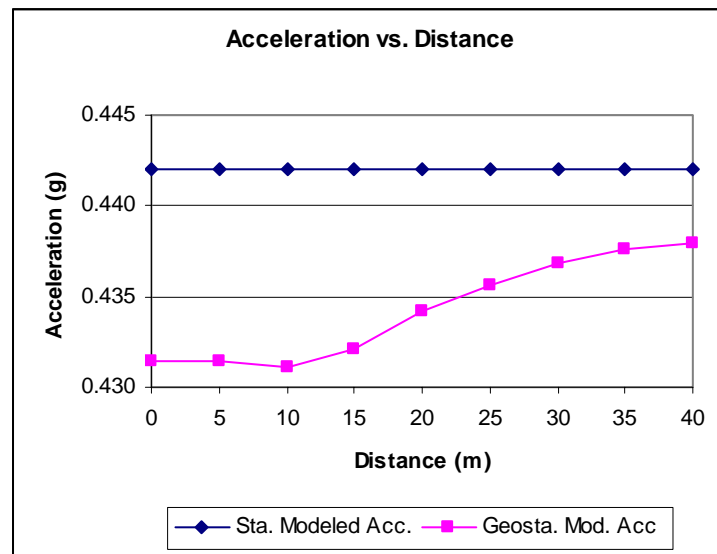


**Figure D-5** Peak acceleration distribution along the line 1 recorded at ground surface for statistically and geostatistically modeled soil profiles

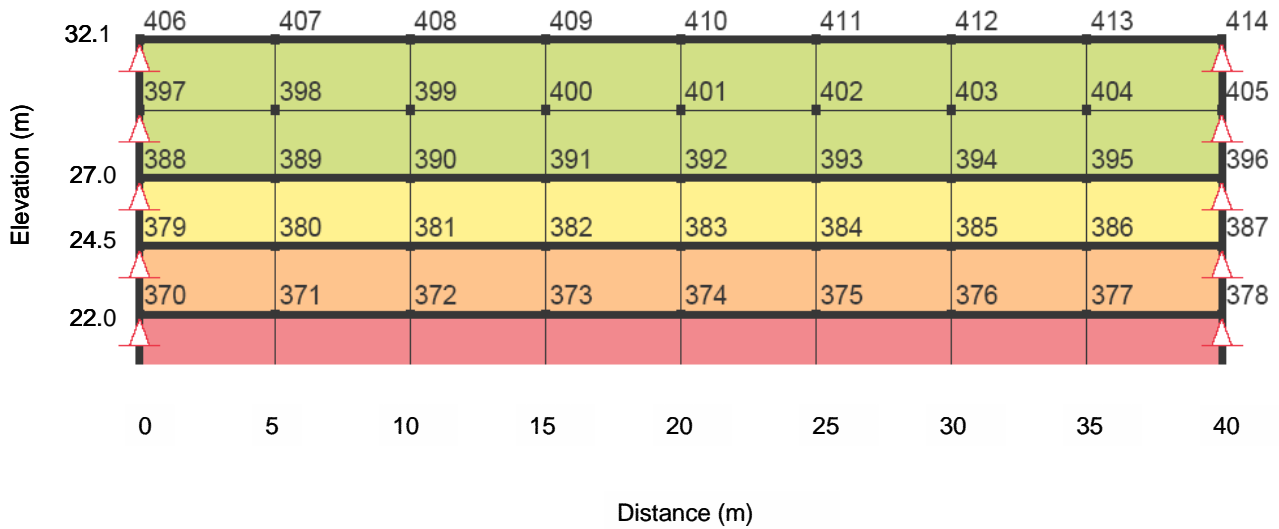


**Figure D-6** Statistically Modeled soil profile for line 2

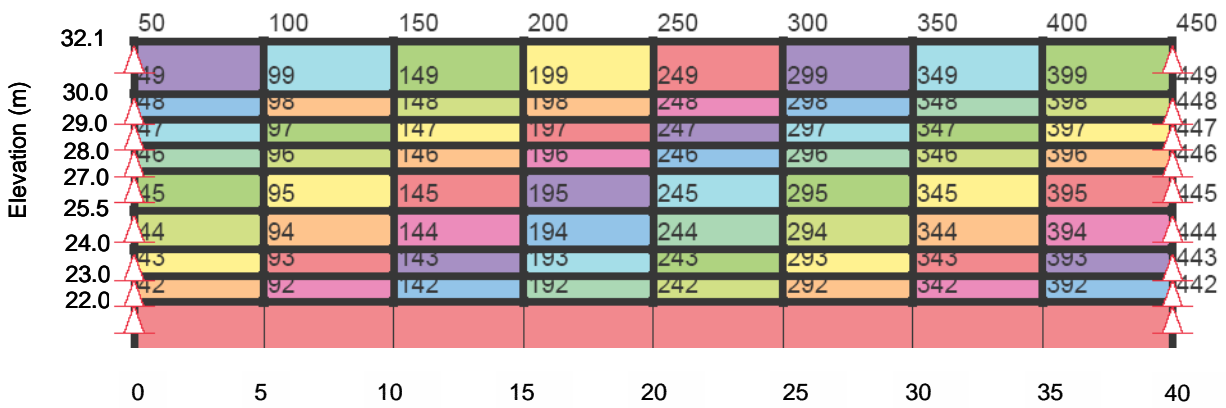


**Figure D-7** Geostatistically Modeled soil profile for line 2

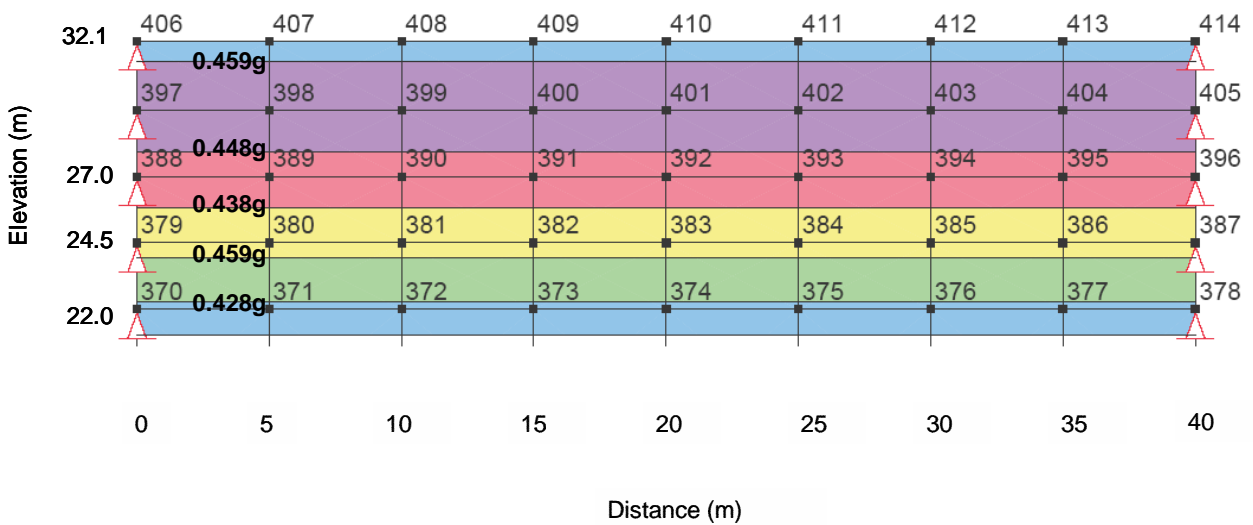


**Figure D-8** Peak acceleration distribution for statistically Modeled soil profile for line 2

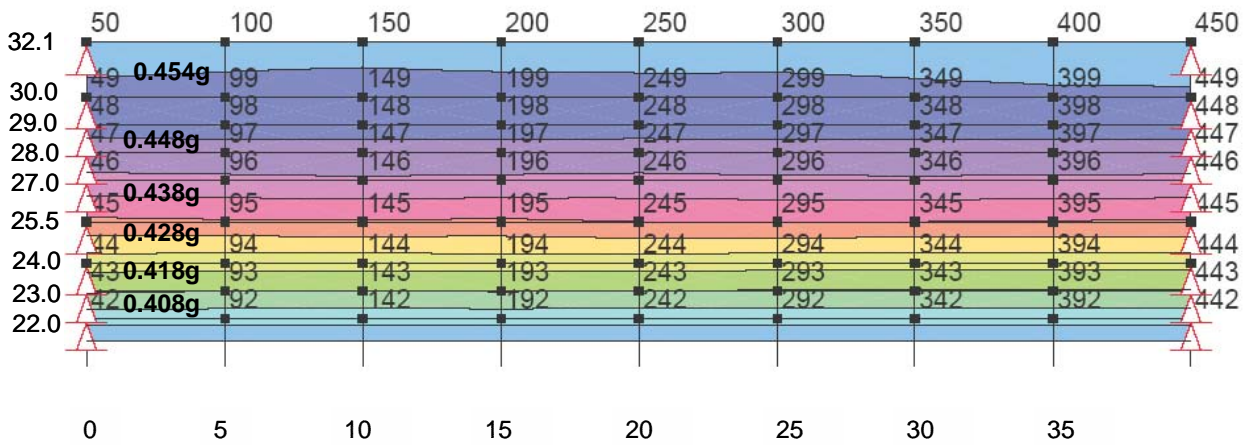


**Figure D-9** Peak acceleration distribution for geostatistically Modeled soil profile for line 2

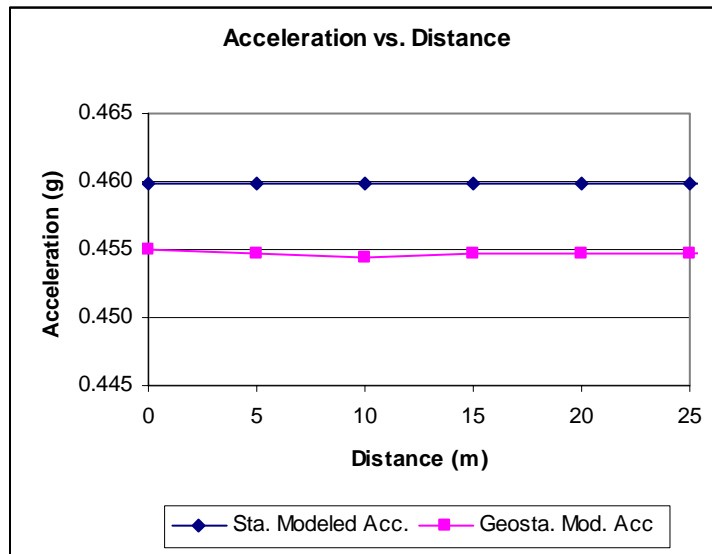


**Figure D-10** Peak acceleration distribution along the line 2 recorded at ground surface for statistically and geostatistically modeled soil profiles

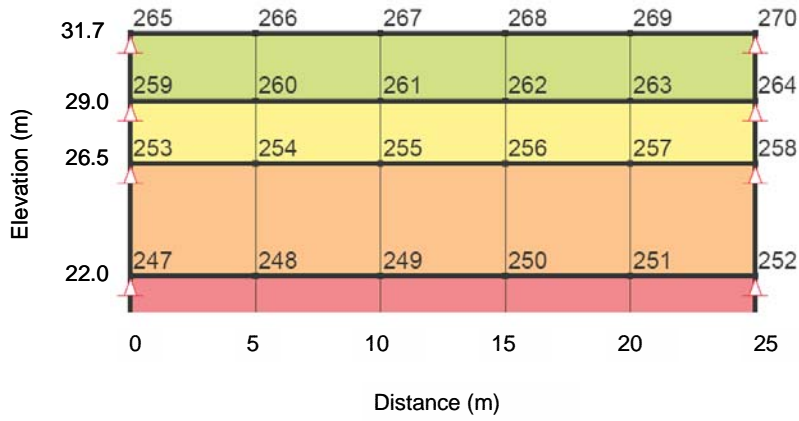


**Figure D -11** Statistically Modeled soil profile for line 3

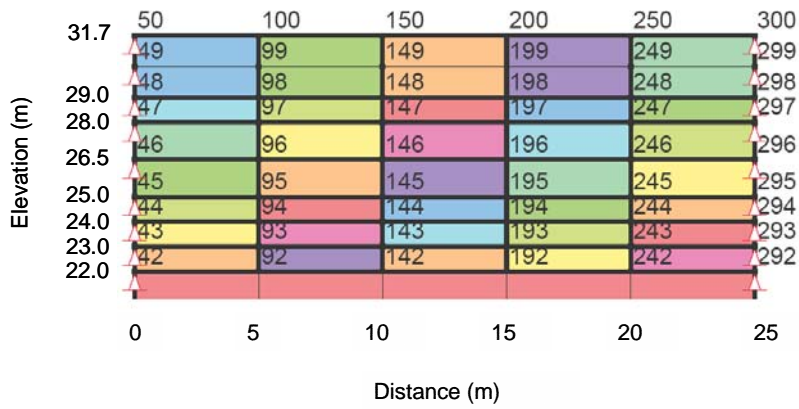


**Figure D-12** Geostatistically Modeled soil profile for line 3

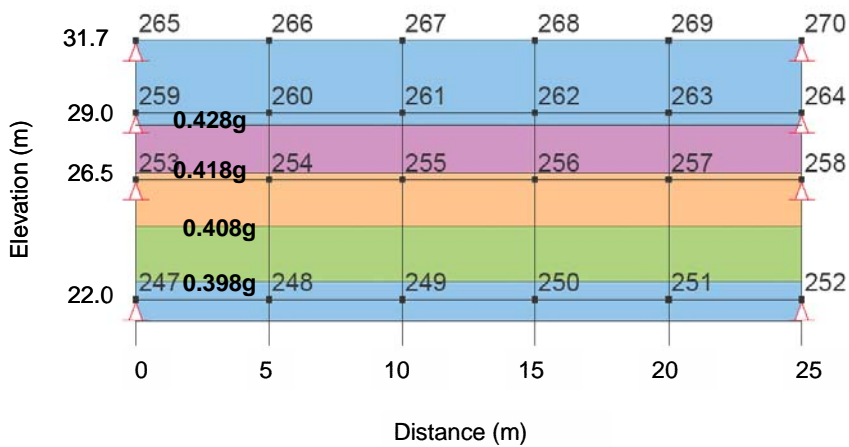


**Figure D-13** Peak acceleration distribution for statistically Modeled soil profile for line 3

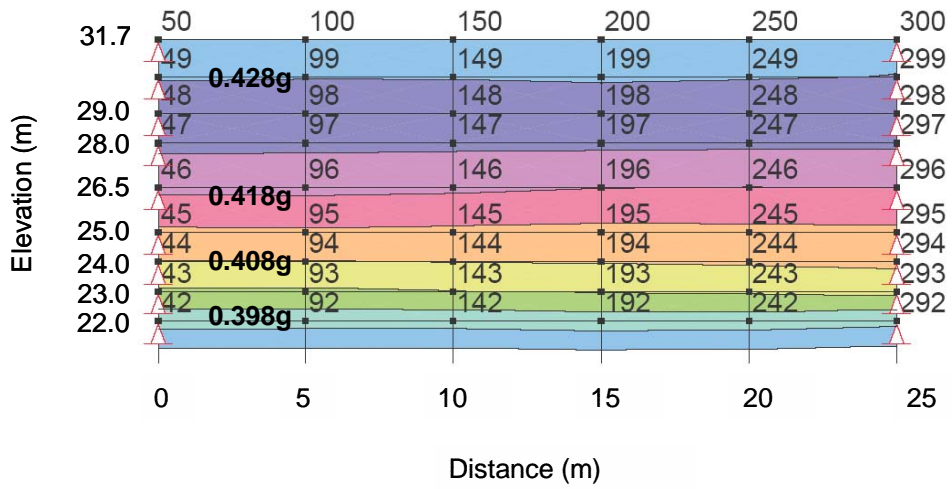


**Figure D-14** Peak acceleration distribution for geostatistically Modeled soil profile for line 3

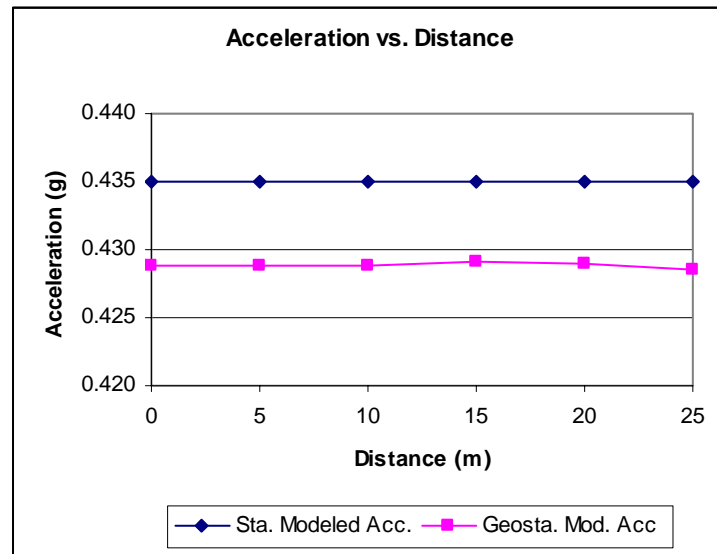


**Figure D-15** Peak acceleration distribution along the line 3 recorded at ground surface for statistically and geostatistically modeled soil profiles

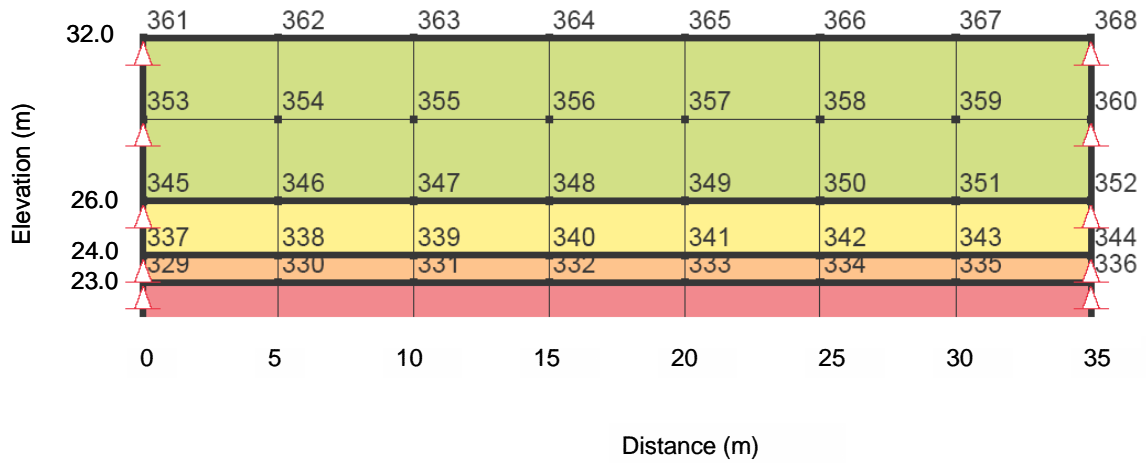


**Figure D-16** Statistically Modeled soil profile for line 4

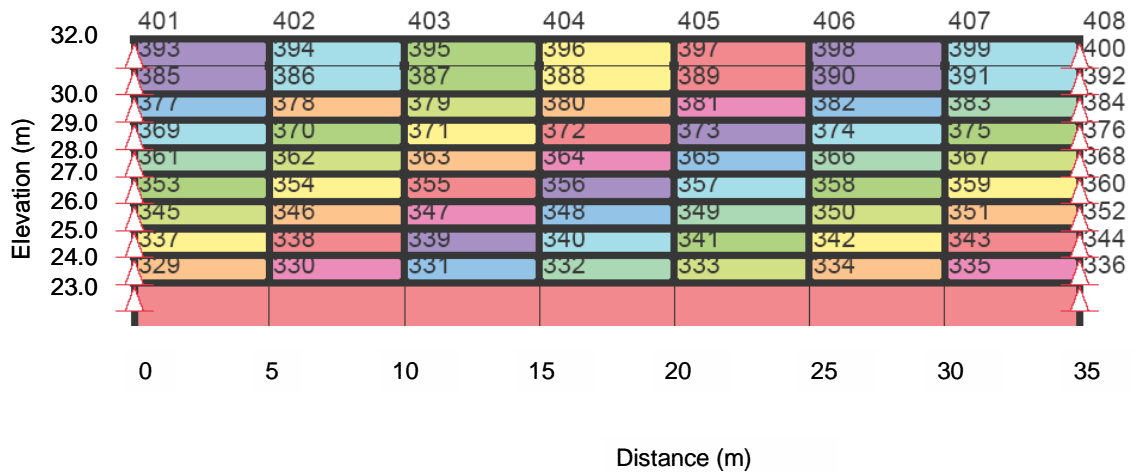


**Figure D-17** Geostatistically Modeled soil profile for line 4

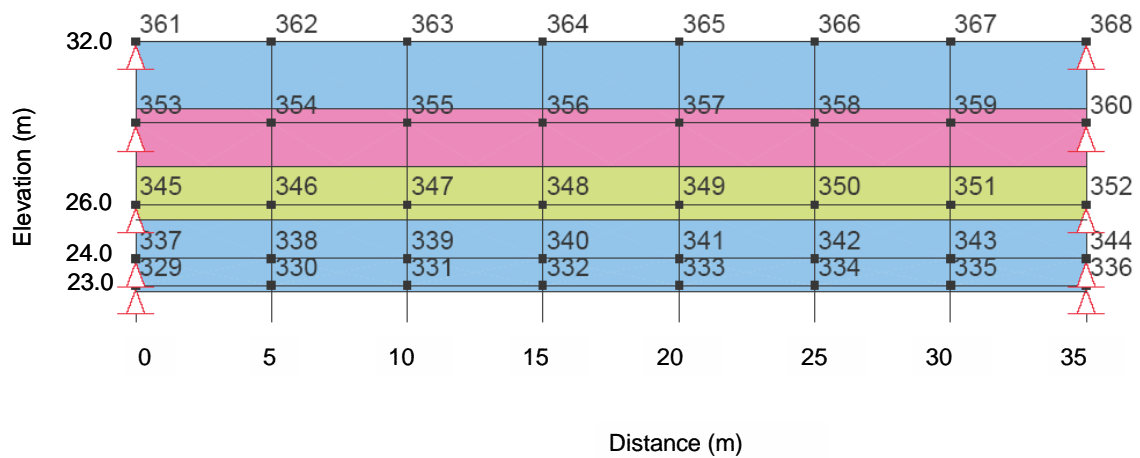


**Figure D-18** Peak acceleration distribution for statistically Modeled soil profile for line 4

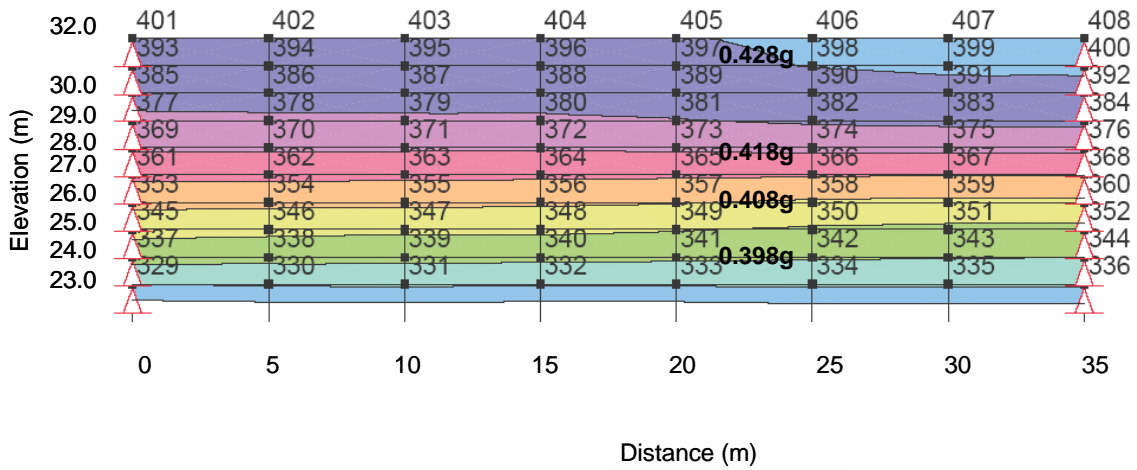


**Figure D-19** Peak acceleration distribution for geostatistically Modeled soil profile for line 4

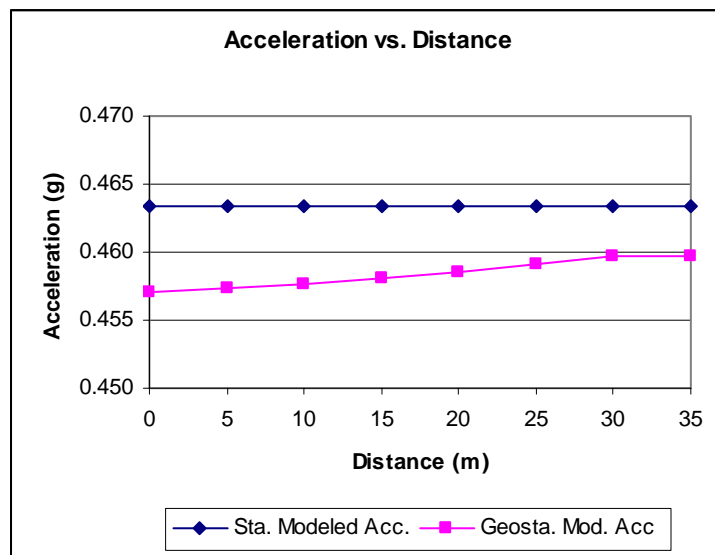


**Figure D-20** Peak acceleration distribution along the line 4 recorded at ground surface for statistically and geostatistically modeled soil profiles

## **CURRICULLUM VITAE**

Serkan ÜLKER was born on June 17, 1981 in Kars. He completed his primary school in Kars in 1992, his secondary school in Ankara in 1996, and his high school in Eskişehir in 1999. He started his BS degree at the Civil Engineering Department of the Istanbul Technical University and completed a four-year undergraduate education and graduated in 2004. At the same year, he started his MS education as a graduate student in the Geotechnical Engineering Division of Civil Engineering Department at the Istanbul Technical University.